

Initial bow imperfection for flexural buckling of steel members

Verification and optimisation regarding analysis of columns and beam-columns

Master's thesis in Structural Engineering and Building Technology

ANGELICA HENRIKSSON
JOSEFIN PANARELLI

MASTER'S THESIS BOMX02-17-100

Initial bow imperfection for flexural buckling of steel members

Verification and optimisation regarding analysis of columns and beam-columns

Master's thesis in Structural Engineering and Building Technology

ANGELICA HENRIKSSON
JOSEFIN PANARELLI

Department of Civil and Environmental Engineering
Division of Structural Engineering
Steel Structures
CHALMERS UNIVERSITY OF TECHNOLOGY
Gothenburg, Sweden 2017

Initial bow imperfection for flexural buckling of steel members
Verification and optimisation regarding analysis of columns and beam-columns
ANGELICA HENRIKSSON
JOSEFIN PANARELLI

© ANGELICA HENRIKSSON , JOSEFIN PANARELLI, 2017

Master's thesis BOMX02-17-100
ISSN 1652-8557
Department of Civil and Environmental Engineering
Division of Structural Engineering
Steel Structures
Chalmers University of Technology
SE-412 96 Gothenburg
Sweden
Telephone: +46 (0)31-772 1000

Colophon:

The thesis was created using $\text{\LaTeX} 2_{\epsilon}$ and `biblatex` and edited on `www.sharelatex.com`. The typesetting software was the `TEX Live` distribution. The text is set in Times New Roman. Graphs were created using `PGFPLOTS` and `Matlab`. Figures were created using `INKSCAPE`.

Cover:

Initial bow imperfection of a axially compressed column. Picture created in `INKSCAPE`.

Chalmers Reproservice
Gothenburg, Sweden 2017

Initial bow imperfection for flexural buckling of steel members
Verification and optimisation regarding analysis of columns and beam-columns
Master's thesis in Structural Engineering and Building Technology

ANGELICA HENRIKSSON

JOSEFIN PANARELLI

Department of Civil and Environmental Engineering
Division of Structural Engineering
Steel Structures
Chalmers University of Technology

ABSTRACT

The procedure of analysing the stability of steel structures has been developed for a long time. Still today, some of the methods are both questioned and complicated to use, especially when considering more advanced load and boundary conditions. The aim of this thesis was therefore to evaluate the accuracy of the method with an initial bow imperfection both analytically and numerically. The contents of this thesis was a beginning of the long-term goal of studying the optimisation of the initial bow imperfection to make it more numerically applicable for a wide range of load and boundary conditions. The study was conducted on columns which were loaded only with axial compression and beam-columns which were loaded with a combination of axial compression and an external bending moment.

The analyses were based on a comparison between the method with an initial bow imperfection and the other already established methods, i.e. the buckling curve method for columns together with Method 1 and 2 for beam-columns. The method with an initial bow imperfection is based on that all steel members have initial material and geometrical imperfections in some extent. Those imperfections is converted into a resulting initial bow in the member which in turn creates a second-order moment. In the case of a beam-column subjected to an external moment, this initial bow imperfection enhances the total moment that acts on the member.

Overall, the original value of the initial bow imperfection gave results on the safe side for columns but varying results for beam-columns. The new and optimised formulas improved the results for columns in both plastic and elastic analysis, for all considered members in both bending directions with one exception: the results were on the unsafe side for the plastic analysis of H and I members in the weak buckling direction. Regarding beam-columns, there were still varying results for the plastic analysis. The unfavourable results for both columns and beam-columns could be explained with the interpretation of the stress-strain relation in the calculations methods. By that, the conclusion that the new formulas worked well was drawn. However, it should be perceived that for a final overall conclusion regarding the numerical analysis, a greater number of analyses needs to be conducted.

Keywords: steel, instability, buckling, initial bow imperfection, second order buckling analysis, interaction, column, beam-column, Eurocode

Initialimperfektion för böjknäckning av stålenheter
Verifiering och optimering avseende analys av pelare och balk-pelare
Examensarbete inom Konstruktionsteknik och Byggnadsteknologi

ANGELICA HENRIKSSON

JOSEFIN PANARELLI

Institutionen för bygg- och miljöteknik
Avdelningen för konstruktionsteknik
Stålkonstruktioner
Chalmers tekniska högskola

SAMMANFATTNING

Stabilitetsanalyser av stålkonstruktioner har varit under utveckling under en lång period. Än idag är vissa av metoderna ifrågasatta och komplicerade att använda, speciellt när hänsyn tas till mer avancerade lastfall och upplagsvillkor. Målet med examensarbetet var därför att utvärdera noggrannheten hos metoden med initialimperfektioner både analytiskt och numeriskt. Innehållet i denna masteruppsats var en början på vägen till målet om att optimera metoden med initialimperfektioner och göra den mer numeriskt applicerbar för en stor variation av lastfall och upplagsvillkor. Studien är genomförd på pelare belastade med enbart axiell last och på balk-pelare belastade med en kombination av axiell last och yttre böjmoment.

Analyserna baserades på en jämförelse mellan metoden med en initialimperfektion och de andra, redan etablerade metoderna dvs. metoden med knäckkurvor för pelare samt Metod 1 och 2 för balk-pelare. Metoden med initialimperfektioner är baserad på att alla stålkonstruktioner har initiella materiella- och geometriska imperfektioner i olika utsträckning. De imperfektionerna omvandlas till en resulterande initialutböjning vilket i sin tur genererar ett böjmoment av andra ordningen. I fallet med balk-pelare belastade med ett ytterligare böjmoment medverkar den initiella imperfektionen till att det totala böjmomentet som verkar på konstruktionen ökar.

Resultatet visade övergripande att det nuvarande värdet för den initiella imperfektionen gav resultat på den säkra sidan för pelare men varierande resultat för balk-pelare. De nya och optimerade formlerna genererade bra resultat beträffande pelare för både plastisk och elastisk analys för alla beaktade konstruktioner i båda knäckningsriktningarna med ett undantag: resultatet var på den osäkra sidan för plastisk analys av H- och I-tvärsnitt i vek knäckningsriktning. För balk-pelare var resultaten fortfarande varierande för den plastiska analysen. De ogynnsamma resultaten för både pelare och balk-pelare förklarades med beräkningsmetodernas tolkning av spänning-töjningsförhållandet. Därmed drogs slutsatsen att de nya formlerna fungerade väl. Däremot bör det uppmärksammas att för att kunna dra en slutgiltig slutsats angående de numeriska resultaten så måste ett större antal analyser utföras.

Nyckelord: stål, instabilitet, knäckning, initialimperfektion, andra ordningens analys, pelare, balk-pelare, Eurokod.

CONTENTS

Abstract	i
Sammanfattning	ii
Contents	iii
Preface	vii
Acronyms	ix
Nomenclature	ix
1 Introduction	1
1.1 Background	1
1.2 Aim and objectives	1
1.3 Method	2
1.4 Limitations	3
2 Theoretical background	4
2.1 Introduction to structural instability	4
2.2 Euler's buckling theory	6
2.2.1 Critical buckling length	10
2.3 Initial imperfections	10
2.3.1 Geometrical imperfections	11
2.3.2 Material imperfections	13
2.4 Sectional response	15
2.4.1 Elastic response	15
2.4.2 Plastic response	16
2.4.3 Cross-section classification	17
2.5 Recently conducted research	18
2.5.1 Verification of flexural buckling using the initial bow imperfection	18
2.5.2 Equivalent member imperfections in steel frames	19
3 Methods for stability analysis	20
3.1 Columns	20
3.1.1 Method with buckling curves	20
3.1.2 Method with initial bow imperfections and second-order moment	23
3.2 Beam-columns	27
3.2.1 Method 1 and 2	27
3.2.2 Method with an initial bow imperfection	31
CHALMERS, Department of Civil and Environmental Engineering, Master's thesis, BOMX02-17-100	iii

4	FE-model	32
4.1	Abaqus	32
4.2	Modelling procedure	32
4.2.1	Considered columns	36
4.3	FE-analyses	36
4.3.1	Static stress analysis	36
4.3.2	Linear buckling analysis	37
4.3.3	Second order buckling analysis	37
5	Results and discussion	39
5.1	Analytical results for columns	39
5.1.1	Verification of Matlab programme	39
5.1.2	Exact vs. simplified cross-section classification	40
5.1.3	The exact method vs. the reduction formula method	42
5.1.4	Results before the optimisation	43
5.1.5	Optimisation of initial bow imperfection	48
5.2	Numerical results for columns	57
5.2.1	Euler-Bernoulli or Timoshenko beam elements	58
5.2.2	Comparison of analytical and numerical results	63
5.2.3	Optimisation of FE-analysis	66
5.3	Analytical results for beam-columns	69
5.3.1	Verification of Matlab programme	69
5.3.2	Analysis of beam-columns	69
5.3.3	Optimisation of initial bow imperfection	81
5.4	Numerical results for beam-columns	85
5.5	Summary of results	86
5.5.1	Reflections over the deviations in the results	88
6	Conclusions	91
	References	93
	Appendix A Considered columns in numerical analysis	94
	Appendix B Comparison of B21 and B23 beam elements.	95
	Appendix C Verification of Matlab programme	96
C.1	Columns	96
C.2	Beam-columns	97
	Appendix D Numerical results for columns	98
D.1	Comparison of analytical and numerical results	99
D.2	Comparison of optimised plastic analyses	101

Appendix E Analytical results for beam-columns	103
E.1 Equal external end-moment (y-y)	104
E.2 Equal external end-moment (z-z)	111
E.3 Uniformly distributed load (y-y)	118
E.4 Uniformly distributed load weak buckling direction (z-z)	125
E.5 Optimisation of initial bow imperfection (y-y)	132
E.6 Optimisation of initial bow imperfection (z-z)	139

PREFACE

As a part of the compulsory assignments for the master's degree in Structural Engineering and Building Technology, this master's thesis was carried out during the spring of 2017 at Chalmers University of Technology, Gothenburg Sweden, at the division of Structural Engineering.

We would like to acknowledge our gratitude to our examiner and supervisor Mohammad Al-Emrani, associate professor at the division of Structural Engineering at Chalmers University of Technology. He always impressed with his expertise within this area of steel research and he were an excellent, committed mentor throughout the project. We also want to declare a special thank you to VBK Konsulterande Ingenjörer AB with supervisor Rasmus Sylvén, Gothenburg Sweden, for letting us be a part of the company during this period. Finally, we would like to thank our opponents Axel Kristensson and Michael Engberg for great feedback and inspirational discussions.

Angelica Henriksson and Josefin Panarelli

Gothenburg, 2017

Acronyms

CAE Computer Aided Engineering or Complete Abaqus Environment. 2

ECCS European Convention for Constructional Steelwork. 1, 27

Nomenclature

Greek letters

α	imperfection factor (-)
$\bar{\lambda}$	relative slenderness ratio (-)
χ	buckling reduction factor (-)
χ_{LT}	buckling reduction factor due to lateral-torsional buckling (-)
χ_y	reduction factor due to flexural buckling, strong axis, y-y (-)
χ_z	reduction factor due to flexural buckling, weak axis z-z (-)
δ	Dischinger factor (correction factor) (-)
$\delta_{0,d}$	unit amplitude critical mode shape initial imperfection (mm)
η	factor (-)
γ_{M0}	partial factor for resistance of cross-sections (-)
γ_{M1}	partial factor for resistance of members to instability (-)
κ_y	factor (-)
$\lambda_{(1)}$	slenderness (-)
$\lambda_{(2)}$	eigenvalue (-)
λ_1	reference relative slenderness (-)
μ	factor (-)
ω	frequency (1/m)
Φ	factor to determine the reduction factor (-)
ϕ	eigenvector (-)
π	constant (-)
$\psi_{(1)}$	interaction factor (-)
$\psi_{(2)}$	factor used in equivalent moment factor (-)
σ	stress (MPa)

σ_{cr}	critical buckling stress (MPa)
σ_{Ed}	stress design value (MPa)
σ_{max}	maximum stress (MPa)
ε	strain (-)
ε_{el}	elastic strain (-)
ε_{pl}	plastic strain (-)
φ	curvature (rad)
φ_y	curvature at yielding (rad)

Roman lower case letters

a	ratio of web area to gross area (-)
a_f	ratio of flange area to gross area, hollow core sections (-)
a_w	ratio of web area to gross area, hollow core sections (-)
b	member width (mm)
b_1	member bottom flange width (mm)
b_2	member top flange width (mm)
$e_{0,d}$	design values for the initial bow imperfection (mm)
e_0	initial bow imperfection (mm)
e_1	lateral deflection (mm)
e_{max}	total amplitude of lateral deflection (mm)
f	factor (-)
f_u	ultimate stress (MPa)
f_y	yield stress (MPa)
h	member height (mm)
h_w	member web height (m)
i	radius of gyration (m)
j	ratio between initial bow imperfection and length (-)
k_{yy}	interaction factor for Method 1 and 2 (-)

k_{yz}	interaction factor for Method 1 and 2 (-)
k_{zy}	interaction factor for Method 1 and 2 (-)
k_{zz}	interaction factor for Method 1 and 2 (-)
l	length at x (mm)
n	ratio of design value of axial compression force and plastic design plastic resistance to axial compression force (-)
t_1	member bottom flange thickness (mm)
t_2	member top flange thickness (mm)
t_3	member web thickness (mm)
t_f	member flange thickness (mm)
t_w	member web thickness (mm)
x	coordinate in x-direction (m)
$x-x$	axis along the member (-)
y	coordinate in y-direction (m)
$y-y$	axis of a cross-section (-)
y_{max}	maximum lateral displacement (mm)
y_n	(distance to neutral axis from centre of cross-section mm)
z	coordinate in z-direction (m)
$z-z$	axis of a cross-section (-)

Roman capital letters

$\Delta M_{y,Ed}$	moments due to shift in the centroidal axis, y-y axis (kN m)
$\Delta M_{z,Ed}$	moments due to shift in the centroidal axis, z-z axis (kN m)
A	surface area (m ²)
A_{eff}	effective surface area
C_m	equivalent uniform moment factor (-)
E	Young's modulus (MPa)
F	maximum compression or tension force (kN)
I	moment of inertia (m ⁴)
I_{eq}	equivalent moment of inertia (m ⁴)
K	basic matrix (-)
K_G	basic identity matrix (-)
$L_{(1)}$	member length (m)
$L_{(2)}$	element length (mm)
L_{cr}	critical buckling length (m)
M	bending moment (kN m)
$M_{Ed,max}^{II}$	maximum second order design bending moment (kN m)
M_{Ed}	design bending moment (kN m)

M_{El}	elastic bending moment (kN m)
M_{el}	elastic bending moment (kN m)
M_{ext}	External bending moment (kN m)
M_{Ex}	external bending moment (kN m)
M_{II}	second order bending moment (kN m)
M_{int}	Internal bending moment (kN m)
M_I	first order bending moment (kN m)
M_{max}	maximum bending moment (kN m)
$M_{N,Rd}$	reduced design values of the resistance to bending moment (kN m)
$M_{N,y,Rd}$	reduced design bending moment resistance, y-y axis (kN m)
$M_{N,z,Rd}$	reduced design bending moment resistance, z-z axis (kN m)
$M_{pl,y,Rd}$	plastic design bending moment resistance, y-y axis (kN m)
$M_{pl,z,Rd}$	plastic design bending moment resistance, z-z axis (kN m)
M_{pl}	plastic bending moment (kN m)
M_{Rd}	design bending moment resistance (kN m)
$M_{y,Ed}$	design bending moment, y-y axis (kN m)
$M_{y,Rk}$	characteristic value of resistance to bending moment, y-y axis (kN m)
M_y	bending moment at yielding (kN m)
$M_{z,Ed}$	design bending moment, z-z axis (kN m)
$M_{z,Rk}$	characteristic value of resistance to bending moment, z-z axis (kN m)
N	axial compression force (kN)
$N_{b,Rd}$	design buckling resistance (kN)
N_{cr}	critical buckling force (kN)
N_{Ed}	design value of the axial compression force (kN)
N_{max}	maximum axial compression force (kN)
$N_{N,y,Rd}$	reduced design axial compression resistance, y-y axis (kN)
$N_{N,z,Rd}$	reduced design axial compression resistance, z-z axis (kN)
$N_{pl,Rd}$	design plastic resistance to axial compression force (kN)
N_{Pl}	plastic axial compression force (kN)
N_{Rd}	design resistance to axial compression force (kN)
N_{Rk}	characteristic value of resistance compression (kN)

N_u	ultimate axial compression force (kN)		
N_y	axial compression force when yielding (kN)		ing the data from method with initial bow imperfection (-)
P_0	dead load (kN)	S_{11}	axial principal stress (MPa)
P_{cr}	critical buckling load (kN)	U	deflection (mm)
P_{ref}	pre-loaded reference load (kN)	W	section modulus (m ³)
P_{total}	total load (kN)	W_{el}	elastic section modulus (m ³)
Q	uniformly distributed load (kN/m)	$W_{pl,y}$	plastic section modulus, y-y axis (m ³)
R	resulting ratio from Method 1 or 2 by us-	W_{pl}	plastic section modulus (m ³)

1 Introduction

The contents of this master's thesis concern the study of the stability of steel structures focusing on how the available calculation methods in EN-1993-1-1 (2005) are related to each other and to the behaviour of an actual structural member. The various methods were thoroughly examined for various columns and beam-columns, steel strength classes and load conditions.

1.1 Background

Stability analyses of steel structures began over two centuries ago, with Leonhard Euler presenting the elastic buckling theory for compressed steel columns in 1759, Bjorhovde (1972). Theories for the complex non-linear behaviour of steel columns were not developed until over a hundred years later and the phenomenon was further analysed throughout the years. Research on the effect of initial imperfections was initiated around 1950. The outcome was an early proposal of buckling curves based on a probabilistic method presented by Bjorhovde (1972). In 1976, the European Convention for Constructional Steelwork presented the current buckling curves which were based on an extensive experimental research, da Silva, Simões, and Gervásio (2010). Since then, the ECCS has further developed Eurocode and the calculation methods in it. The version currently in use, Eurocode 3, was presented in 2005.

In this standard, there are two ways for calculation of stability against buckling for compressed members, either with buckling curves or with the use of initial bow imperfections. For members subjected to both bending and compression there are additional methods given. The buckling curves are suitable for analyses of simpler members subjected to compression and to some extent also lateral-torsional buckling. For more advanced models the method with buckling curves are not applicable and the other methods must be used. The accuracy of the stability design calculation methods in EN-1993-1-1 (2005) has been under discussion and there are still some uncertainties towards the more complex methods.

The method with initial bow imperfections is based on that all steel members have initial imperfections by some extent, which can be of material or geometrical type. Those imperfections lead to an initial bow in the member which in turn creates a second order moment. In the case of a beam-column subjected to an external moment this initial bow imperfection enhances the total moment that acts on the member. The goal of developing this method was that it should be applicable on a wide variation of loading and boundary conditions and thus simplify the calculations.

1.2 Aim and objectives

The aim of this thesis was to analyse and evaluate the accuracy of the method with an initial bow imperfection for stability analysis regarding flexural buckling of steel members which was presented in EN-1993-1-1 (2005). The purpose was to find the deviations in this method compared to the other calculation methods and the behaviour of a "real" structural member. It was also of interest to evaluate the possibility to optimise the results by either improving the initial bow imperfection or develop the calculation method itself. Today, the initial bow imperfection is dependent on the length of the structural

member. An additional goal was therefore to make it dependent of the relative slenderness $\bar{\lambda}$ instead. More specific, the aim was divided into the following objectives:

1. Perform a thorough literature study regarding facts, current calculation methods and more recent research to achieve a sufficient background of the subject.
2. Part one: Study of a pinned-pinned column subjected to an axial compressive load.
 - a) compare the method with an initial bow imperfection to the method with buckling curves.
 - b) for the deviations, make an optimisation.
 - c) perform FE-analyses with the same prerequisites. Verify the accuracy and compare with the results from the analytical calculations.
3. Part two: Study of a pinned-pinned beam-column subjected to a combination of an axial compressive load and an external bending moment.
 - a) compare the method with an initial bow imperfection to Method 1 and 2.
 - b) perform FE-analyses with the same prerequisites and compare with the results from the analytical calculations.

1.3 Method

Initially, a literature study was performed to examine documented facts and the background of both the subject and the general behaviour of structural steel members. Further, the current calculation methods from EN-1993-1-1 (2005) and their associated information were studied. Finally, the literature study included a review of more recent research of the subject.

Part one, which concerned the study of a pinned-pinned column subjected to an axial compressive load as in figure 1.1a, was initiated by hand-calculations in Mathcad to obtain reference values for design loads and stresses. Both the method with an initial bow imperfection and the method with buckling curves were evaluated. Then, the same calculations were carried out by iteration in Matlab for many columns and was later compared to the first calculations for verification of the programme. The analytical results were presented in tables and plots that clearly showed the differences between the methods. The next step was to compare the methods and further optimise the initial bow imperfection for the deviations. Also, FE-analyses were performed in Abaqus/CAE (from now referred to as just Abaqus) to obtain numerical results for verification of the analytical results. The numerical analyses were divided into three parts:

1. A static analysis to receive stresses, deformations and reaction forces.
2. A linear buckling analysis to get the first eigenvalue used for calculating the critical buckling load.
3. A non-linear buckling analysis where the buckling resistance of the compression member was found for an elastic-perfectly plastic material behaviour.

In the second part of this study, which concerned the study of a pinned-pinned beam-column subjected to a combination of an axial compressive load and an external bending moment as in figure 1.1b, the Matlab programme was developed to include this type of member. A real example of a beam-column is an axially loaded member which is also subjected to a transverse wind load. The hand-calculations were similar to those used on columns. Though, with a difference being that the second-order moment now included the additional external moment. The analytical results from the method with initial bow imperfection were compared to the analytical results for Method 1 and 2 with utilisation ratios in tables and plots. Also in this part, FE-analyses were carried out in the same manner as for columns. Though, the results were treated in another way. Instead of just verifying the hand-calculations, the analytic results were now used as data to compare with the analytical results obtained from Method 1 and 2.

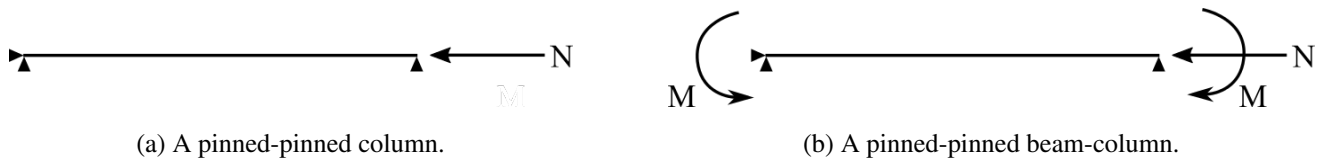


Figure 1.1: Load and boundary conditions for a column and a beam-column. Axial compressive load, N , and external bending moment, M .

1.4 Limitations

All analyses in this study were based on a pinned-pinned standard hot or cold rolled double-symmetric structural column or beam-column. The considered cross-sections were HEA, HEB, HEM and IPE sections with outstanding flanges together with hollow core KKR and VKR cross-sections. The failure mode of interest was flexural buckling since the members were assumed to be restrained against spatial behaviour such as lateral-torsional. The analyses were confined to steel strength classes $S235 - S420$. Both elastic and plastic analyses were considered and later presented separately. Only global buckling was included, hence, just cross-section classes 1 – 3 were studied since members in cross-section class 4 might fail due to local buckling. When the cross-section class was determined, a simplified method described in section 2.4.3 was used.

By reasons further described in section 2.4, plastic analyses were only carried out for cross-section class 1 and 2. Elastic analyses on the other hand were performed for all cross-section classes. The reason was that structural engineers sometimes only perform the elastic analyses due to its simplicity and because the results are on the safe side since plasticity is neglected. However, the results from the plastic analyses were considered more interesting due to the optimisation possibility. If a greater part of the cross-section could plasticise, material usage and construction costs could be decreased. When the FE-analyses were performed, a limitation in the cross-section geometry had to be made because of restrictions in Abaqus. Thus, the rolled parts of the cross-section had to be neglected which is further described in section 4.2.

2 Theoretical background

Major research upon the study of structural instability of steel members have been conducted to reach the design calculations of today. To comprehend the calculation methods used for buckling analysis more thoroughly, this chapter provides the reader with a synopsis concerning the fundamentals regarding the general behaviour, with a focus on buckling, of steel members. First, an overview of the phenomenon of structural instability is given. After that, Euler's buckling theory is derived followed by deeper knowledge regarding initial imperfections. Later, the section about sectional response provides the reader with knowledge regarding elastic and plastic material behaviour. Subsequently in this chapter, a brief review of recent conducted research is presented.

2.1 Introduction to structural instability

Buckling is the instability phenomenon arising from predominantly compressive stresses in a structural member subjected to either axial compression, bending moment or a combination of both. As defined in Galambos and Surovek (2008), the definition of instability is that a small change in load will generate a large change in displacement. Buckling, which is more commonly termed structural or geometrical instability, is distinguished by the occurrence of transverse deformations and is particularly important for axially compressed steel members since the slenderness often is relatively high. This type of structural collapse can occur both local, in a specific member, or global which may cause failure of the whole structure. As pointed out in Gambhir (2004), the load magnitude at which instability occur is more determined by the stiffness of the structure than the material strength itself. Further, instability is prevented by fulfilling a stable state of equilibrium where the structural member in consideration can keep its position and handle the loads even though the member is somewhat displaced out of its original position. As in figure 2.1a, an ideal pinned-pinned column with length L , is loaded with an axial load N until it reaches collapse. The definition of an ideal column is further described in section 2.2. The resulting deflection U has the shape of the first buckling mode in this case.

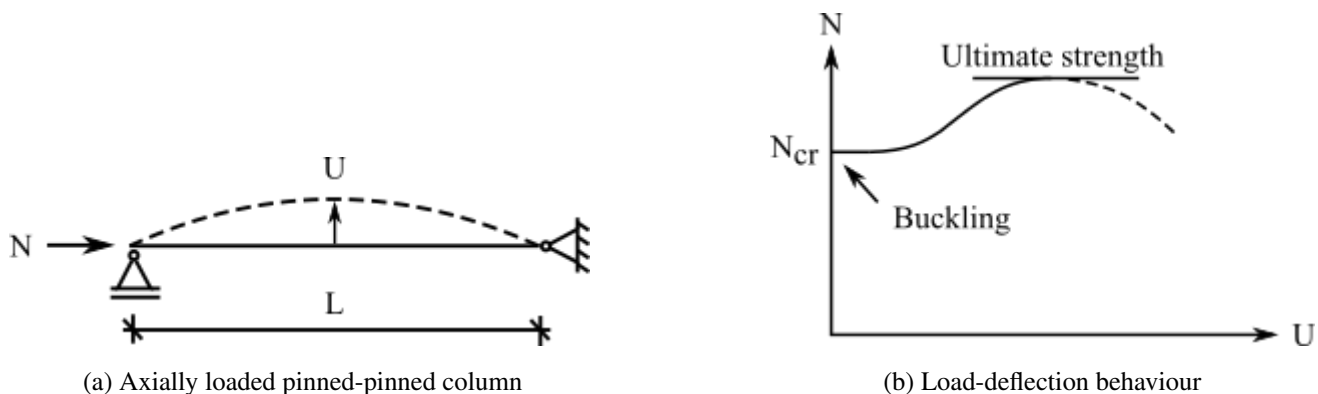


Figure 2.1: The axially compressed column in a) has the load-deflection relation described in b). Figure based on Gambhir (2004).

In figure 2.1b the corresponding load-deflection behaviour is presented in a graph. This ideal column will remain in its initially perfect state until the critical load N_{cr} at which yielding occur, is reached and buckling takes place. Before the yielding in the material is reached, adding or removal of any eventual lateral load would result in a return to the previous loaded position, Ziemian (2010). The critical point at the branch point is also called the bifurcation point. No bending moment may arise before that. Axially compressed columns have a distinct initial post-buckling behaviour. When the critical load is reached and buckling has occurred, the stiffness of the column will decrease. This happens because of the release of strain energy for the structure to keep its equilibrium, SIMULIA (2014). Instability take place at the maximum point of the load deflection curve, i.e. the ultimate strength in figure 2.1b. This post-buckling behaviour is visualised in an additional load-deflection relation in figure 2.2, from which two configurations are valid due to the symmetry. This relation is called an unstable symmetric post-buckling behaviour.

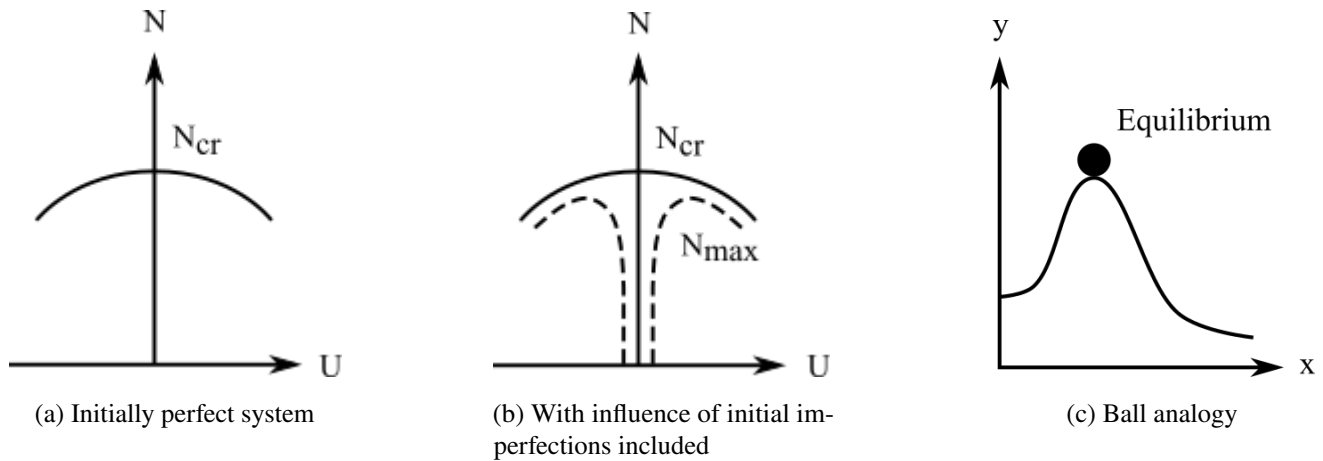


Figure 2.2: Unstable symmetric post-buckling curves for an initially perfect system and with and without imperfections included together with the ball analogy. Figure based on Gambhir (2004) and Ziemian (2010).

For initially imperfect systems, the initial imperfections and eccentricities of loading must be considered. The influence of these are visualised with dashed lines. The unstable symmetric post-buckling behaviour may be described as in Gambhir (2004) using a ball with arbitrary weight placed in the x - y plane as in the same figure. Equilibrium is assumed at the zero-curvature position. A minor perturbation of the ball will cause a corresponding response as to an unstable collapse of an axially compressed column. When the disturbance is removed, the energy will be released and the movement of the ball will gradually increase. As indicated in the figure, unstable systems may fail at loads below the critical load due to initial imperfections. Thus, unstable systems are imperfection sensitive.

2.2 Euler's buckling theory

Euler's buckling theory for columns is based on a derivation of the critical elastic load, which is referred to as Euler's critical load, N_{cr} . The derivation follows the theory of elasticity and includes the following assumptions for ideal design conditions:

1. Initially perfect column without geometrical imperfections
2. All load is applied in the centre of the column
3. Linear elastic material response
4. No residual or other inner stresses
5. Cross-section and support conditions are such that only plane-buckling occur in one direction
6. Small displacement theory is valid

Based on those conditions, a value of the axial load for which the column start exhibiting deformations that are not completely axial can be derived. This may be referred to as flexural buckling. Figure 2.3 shows the load and boundary conditions for the considered column.

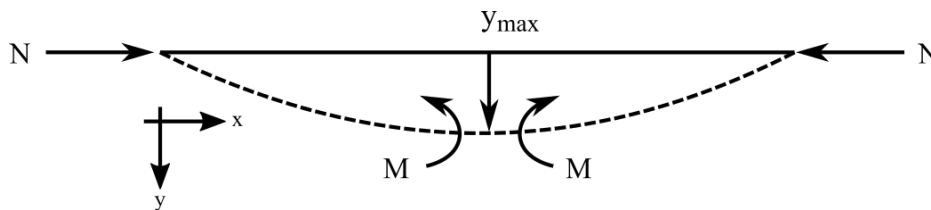


Figure 2.3: The column used in the derivation of Euler's buckling theory. The column is subjected to an axial load, N , an resulting bending moment, M , leading to the deflection y in the temporary defined coordinate system.

The deflection follows the first buckling mode, a half-sine wave, for a pinned-pinned column in this derivation. As described in section 2.1 the column will remain perfect until the critical buckling load is reached. At that point, the external bending moment at an arbitrary point of the column is defined as in equation 2.1.

$$M_{ext}(x) = N_{cr} \cdot y(x) \quad (2.1)$$

The corresponding internal bending moment is expressed as in equation 2.2.

$$M_{int}(x) = -EI \frac{d^2y}{dx^2} \quad (2.2)$$

The external and internal bending moment should be equal to fulfil equilibrium. By combining them, a differential equation expressing small buckling deformations arises, see equation 2.3.

$$-EI \frac{d^2 y}{dx^2} = N_{cr} \cdot y(x) \quad \leftrightarrow \quad \frac{d^2 y}{dx^2} + \frac{N_{cr}}{EI} y(x) = 0 \quad (2.3)$$

Which also can be written as:

$$y'' + \omega^2 y(x) = 0 \quad \text{with} \quad \omega^2 = \frac{N_{cr}}{EI} \quad (2.4)$$

The way to solve the differential equation follows the general solution in equation 2.5. Additionally, the first and second derivatives are as in equation 2.6 and 2.7.

$$y(x) = A \cdot \sin(\omega x) + B \cdot \cos(\omega x) \quad (2.5)$$

$$y'(x) = A\omega \cdot \cos(\omega x) - B\omega \cdot \sin(\omega x) \quad (2.6)$$

$$y''(x) = -A\omega^2 \cdot \sin(\omega x) - B\omega^2 \cdot \cos(\omega x) \quad (2.7)$$

For the pinned-pinned column, there are no translations in y-direction at the supports. Hence, boundary conditions yields as following:

$$y(0) = 0 \quad \text{and} \quad y(L) = 0$$

By inserting the boundary conditions into the general solution, the constants A and B can be derived as following:

$$y(0) = 0 \quad \rightarrow \quad A \cdot \sin(0) + B \cdot \cos(0) = 0 \quad \rightarrow \quad B = 0$$

$$y(L) = 0 \quad \rightarrow \quad A \cdot \sin(\omega L) = 0$$

This is fulfilled for all $\omega L = n\pi$ where $n = 1, 2, 3, \dots$ etc. and results in the expression presented in equation 2.8.

$$\omega^2 = \frac{N_{cr}}{EI} = \frac{n^2 \pi^2}{L^2} \quad (2.8)$$

By extracting the critical buckling load N_{cr} from equation 2.8 and using the radius of gyration $i = \sqrt{I/A}$ together with that the minimum value for n is equal to 1, the critical buckling load is expressed in terms of a load as in equation 2.9 or as a stress as in equation 2.10. Notice that the term for the length, L , was replaced by the critical buckling length L_{cr} . This is further described in section 2.2.1.

$$N_{cr} = \frac{\pi^2 EI}{L_{cr}^2} \quad (2.9)$$

$$\sigma_{cr} = \frac{\pi^2 E}{\left(\frac{L_{cr}}{i}\right)^2} \quad (2.10)$$

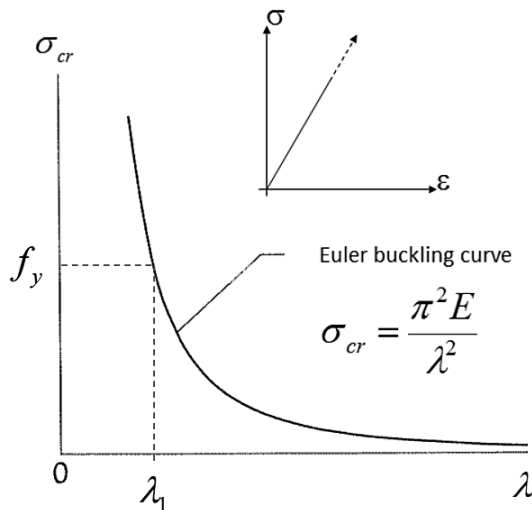
The new parameter that arose, L_{cr}/i indicates the slenderness λ of the column. A rewriting of the previous equation using the slenderness parameter results in the expression visualised in equation 2.11:

$$\sigma_{cr} = \frac{\pi^2 E}{\lambda^2} \quad (2.11)$$

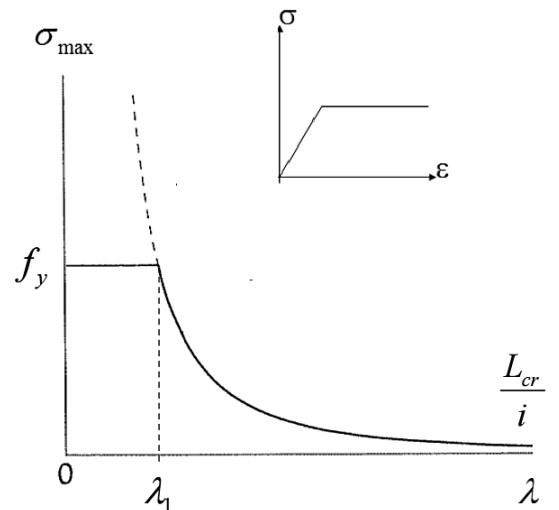
At this stage, the critical buckling stress is independent of the yield strength of the material, i.e. it follows an infinite linear elastic material behaviour. Therefore, the yield limit is included by introducing a reference relative slenderness as in 2.12. The reference relative slenderness is received by assuming that the critical buckling stress is equal to the yield stress and then extract the parameter.

$$\sigma_{cr} = \frac{\pi^2 E}{\lambda_1^2} = f_y \quad \rightarrow \quad \lambda_1 = \pi \sqrt{\frac{E}{f_y}} \quad (2.12)$$

The relation between the critical buckling stress and slenderness is shown in figure 2.4a and the relation for when the yield limit is included is shown in figure 2.4b.



(a) Linear elastic material behaviour



(b) With yield limit included in the material behaviour

Figure 2.4: Relation between the critical buckling stress and the slenderness of the column. Figures from Al-Emrani and Åkesson (2013).

The relation can be further developed by normalising the parameters and introducing two new parameters; the relative slenderness ratio $\bar{\lambda}$ and the reduction factor with regard to buckling χ .

$$\bar{\lambda} = \frac{\lambda}{\lambda_1} = \sqrt{\frac{N_y}{N_{cr}}} \quad (2.13)$$

$$\chi = \frac{\sigma_{max}}{f_y} \quad (2.14)$$

The relation between the relative slenderness and the buckling reduction factor is shown in figure 2.5.

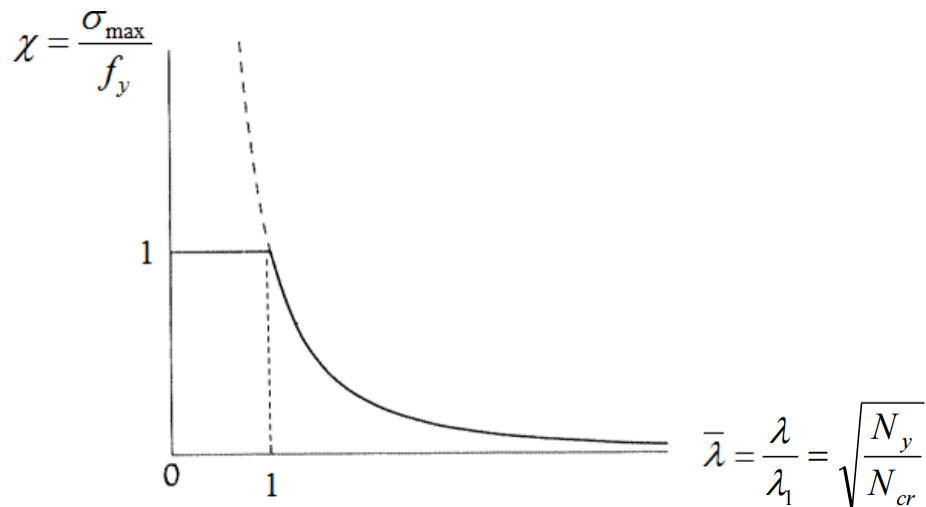


Figure 2.5: Relation between the buckling reduction factor and relative slenderness. Figure from Al-Emrani and Åkesson (2013)

2.2.1 Critical buckling length

As mentioned, the theoretical critical buckling load for a compressed member, see equation 2.9, is the load at which the column becomes unstable based on theory of elasticity. The buckling length can be derived with forth-order differential equations. Though, for columns with boundary conditions e.g. as in figure 2.6, the buckling length can be determined according to Euler's defined buckling cases. Where the critical buckling length ranges from left to right: $2L$, L , $0.75L$, $0.5L$ and L depending on boundary condition. Since only pinned-pinned members (case 2) was considered in this thesis the critical buckling length was set to L .

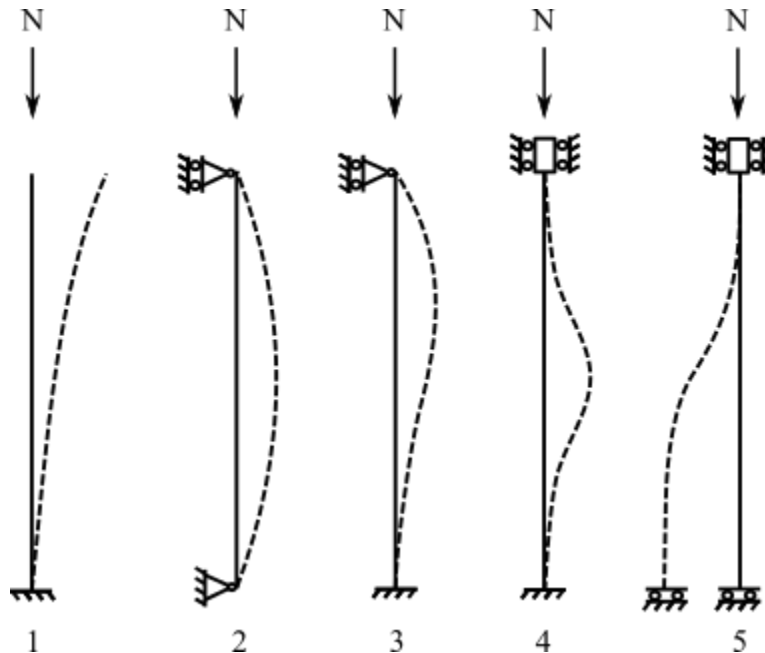


Figure 2.6: Euler buckling cases 1-5.

2.3 Initial imperfections

When a buckling curve is compared to the theoretical Euler buckling curve as in figure 2.7, it can be seen that depending on relative slenderness, the load carrying capacity differs. The difference is largest for columns with intermediate slenderness, i.e. a relative slenderness about 1. The reason for this behaviour is the initial imperfections of the column. Members with low relative slenderness are not affected by this as much since the load-carrying capacity is governed by yielding and not by buckling. The load-carrying capacity for members with very high slenderness is governed by elastic buckling where the stresses are much lower than the yield stress. Hence, the effect of the initial imperfections is not as decisive. The initial imperfections can be divided into two categories: geometrical and material imperfections.

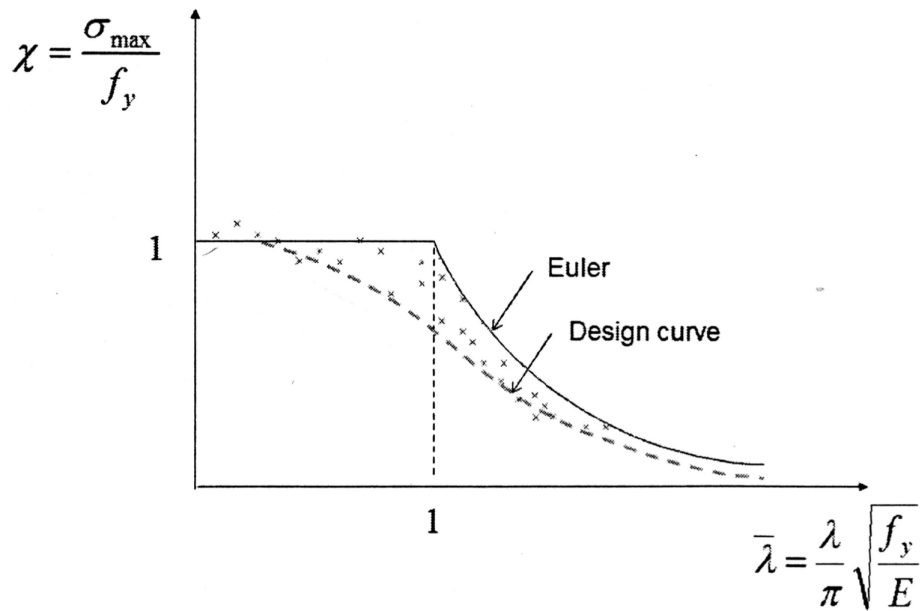


Figure 2.7: How a buckling curve is related to Euler's buckling theory shown with the relation between the buckling reduction factor and the relative slenderness. Figure from Al-Emrani and Åkesson (2013).

2.3.1 Geometrical imperfections

Steel members always experience some initial crookedness or other geometrical imperfections in some extent which leads to second-order moments because of the axial compression. This second-order moment will have an impact on the load-carrying capacity. Additionally, the second-order moment increases with increasing initial imperfections. When regarding beam-columns the second order moment as well as the external moment affects the final deflection. The effect of geometrical imperfections can be visualised by considering a pinned-pinned, axially loaded column with an initial bow imperfection e_0 shaped as a half-sine wave as in figure 2.8.

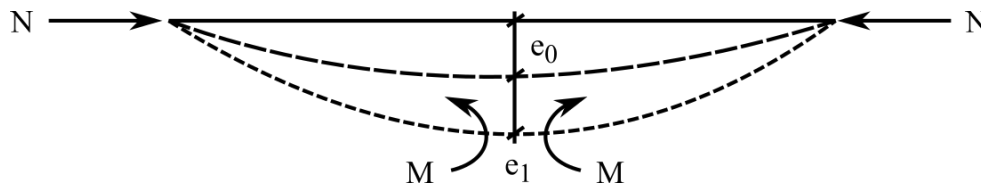


Figure 2.8: A member with an initial bow imperfection, e_0 , shaped as a half-sine wave. The member is loaded with an axial load, N , and obtains the bending moment, M . The loads cause additional deflection, e_1 .

For this case, the initial bow imperfection is captured at the midpoint since the magnitude is largest. It is calculated according to equation 2.15.

$$e_0 = a \cdot \sin\left(\frac{\pi x}{l}\right) \quad (2.15)$$

Due to the initial bow imperfection, a first order bending moment, M , arises which is expressed as:

$$M_I = N (e_0 + e_1) \quad (2.16)$$

This bending moment will cause an additional lateral deformation. Thus, an even larger deflection and bending moment. This iterative process can be written in form of a differential equation:

$$EI \frac{d^2 e}{dx^2} + N (e_0 + e_1) = 0 \quad (2.17)$$

By inserting equation 2.15 into the differential equation and later divide by EI , the following expression arises:

$$\frac{d^2 e}{dx^2} + \frac{N}{EI} \left(a \cdot \sin \frac{\pi x}{l} + e_1 \right) = 0 \quad (2.18)$$

The general solution of the differential equation is:

$$e_1 = A \sin(\omega x) + B \cos(\omega x) + \frac{\frac{Na}{EI}}{\frac{\pi^2}{l^2} - \frac{N}{EI}} \sin\left(\frac{\pi x}{l}\right) \quad (2.19)$$

Where:

$$\omega = \sqrt{\frac{N}{EI}} \quad (2.20)$$

The boundary conditions for the pinned-pinned column are:

$$e(0) = 0 \quad \text{and} \quad e(L) = 0$$

By inserting the boundary into the general solution, the additional deformation at the midpoint becomes:

$$e_1 \left(x = \frac{L}{2} \right) = \frac{\frac{N}{N_{cr}}}{1 - \frac{N}{N_{cr}}} \cdot e_0 \quad (2.21)$$

The total deformation e_{max} is obtained by adding the initial bow imperfection with the additional deformation. The final simplification of the expression is:

$$e_{max} = a + \frac{\frac{N}{N_{cr}}}{1 - \frac{N}{N_{cr}}} \cdot e_0 = \frac{1}{1 - \frac{N}{N_{cr}}} \cdot e_0 \quad (2.22)$$

This can be inserted in equation 2.16 to get the maximum bending moment M_{max} .

$$M_{max} = \frac{e_0}{1 - \frac{N}{N_{cr}}} \cdot N \quad (2.23)$$

Finally, the second-order moment can be written as:

$$M_{II} = \frac{1}{1 - \frac{N}{N_{cr}}} \cdot M_I = \frac{N}{1 - \frac{N}{N_{cr}}} \cdot e_0 \quad (2.24)$$

2.3.2 Material imperfections

Material imperfections, which also is referred to as residual stresses, is a phenomenon arising from when the steel is exposed to heating or cooling. This is the case for e.g. hot or cold-rolling in the manufacturing stage which creates a state of inner stresses in the cross-section, Al-Emrani and Åkesson (2013). According to Ziemian (2010), the residual stresses are self-balancing as well as dependent on the material properties, cross-section geometry and manufacturing method. This causes a wide spectrum of residual stresses which in turn causes a variation in the stress pattern. As explained by Jönsson and Stan (2017), the most appropriate stress pattern for an I-cross-section is the parabolic shape as in figure 2.9a. Though, the most common used model, which is the model used in the buckling curves, is the simplified linear distribution in figure 2.9b.

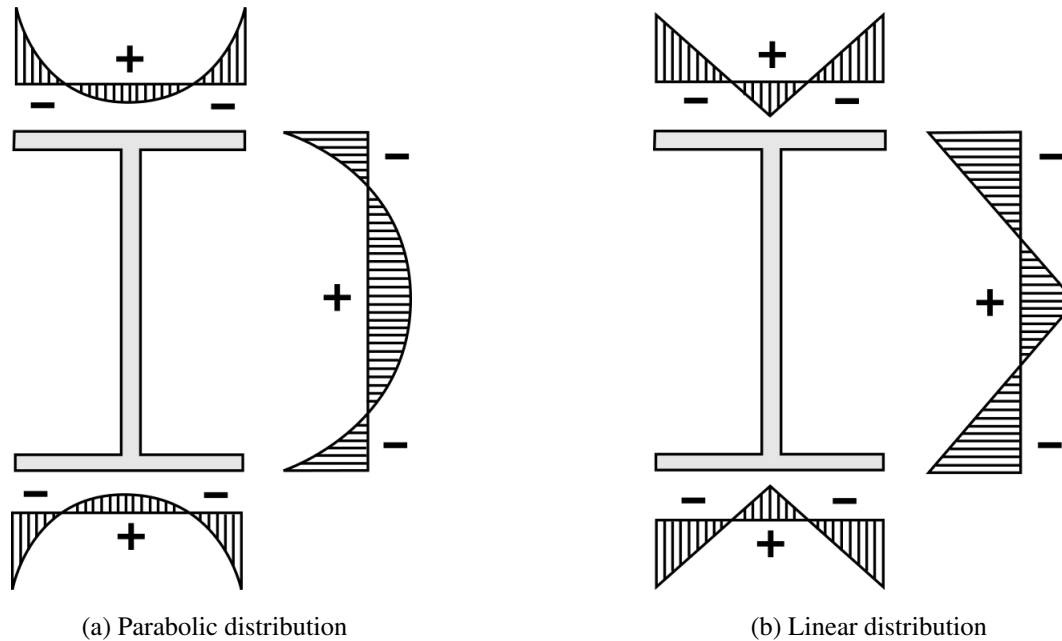


Figure 2.9: Distribution of residual stresses in a doubly symmetrical cross-section with outstanding flanges.

The residual stresses is added to the stresses caused by the loading of the member. For a member in compression, the resulting compressive stresses becomes even larger and the yield limit is reached faster. In members with low relative slenderness, this have a limited effect since the residual stresses are self-balancing and the ultimate load is not affected, Al-Emrani and Åkesson (2013). In very slender members, the ultimate load will be close to the elastic buckling load as previously mentioned, and therefore not affected by residual stresses in such great extent. For members with intermediate relative slenderness, the partial yielding that occur due to the uneven distribution of the residual stresses will affect the axial and bending stiffness of the member. Thus, resulting in increased deformations and second-order moments.

2.4 Sectional response

The sectional response of structural members is divided into elastic or plastic material behaviour. A steel member experience a linear material behaviour in the elastic range and a non-linear behaviour in the plastic range.

2.4.1 Elastic response

For a linear-elastic material behaviour, the Euler-Bernoulli beam theory is valid for slender beams with small deformations. The beam theory is based the following assumptions:

1. Only pure bending may take place
2. Initially straight member
3. Isotropic material with known stress-strain relation
4. Plane sections remain plane
5. The sections remain perpendicular to the centre-line of the beam

Elastic response can only be considered when the extreme fibre of the cross-section has not yet exceeded the yield limit. When Euler-Bernoulli beam theory is valid, both stress- and strain distribution varies linearly starting from the neutral axis. The elastic response is shown for a prismatic cross-section, i.e. the simplest model, in figure 2.10.

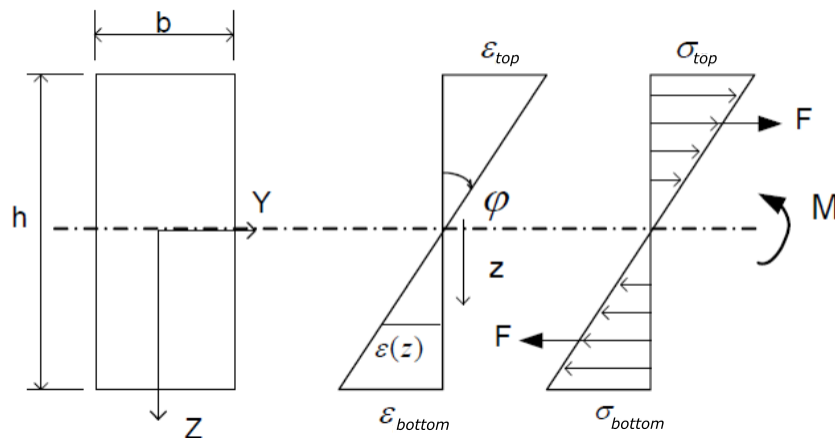


Figure 2.10: Linear-elastic sectional response for a prismatic cross-section. Figure from Al-Emrani, Engström, Johansson, and Johansson (2013).

The curvature φ is a result of the imposed bending moment M . The relation between the curvature and the strain ε at distance z from the neutral axis is expressed in equation 2.25.

$$\varphi = \frac{\varepsilon(z)}{z} \quad (2.25)$$

The stress distribution σ in the cross-section is caused by the curvature which in turn results in an elastic bending moment as in equation 2.26. The term W_{el} corresponds to the elastic section modulus.

$$M_{el} = \sigma \cdot W_{el} \quad (2.26)$$

As long as the yield strength is not exceeded, the relation can be written as in equation 2.27 since the relation between moment and curvature acts linearly in a triangular distribution determined by the material and cross-sectional constants EI .

$$\varphi = \frac{M}{EI} \quad (2.27)$$

The response will remain elastic until the yield limit is reached, i.e. when $\sigma = f_y$. After that, plastic material response is valid.

2.4.2 Plastic response

After the yield limit is reached, plasticity gradually takes place with increasing imposed bending moment until the cross-section eventually reach full plasticity. The transition from elastic to fully plastic response is shown in figure 2.11.

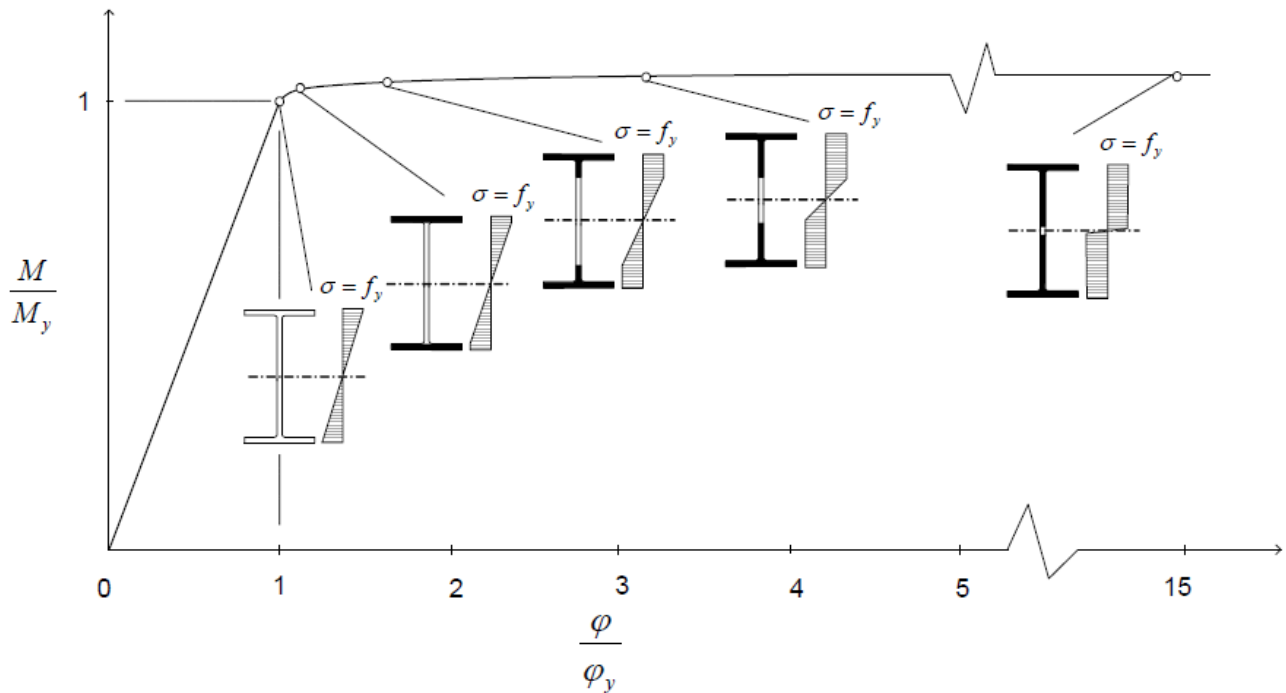


Figure 2.11: Relation between bending moment capacity and curvature for an I-section, normalised with respect to the elastic moment capacity and the corresponding curvature. Figure from Al-Emrani, Engström, Johansson, and Johansson (2013).

It is seen in the figure that the stress-strain relation becomes bi-linear. Though, the strain distribution remains linear, although increasing due to the growing bending moment. By using the relations for elasticity and plasticity, the sectional response at any point can be calculated, it is only the degree of plasticity that differs. When the cross-section has reached full plasticity, the plastic bending moment M_{pl} can be expressed as in equation 2.28. The term σ represents the stress distribution and the term W_{pl} corresponds to the plastic section modulus.

$$M_{pl} = \sigma \cdot W_{pl} \quad (2.28)$$

2.4.3 Cross-section classification

According to EN-1993-1-1 (2005), a structural member is divided into different classes depending on the width-to-thickness ratio of the cross-section and the type of loading (pure compression/tension, pure bending or a combination of both). The cross-section class considers the risk of local instability where a higher class represents a higher risk. Also, the cross-section class determines the way of calculating the capacity. In figure 2.12a to 2.12c, the load and deflection relations which represents the calculation model for each class is shown. A cross-section is classified according to the least favourable class. In fact, there are four cross-section classes but as mentioned in the limitations, cross-section class 4 was not treated in this thesis.

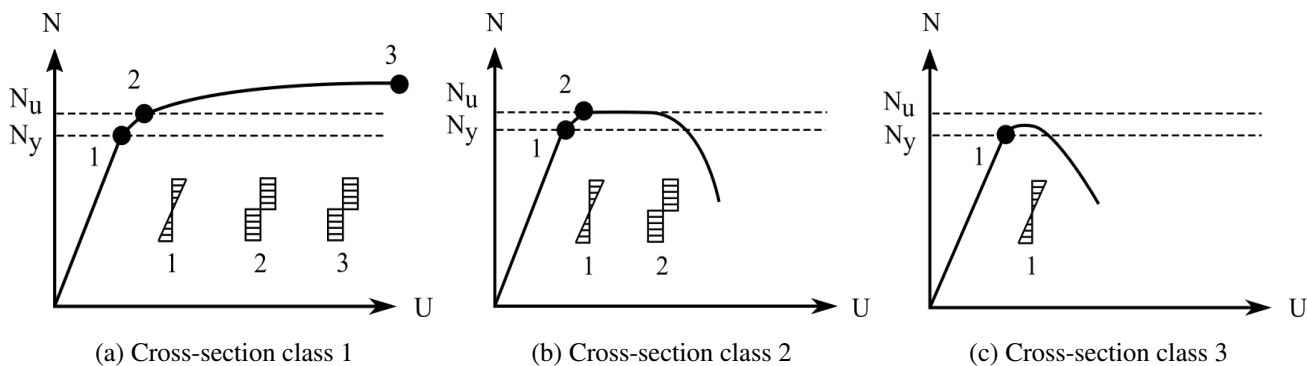


Figure 2.12: Load-deflection relation for cross-section class 1-3. N_y corresponds to the yield limit while N_u represents the limit of the ultimate load. Figure based on Al-Emrani, Engström, Johansson, and Johansson (2013).

Cross-sections in class 1 have the ability to reach full plasticity and develop a failure mechanism with plastic hinges for statically indeterminate systems due to its high rotation capacity. Since plastic moment redistribution can take place, the cross-section obtains a higher load-carrying capacity. Members in cross-section class 1 have a low relative slenderness. Therefore, the probability of failure due to yielding is higher than the risk of failure due to instability. Plastic response is used in design for both local and global analysis without any reduction of the resistance. Cross-sections in class 2 also have the ability to reach full plasticity. Though, only at the most critical section. In that section, a plastic hinge will develop and the load-carrying capacity will be governed by that. Because of the limited rotational capacity, no moment redistribution can take place in statically indeterminate systems, which means local buckling will occur before a mechanism can develop. At any section besides the most critical section, the load

bearing capacity should be governed by elastic response. However, there is no difference in calculations for cross-section class 1 and 2 if the system is statically determined. Lastly, the load-carrying capacity for cross-sections in class 3 is determined by the stress in the most extreme compression fibre which indicates a level of full elastic moment capacity corresponding to the yield strength of the material. Plastic capacity cannot be utilised due to the risk of local buckling. Therefore, elastic response should be used both locally and globally.

2.5 Recently conducted research

In this section, two recently conducted research projects that have influenced the subject of this thesis are briefly described focusing on the main conclusions.

2.5.1 Verification of flexural buckling using the initial bow imperfection

In 2016, an article which concerned the verification of flexural buckling according to Eurocode 3 using a bow imperfection was published by Lindner, Kuhlmann, and Just (2016). The research included both columns and beam-columns. The researchers assumed that the buckling curves in EN-1993-1-1 (2005) were accurate and that the cross-sectional analysis based on a second-order theory would result in the same load-carrying capacity. Based on that, the initial bow imperfection $e_{0,d}$ was derived based on the load-carrying capacity and the relative slenderness $\bar{\lambda}$ and further compared to the values for the initial bow imperfection presented in table 5.1 of EN-1993-1-1 (2005). According to Lindner et al. (2016), it was more appropriate to compare the ratios between the member length and the initial bow imperfection, i.e. a non-dimensional value. Thus, a factor j was introduced. Also in the article, several alternative reduction factors were presented and compared to the results from the current ones. Furthermore, FE-calculations for the ultimate load were carried out for verification. The calculations included both plastifying of the cross-section, residual stresses, elastic-perfectly plastic material behaviour and an initial bow imperfection of $L/1000$.

Most results which concerned columns were on the safe side with a few exceptions for the weak buckling direction. The authors seemed to find the deviant results acceptable. Another conclusion for columns was that for steel grade $S235$ and higher, the initial bow imperfection from EN-1993-1-1 (2005) may be retained for rolled I and H sections, partly based on the results from FE-calculations. However, exceptions were made for steel grade $S460$, since more results were on the unsafe side. For beam-columns, nearly all results were more unfavourable than for the columns. Additionally, many results were on the unsafe side. The researchers also presented some solutions to that problem.

Besides that some alternative interaction factors ψ used in the reduction formula presented in chapter 3.1.2, for normal load and bending moment were presented. One of the examples was an interaction factor from the German code DIN 18800 – 1. The interaction factor for I and H cross-sections in strong buckling direction is:

$$\psi = \frac{1 - \chi}{0.9} \quad \text{but} \quad \psi \leq 1 \quad (2.29)$$

The corresponding interaction formula for weak buckling direction is:

$$\psi = \frac{1 - \chi^2}{0.91} \quad \text{but} \quad \psi \leq 1 \quad (2.30)$$

In addition to those interaction factors, some new suggestions for the upcoming version of Eurocode 3 were given.

2.5.2 Equivalent member imperfections in steel frames

A while ago, Goncalves and Camotim (2005) published an article with the objective of clarifying the preliminary version of Eurocode concerning the incorporation of equivalent member imperfections in the elastic second-order global analysis. The main goal was to propose a general and consistent method to evaluate the equivalent initial imperfection that complied with EN-1993-1-1 (2005). Though, most of this article was focused on frames. In the first part, the authors republished an expression for the equivalent bow imperfection originally presented by Maqoui in 1980, here presented in equation 2.31, The formula is based on a sinusoidal shape of the imperfection.

$$e_{0,d} = \alpha (\bar{\lambda} - 0.2) \frac{W}{A} \quad (2.31)$$

3 Methods for stability analysis

In this chapter, the calculation methods that were used in this study are presented. For columns, there was the method with buckling curves and the method with initial imperfections. Regarding beam-columns, the method with initial imperfections were analysed in comparison with Method 1 and 2. All calculation methods are included in EN-1993-1-1 (2005) where the complete set of equations and coefficients can be found.

3.1 Columns

As already mentioned, there are two methods in EN-1993-1-1 (2005) for columns, i.e. a structural member subjected to axial compression, which are:

- 1) The method with buckling curves
- 2) The method based on initial imperfections and second-order moment where the bending moment is calculated using either:
 - a) a reduction formula, or
 - b) an exact method established on cross-section equilibrium

3.1.1 Method with buckling curves

In EN-1993-1-1 (2005), one of the design methods used to determine the buckling resistance of a column is based on the five buckling curves in figure 3.1.

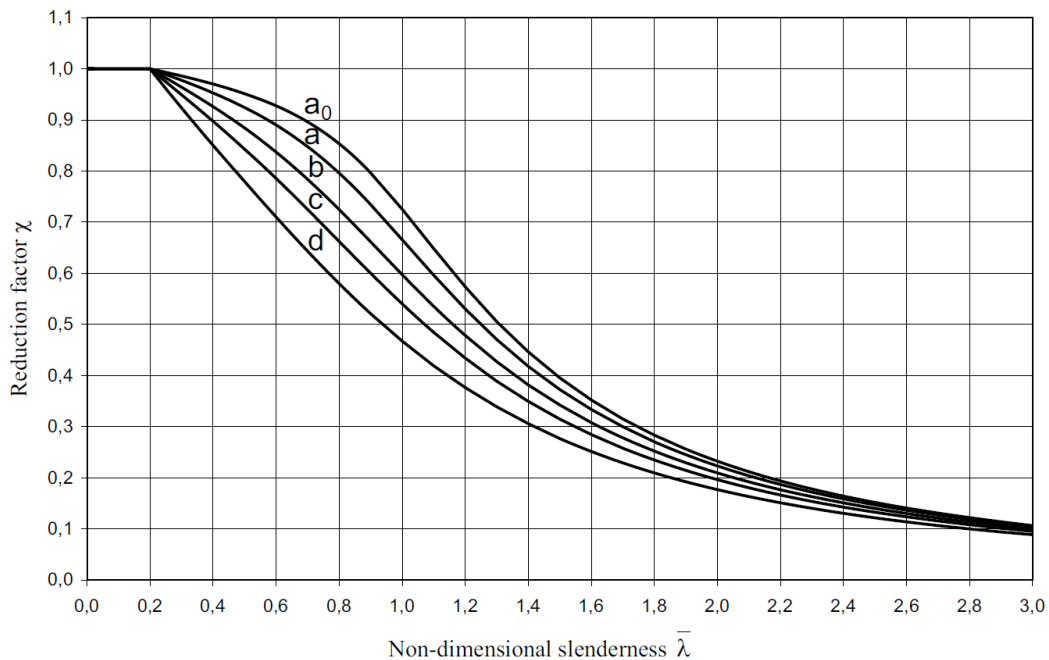


Figure 3.1: Buckling curves for flexural buckling. Figure from EN-1993-1-1 (2005).

The compressed member should be verified against buckling failure by calculating the ratio between the design value of the compression force, N_{Ed} and the design buckling resistance, $N_{b,Rd}$, according to equation 3.1.

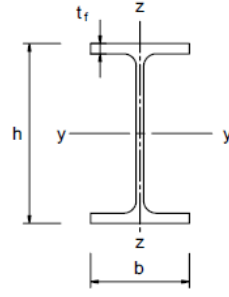
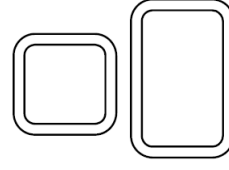
$$\frac{N_{Ed}}{N_{b,Rd}} \leq 1.0 \quad (3.1)$$

For cross-section class 1 – 3, the buckling resistance is calculated as in equation 3.2. As mentioned in the limitations, cross-section class 4 was not treated in this thesis.

$$N_{b,Rd} = \frac{\chi A f_y}{\gamma_{M1}} \quad (3.2)$$

The reduction factor χ can be calculated analytically (see equation 3.13), but also directly from the buckling curves. The correct buckling curve is selected by following table 3.1, which is a simplified version of the one in EN-1993-1-1 (2005). Further, the non-dimensional slenderness $\bar{\lambda}$ which in this thesis was called the relative slenderness ratio, is calculated by using equation 2.13, found in the previous chapter.

Table 3.1: Buckling curve selection for a cross-section with steel quality S235, S275, S355 and S420.

Cross section		Limits	Buckling about axis	Buckling curve	
Rolled section		$h/b > 1.2$	$t_f \leq 40$ mm	y-y z-z	a b
			$40 \text{ mm} < t_f \leq 100$ mm	y-y z-z	b c
		$h/b \leq 1.2$	$t_f \leq 100$ mm	y-y z-z	b c
			$t_f > 100$ mm	y-y z-z	d d
Hollow section		hot finished		any	a
		cold formed		any	c

The analytical way of calculating the buckling reduction factor is based on the Ayrton-Perry formula which was derived in 1978, Jönsson and Stan (2017). Initially, the Ayrton-Perry formula was applied for the case of a geometrically imperfect, elastic, pinned-pinned column loaded in uniform compression, Szalai and Pappb (2010).

This was described with the differential equation in expression 3.3, where N is the axial compression load, e the lateral displacement and e_0 represents the initial imperfection.

$$EI \frac{d^2 e(x)}{dx^2} + N (e(x) + e_0(x)) = 0 \quad (3.3)$$

This differential equation is similar to equation 2.17. Though, at position x along the member instead of at the midpoint. Just as in section 2.3.1, by assuming a sinusoidal imperfection, the total translation, e , becomes:

$$e = \frac{1}{1 - \frac{N}{N_{cr}}} \cdot e_0 \quad (3.4)$$

Yielding of the cross-section occurs when the following condition is fulfilled:

$$\frac{N_{max}}{A} + \frac{N_{max} \cdot e}{W_{el}} = f_y \quad (3.5)$$

By inserting equation 3.4 into equation 3.5, the following expression arises:

$$\chi + \frac{\chi}{(1 - \chi \bar{\lambda}^2)} \frac{e_0 \cdot A}{W_{el}} = 1 \quad (3.6)$$

Or, written in the form of the Ayrton-Perry formula as in equation 3.7, according to da Silva et al. (2010).

$$(1 - \chi) (1 - \chi \bar{\lambda}^2) = \frac{e_0 \cdot A}{W_{el}} \cdot \chi = \eta \chi \quad (3.7)$$

The factor η correlates to expression 3.8, with α representing the imperfection factor.

$$\eta = \alpha (\bar{\lambda} - 0.2) \quad (3.8)$$

The imperfection factor is determined by the following table, which is found in EN-1993-1-1 (2005).

Table 3.2: Imperfection factors for buckling curves.

Buckling curve	a_0	a	b	c	d
Imperfection factor, α	0.13	0.21	0.34	0.49	0.76

Further, the Ayrton-Perry equation can be written on a quadratic form:

$$(1 - \chi \bar{\lambda}^2)(1 - \chi) = \eta \chi = \alpha \chi (\bar{\lambda} - 0.2) \quad (3.9)$$

The minimum solution for the buckling reduction factor, χ , in the quadratic equation is:

$$\chi = \frac{\Phi - \sqrt{\Phi^2 - \bar{\lambda}^2}}{\bar{\lambda}^2} \quad (3.10)$$

The factor Φ is determined by:

$$\Phi = 0.5 [1 + \alpha (\bar{\lambda} - 0.2) + \bar{\lambda}^2] \quad (3.11)$$

Further, equation 3.10 is multiplied with the following expression:

$$\Phi + \sqrt{\Phi^2 - \bar{\lambda}^2} \quad (3.12)$$

Resulting in that, the final form of the critical buckling factor becomes as in equation 3.13, which is the formula used in EN-1993-1-1 (2005).

$$\chi = \frac{1}{\Phi + \sqrt{\Phi^2 - \bar{\lambda}^2}} \quad (3.13)$$

3.1.2 Method with initial bow imperfections and second-order moment

The other design method used to determine the buckling resistance of a column is the one based on an initial bow imperfection. Due to that imperfection, a second-order bending moment arises when the member is loaded. The value of this initial bow imperfection is shown in the following table, which is found in EN-1993-1-1 (2005).

Table 3.3: Design values for the initial bow imperfection.

Buckling curve	Elastic analysis	Plastic analysis
	$e_{0,d}/L$	$e_{0,d}/L$
a_0	1/350	1/300
a	1/300	1/250
b	1/250	1/200
c	1/200	1/150
d	1/150	1/100

In this method, the critical buckling load is found by iteration. The second-order design moment M_{Ed} that arises in the member is calculated using the following equation:

$$M_{Ed} = N_{Ed} \left(\frac{N_{cr}}{N_{cr} - N_{Ed}} \right) \cdot e_{0,d} \quad (3.14)$$

Buckling is prevented as long as the condition in equation 3.15 is fulfilled. The term $M_{N,Rd}$ represents the design moment resistance.

$$M_{Ed} \leq M_{N,Rd} \quad (3.15)$$

The way of calculating the moment resistance depends on if the exact method or the method with a reduction formula is used. Though, this is only valid for plastic analyses, i.e. for cross-sections in class 1 and 2. For cross-sections in class 3, the moment resistance is calculated using Navier's formula as in equation 3.16. Additionally, the axial compression force N_{Ed} has to be completely utilised with regard to the buckling factor.

$$\sigma_{Ed} = \frac{M_{Ed}}{W_{el}} + \frac{N_{Ed}}{A} \leq \frac{f_y}{\gamma_{M0}} \quad (3.16)$$

Moment resistance calculated using the reduction formula

When a combination of axial load and a bending moment is acting on a member, the effect the axial load has on the bending moment needs to be considered in the calculations of the plastic moment resistance. For columns, the bending moment corresponds to the second-order moment while for beam-columns the total bending moment is the external bending moment in combination with the second-order moment. For double symmetrical cross-sections with outstanding flanges, the reduced moment resistance $M_{N,y,Rd}$ in strong buckling direction is:

$$M_{N,y,Rd} = M_{pl,y,Rd} \frac{(1-n)}{(1-0.5a)} \quad \text{but} \quad M_{N,y,Rd} \leq M_{pl,y,Rd} \quad (3.17)$$

For weak buckling direction, the equation is as following:

$$M_{N,z,Rd} = M_{pl,z,Rd} \quad \text{for} \quad n \leq a \quad (3.18)$$

$$M_{N,z,Rd} = M_{pl,z,Rd} \left(1 - \left(\frac{n-a}{1-a} \right)^2 \right) \quad \text{for} \quad n > a \quad (3.19)$$

The factors a and n found in both expressions corresponds to equations:

$$a = \frac{(A - 2bt_f)}{A} \quad \text{but} \quad a \leq 0.5 \quad (3.20)$$

$$n = \frac{N_{Ed}}{N_{pl,Rd}} \quad (3.21)$$

This reduction does not have to be accounted for if the following criteria in equation 3.22 are fulfilled for the strong buckling direction and equation 3.23 for the weak buckling direction.

$$N_{Ed} \leq 0.25N_{pl,Rd} \quad \text{and} \quad N_{Ed} \leq \frac{0.5h_w t_w f_y}{\gamma_{M0}} \quad (3.22)$$

$$N_{Ed} \leq \frac{h_w t_w f_y}{\gamma_{M0}} \quad (3.23)$$

The corresponding formulas for the reduced moment capacity for rectangular hollow sections are as in equation 3.24 for columns in strong buckling direction and equation 3.25 for weak buckling direction.

$$M_{N,y,Rd} = M_{pl,y,Rd} \frac{(1 - n)}{(1 - 0.5a_w)} \quad \text{but} \quad M_{N,y,Rd} \leq M_{pl,y,Rd} \quad (3.24)$$

$$M_{N,z,Rd} = M_{pl,z,Rd} \frac{(1 - n)}{(1 - 0.5a_f)} \quad \text{but} \quad M_{N,z,Rd} \leq M_{pl,z,Rd} \quad (3.25)$$

The terms a_w and a_f are determined by the following equations:

$$a_w = \frac{(A - 2bt)}{A} \quad \text{but} \quad a_w \leq 0.5 \quad (3.26)$$

$$a_f = \frac{(A - 2ht)}{A} \quad \text{but} \quad a_f \leq 0.5 \quad (3.27)$$

Moment resistance calculated using the exact formula

The moment resistance can also be determined by an exact method which is based on an equilibrium analysis concerning the stresses in the cross-section. The way of calculation depends on whether the neutral axis is in the web or the flanges. For the strong buckling direction, the cross-section equilibrium results in the following two cases presented in figure 3.2.

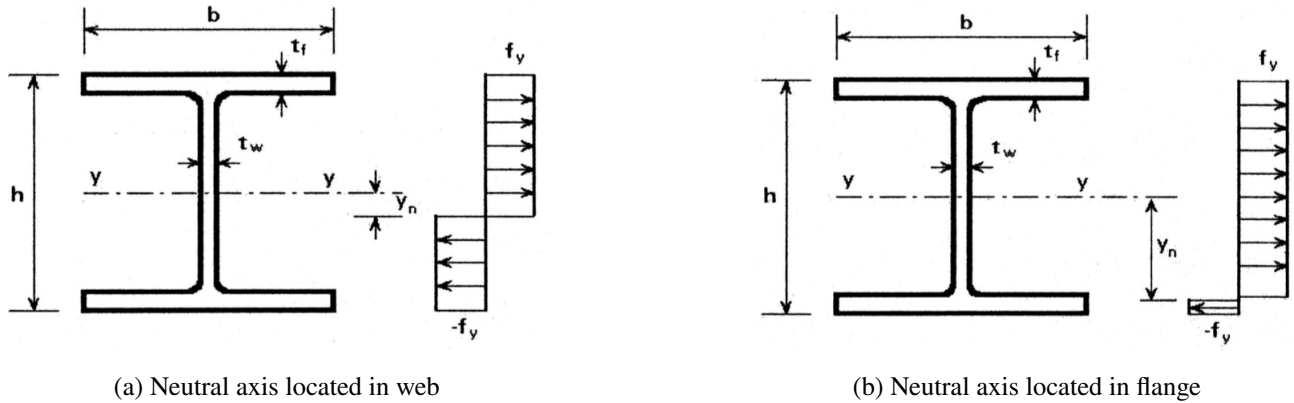


Figure 3.2: Two cases of equilibrium depending on the location of the neutral axis. Figure from Al-Emrani and Åkesson (2013).

In figure 3.2a, the neutral axis is located in the web. The axial load capacity is calculated as in equation 3.28 and the moment capacity according to equation 3.29.

$$N_{N,y,Rd} = \frac{2 \cdot y_n t_w f_y}{\gamma_{M0}} \quad (3.28)$$

$$M_{N,y,Rd} = \frac{(W_{pl,y} - y_n^2 t_w)}{\gamma_{M0}} \quad (3.29)$$

In the other case, figure 3.2b, when the neutral axis is located in one of the flanges, the axial load capacity is determined by equation 3.30 and the moment capacity according to equation 3.31.

$$N_{N,y,Rd} = \frac{\left[A - 2 \left(\frac{h}{2} - y_n \right) b_f \right] f_y}{\gamma_{M0}} \quad (3.30)$$

$$M_{N,y,Rd} = \frac{2b_f \left(\frac{h}{2} - y_n \right) \left[\frac{1}{2} \left(\frac{h}{2} - y_n \right) + y_n \right] f_y}{\gamma_{M0}} \quad (3.31)$$

The next step, is the same as for the method with the reduction formula. Yielding is found by iteration until the ratio between the design moment M_{Ed} and the reduced design moment $M_{N,Rd}$ is equal to 1.

3.2 Beam-columns

In this chapter, Method 1 and 2 and the method using an initial bow imperfection will be described briefly. All three methods treat members subjected to an axial load in combination with a bending moment, i.e. beam-columns. Method 1 and 2 are based on interaction formulae while the method with an initial imperfection follow the same calculation procedure as for columns. Though, with an additional bending moment included.

3.2.1 Method 1 and 2

The methods are based on an extensive research performed by two research teams under the auspices of European Convention for Constructional Steelwork and are used to solve the interaction formulae for beam-columns, Boissonnade, Greiner, Jaspert, and Lindner (2006). Method 1 was developed by a French-Belgian team, Boissonnade, Jaspert, Muzeau, and Villette (2004), and Method 2 was developed by an Austrian-German, Greiner and Lindner (2006). Even though the research resulted in two methods, the authors of EN-1993-1-1 (2005) agreed to keep both because of the differences in philosophy between the methods. The detailed background and solution techniques of the methods can be found in a book written by Boissonnade et al. (2006). Both approaches treat complex behaviour of a single-span structural member including all potential interactions and non-linear effects. The two provide accurate results since the verification for both methods were based on about 15000 FE-analyses.

Both methods are based on a second-order in-plane theory. The structural model is a single-spanned beam-column with doubly symmetrical cross-section. The boundary conditions are defined as in figure 3.3, i.e. with fork-conditions. By that, translations in x , y and z and rotations about the longitudinal axis are prevented. The loads are a fixed axial load in combination with a bending moment induced by either end moments or transverse loads. Intermediate lateral restraints can be included if prevention of torsional movements is desired. In the case of combined axial compression and bending moment, there are convenient derivations for the buckling modes of in and out-of-plane flexural buckling based on linear elastic behaviour. Though, as mentioned in the limitations, out-of-plane flexural buckling was not considered in this thesis.

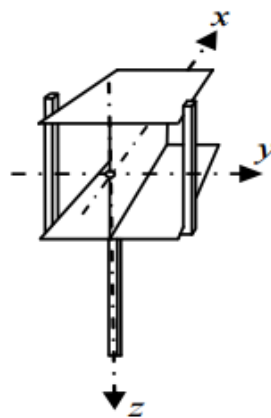


Figure 3.3: Fork boundary condition. Figure from Al-Emrani and Åkesson (2013).

The interaction formulae are based on the case with only an elastic axial compressive load. Hence, equation 3.14 and 3.15 are re-written into:

$$\frac{N_{Ed}}{N_{Rd}} + \frac{1}{1 - \frac{N_{Ed}}{N_{cr}}} \frac{N_{Ed} \cdot e_{0,d}}{M_{Rd}} \leq 1 \quad (3.32)$$

If an additional moment is acting on the member, the previous equation is extended into the following equation where an extra factor corresponding to the ratio between the first and second-order moment is added.

$$\frac{N_{Ed}}{N_{Rd}} + \frac{1}{1 - \frac{N_{Ed}}{N_{cr}}} \cdot \frac{N_{Ed} e_{0,d}}{M_{Rd}} + \frac{M_{Ed,II,max}^{II}}{M_{Rd}} \leq 1 \quad (3.33)$$

Also, by introducing the additional first-order moment, there will be a shift of shape in the deflection and bending moment diagrams due to an arising lever arm to the axial load. This would constitute a difficulty when determining the location of the critical section. Therefore, the solution is to introduce an equivalent moment concept shown in figure 3.4. The concept involves a re-establishment of the current first-order bending system into a sinusoidal first-order bending moment corresponding to the same amplification as the first, Boissonnade et al. (2006). Also in the article, it is stated that an equivalent uniform moment factor C_m is used for taking different moment variations into account and to simplify the process of finding the critical section.

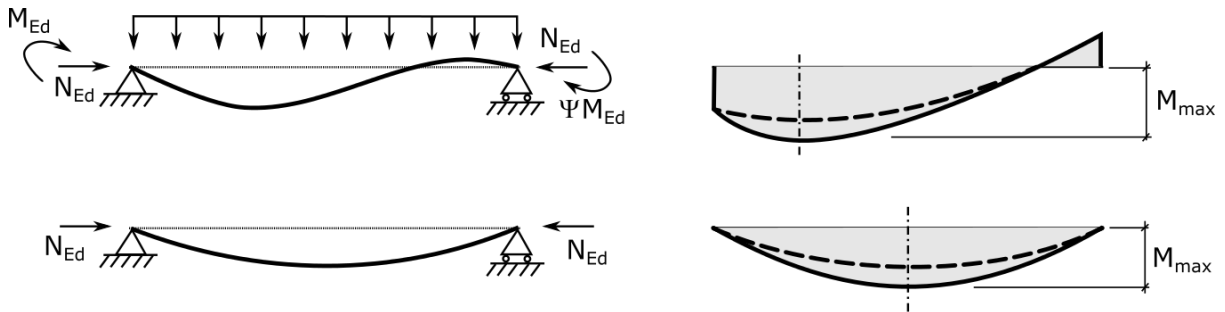


Figure 3.4: The basis of the equivalent moment concept where the actual second order bending moment is replaced by a sinusoidal one. Figure based on Boissonnade, Greiner, Jaspart, and Lindner (2006).

As a result, the second-order moment can be calculated more convenient by using equation 3.34, which includes the equivalent moment factor.

$$M_{Ed,max}^{II} = \frac{C_m M_{Ed,max}}{1 - \frac{N_{Ed}}{N_{cr}}} \quad (3.34)$$

Further, by inserting equation 3.34 into equation 3.33 and rewrite the expression into a so-called μ -format, equations 3.35 and 3.36 are obtained.

$$\frac{N_{Ed}}{\chi N_{Rd}} + \mu \frac{1}{1 - \frac{N_{Ed}}{N_{cr}}} \cdot \frac{C_m M_{Ed}}{M_{Rd}} \leq 1 \quad (3.35)$$

Where the factor μ is equal to:

$$\mu = \frac{1 - \frac{N_{Ed}}{N_{cr}}}{1 - \frac{\chi N_{Ed}}{N_{cr}}} \quad (3.36)$$

This can also be done for elastic-plastic flexural buckling with similar results. For more details concerning that, study the book written by Boissonnade et al. (2006). However, this constitutes the base for the final equations regarding interaction to be solved using both methods. The equations in EN-1993-1-1 (2005) are in accordance with equation 3.37 and 3.38.

$$\frac{\frac{N_{Ed}}{\chi_y N_{Rk}}}{\gamma_{M1}} + k_{yy} \frac{\frac{M_{y,Ed} + \Delta M_{y,Ed}}{\chi_{LT} \frac{M_{y,Rk}}{\gamma_{M1}}}}{\chi_{LT} \frac{M_{y,Rk}}{\gamma_{M1}}} + k_{yz} \frac{\frac{M_{z,Ed} + \Delta M_{z,Ed}}{\chi_{LT} \frac{M_{z,Rk}}{\gamma_{M1}}}}{\chi_{LT} \frac{M_{z,Rk}}{\gamma_{M1}}} \leq 1 \quad (3.37)$$

$$\frac{\frac{N_{Ed}}{\chi_z N_{Rk}}}{\gamma_{M1}} + k_{zy} \frac{\frac{M_{y,Ed} + \Delta M_{y,Ed}}{\chi_{LT} \frac{M_{y,Rk}}{\gamma_{M1}}}}{\chi_{LT} \frac{M_{y,Rk}}{\gamma_{M1}}} + k_{zz} \frac{\frac{M_{z,Ed} + \Delta M_{z,Ed}}{\chi_{LT} \frac{M_{z,Rk}}{\gamma_{M1}}}}{\chi_{LT} \frac{M_{z,Rk}}{\gamma_{M1}}} \leq 1 \quad (3.38)$$

Where:

N_{Ed} , $M_{y,Ed}$ and $M_{z,Ed}$ are design values of the compression force and the maximum moments about the strong and weak axis along the member, respectively

$\Delta M_{y,Ed}$ and $\Delta M_{z,Ed}$ are the moments due to shift of the central axis. Only for members in cross-section class 4.

χ_y and χ_z are the reduction factors due to flexural buckling

χ_{LT} is the reduction factor due to lateral-torsional buckling

k_{yy} , k_{yz} , k_{zy} and k_{zz} are the interaction factors obtained in Method 1 or 2

The equations are based on an elastic second-order theory and are the same for all cross-section classes. Since plastic response must be considered for cross-section class 1 and 2, the interaction factors consist of extra factors in those cases. Since out-of-plane buckling and cross-section class 4 were neglected, all moments due to shift of the central axis and the interaction factors concerning a combination of buckling direction are set to zero. Additionally, the reduction factor due to lateral-torsional buckling was set to one.

Basically, Method 1 and 2 represents different ways to find the interaction factors in equation 3.37 and 3.38. The main difference between the two methods is that Method 1 includes the structural effects by using various coefficients. Those represents all impacts of material and geometrical non-linearities. Also, the interaction between loading components, which may be more advantageous when determining and accounting for the structural effects. For Method 2 on the other hand, there is only one compact factor, which is the outcome of a globalisation of several effects such as cross-section shape, buckling mode and intermediate lateral restraints. The buckling mode is either about the strong or the weak axis. Additionally, the formulae were intended exclusively for beam-columns with fork boundary-conditions, but was later adapted to consider cases with intermediate supports. This approach is more focused on the direct design of standard cases, Boissonnade et al. (2006).

The equivalent uniform moment factor is calculated differently depending on method choice. For the load case with end moments related to each other with the ratio ψ ($-1 \leq \psi \leq 1$), the equivalent uniform moment factor is derived as in equation 3.39 for Method 1 and equation 3.40 for Method 2. In the first equation, the influence of the axial load is included in the last term. The second equation is based on the commonly used Austin-Perry formula.

$$C_m = 0.79 + 0.21\psi + 0.36(\psi - 0.33) \frac{N_{Ed}}{N_{cr}} \quad (3.39)$$

$$C_m = 0.6 + 0.4\psi \geq 0.4 \quad (3.40)$$

A drawback of Eurocode 3 is that it was not stated which method that is most suitable for which case. Luckily, Greiner and Lindner (2006) stated some helpful guidance. The first difference between the methods was regarding the C_m -factors. In Method 1 these factors were based on equivalent sinusoidal moments which relied on the critical flexural buckling load and were derived presuming an elastic buckling theory. The C_m -factors in Method 2 on the other hand were based on equivalent uniform moments following the Austin-formula. Since the factors were not derived on the same basis, their magnitude generally differs. Another difference was concerning the transition from flexural buckling to lateral torsional buckling which is smooth for method 1 due to an approximation of the member's torsional rigidity, but regarded as two separate cases in Method 2. Further, Method 1 covers out-of-plane buckling more closely while Method 2 might be more suitable for in-plane buckling and generates an approximate value for out-of-plane buckling. That is the reason for the individual coefficients in Method 1 while Method 2 only have one integrate based on calibration of the elastic-plastic member capacity. The final difference between the methods that Greiner and Lindner (2006) declared was due to the practical use. Computational effort might be needed when using Method 1 since there are a considerable number of factors while Method 2 is more suitable for hand-calculations.

3.2.2 Method with an initial bow imperfection

According to Lindner et al. (2016) and Al-Emrani and Åkesson (2013), the stability analysis of beam-columns considering only flexural buckling can be done similarly as for columns. Though there is a difference within the design moment since the beam-column is subjected to an external moment as well as axial compression force. The design moment for columns is calculated by:

$$M_{Ed} = N \cdot e_{0,d} \cdot \frac{1}{1 - \frac{N}{N_{cr}}} \quad (3.41)$$

For the beam-columns, the expression is extended into the following equation.

$$M_{Ed} = N \cdot e_{0,d} \cdot \frac{1}{1 - \frac{N}{N_{cr}}} + M_{Ex} \frac{1 + \delta \cdot \frac{N}{N_{cr}}}{1 - \frac{N}{N_{cr}}} \quad (3.42)$$

The approximation was presented by Lindner et al. (2016). The term δ represents a load-case dependent correction factor referred to as the Dischinger factor. For the load cases considered for beam-columns in this thesis, the correction factor corresponds to the values in table 3.4.

Table 3.4: Correction factor δ , based on Lindner, Kuhlmann, and Just (2016)

Load case	Correction factor δ
	0.273
	0.032

4 FE-model

The FE-analyses were carried out in the software Abaqus which is suitable for analysis, visualisation and post processing. The purpose was to obtain viable numerical results as a ground for further use of FE-analysis in combination with initial bow imperfections. The results were verified against Matlab calculations. Both linear and non-linear analyses were performed. The structural member in the models followed Euler's second buckling case, i.e. pinned supports at both ends.

4.1 Abaqus

The software Abaqus is provided by SIMULIA and is based on the open-source scripting language Python. At the time of this thesis, version 6.14 (released 2014) was used. A solution sequence in Abaqus consists of three parts; pre-processing/modelling, evaluation and simulation and finally post-processing/visualisation. Abaqus is built on modules (i.e. part module, property module, mesh module and visualisation module etc.) following a logical order of the modelling process. Simultaneously as the model is built manually, Abaqus generates an input file (*.INP) where modifications easily can be performed by Python scripting if desired. After the pre-processing, the analysis is performed and the output database is generated. Lastly, the visualisation module allows the designer to read the output database and see the results. Deeper knowledge of the software has been received by reading the user manual SIMULIA (2014). The manual was essential for the contents of this chapter.

4.2 Modelling procedure

The model database in Abaqus was a standard/explicit. Since Abaqus is unitless, the designer must be consistent to get the correct magnitude of the results. The models were chosen to follow SI units in terms of N, mm and MPa. The steel used for analytic evaluation was exclusively standard steel grades presuming a nominal thickness less than 40 mm. Characteristic values were used to specify material properties. To access isotropic linear-elastic material properties, Young's modulus was set to 210 MPa and Poisson's ratio to 0.3. As can be read in appendix C of EN-1993-1-5 (2006), there were several ways to take plasticity into account in the model:

1. Elastic-plastic without strain hardening (elastic-perfectly plastic)
2. Elastic-plastic with a nominal plateau slope
3. Elastic-plastic with linear strain hardening
4. True stress-strain curve modified from the test results as follows:
 - a) true stress-strain curve
 - b) stress-strain curve from tests

These relations between stress and strain regarding the material behaviour models are seen in figure 4.1.

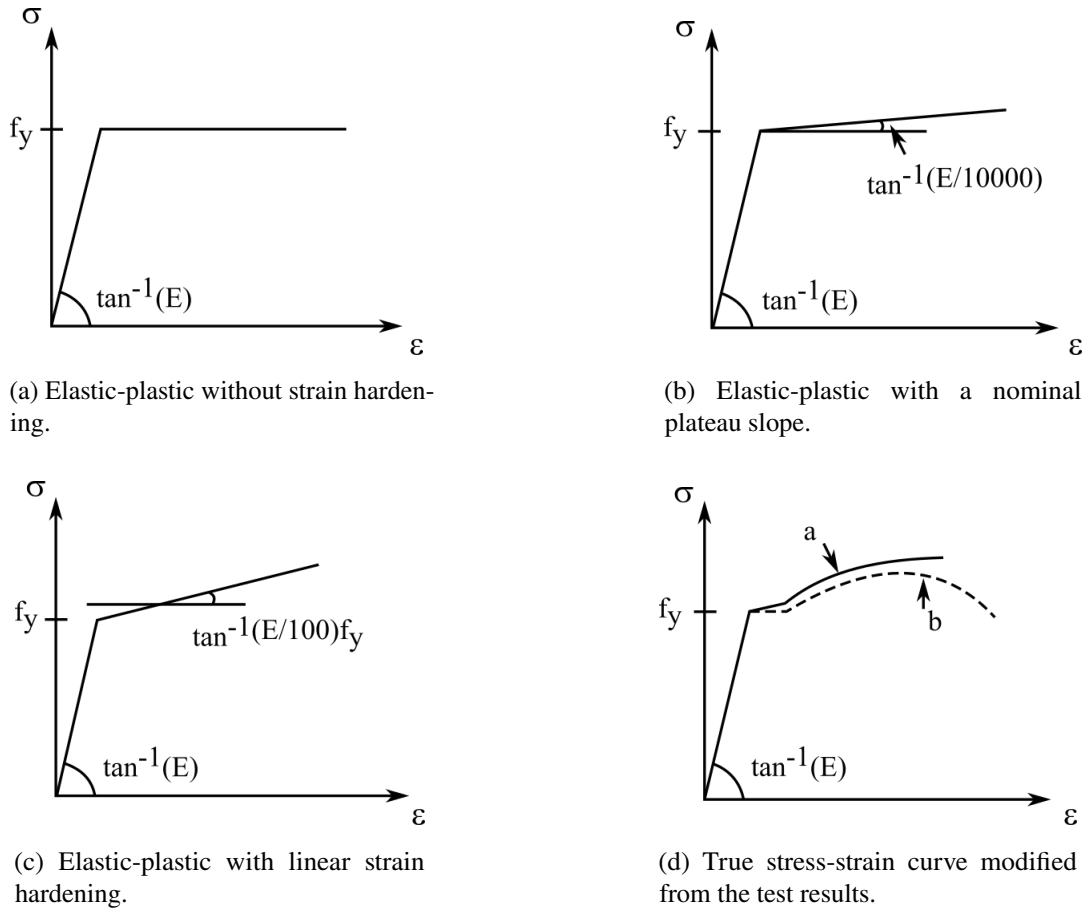


Figure 4.1: Modelling of elastic-plastic material behaviour. Figure based on EN-1993-1-5 (2006).

In the FE-models regarded in this thesis, the case in figure 4.1a was chosen due to simplicity and flexibility. The meaning of perfect plasticity is that the yield stress does not change with plastic strain ($\epsilon_{pl} - \epsilon_{el}$), unlike for an elastic-plastic material behaviour. This stress-strain relation was chosen since steel grades *S235*, *S275*, *S355* and *S420* have different slopes for the strain hardening. To specify such behaviour in Abaqus, the inputs were yield stress and plastic strain. The first parameter was set to 355 MPa and the latter zero. Depending on chosen element type, there are primary element characteristics that made it suitable for different kinds of modelling.

Beam elements were chosen for the analyses in this thesis, which are convenient for geometrically non-linear analyses where large displacements and rotations may take place. Beam elements is a simplification of a structure since the beam theory approximate 3D continuum elements with a 1D theory, as seen in figure 4.2. Hence, the model was based on a 2D planar, deformable wire with user specified length. By that, the geometrical simplicity together with the fewer degrees of freedom forms two advantages for beam elements.

Further benefits were faster computational time along with user flexibility since only the length of the member had to be changed and not the cross-section as would have been the case for example solid elements.

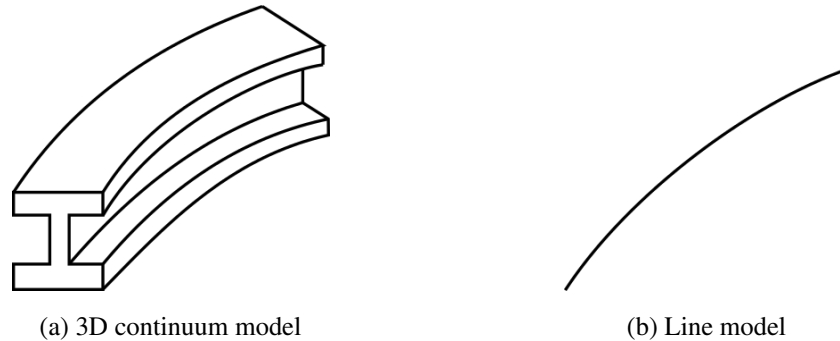


Figure 4.2: Approximation from a 3D continuum element (a) to a 1D theory line model (b) for beam elements.

The structural member was, as mentioned, assumed to be pinned-pinned. For implementation in Abaqus, the boundary conditions were set so that no horizontal or vertical translations took place at one end and no vertical translations at the other end could occur. When modelling the beam-column, also an additional line restraint along the member was applied. The loads were applied in two cases where the first represents column behaviour and the other beam-column behaviour, see figure 4.3. In the first case, a concentrated compressive axial force (N) was applied at the end where no translations in only vertical direction was allowed. In the second case, also an external bending moment (M) was added at both supports. The self-weight of the member was neglected.

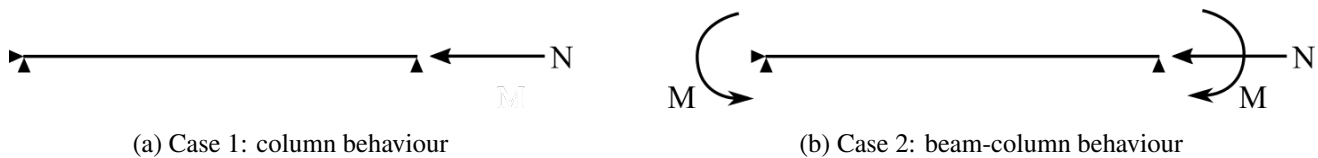


Figure 4.3: Model of support and load conditions in Abaqus.

The most accurate way of analysing members in Abaqus and later compare them with analytic calculations would presumably be to model the exact same cross-sections and corresponding lengths. The cross-sections used in the analytic calculations were standardised with rolled parts between web and flanges. When beam elements are used, there are two ways of assigning a cross-section to the line model,

1. cross-sectional properties as an I or box-section
2. cross-sectional properties as a generalised section

The accuracy of the results differed depending on chosen modelling procedure of the cross-section assignment. For I or box sections the cross-section dimensions (flange thickness, web thickness, height etc.) are manually inserted as in figure 4.4. The axes followed the general coordinate system of a cross-section, i.e. with axis 1 corresponding to the Cartesian y-axis and 2 to the Cartesian z-axis. The

inputs for the generalised section are the cross-section properties; area, moment of inertia for bending about the 1-axis, moment of inertia for cross bending, moment of inertia for bending about the 2-axis, torsional constant, sectorial moment and warping constant.

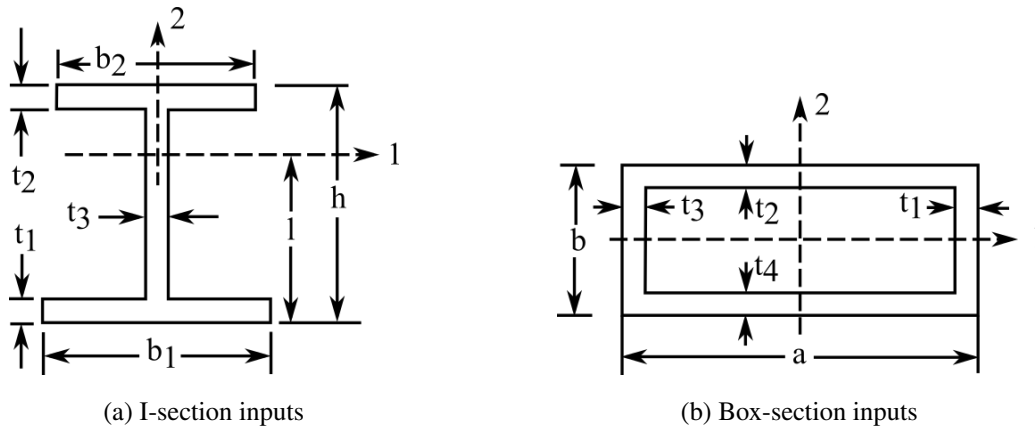


Figure 4.4: Axis and cross-section definition of an I section (a) and a box section (b) in Abaqus.

Unfortunately, there are drawbacks for both alternatives. The drawback regarding an I or box section is that the rolled part of the cross-section is neglected. By that, the area of those parts multiplied with the lever arm to the neutral axis of the section will form a bending moment that would be lost in the results. Despite that, this modelling procedure was chosen because the drawbacks for the generalised way had an unfortunate disadvantage: Abaqus do not support non-linear material behaviour of generalised sections. After the I or box profile was generated, it was assigned into a section with beam elements and material properties included. Beam elements generates that each node consists of three degrees of freedom; two for translations and one for rotation. The section integration was set to take place during analysis. Further, the section was assigned to the wire and an instance of dependent type was created. Because of that, the mesh was created on the part instead of the instance. Since the model itself did not require a lot of computational effort, the element size was set to approximately 50 mm. A drawback was short members obtained less number of elements than the long ones. A quick study concerning adequate element size resulted in that no convergence study was needed for the selected mesh size. Also, there were problems due to curvature if the mesh density was specified using a specific number of nodes along the member. For beam elements with linear geometrical order in the standard element library, there are two options regarding element type:

1. Shear-flexible (B21); a 2-node linear beam in a plane (Timoshenko beams).
2. Cubic formulation (B23); a 2-node cubic beam in a plane (Euler-Bernoulli beams).

The naming convention in Abaqus gives the beam names as B21 and B23 where B stands for beam element, 2 stands for beam in plane and the last number represents linear (1) or cubic (3) geometric order. Timoshenko beam elements (B21) is taking transverse shear deformations into account and may be used for both slender and stocky beams. The Timoshenko beam theory gives convenient results for beams with uniform material and with a slenderness ratio up to 1/8 (between the width of the cross-section and the length of the member). This element type makes it possible for the beam to be subjected to large

axial strains. Euler-Bernoulli beam elements (B23) is suitable for modelling of slender beams where plane sections are assumed to remain plane and normal to the beam axis. Transverse shear deformation is neglected using this element type. The Euler-Bernoulli beam theory gives convenient results for beams with uniform material and a slenderness ratio up to 1/15. The cubic interpolation functions within this element type makes it suitable for situations with distributed load conditions along the beam. Because of the cubic formulation, this element type is appropriate for small-strain, large-rotation analysis but not for torsional stability problems. The comparison of these element types is found in section 5.2.1, where it can be read that Timoshenko beam elements (B23) was chosen for the analyses.

4.2.1 Considered columns

In the FE-analyses, the examined cross-sections were standard hot-rolled HEB 220, IPE 140 and VKR 90x50 t = 4 profiles with their rolled parts between web and flanges neglected. Each cross-section was assigned to a model with length depending on the relative slenderness (equation 2.13). Values for $\bar{\lambda}$ corresponding to 0.4 (stocky member), 1.0 (intermediate member) and 1.8 (slender member) were chosen. For exact lengths, see tables in appendix A.

4.3 FE-analyses

The procedure of the FE-analyses of this thesis was divided into three types of analyses depending on requested output data: a static analysis, a buckling analysis and a second order buckling analysis. The differences between them are specified in the step manager in which the designer can request which analysis Abaqus will perform and what data outputs should be generated. Within each of the three models there are two stages; the initial and the analysis specific. The support and load conditions are applied in the latter. The first analysis type is a *Static, General*, which was used for the static stress analysis since it is suitable for stable problems which may include both linear and non-linear elastic material behaviour. The second type is called *Linear perturbation, Buckle* and was used for the buckling analysis. This analysis includes a linear perturbation procedure and may also be referred to as an eigenvalue buckling analysis used to estimate the critical buckling load (bifurcation load). Finally, for the second order buckling analysis (or post-buckling analysis), an analysis type called *Static, Riks* was used. This analysis type is suitable to obtain the limit load for structures that experience unstable collapse. It is possible to include geometrical and material non-linear collapse.

4.3.1 Static stress analysis

To verify the cross-section capacity the stress components, invariants (S), deformations (U) in transverse direction, reaction forces (RF) and moments from a step procedure called *Static, General* was compared to hand-calculations. As can be read in the manual of Abaqus, a static stress analysis involves the specification of load cases and appropriate boundary conditions. The maximum number of increments was chosen to the fixed value of 100 with increment size 1. The equation solver method was direct with full Newton as solution technique. Linear elastic material behaviour was valid since Nlgeom (geometrical non-linearity) was not included. The analysis provided verification of the cross-section by comparing the results of the axial stress (S11), which was constant along the member, by simple hand-calculations where the stress is equal to the axial load (N) divided by the cross-sectional area (A).

4.3.2 Linear buckling analysis

In the linear buckling analysis, the linear buckling load capacity was estimated in a step procedure type called *Linear perturbation-Buckle*. By using this method, a small deformation is assumed before the collapse. Since only the first buckling mode was of interest, the subspace iteration eigenvalue extraction method was used which is more suitable for a few number of eigenmodes than e.g. Lanczos. The shape of the buckling mode was saved into a (*.fil) file which was generated by adding two lines into the keywords of Abaqus. This file was later used in the non-linear buckling analysis so the eigenvalue buckling analysis could provide complete information about the collapse of the structure. These lines were:

```
*NODE FILE, GLOBAL=YES, LAST MODE=1  
U
```

The background of the eigenvalue buckling problem is that loads, for which the stiffness matrix become singular, are searched for to obtain non-trivial solutions. If desired, a thorough derivation of the eigenvalue buckling problem is found in SIMULIA (2014). Though the problem can be more easily explained by saying that the algorithm solves a linearized eigenvalue problem as in Al-Emrani (2014):

$$(K - \lambda K_G) \phi = 0 \quad (4.1)$$

The structure is pre-loaded with a reference load called P_{ref} . The critical buckling load P_{cr} (in this thesis referred to as N_{cr}) is obtained as a reference (perturbation) multiplier load as in equation 4.2 where λ represents the eigenvalues. In this thesis, only the first eigenvalue was by interest since it gave the greatest magnitude (half sine shape).

$$P_{cr} = \lambda P_{ref} \quad (4.2)$$

The eigenvalue λ obtained from Abaqus was compared to the reduction factor χ in equation 3.13 for comparison of the FE-results and hand-calculations.

4.3.3 Second order buckling analysis

The solution method for the work of this thesis was based on a static stress analysis method. Though, since buckling or collapse should be included, a special approach called *the modified Riks method* was used. This method has an algorithm that computes the non-linear buckling load capacity for a more realistic structural behaviour, i.e. with geometrical imperfections, residual stresses and non-linear material behaviour. When such geometrically non-linear analysis is performed, "a quasi-static solution can be obtained only if the magnitude of the load does not follow a prescribed history; it must be part of the solution", as can be read in the Abaqus documentation. The modified Riks method is valid when the loading has the possibility to be scaled with one parameter, and be treated as proportional in this case it is called the load proportionality factor (LPF). To introduce geometrical imperfections, an initial bow imperfection was added to the first buckling mode obtained from the linear buckling analysis in accordance with Table 5.1 of EN-1993-1-1 (2005). A solution would be obtained regardless of a stable or unstable response. In the algorithm, the load multiplier λ was considered unknown at

every iteration. In the non-linear buckling analysis, the load was applied in 100 increments with fixed arc length increments of 0.05 and the function *Nlgeom* activated to control the inclusion of non-linear effects of large displacements and affect subsequent steps. The mentioned geometrical imperfection was included by editing the keywords of the non-linear model by adding these lines into the keywords:

```
*IMPERFECTION, FILE=*.fil, STEP=1
1, (e0/L)
```

The name of the (*.fil) file was inserted in the first row and the value for the initial bow imperfection into the second. The load magnitude was used as a supplementary unknown variable which solves simultaneously for loads and displacements. Because of that, Abaqus used arc lengths along the static equilibrium path in load-displacement space to measure the development of the solution. This would occur irrespective of a stable or unstable solution. The total load P_{total} at each increment was calculated as:

$$P_{\text{total}} = P_0 + \lambda (P_{\text{ref}} - P_0) \quad (4.3)$$

where λ is the LPF and P_0 is represented by the dead load of the structure. Since the dead load was neglected, the expression yields:

$$P_{\text{total}} = \lambda P_{\text{ref}} \quad (4.4)$$

To solve the non-linear equilibrium equation, Newton's method was chosen as solution method. To find the point of yielding, the reaction force along the member (RF) at the pinned support (with no translations in x and y-direction) was plotted against the displacement (U) in the middle of the member where the magnitude was the greatest. To find the bending moment at the ends or in the midpoint of the member, the probe value for the nodal moment (NFORC) in the same step as yielding was selected.

5 Results and discussion

This chapter provides the reader with the results obtained from the conducted research. The results are presented together with associated reflections and conclusions to easier follow the reasoning. The chapter is divided into the two main parts, columns, and beam-columns. Each part regards both analytical and numerical results. The analytical results are obtained from Matlab (hand-calculations) and the numerical results are collected from Abaqus (FE-analysis). The results are presented separately for strong ($y - y$) and weak ($z - z$) buckling direction throughout the whole chapter.

5.1 Analytical results for columns

This first section of this chapter only treats the first part of this study, i.e. pinned-pinned columns subjected to axial compression. The varying parameters were cross-section type and size, buckling direction and steel strength class. Initially, the Matlab programme was verified and after that, the reduction formula method was compared to the exact method. The following step was to obtain the general results and lastly, the initial bow imperfection was optimised.

5.1.1 Verification of Matlab programme

To make sure that all iterations in Matlab were correct, the programme was verified against hand-calculations for a number of columns. This verification was computed for both strong and weak buckling direction and relative slenderness ratios $\bar{\lambda}$ equal to 0.4, 1.0 and 1.8. The accuracy was consistent with values from 99.5 to 100.0% which was considered ideal. The complete results for the verification are found in appendix C. The verification was based on the buckling reduction factor χ calculated using the initial bow imperfection method with the reduction formulas presented in chapter 3.1.2.

The Matlab programme and hand-calculations were also verified against the results presented in the article written by Lindner et al. (2016), which was declared briefly in chapter 2.5.1 of this thesis. They presented their results with a non-dimensional value j on the y-axis instead of the buckling reduction factor χ . Because of that, the results obtained in this study also had to be presented with the non-dimensional value j for an accurate comparison. Figure 5.1 shows the results regarding IPE columns with steel strength class $S235$ associated with buckling curve a . The results considers the plastic analysis for bending about the strong axis and are presented with non-dimensional value j vs. relative slenderness ratio $\bar{\lambda}$. The analysis was based on the assumption that the cross-section should first reach full capacity according to buckling curve analysis and after that, the initial bow imperfection needed to reach full capacity was calculated. The black line represents all results for the IPE columns obtained in Matlab. The blue line shows where the initial bow imperfection according to EN-1993-1-1 (2005) was located and the green line marks the lowest value presented in Lindner et al. (2016).

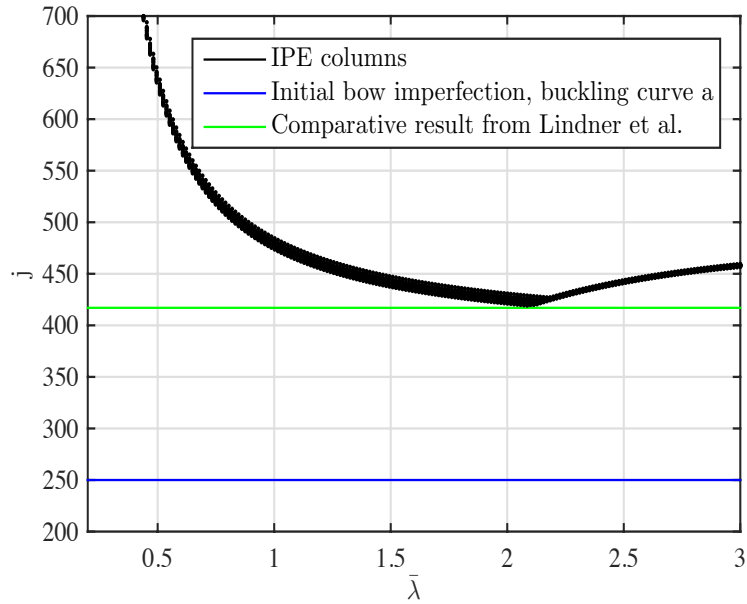


Figure 5.1: Verification of results from Matlab calculations with the results presented by Lindner, Kuhlmann, and Just (2016). Results visualised as non-dimensional value j vs. relative slenderness ratio, $\bar{\lambda}$.

A conclusion was that the Matlab programme corresponded well with the results presented in Lindner et al. (2016) and that the minimum values were equal, i.e. the lowest point of the black line is located on the green line. Hence, the Matlab programme was considered correct and approved for usage in the following analysis. A similar verification, but for HEA members can be found in appendix C.

5.1.2 Exact vs. simplified cross-section classification

As explained in section 2.4, a cross-section can be classified either by considering parts subjected to compression, bending or by a combination of both. Although an axially compressed column may be considered as only compressed, a second-order moment arising from the initial bow imperfection justifies the fact that the column is always subjected to a combination of compression and bending. The simple way of classifying the cross-section was to neglect the influence of bending. Therefore, a comparison between the exact and simplified cross-section classification was performed to evaluate the margin of error. In figure 5.2, the results for a HEA 650 cross-section using exact cross-section classification is presented. If the simplified cross-section classification would have been used, this column would have been in cross-section class 4. The black line represents buckling curve a while the blue line represents the plastic analysis and the red line the elastic analysis.

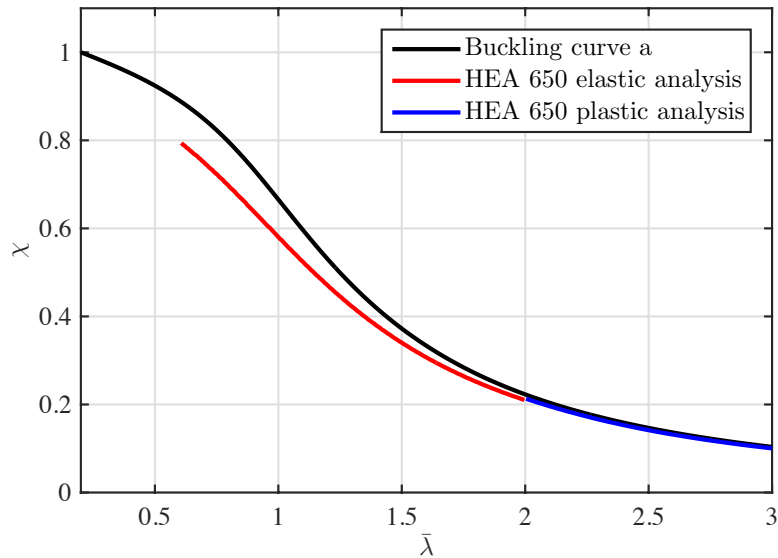


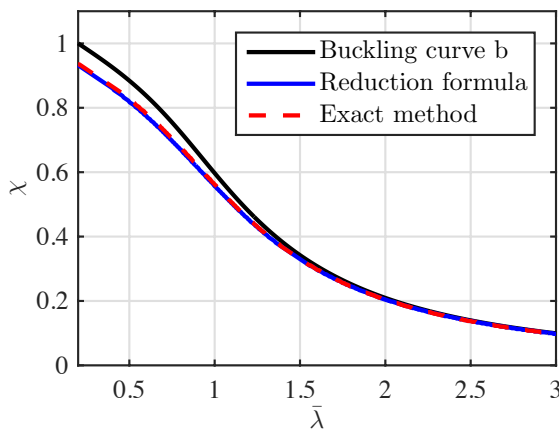
Figure 5.2: Results for a HEA 650 column using the exact cross-section classification. Strong buckling direction.

The figure shows that for columns with a relative slenderness less than approximately 0.6, the column was still in cross-section class 4. Thus, the Matlab programme stopped and no curve was created. When the relative slenderness increased, also the second-order moment increased and suddenly, the column was in cross-section class 3 (red line). When the relative slenderness was high enough (in this case over 2.0) the column was in class 1 or 2 (blue line). Even though the column changed cross-section class, both the plastic and elastic curves reached the same maximum capacities as they would have done by using a simple cross-section classification. The only difference was which relative slenderness that was covered with the current analysis. Thus, it was not as important in which cross-section class the members belonged. The decision was whether plastic or elastic analysis should be compiled. For example, in a plastic analysis all members corresponding to buckling curve *a* ended up on approximately the same capacity for the same relative slenderness ratio regardless if the member belonged to cross-section class 1, 2 or 3.

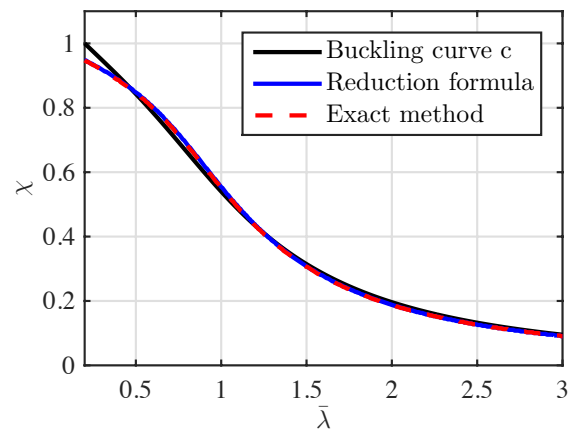
The same was true for the elastic analysis. Therefore, to avoid that the analysis type shifted between elastic and plastic for a specific cross-section, it was decided to use the simplified cross-section classification. This did not affect the study more than that the number of considered members was slightly reduced. It is however important to make sure that the member is in cross-section class 1 or 2 to use the plastic analysis, otherwise the assumption of full plastic capacity is inaccurate and might cause failure of the member. All columns in cross-section class 1, 2 and 3 were investigated with an elastic analysis in Matlab to increase the number of analysed members compared to if only members belonging to cross-section class 3 would have been analysed. It turned out that it was possible to perform the elastic analysis for all columns without reaching the maximum capacity. This was because the elastic analysis did not consider the plastic capacity and therefore always resulted in a lower capacity than for the plastic analysis.

5.1.3 The exact method vs. the reduction formula method

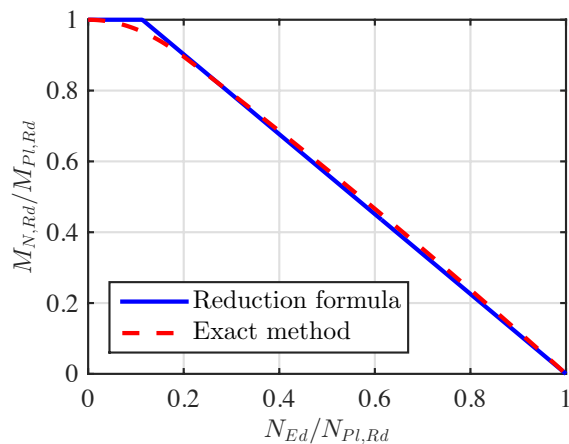
As explained in section 3.1.2, the moment resistance of a cross-section could either be calculated by using the exact method with equilibrium conditions of the cross-section or by using the approximated reduction formulas presented in EN-1993-1-1 (2005). In this section, the comparison between these two calculation methods is presented. The results for a HEB 220 cross-section calculated with a plastic analysis in strong buckling direction and with steel strength class S355 is presented in figure 5.3a where the buckling reduction factor χ plotted against the relative slenderness $\bar{\lambda}$. In figure 5.3b, the same analysis but for weak buckling direction is shown. The black line represents buckling curve *b*, which in this case corresponds to the requested result. The blue line represents the results for the reduction formula method and the red line represents the results for the exact method.



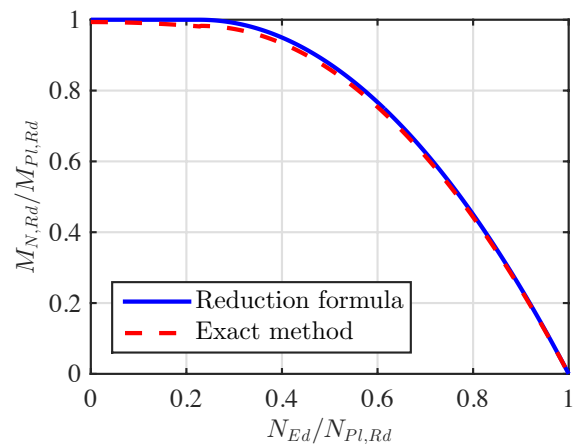
(a) The reduction formula method and the exact method vs. buckling curve *b*. Strong buckling direction.



(b) The reduction formula method and the exact method vs. buckling curve *c*. Weak buckling direction.



(c) The reduction formula method vs. the exact method. Strong buckling direction.



(d) The reduction formula method vs. the exact method. Weak buckling direction.

Figure 5.3: Comparison of reduction formula and exact method regarding the plastic analysis for a HEB 220 column with steel strength class S355.

Although the curves for both methods were located at a small distance from the buckling curve, they corresponded quite well. It was therefore assumed that the reduction formula was a valid approximation of the cross-section equilibrium. In figure 5.3c and 5.3d, the same results are presented independent of the buckling factor and relative slenderness. The ratio between the axial load and the axial plastic compressive capacity was plotted against the ratio between the reduced moment capacity and the full plastic moment capacity. Also, this figure indicates that the two methods corresponded well. Regarding the weak buckling direction, the behaviour was similar and the reduction formula method corresponded well to the exact method.

The equations presented for the exact formula in chapter 3.1.2 was based on simplified cross-sections i.e., cross-sections without rolled corners. Though, the considered cross-sections were standard cross-sections with rolled parts included, as stated in chapter 1.4. Therefore, the curve representing the exact formula is deviating slightly. A short comparison between cross-sections with and without rolled corners for the exact method was conducted for a few cross-sections and the results showed small deviations for cases with high moment only i.e. cases where the design moment was close to the moment resistance. The conclusion of the comparison between the reduction formula and the exact method was that the reduction formula should be used in the following analysis for columns, and that the deviations between cross-sections with or without rolled corners could be neglected in those cases where the exact method was used.

5.1.4 Results before the optimisation

In figure 5.4a, the results for all considered cross-sections (HEA, HEB, HEM, IPE, VKR and VKK) with steel strength class was *S355* in strong buckling direction are presented. The black line represents buckling curve *a*, the blue line is the result from the plastic analysis and the red line is from the elastic analysis.

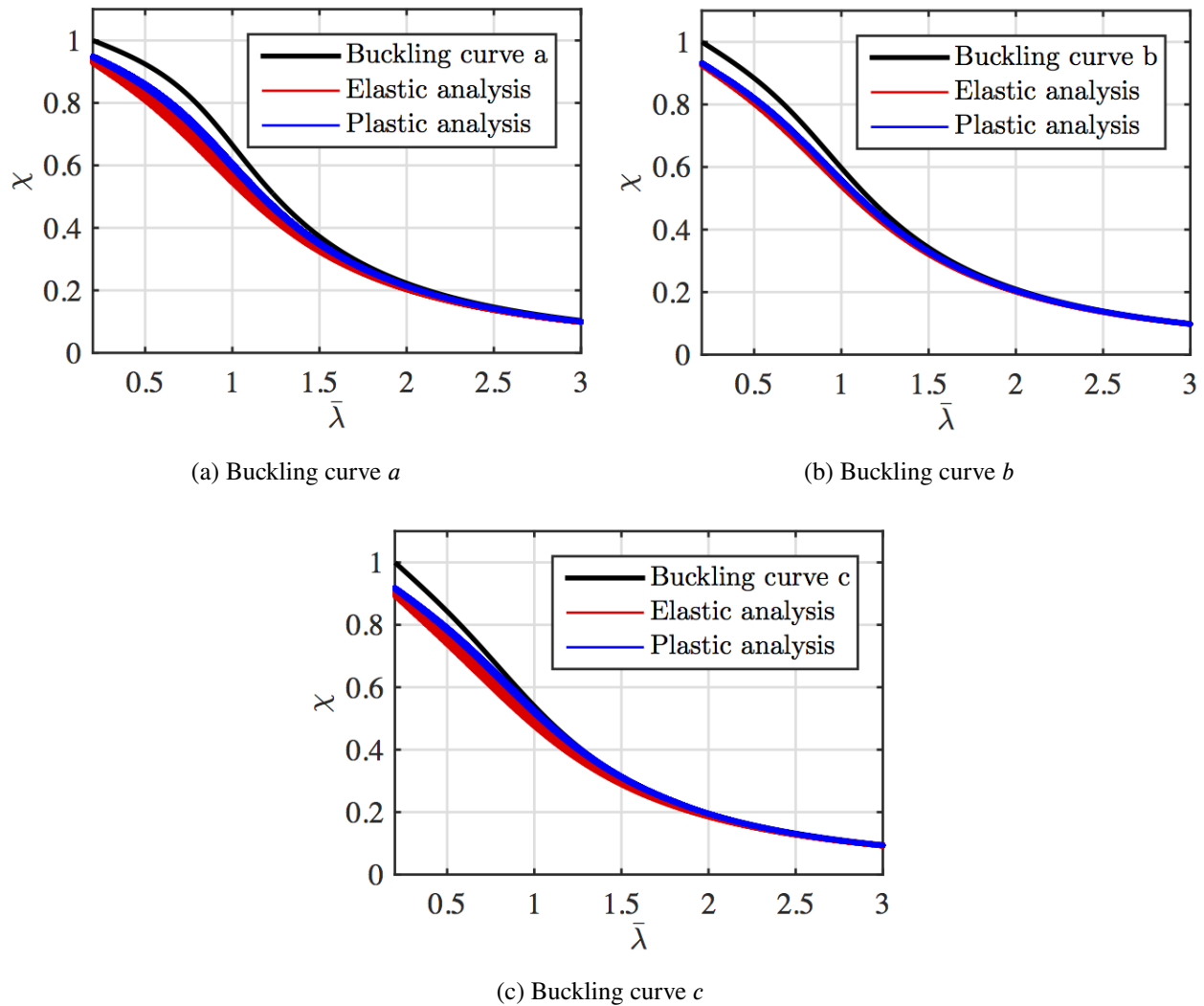


Figure 5.4: How the method with an initial bow imperfection is related to the corresponding buckling curve based on all considered cross-section types. The elastic and plastic results are visualised with the relation between the buckling reduction factor and the relative slenderness. Steel strength class S355 and strong buckling direction.

It was seen that both plastic and elastic analysis gave lower values than the buckling curve itself. Hence, the method with an initial bow imperfection resulted in a lower maximum capacity compared to the buckling curve. It was also noticed that the elastic and plastic behaviour were similar. However, it was reasonable that the plastic analysis gave higher results than the elastic because of the possibility to reach higher capacity. Regarding the elastic analysis, the lack of plastic material behaviour was compensated by using a lower value of initial bow imperfection, see table 3.3 in chapter 3.1.2. Also for buckling curve *b* and *c* the behaviour was similar. The conclusion was that for all cross-section types with steel strength class S355 in strong buckling direction, the method with initial bow imperfection resulted in lower maximum capacities for a theoretical column than for a real column. The corresponding analysis was conducted for the weak buckling direction and the results are found in figure 5.5.

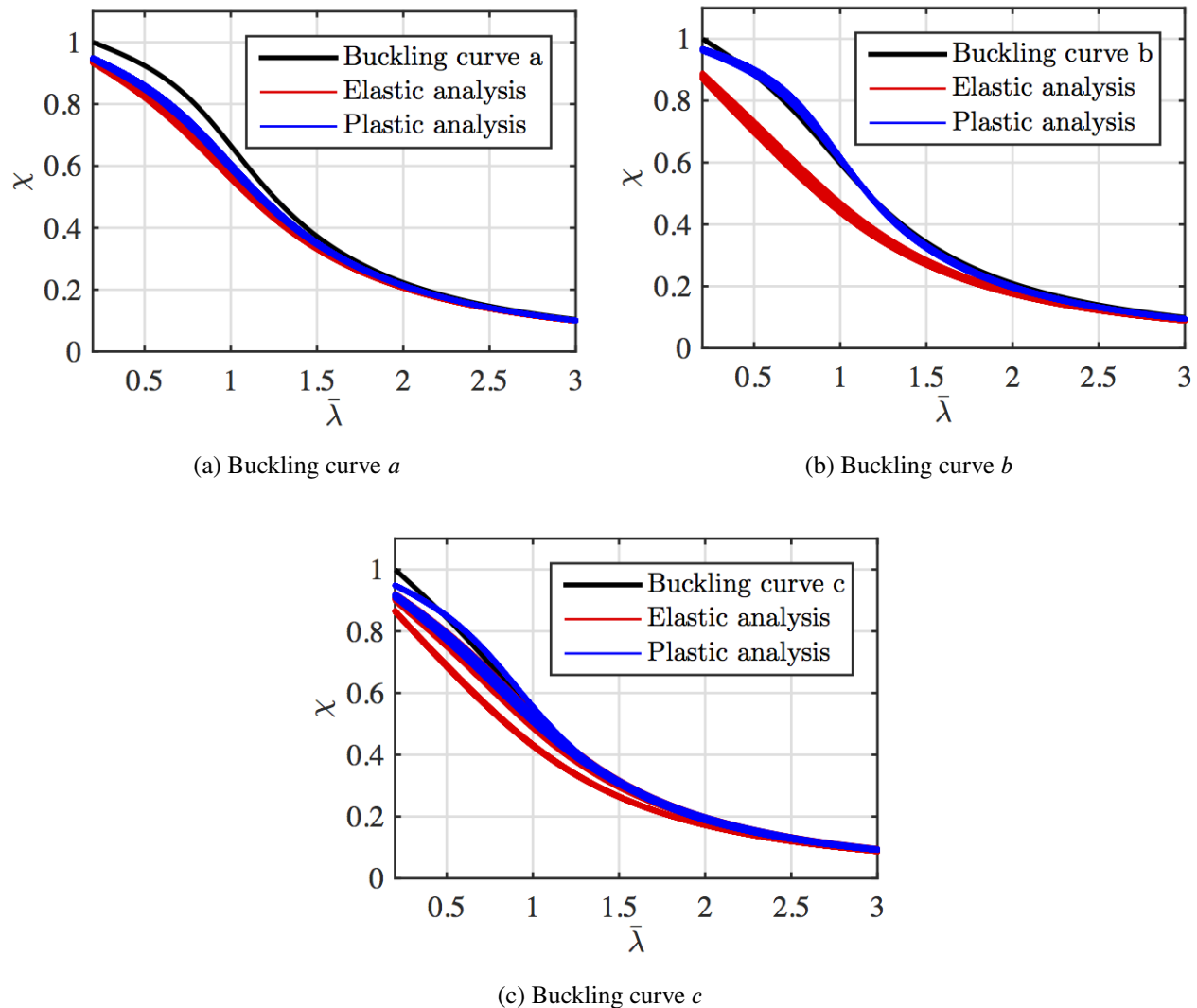


Figure 5.5: How the method with an initial bow imperfection is related to the corresponding buckling curve based on all considered cross-section types. The elastic and plastic results are visualised with the relation between the buckling reduction factor and the relative slenderness. Steel strength class S355 and weak buckling direction.

It was seen that the result for buckling curve *a* in the weak buckling direction was similar to the result for the strong buckling direction. The reason was that for the weak buckling direction, only VKR cross-sections were found in cross-section class *a* and those members have similar geometry about both axes. For the results corresponding to buckling curve *b* and *c*, a distinct difference in the behaviour was noticed. The reason was that H and I cross-sections have outstanding flanges and therefore different cross-section properties depending on which direction buckling occurs. Regarding the plastic analysis, the results were close to the buckling curve. Though, slightly on the unsafe side for a relative slenderness between 0.4 and 1.0. The elastic analysis showed results on the safe side, even more favourable than for the strong buckling direction. For buckling curve *c*, there were more variation for both elastic and plastic analysis. This was because both KKR and H cross-sections corresponded to that curve. The result for buckling curve *c* is clarified in figure 5.6 where the black line represents the buckling curve while the

blue and red line represents plastic and elastic analysis for KKR columns and the green and magenta lines represents the plastic and elastic analysis of H columns. It was obvious that the H columns behaved in the same manner as in the analysis corresponding to buckling curve *b* and the KKR columns behaved the same way as the VKR columns in figure 5.5a.

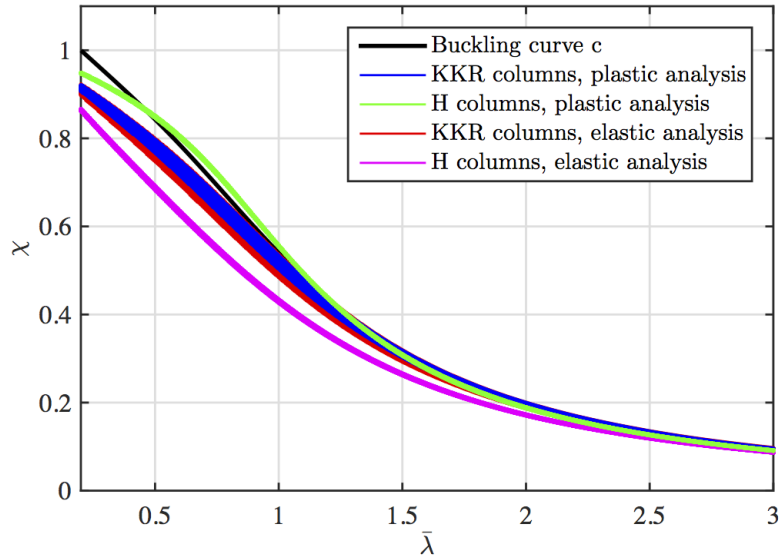
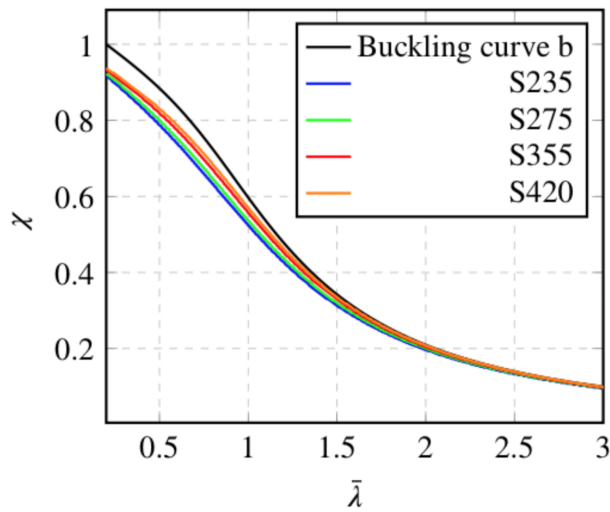


Figure 5.6: Closer analysis of the results from first analysis regarding buckling curve *c* and bending about weak axis. The results are visualised as the buckling reduction factor vs. the relative slenderness ratio.

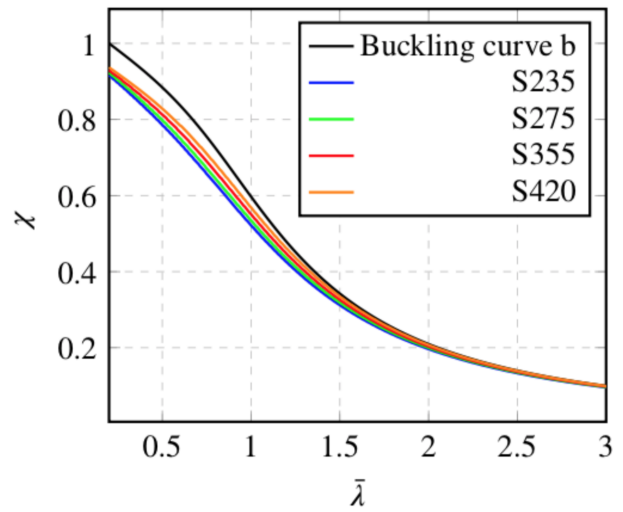
Comparison of different steel strength classes

Until this point of the study, the preformed analysis only covered one steel strength class at a time. However, one of the goals was to reach general results compatible to all steel strength classes between *S235* and *S420*. Therefore a comparison of steel strength classes was performed for all considered columns although only the results regarding an example column with HEB 220 cross-section is presented in figure 5.7. The results for each steel strength class were compared to the corresponding buckling curve. The black line forms the buckling curve while the blue, green, red and orange lines represents steel strength classes *S235* to *S420*, respectively.

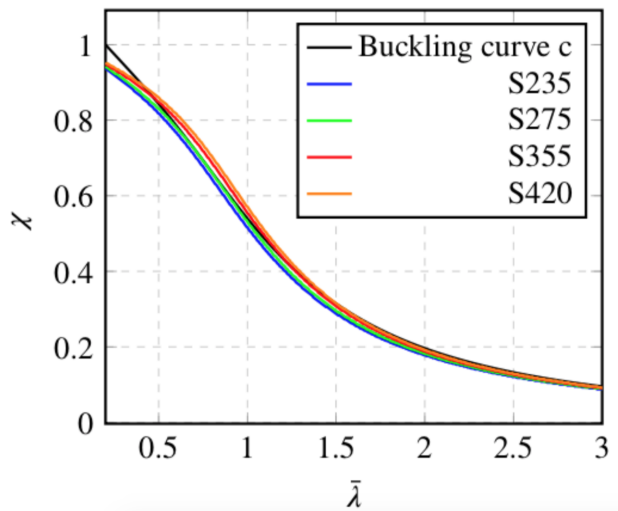
The analysis showed similar results, regardless plastic or elastic analysis or bending about strong or weak axis, the calculated capacity clearly differed between steel strength classes. The highest steel strength class reached the highest capacity. This result agreed with analysis for multiple cross-section types. Thus, while the buckling curve calculations were independent of the steel strength class while the method with initial bow imperfections was not.



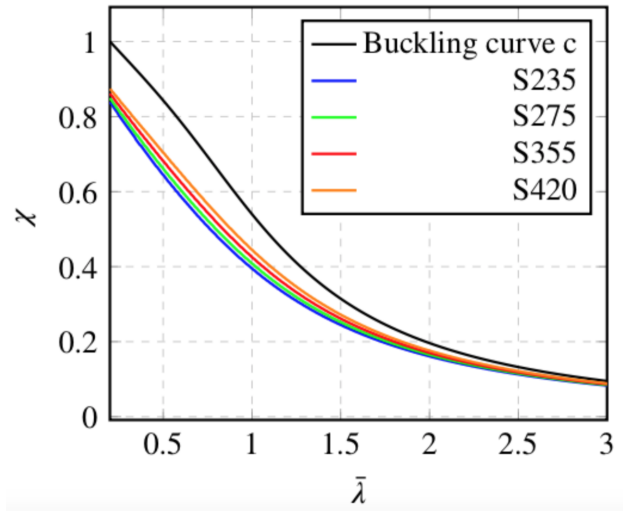
(a) Plastic analysis, strong buckling direction



(b) Elastic analysis, strong buckling direction



(c) Plastic analysis, weak buckling direction



(d) Elastic analysis, weak buckling direction

Figure 5.7: Comparison of steel strength classes S235 – S420 for a HEB 220 cross-section with the relation between the buckling reduction factor and the relative slenderness.

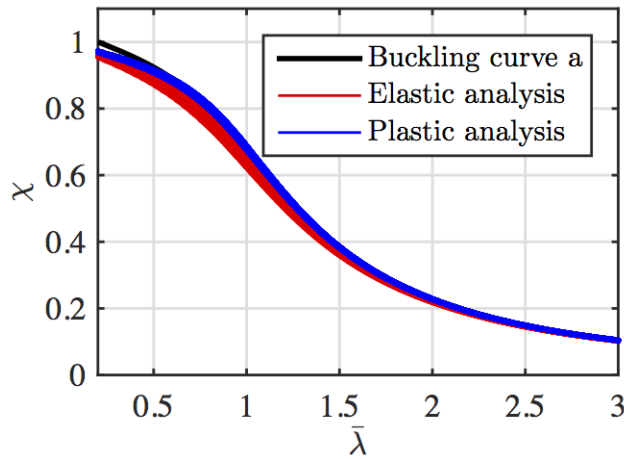
5.1.5 Optimisation of initial bow imperfection

The general result for columns was that the analysis conducted with the method using the initial bow imperfection resulted in column capacities mostly on the safe side. This indicated that if this method were to be used in design, there would be a loss in capacity compared with the buckling curve method. A consequence could be economical losses and unnecessary material usage due to the greater cross-section needed to achieve the adequate capacity. Therefore, the possibility to optimise the initial bow imperfection and by that reach a better correlation between this method and the buckling curve analysis is examined in this section. A way to improve the results was to decrease the value of the initial bow imperfection which lead to a smaller second-order moment. Hence, the columns could reach higher capacities. Instead of using the values for the initial bow imperfections presented in table 3.3, the values in table 5.1 were used.

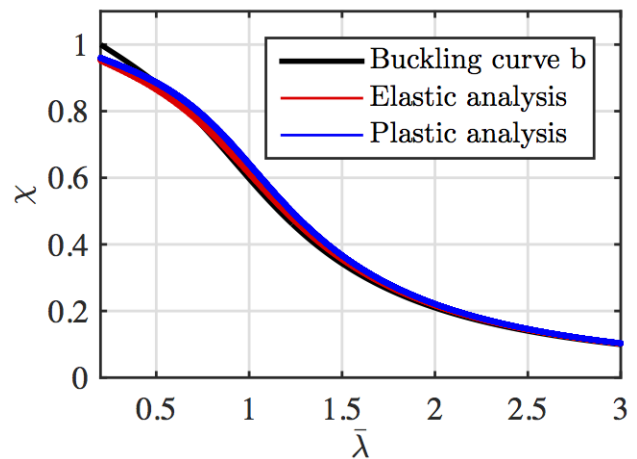
Table 5.1: New, optimised design values of the initial local bow imperfection.

Buckling curve	Elastic analysis $e_{0,d}/L$	Plastic analysis $e_{0,d}/L$
<i>a</i>	1/500	1/450
<i>b</i>	1/400	1/350
<i>c</i>	1/300	1/250

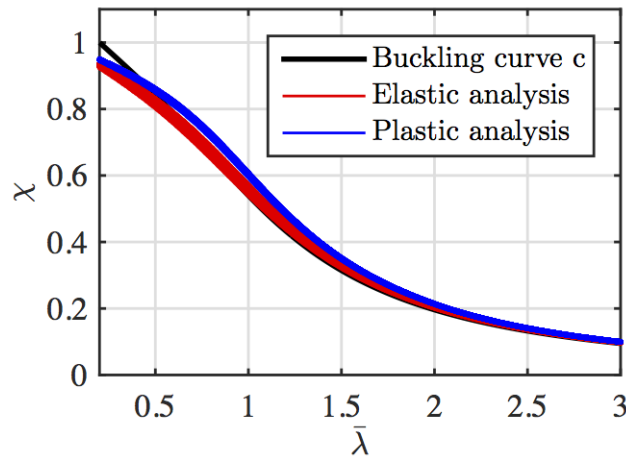
Results regarding the change are presented in figure 5.8a to 5.8c where bending about strong axis for HEA, HEB, HEM, IPE, VKR and KKR columns and steel strength class S355 were chosen as the example. The black line represents the buckling curve while the blue and red lines corresponds to the plastic and elastic analysis, respectively. It was clear that the correlation was better when using the decreased value for the initial bow imperfection. However, the match was not perfect for all columns and for all values of relative slenderness. Some results were even on the unsafe side after this optimisation. Also, the difference that occurred when analysing different steel strength classes was still a problem.



(a) Buckling curve *a*



(b) Buckling curve *b*



(c) Buckling curve *c*

Figure 5.8: Optimisation of the initial bow imperfection by using decreased values. The columns were divided into corresponding buckling curve and the results are visualised as the buckling reduction factor vs. the relative slenderness. Strong buckling direction and steel strength class S355.

An additional way to achieve better results for all columns and all values of relative slenderness, was to make the initial bow imperfection dependent on relative slenderness instead of the column length. An example of this was presented by Goncalves and Camotim (2005) and was described in chapter 2.5.2 of this thesis. The new expression used for the initial bow imperfection is found in equation 5.1.

$$e_{0,d} = \alpha (\bar{\lambda} - 0.2) \frac{W_{el}}{A} \quad (5.1)$$

The results from introducing this new value of the initial bow imperfection into the analysis are presented in figure 5.9a to 5.9c. Again, columns with HEA, HEB, HEM, IPE, VKR and KKR cross-sections, steel strength class *S355* and strong buckling direction were considered. The black line represents the buckling curve while the blue and red lines corresponds to the plastic respectively elastic analysis.

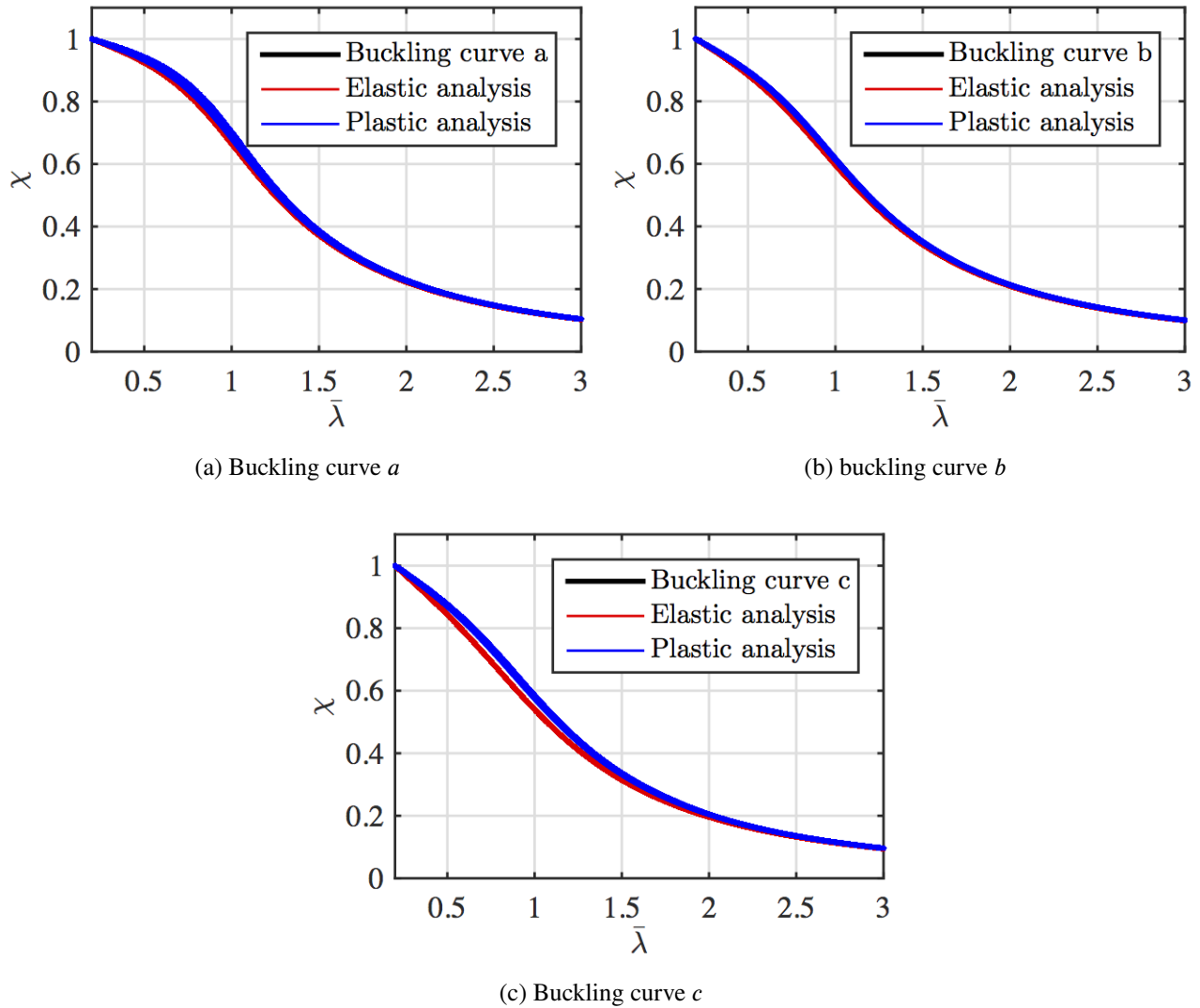


Figure 5.9: Optimisation of the initial bow imperfection by using the formula in equation 5.1. The columns were divided into corresponding buckling curve and the results are visualised as the buckling reduction factor vs. the relative slenderness ratio.

At first glance, these results seemed to correlate well for both buckling curve *a* and *b* but a large number of columns were evaluated at the same time which made it hard to interpret how well the results really corresponded to the buckling curves. To be able to draw a better conclusion, the same analysis but only considering HEB 220 cross-sections which corresponded to buckling curve *b* was performed. The results are presented in figure 5.10.

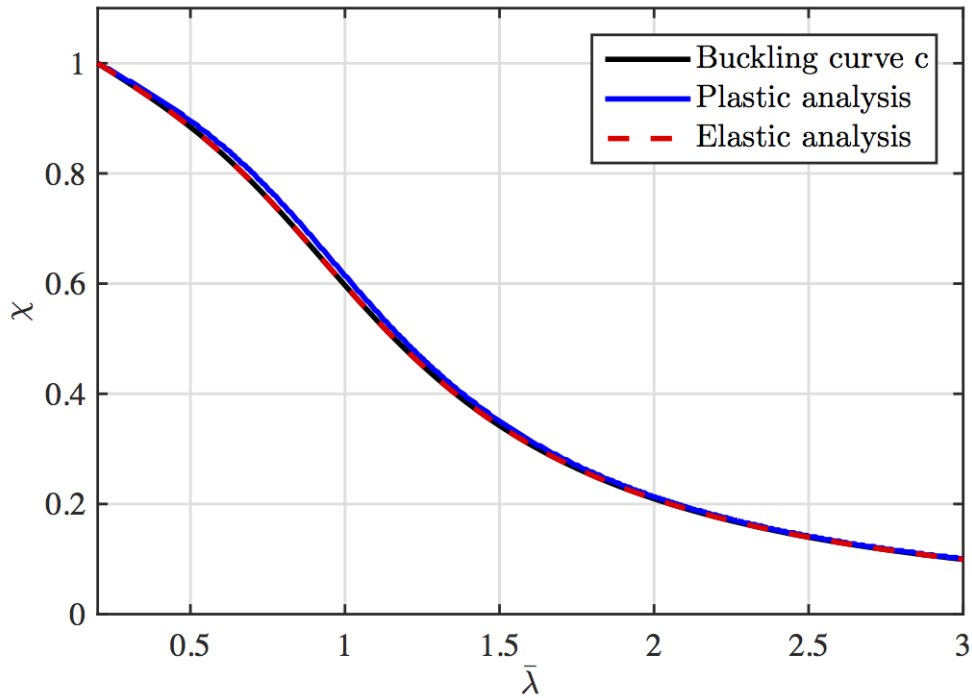


Figure 5.10: Optimisation of the initial bow imperfection as in figure 5.9 although only for cross-section type HEB 220.

It was observed that the elastic analysis achieved an excellent fit with buckling curve *b* while the plastic analysis showed overestimated capacity. This was the case for all columns which was even more clear for other cross-section types. To overcome the problem with overestimated capacity for the plastic analysis, the expression for the initial bow imperfection needed to be corrected to cover the extra capacity the cross-section achieved when it plasticised. This was achieved by adding a factor that corresponded to the ratio between the plastic and elastic section modulus. The new expression for the initial bow imperfection used in the plastic analysis is presented in equation 5.2.

$$e_{0,d} = \alpha (\bar{\lambda} - 0.2) \cdot \frac{W_{pl}}{A} \cdot \frac{W_{pl}}{W_{el}} \quad (5.2)$$

If analysing the HEB 220 columns with this initial bow imperfection for the plastic analysis the results corresponded very well, as seen in figure 5.11. Also here, HEB 220 columns associated to buckling curve *b* with steel strength class *S355* and buckling about the strong axis were examined. The black line represents buckling curve *b* while the blue and red lines corresponds to the plastic and elastic analysis respectively.

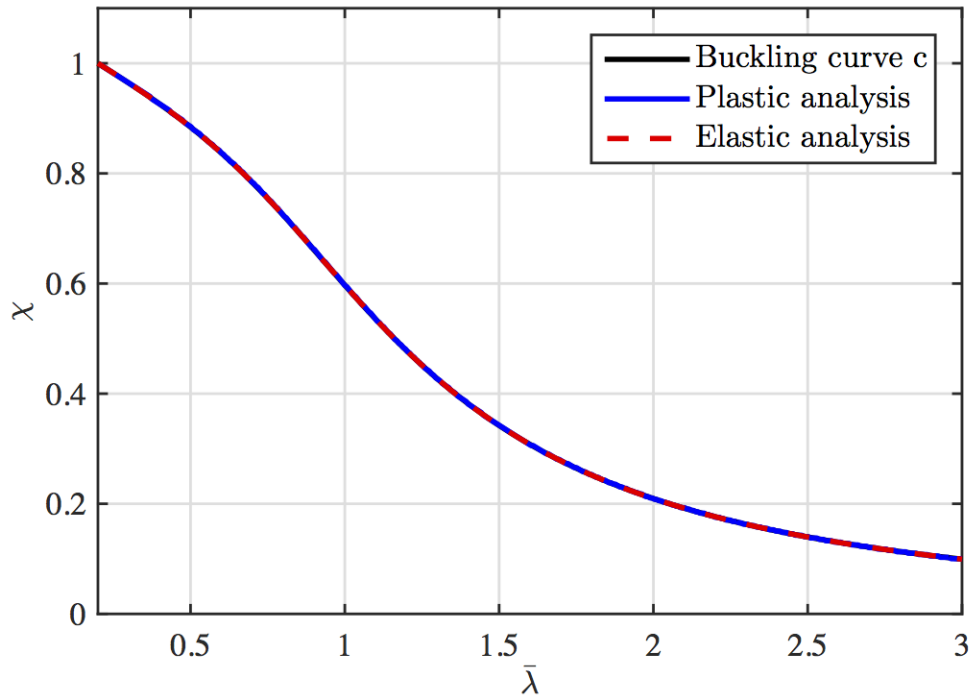
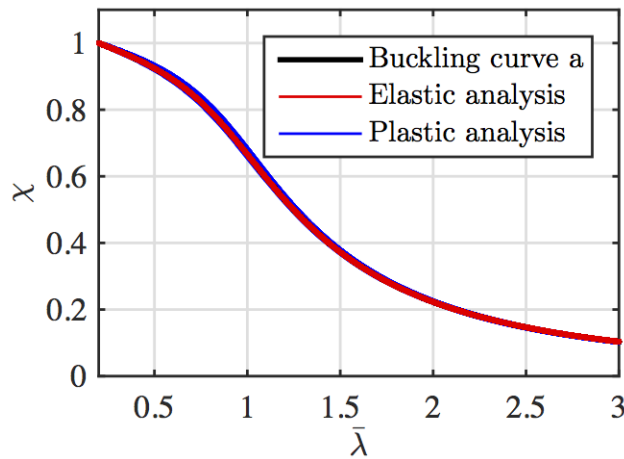
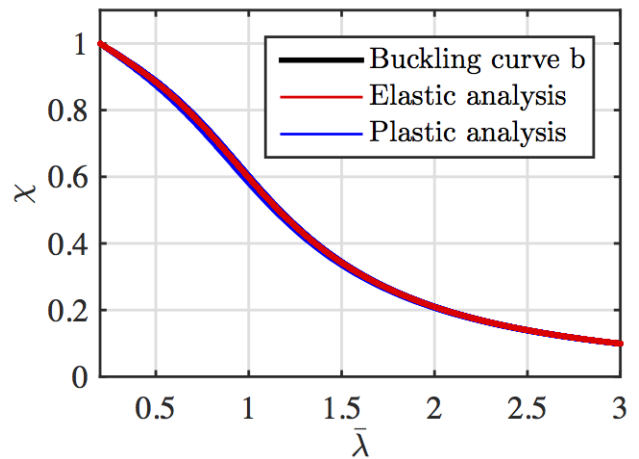


Figure 5.11: Optimisation results of initial bow imperfection regarding separate formulas for the initial bow imperfection for plastic and elastic analysis, strong axis. The results are visualised as the buckling reduction factor vs. the relative slenderness ratio.

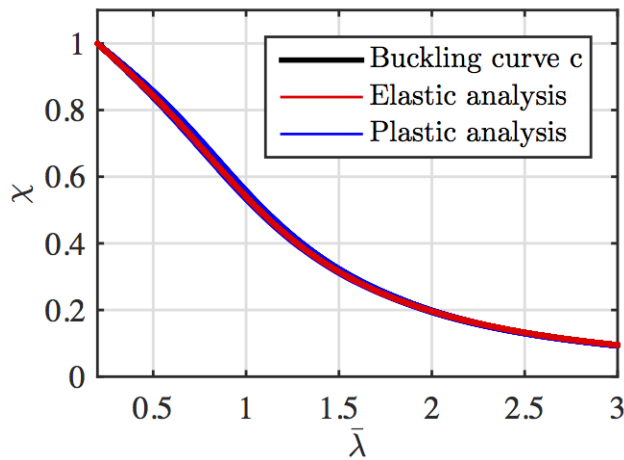
When this new equation was used in the plastic analysis for all columns, the result had a very good conformity as seen in figure 5.12a to 5.12c where strong buckling direction for all three buckling curves were considered. The black line represents the buckling curve while the blue and red lines corresponds to the plastic and elastic analysis respectively. Using those equations also solved the problem with varying results for different steel strength classes. The reason was that those formulas are dependent on the relative slenderness which in turn considers the steel strength class. The original expression for the initial bow imperfection only depends on the column length.



(a) Buckling curve a



(b) Buckling curve b



(c) Buckling curve c

Figure 5.12: Optimisation of the initial bow imperfection by using the final formulas. The results are visualised as the buckling reduction factor vs. the relative slenderness ratio for each buckling curve separately. All results concern the strong buckling direction.

For buckling about the weak axis, figure 5.6 shows that the results varied for different types of columns (H or KKR) and analysis type (plastic or elastic). When the new formulas for the initial bow imperfection were implemented, the results became as in figure 5.13.

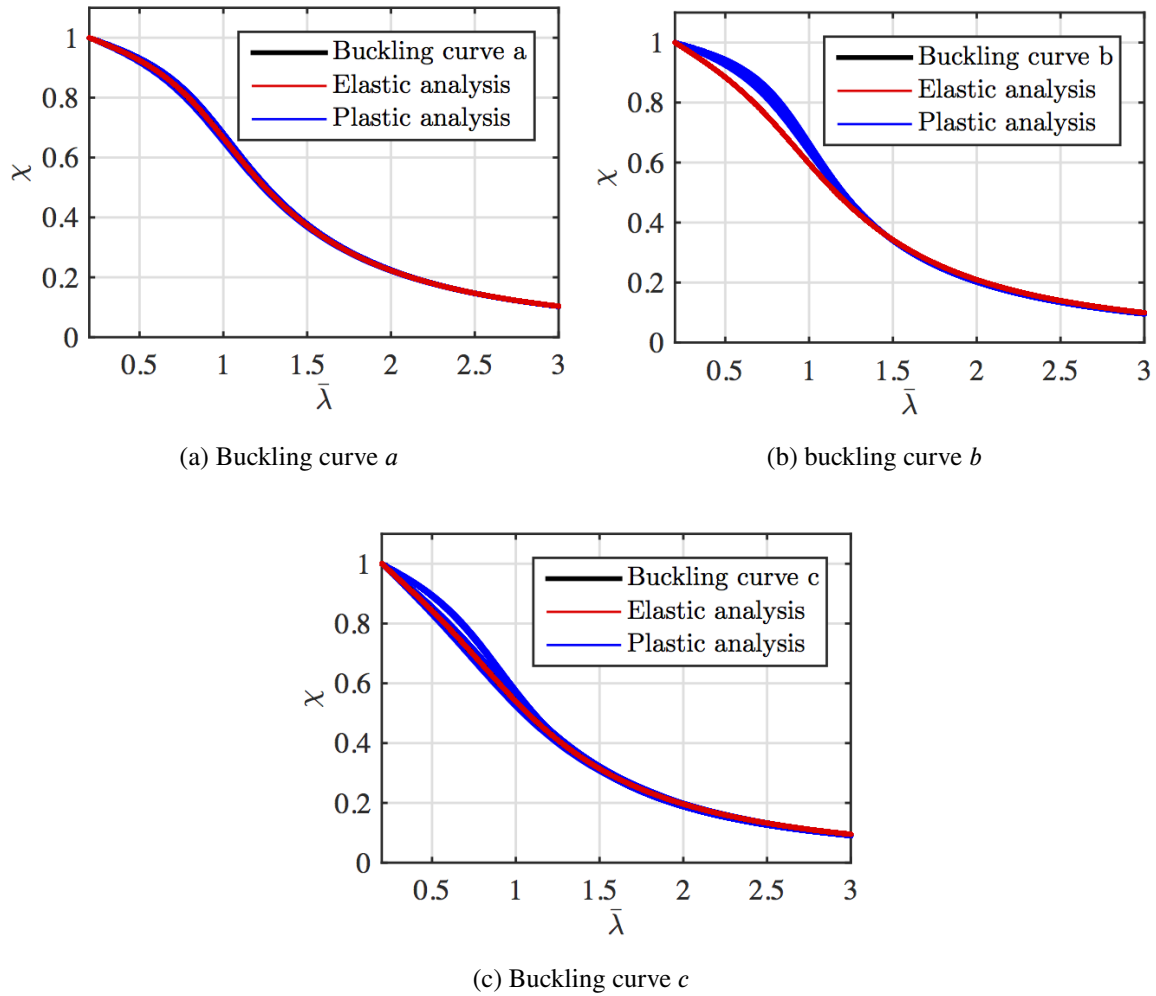


Figure 5.13: Optimisation results of initial bow imperfection regarding separate formulas for the initial bow imperfection for plastic and elastic analysis in weak buckling direction. The results are visualised as the buckling reduction factor vs. the relative slenderness ratio.

It was observed that the new formulas fit very well for the elastic analysis which also was true for the plastic analysis of VKR and KKR columns. Though, there was a problem for the plastic analysis of H and I columns, as seen in figure 5.13b and 5.13c where the plastic curve is located above the buckling curve. Thus, the second-order moment and the column capacity were overestimated for the interval where the initial imperfections have the highest influence. One way to improve the results was to add a factor of 1.4 to the formula for the plastic analysis just as in equation 5.3.

$$e_{0,d} = \alpha (\bar{\lambda} - 0.2) \cdot 1.4 \cdot \frac{W_{pl}}{A} \cdot \frac{W_{pl}}{W_{el}} \quad (5.3)$$

The consequence was that the whole plastic curve was moved downwards as in figure 5.14 where the highest point was on the buckling curve but below the buckling curve for higher relative slenderness. The conclusion was that the shape of the plastic curve did not fit good enough to the buckling curve.

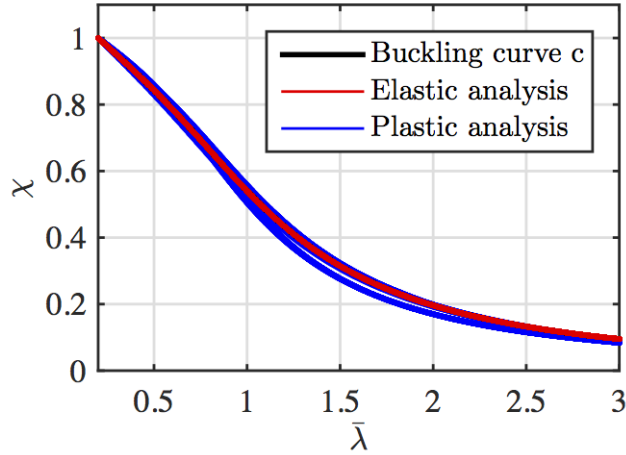


Figure 5.14: Optimisation of the initial bow imperfection by adding a factor of 1.4 to the new formula for the plastic value. The results are visualised as the buckling reduction factor vs. the relative slenderness ratio. Buckling curve c and weak buckling direction.

A way to further improve the results was to develop the formula with another factor for a better match to the buckling curve. The formula for the plastic analysis was accurate for the strong buckling direction and was therefore used as a base for the formula in weak buckling direction. By curve fitting, the factor f in equation 5.4 was found.

$$f = \frac{1}{0.55 \cdot \sqrt{(1 + \bar{\lambda}^2)}} \quad (5.4)$$

The factor was inserted into equation 5.2, which resulted in the formula presented in equation 5.5.

$$e_{0,d} = \frac{\alpha (\bar{\lambda} - 0.2) \cdot \frac{W_{pl}}{A} \cdot \frac{W_{pl}}{W_{el}}}{0.55 \cdot \sqrt{(1 + \bar{\lambda}^2)}} \quad (5.5)$$

Of course, curve fitting could generate other solutions than this. With this new formula applied on the plastic analysis and bending about the weak axis for H and I columns only. The result was as presented in figure 5.15 where it can be seen that the result was consistent with the buckling curve for all cases.

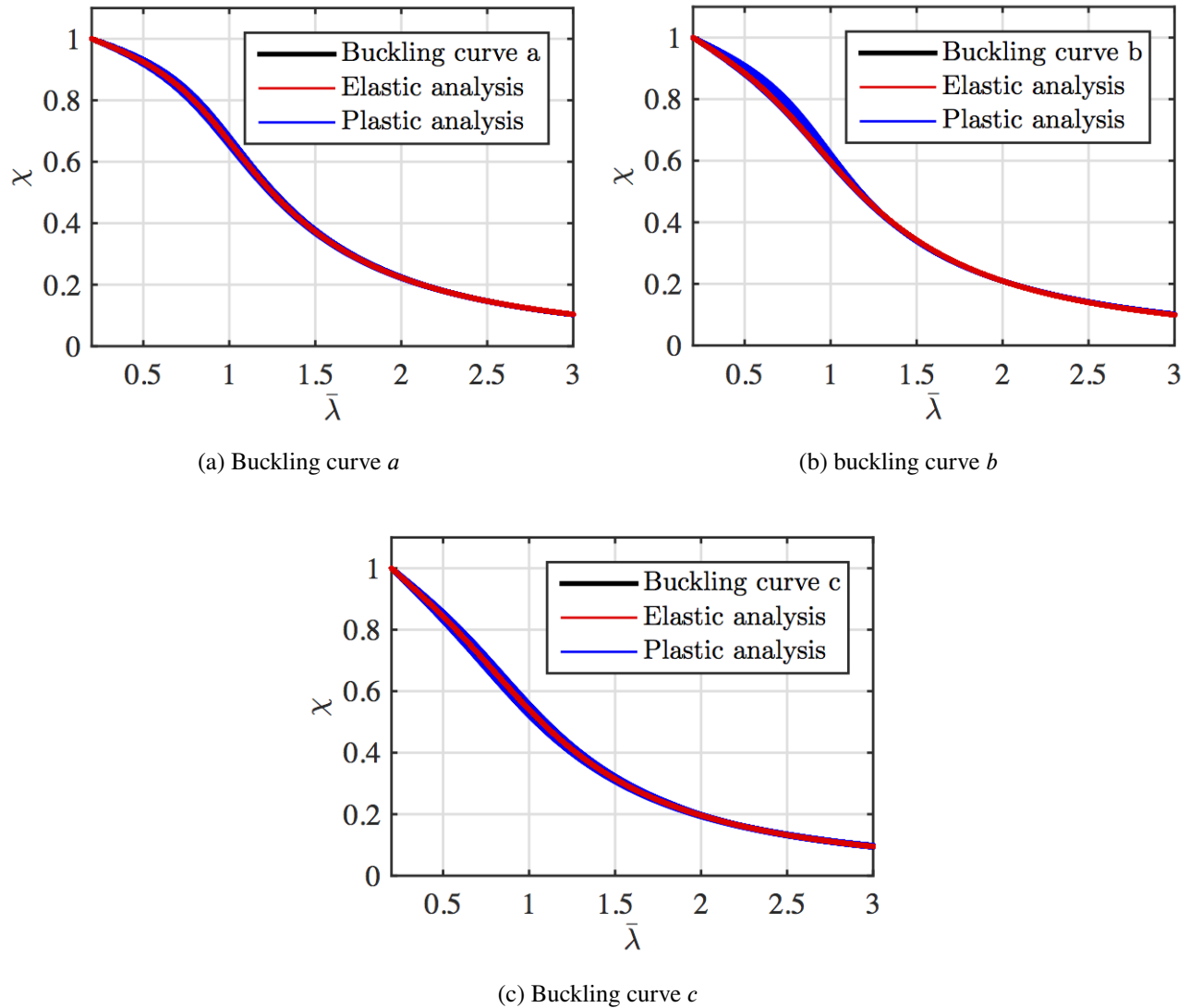


Figure 5.15: Optimisation of the initial bow imperfection by adding a factor f to the new formula for the plastic value. The results are visualised as the buckling reduction factor vs. the relative slenderness ratio. Weak buckling direction.

The interaction factor and reduction formula presented in EN-1993-1-1 (2005) were used during the analysis but as mentioned by Lindner et al. (2016), the German code uses another interaction factor. In the same article, several potential interaction factors for future versions of Eurocode were presented. Therefore, it was investigated whether the German code gave similar results as in this study. The analysis was conducted for a HEB 220 cross-section in weak buckling direction and by using the new formulas for the initial bow imperfection presented in (equation 5.2). The results can be seen in figure 5.16 where the black line represents buckling curve c while the blue and green lines represents the interaction factors from EN-1993-1-1 (2005) respectively the German code. The red line shows the result for the exact solution.

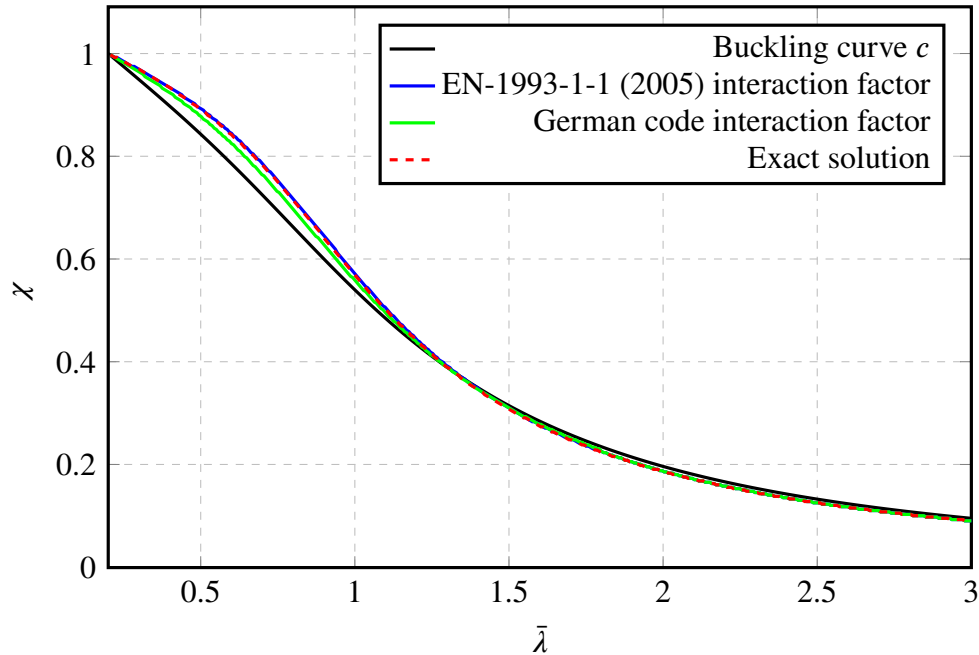


Figure 5.16: Comparison of interaction factors from the German code DIN 18800-1 and corresponding factors presented in EN-1993-1-1 (2005).

As can be seen, the interaction factor from the German code resulted in a slightly lower buckling reduction factor where the magnitude of the overestimation was highest. Compared with the buckling curve, this was a better result than for the reduction formula presented in EN-1993-1-1 (2005) since the differences are smaller. However, since the formula from the German code deviated from the exact method the conclusion was drawn that this formula was a slightly less exact approximation compared to the formula in EN-1993-1-1 (2005). This result was conclusive only for this particular column, not as a general result.

5.2 Numerical results for columns

The intention of performing a FE-analysis in Abaqus was mainly to verify the consistency between the numerical and analytical results. Also, to deepen the understanding of FE-analysis and how the initial bow imperfection was interpreted numerically. A long-term goal was to simplify calculations procedures by applying the initial bow imperfections directly into numerical analysis. To verify the FE-model, the results were compared to the hand-calculations and a convergence study was performed using different beam elements and number of section points. The adequate FE-model was then used to access the results. An optimisation test of the FE-analysis was also conducted where the new formulas for the initial bow imperfection, presented in section 5.1.5 were applied. The numerical results were presented in a direct comparison with the analytical results.

5.2.1 Euler-Bernoulli or Timoshenko beam elements

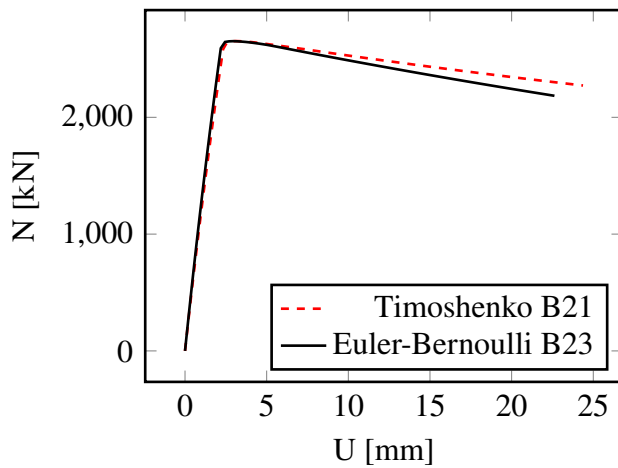
A study was performed in Abaqus in order to find the optimal beam element type. The study was carried out on an axially loaded model, i.e. a column, because of the simplicity. Also, the hand-calculations for a structural member subjected to exclusively axial compression was easier and more accurate. The final model configuration was later used for all analyses, including for beam-columns. The compared beam elements were Timoshenko (B21) and Euler-Bernoulli (B23) beam elements. As specified in chapter 4.2, the cross-sections used in the FE-analysis were HEB 220, IPE 140 and VKR 90 × 50 with thickness $t = 4$ (from now on referred to as HEB, IPE and VKR). The member lengths corresponded to the chosen relative slenderness ratios $\bar{\lambda}$ of 0.4, 1.0 and 1.8 as declared in chapter 4.2.1. Both buckling about strong and weak axis was considered.

One method to examine the applicability of the considered beam elements was to investigate whether the cross-section's width-to-length ratio met the requirements, i.e. if they were below 1/8 respectively 1/15 as described in chapter 4.2. The requirement for B23 beam elements was not met for the HEB with lowest slenderness for strong axis buckling direction, neither for the IPE with low and intermediate slenderness in weak axis buckling direction. The conclusion of this was that the requirements were fulfilled in a greater extent when using Timoshenko beam elements. For more certainty over the decision regarding beam element type, a more thorough comparison was performed for a HEB member for buckling about strong axis. The differences between the critical buckling load obtained from both the linear buckling analysis and the hand-calculations are summarised in table 5.2.

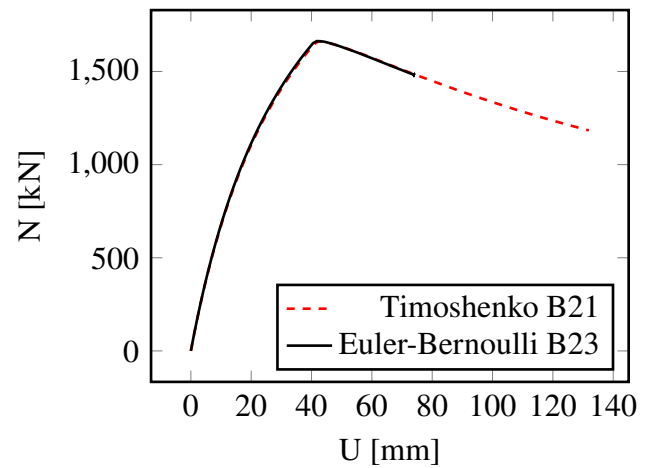
Table 5.2: The difference between FE-results and hand calculations for an HEB 220 cross-section. Strong buckling direction.

Relative slenderness $\bar{\lambda}$ [-]	B21, difference [%]	B23, difference [%]
0.4	-6.6	-0.4
1.0	-1.3	-0.3
1.8	-0.7	-0.4

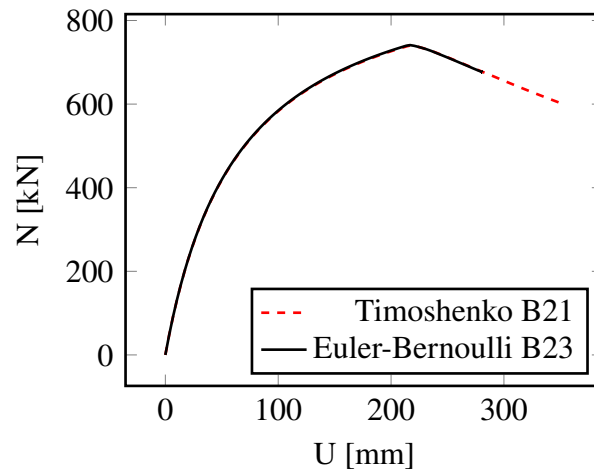
The general result was that the FE-results yielded a lower critical load than the hand-calculations. It was reasonable that the difference when using B23 elements are lower since the hand-calculations are based on the Euler-Bernoulli beam theory. Regarding the Timoshenko beam elements, the difference decreases with increasing slenderness. The critical load was further compared using B21 beam elements for all members. The difference turned out to be of almost the same magnitude with intervals of -6.05 to -6.57% for members with low relative slenderness, -1.04 to -1.51% for members with intermediate relative slenderness and -0.35 to -0.85% for members with high relative slenderness. The results for the second-order non-linear buckling analysis of an axially compressed member (column) were summarised into figure 5.17. The normal force N was obtained from the reaction force (RF1) in longitudinal member direction at the pinned support free to translate in x-direction and the deflection U was the obtained from the transverse member translation (U2) at the mid-point. The maximum point of the curve was represented by the yielding point (or bifurcation point). The arc length increment had a fixed value of 0.05 in all simulations.



(a) Low relative slenderness



(b) Intermediate relative slenderness

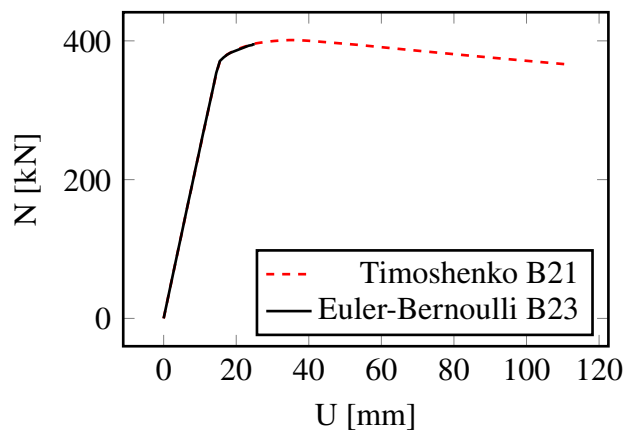


(c) High relative slenderness

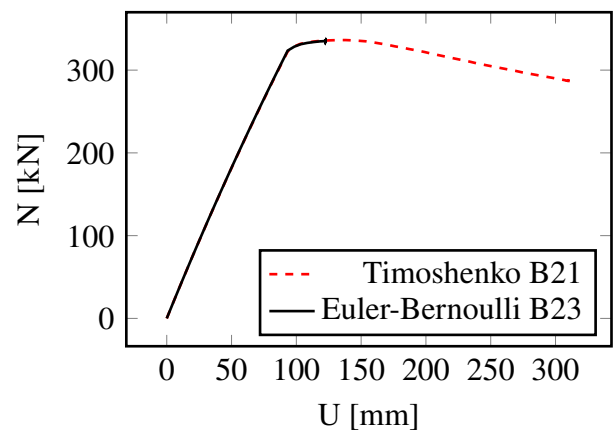
Figure 5.17: Load vs. deflection relation for a column with a HEB 220 cross-section subjected to an axial load. Strong buckling direction.

The initial imperfection $e_{0,d}$ was excluded from the deflection in Abaqus. Thus, it had to be added to obtain the actual total deflection if desired. All results were from the point of yielding, i.e. the maximum load. It can be seen in all graphs that the critical buckling load were approximately equal for both beam element types but the post-critical behaviour was somehow varying. For the member with lowest relative slenderness, B21 beam elements had a higher post-critical load for the corresponding deflection while for the members with intermediate and high relative slenderness the values were equal. Though, the values for B23 beam elements were interrupted earlier. The exact differences between the FE-analysis and hand-calculations, at the critical point, when using both B21 and B23 beam elements are found in appendix B. The values for the arising second-order moment were also included. Also there, the results were similar.

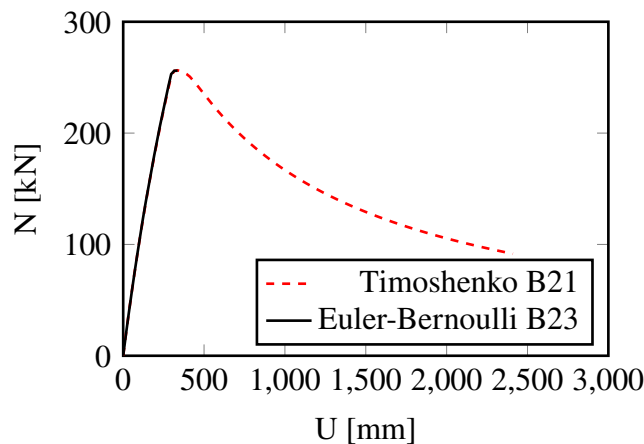
The last part of the convergence study concerning beam element types included a combination of axial load and bending moment at both ends, i.e. a beam-column. The applied loads in Abaqus were related to each other with a factor 1.6, i.e. for an axial load of 800 kN, the bending moment was ± 500 kN m etc. In the previous part, the arc length increment was exclusively 0.05. When the bending moment was added, there were convergence problems when using B23 beam elements when considering the same loading as for B21 beam elements. The arc length increment for the member with low relative slenderness had to be changed into 0.03 and for the member with intermediate relative slenderness into 0.045 in order to find convergence. As a result, the arc length increment for the simulations including B21 beam elements was changed too corresponding B23 value to be equal. The comparison of B21 and B23 beam elements when the member was subjected to a combination of bending moment and axial load are shown in figure 5.18.



(a) Low relative slenderness with arc length increment 0.03



(b) Intermediate relative slenderness with arc length increment 0.045



(c) High relative slenderness with arc length increment 0.05

Figure 5.18: Load vs. deflection relation for a column with a HEB 220 cross-section subjected to an axial load. Weak buckling direction.

In all cases, the results for B21 and B23 beam elements followed the same curve almost up to the point of yielding and then, for B23 beam elements, the curve stopped. Thus, no post-buckling behaviour was seen for B23 beam elements. This was the main reason Timoshenko beam elements were finally chosen for all further analysis. The size of the arc length increment was set to 0.05 for all members.

Section point analysis

In the second order non-linear buckling analysis, it was discovered that the cross-section did not reach full plasticity at the ultimate load. Therefore, it was interesting to investigate the cross-section more thoroughly, i.e. with more section points over the cross-section. The default integration for an I and box section in plane and space are seen in figure 5.19.

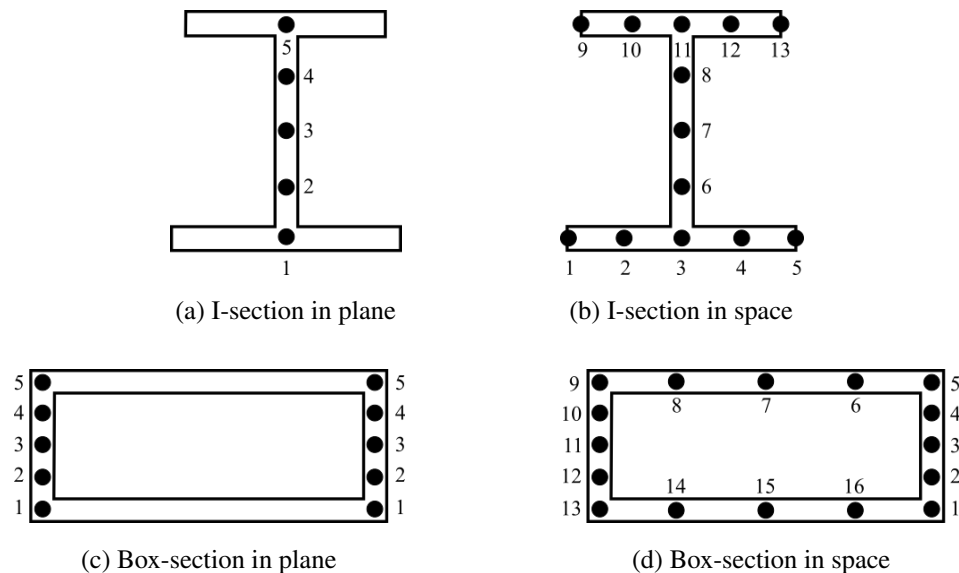
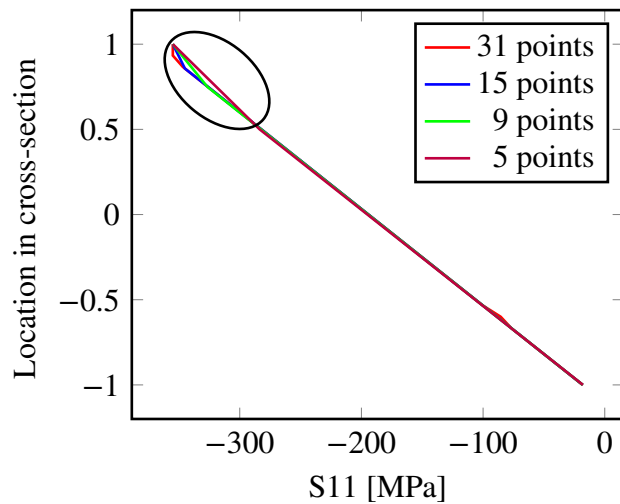
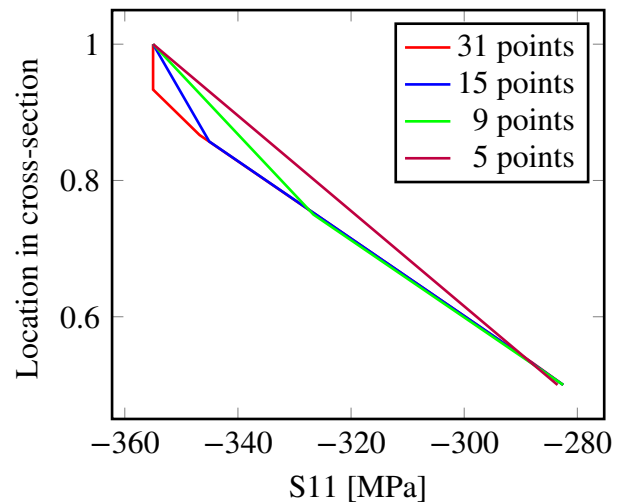


Figure 5.19: Default integration for I and box-sections in ABAQUS.

The number of section points were selected to 5 (default), 9, 15 and 31. The principle stress (S11) was plotted over the whole cross-section. When the ultimate load was reached, the principle stress at each section point was collected and summed into figure 5.20. The considered member was a HEB 220 column in strong buckling direction with assigned Timoshenko beam elements. Since the steel strength class was S355, the principle stress should be 355 MPa in case of full plasticity. The cross-section was divided into local coordinates in ABAQUS where zero represented the mid-point. Coordinates above the mid-point had positive values and coordinates under got negative.



(a) The principal stress (S11) distribution over the cross-section. The black ellipse marks the area with varying results.



(b) Enlargement of the area in the ellipse.

Figure 5.20: Section point analysis of a HEB 220 cross section at the point of yielding. Strong buckling direction.

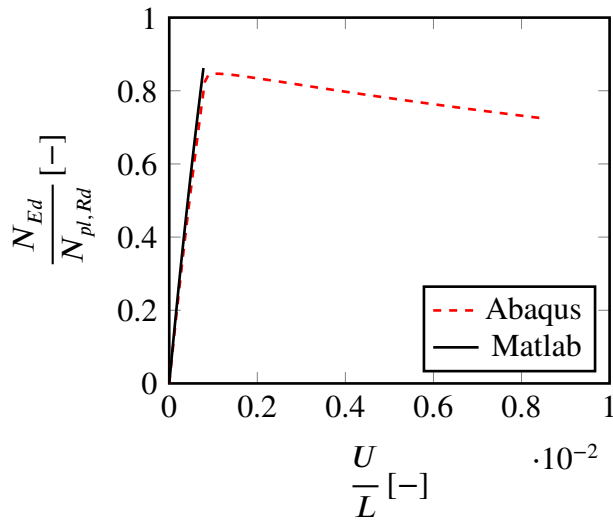
By observing the graphs it was quickly verified that the entire cross-section was in compression due to the negative values of the principle stress. The graphs also revealed that there were only some deviations in the top of the cross-section and that only in the case of 31 section points some plasticity was seen as a vertical line. Perhaps, this was a consequence of the fact that Abaqus gives a warning when the strain increment has exceeded fifty times the strain to cause yielding. Hence, the strain increment was too large for the software to not attempt the plasticity calculation along many points of the member. Overall, the number of section points did not affect the principle stress at the outermost fibre. Hence, the default integration may be used if desired. The same procedure was carried out using Euler-Bernoulli beam elements as a comparison. The result was that the cross-section plasticised in a greater extent. Though, since those beam elements were not used, the study was not presented.

5.2.2 Comparison of analytical and numerical results

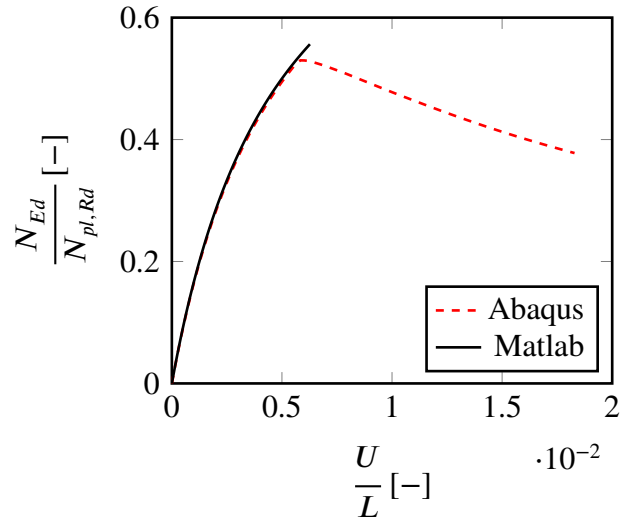
The main results obtained from the FE-analysis is presented in this section. All the results were compared directly with the results from Matlab and presented in plots and tables. Throughout the whole study, the analytical and numerical results were compared so that the analytical value was the numerator and the numerical value was the denominator. Hence, negative differences meant that the numerical results were lower. The considered columns had cross-sections HEB 220, IPE 140 or VKR 90 × 50 with thickness $t = 4$ (from now referred to as HEB, IPE and VKR in this section). The member lengths corresponded to the chosen relative slenderness ratios, $\bar{\lambda}$, of 0.4, 1.0 and 1.8. The applied axial load and external bending moment were related to each other by a factor 1.6 in ABAQUS, as mentioned in 5.2.1. The results were divided after the buckling direction. Thereafter, plotted dimensionless with the ratio between the actual load N_{Ed} and the maximum axial normal force $N_{Pl,Rd}$ on the y-axis and the ratio between the deflection U and the element length L on the x-axis.

Strong buckling direction

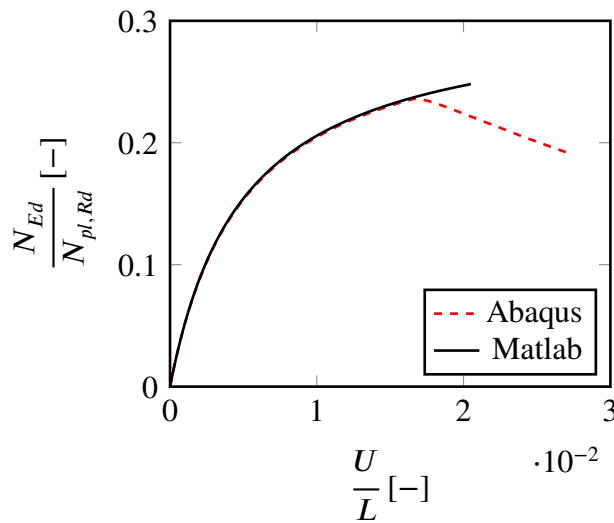
The numerical results obtained in the second order non-linear buckling analysis for the considered columns were compared to the analytical results and summed into plots. The results for the HEB cross-sections are found in figure 5.21. Due to the fact that the structural behaviour for the IPE and VKR cross-sections were similar, those results are found in appendix D.1 for comparison. The difference presented in exact values are found in the same appendix. The plots show that there were distinct differences between the numerical and analytical results. Analogously, both ratios yielded lower results in Abaqus which meant that the columns had lower capacity in Abaqus and therefore reached collapse faster. The largest difference was for columns with intermediate relative slenderness, which could be explained by that fact the initial bow imperfection have the greatest impact there as was explained in chapter 2.3.



(a) Low relative slenderness



(b) Intermediate relative slenderness

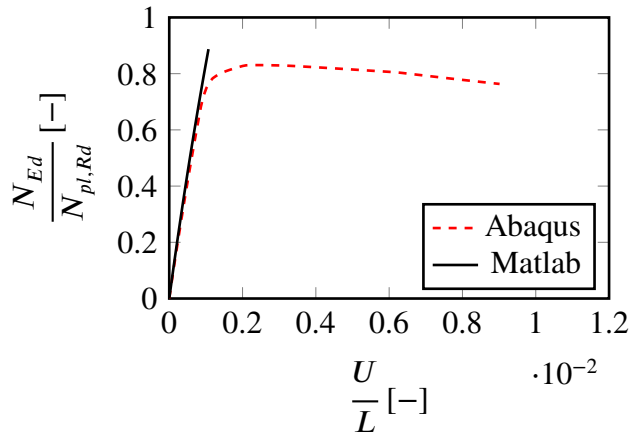


(c) High relative slenderness

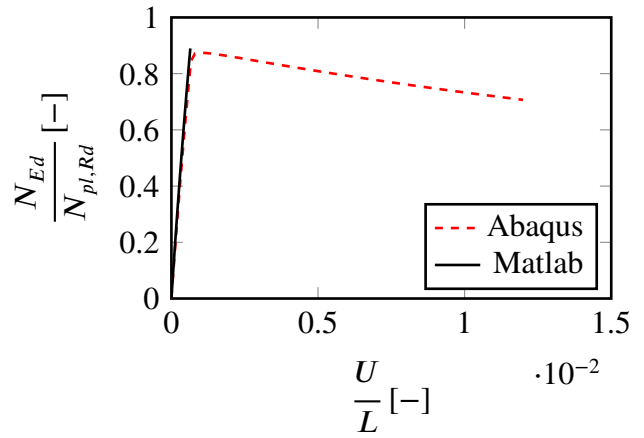
Figure 5.21: Load-deflection relation for a HEB 220 column. Strong buckling direction.

Weak buckling direction

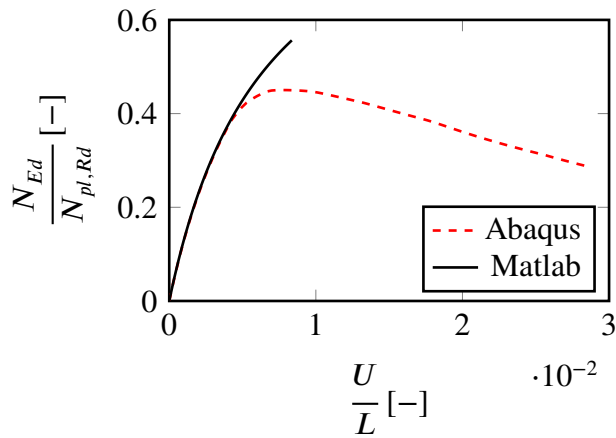
In the second order non-linear analysis in weak buckling direction, the structural behaviour for HEB and IPE cross-sections were similar. Hence, just the results for HEB and VKR cross-sections are presented here. The results for the IPE cross-section columns are found in appendix D.1. In the same appendix, all differences are presented with exact values. The results were similar as for for strong axis buckling direction. Though, the differences between the analysis was greater. Also here, the difference was largest for columns with IPE cross-section with intermediate relative slenderness.



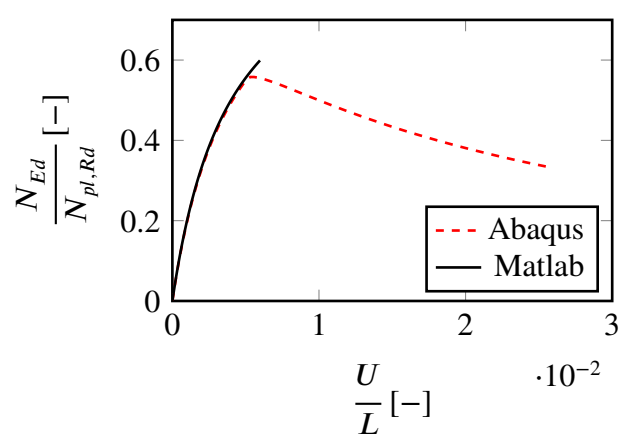
(a) HEB with low relative slenderness



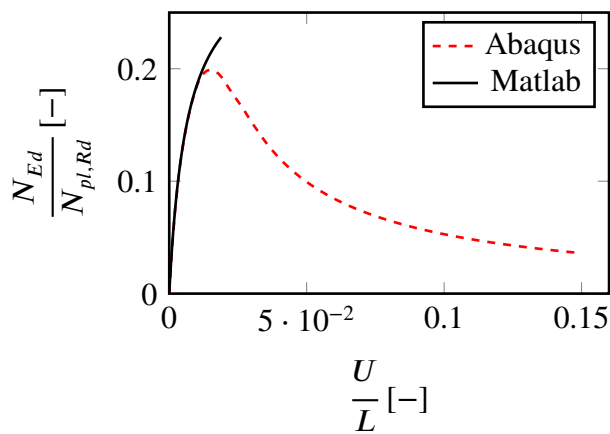
(b) VKR with low relative slenderness



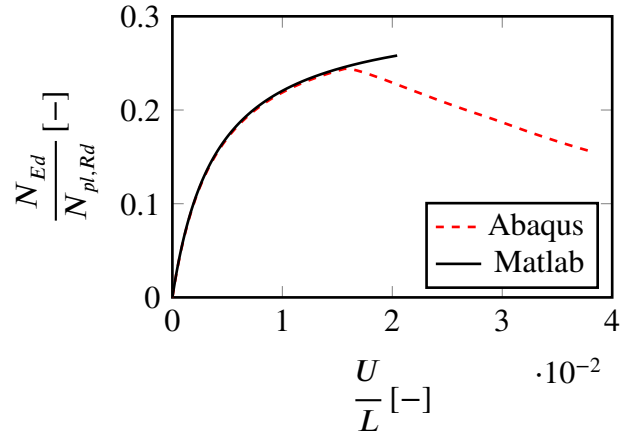
(c) HEB with intermediate relative slenderness



(d) VKR with intermediate relative slenderness



(e) HEB with high relative slenderness



(f) VKR with high relative slenderness

Figure 5.22: Load-deflection relation for a HEB 220 and VKR 90 × 50 ($t = 4$) column. Weak buckling direction.

Summary of differences

The results for all considered columns in both buckling directions may be summed into figure 5.23. The plots represent the ratio between the maximum numerical and analytical results for relative slenderness 0.4 to 1.8. The plots were created using smooth curve fitting. Hence, it must be noted that the relation is only theoretical for the in-between relative slenderness. The accuracy would have been better if multiple cases of relative slenderness were taken into consideration. Thus, the illustration might be slightly unreliable but gives a good picture of the overall behaviour.

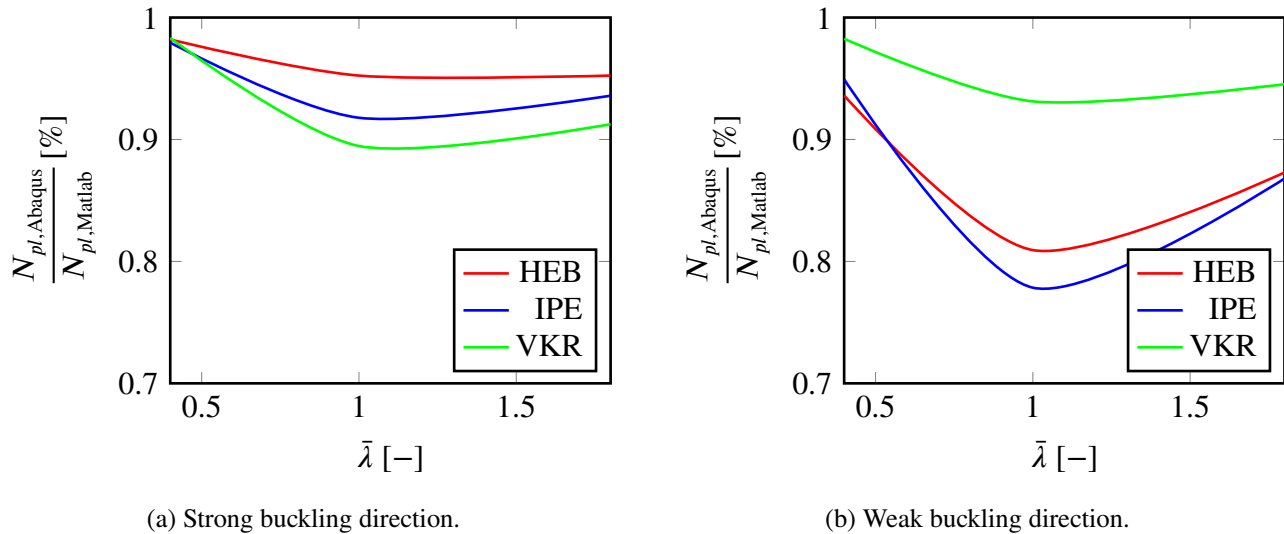


Figure 5.23: Ratio between the plastic capacity obtained from the numerical and analytical results vs. the relative slenderness for all considered columns.

5.2.3 Optimisation of FE-analysis

The performed optimisation in the analytical part generated new formulas for the initial bow imperfection which were later implemented into the FE-analysis. Within this part, also an elastic analysis was performed to verify the fact that the analytical and numerical results should be equal using the developed formula for the initial bow imperfection. The values for the initial bow imperfection were calculated using equation 5.1. For the comparison of the elastic analysis, the results were compared to the maximum capacity obtained in the buckling curve analysis instead of the second-order moment analysis since that was the capacity to aim for. The results for columns with intermediate relative slenderness and strong buckling direction are found in table 5.3. Again, the largest differences were for this relative slenderness because of the initial imperfections within the member. Therefore, the result is only presented for this relative slenderness.

Table 5.3: Difference between the analytical and numerical results for columns with intermediate relative slenderness. Elastic analysis in strong buckling direction.

Cross-section type	Difference, [%] ($e_{0,d}$ from Eurocode)	Difference, [%] ($e_{0,d}$ from new formula)
HEB	-4.61	2.22
IPE	-14.39	0.59
VKR	-18.62	0.46

It was concluded that all values had exceptionally better conformity with differences closer to zero. Though, it was noticed that the numerical results now yielded a slightly higher capacity than the analytical. The results for the intermediate columns in weak buckling direction are shown in table 5.4.

Table 5.4: Difference between the analytical and numerical results for columns with intermediate relative slenderness. Initial bow imperfection from both Eurocode and new formula. Elastic analysis in weak buckling direction.

Cross-section type	Difference, [%] ($e_{0,d}$ from Eurocode)	Difference, [%] ($e_{0,d}$ from new formula)
HEB	-24.9	-0.29
IPE	-32.6	-0.31
VKR	-18.9	1.08

Also here, the difference between the numerical and analytical results were considerably reduced into almost zero. For the weak buckling direction, the numerical results for the HEB and IPE columns were still lower than the analytical results. Overall, the largest difference was only about 2% for the new formula which was considered as small. Perhaps this would have been even less if the strain hardening (elastic-plastic material behaviour) in the material had been taken into account. The same type of analysis, but plastic, was performed with new values for the initial bow imperfections obtained from the formula in equation 5.2. For recurrence, the original (optimised) formula for the initial bow imperfection was:

$$e_{0,1} = \alpha (\bar{\lambda} - 0.2) \cdot \frac{W_{pl}}{A} \cdot \frac{W_{pl}}{W_{el}}$$

Also, an investigation was made using a modification of the formula where the last term was excluded, see equation 5.6. Temporary in this section, the modified and original formula are referred to as Equation 1 and 2, respectively.

$$e_{0,2} = \alpha (\bar{\lambda} - 0.2) \cdot \frac{W_{pl}}{A} \tag{5.6}$$

The comparison for columns with intermediate relative slenderness for both Equation 1 and 2 in strong buckling direction is found in table 5.5. Corresponding results for low and high relative slenderness are found in appendix D.2.

Table 5.5: Difference between the analytical and numerical results for both Equation 1 and 2 for columns with intermediate relative slenderness. Initial bow imperfection from both new formulas. Plastic analysis in strong buckling direction.

Cross-section type	Difference, [%] ($e_{0,1}$ from Equation 1)	Difference, [%] ($e_{0,2}$ from Equation 2)
HEB	-4.51	-1.41
IPE	-4.89	-1.96
VKR	-8.14	-3.13

It was noticed that the modified formula (Equation 2) generated the most accurate results compared to analytical calculations with a maximum difference about 3%. The results from same analysis but for weak buckling direction is found in table 5.6. Also here, Equation 2 gave the most preferable results. Though, with a slightly larger difference of about 4%. Corresponding results for low and high relative slenderness are found in appendix D.2.

Table 5.6: Difference between the analytical and numerical results for columns with intermediate relative slenderness. Initial bow imperfection from both new formulas. Plastic analysis in weak buckling direction.

Cross-section type	Difference, [%] ($e_{0,1}$ from Equation 1)	Difference, [%] ($e_{0,2}$ from Equation 2)
HEB	-16.29	-2.51
IPE	-18.38	-4.30
VKR	-5.27	-1.87

5.3 Analytical results for beam-columns

The second part of this study was, as previously stated, devoted entirely to the analysis of beam-columns where the results obtained from two different moment distributions, as in figure 5.24, was studied. The first case is when the member was subjected to an equal end moment and the latter case is when an external moment caused by adding a uniformly distributed load was present.

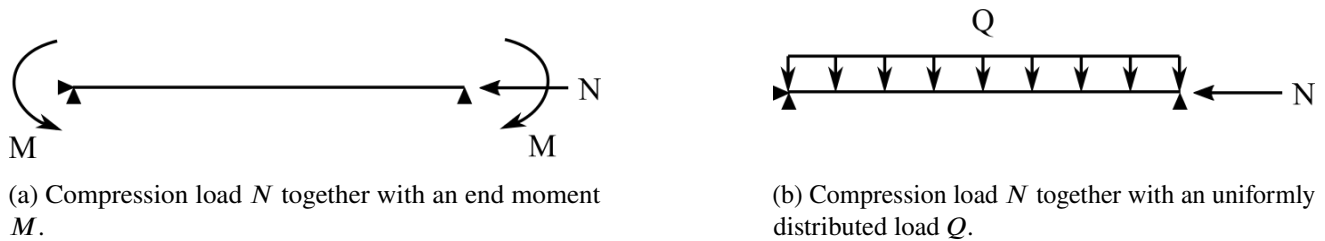


Figure 5.24: Considered moment distributions for the pinned-pinned beam-columns.

The composition was similar to part one where the Matlab programme first was validated, followed by the analytical results obtained for both moment distributions. As it was explained in the beginning of this study, the method with initial bow imperfections was compared to Method 1 and Method 2. Further, the impact of different steel strength classes was examined followed by the optimisation of the initial bow imperfection and after that the numerical FE-analysis was performed.

5.3.1 Verification of Matlab programme

The verification was performed on some beam-columns for both bending about strong and weak axis. As there were an endless number of combinations for axial loads and bending moments, only cases where the external moment was 20% of the maximum plastic moment capacity was analysed. The verification was performed for the method with initial imperfections as well as Method 1 and 2. The first step of the verification included a HEB 220 cross-section with intermediate relative slenderness ($\bar{\lambda} = 1.0$). The results from Matlab compared with the hand-calculations showed a consistency of 99.6 to 100.0% for both the method with initial bow imperfections, Method 1 and Method 2 which was ideal. The exact results are found in appendix C. Hence, the drawn conclusion was that the Matlab programme was sufficient to use for receiving analytical results.

5.3.2 Analysis of beam-columns

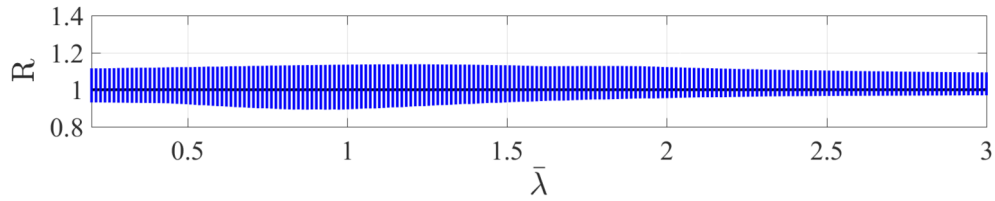
The main task of part two was to analyse all considered beam-columns and compare the results from the method with initial bow imperfections with Method 1 and 2. The difference from part one was that the results were not compared to the buckling curves. A reason was that there were unlimited combinations of axial loads and bending moments. In addition to comparing the maximum capacity of the methods there were also an interest in knowing which combinations of moment and axial load that deviates and by which magnitude. Therefore, instead of comparing the results with the buckling curves, the results in part two was presented in R vs. relative slenderness $\bar{\lambda}$. The programme was created to iterate through a number of different axial loads and work out the corresponding external moment

needed to reach full capacity. This was computed for the method with initial imperfections. Later all the specific combinations of axial load and external moment were inserted into Method 1 and 2. This resulted in a ratio (R), which was interpreted as how well the maximum capacity of the method with initial imperfections corresponded to Method 1 and 2. A ratio (R) above one indicated that the capacity was overestimated compared to Method 1 and 2. A ratio below one displayed results on the safe side. The results were separated for each type of beam-column and further divided into whether the analysis was based on Method 1 or 2.

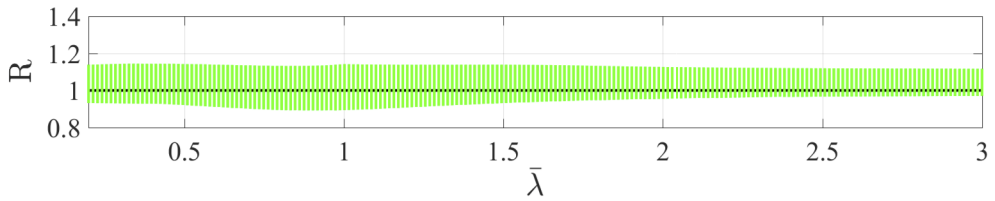
External bending moment from end-moment

Generally, the results for the moment distribution with equal end-moments were similar for all considered beam-columns. Therefore only a few cases that captured the general behaviour was selected for presentation, all results can be found in appendix E.1 for bending about strong axis and in appendix E.2 for bending about weak axis. The first case was HEB cross-sections with steel strength class $S355$. Figure 5.25 shows the results for bending about the strong axis using both plastic and elastic analysis.

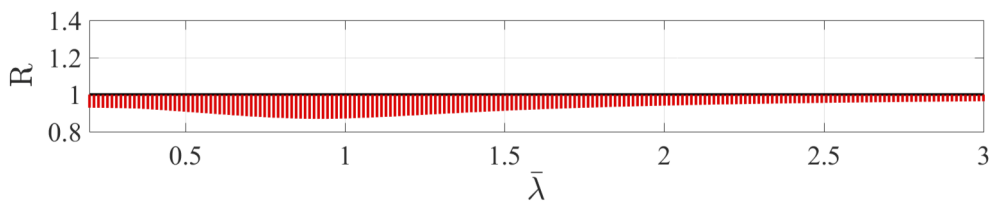
The results for the plastic analysis exhibited a variety of ratio (R) on both the safe and unsafe side. The meaning of that was that for each value of the relative slenderness there were combinations of axial load and external moment resulting in both favourable and unfavourable capacities for the method with initial imperfections compared to Method 1 and 2. For rectangular hollow sections the results were similar, the only observed difference was that the variation of the ratio was slightly larger. When interpreting the results of the elastic analysis it was clear that no load combinations resulted in ratios on the unsafe side. However, there were combinations of axial load and external moment that were considerably on the safe side. Thus, there were thoughts about a possibility for an optimisation of the initial bow imperfections regarding the elastic analysis.



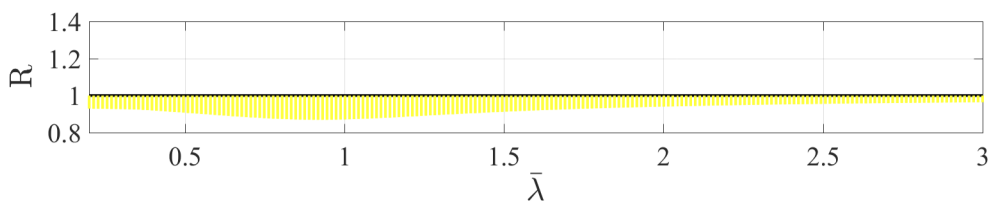
(a) Method 1, plastic analysis



(b) Method 2, plastic analysis



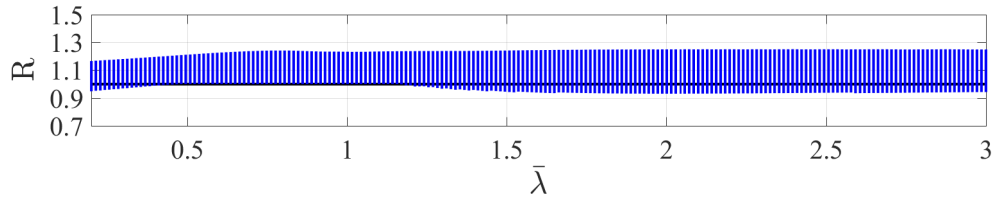
(c) Method 1, elastic analysis



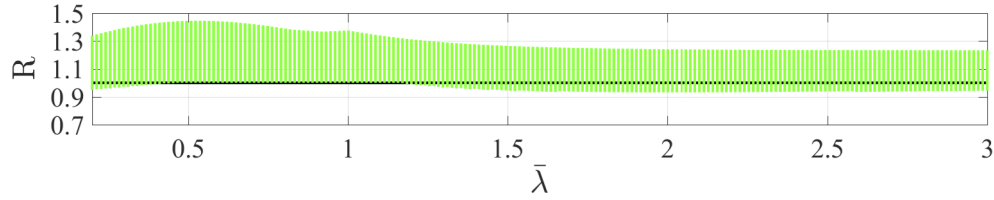
(d) Method 2, elastic analysis

Figure 5.25: Results for beam-columns with HEB cross-sections, steel quality S355 and equal end-moments. Bending about strong axis.

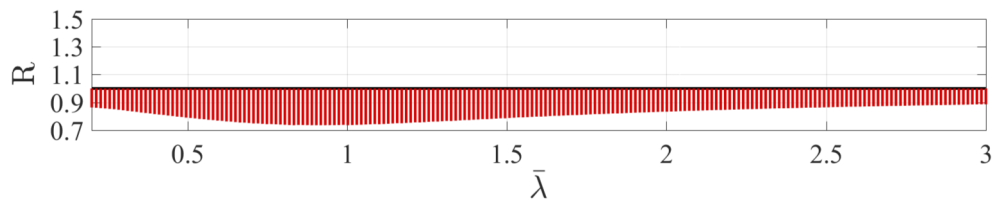
In figure 5.26, the results for the same analysis, but for weak buckling direction is presented. Also here, the results were similar for all beam-columns. Thus, only the HEB members are presented. However, a difference was seen for the Method 2 (plastic analysis) where the maximum ratio was approximately 1.4. In addition to that, the ratio variation was greater than for the strong buckling direction. Also, more results were on the unsafe side. This behaviour was as mentioned also noticed for H and I columns. For the elastic analysis, the results for weak buckling direction were mostly similar to the strong buckling direction. Thus, there were no results on the unsafe side. For some combinations of axial load and external moment there were room for improvement since the ratio was approximately 0.7.



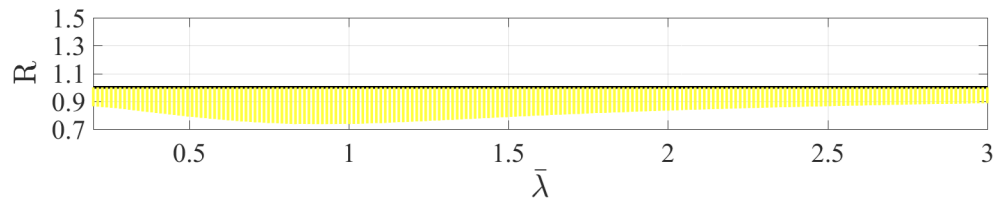
(a) Method 1, plastic analysis



(b) Method 2, plastic analysis



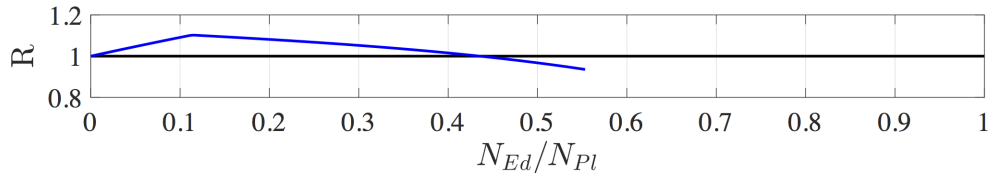
(c) Method 1, elastic analysis



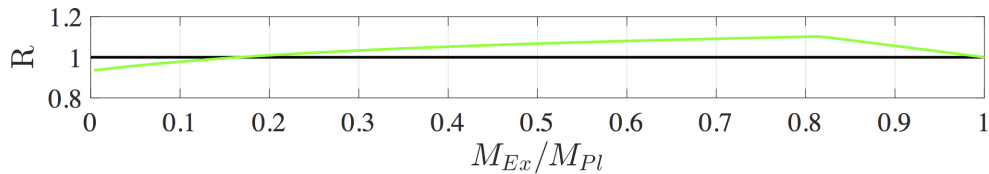
(d) Method 2, elastic analysis

Figure 5.26: Results for beam-columns with HEB cross-sections, steel quality S355 and equal end-moments. Bending about weak axis.

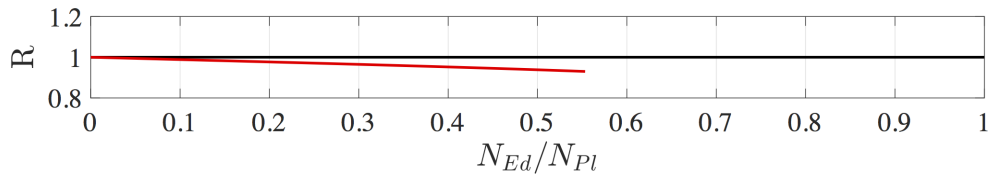
To be able to find exactly which combination of external moment and axial load that resulted in a certain ratio, a HEB 220 member was evaluated in more detail. In figure 5.27, the ratio for Method 1 was plotted against either the relation between the axial compression load and the maximum axial compression load or plotted against the relation between the external moment and maximum moment capacity. This was done for beam-columns with intermediate relative slenderness ($\bar{\lambda} = 1$) and steel strength class S355 in strong buckling direction.



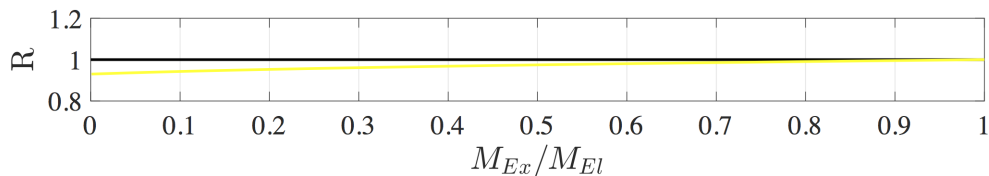
(a) Axial load, plastic analysis



(b) External moment, plastic analysis



(c) Axial load, elastic analysis

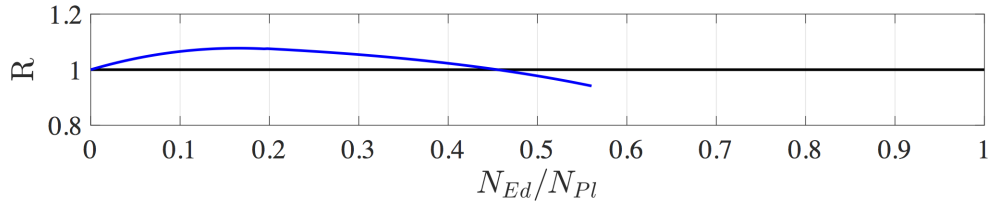


(d) External moment, elastic analysis

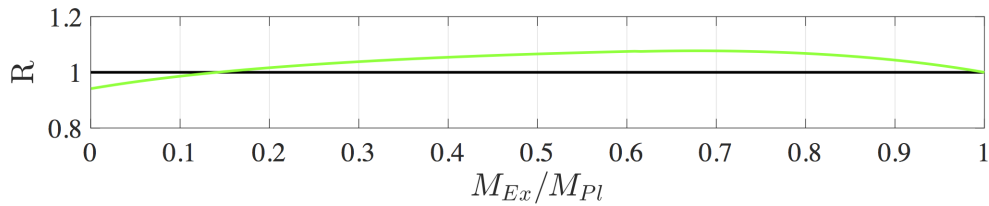
Figure 5.27: Analyse of a HEB 220 beam subjected to different combinations of axial load and external moment. For bending about strong axis, steel strength class S355 and intermediate relative slenderness.

As can be seen in the figure, the unfavourable results for the plastic analysis had largest magnitude for the combination of low axial load and high external bending moment. When the axial load increased and the external moment decreased, the ratio decreased as well. That was consistent with the results achieved for columns where the external moment was zero and the results were on the safe side. Regarding the elastic analysis, the results showed that for cases where the external moment consumes all capacity, the ratio was equal to 1 and with higher axial load, the ratio was lower. Also, this was consistent with the results for columns. The shape of the ratio curve presented here were consistent for all members. Though, with varying magnitude and location of maximum and minimum values. It was also noticed that the curve which presented axial compression ended before it reached the value 1. This was because at this point the full capacity of the member was reached and the axial load could not further increase since the internal

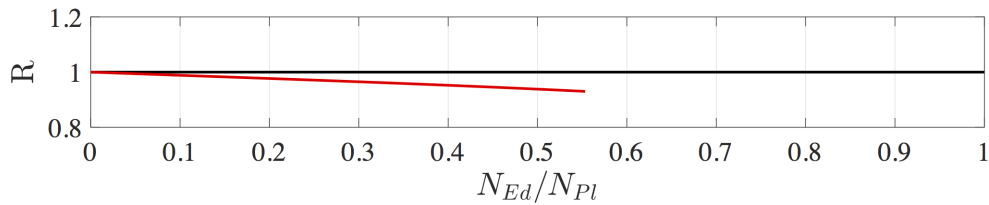
second-order moment withheld the rest of the capacity. Another interesting observation was seen in figure 5.27 where the absolute maximum value of the ratio for the plastic analysis has a pointy tip. The phenomenon was due to the reduction formula presented in chapter 3.1.2. If the exact method would have been used instead of the reduction formula, the result would be as in figure 5.28.



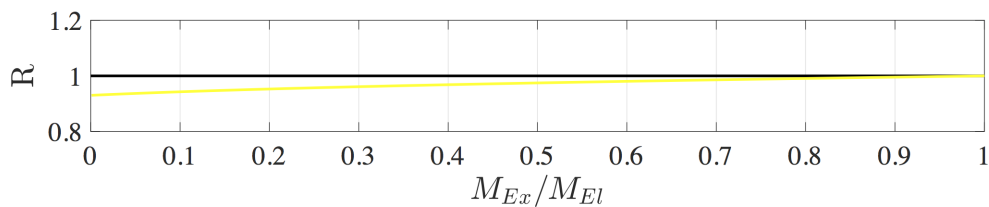
(a) Axial load, plastic analysis



(b) External moment, plastic analysis



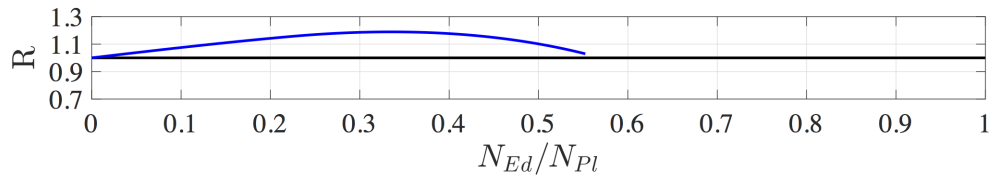
(c) Axial load, elastic analysis



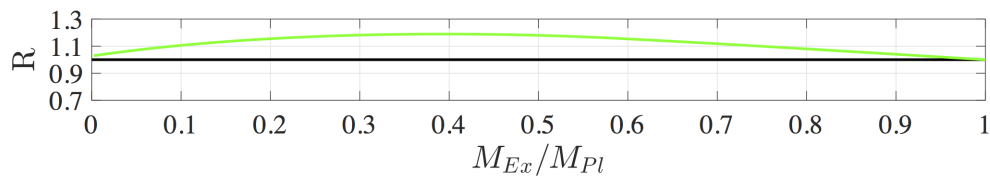
(d) External moment, elastic analysis

Figure 5.28: Analysis of a HEB 220 cross-section subjected to different combinations of axial load and external moment by using the exact method instead of reduction formula. For bending about strong axis, steel strength class S355 and intermediate relative slenderness

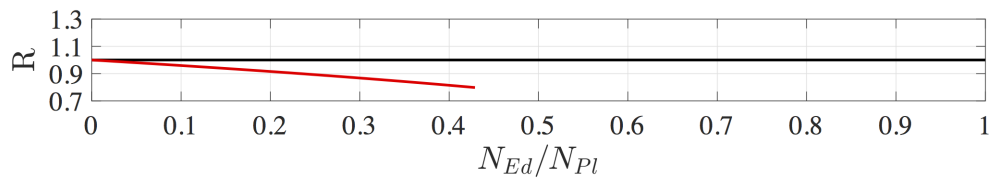
In this case, the curves were smooth instead of pointy. It can also be seen that the differences were small between the exact method and the method with the reduction formula. In figure 5.29, the result when using the reduction formula for weak buckling direction is shown.



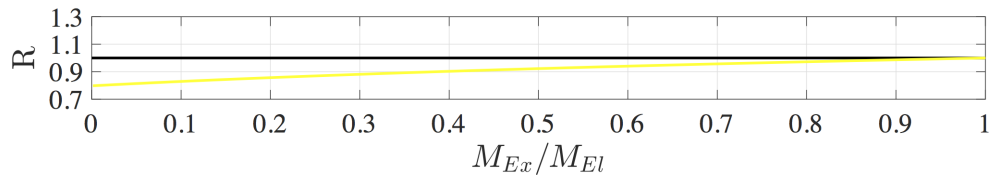
(a) Axial load, plastic analysis



(b) External moment, plastic analysis



(c) Axial load, elastic analysis



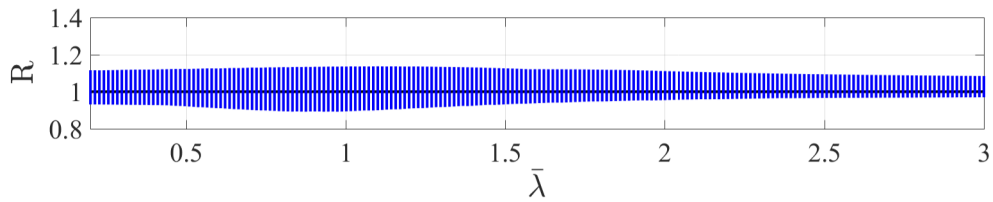
(d) External moment, elastic analysis

Figure 5.29: Analyse of a HEB 220 cross-section subjected to different combinations of axial load and external moment. Weak buckling direction, steel strength class S355 and intermediate relative slenderness.

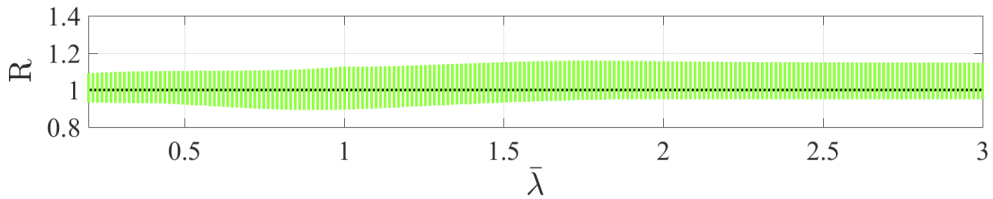
The figure shows that all combinations of axial load and external moment were on the unsafe side for the plastic analysis. This corresponded to the results obtained in figure 5.26. It was also observed that the maximum value was reached with a combination of relatively high axial load and low external moment compared to strong buckling direction. However, this was unique for the H and I cross-sections for weak buckling direction. Also, the curve did not have the pointy tip as for the strong buckling direction. This was consistent with the results received in figure 5.3d, where there was a smaller difference between the reduction formula and exact method.

External bending moment from an uniformly distributed load

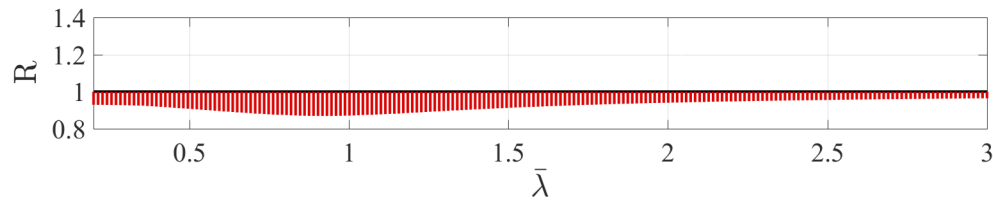
The other considered way to obtain an external bending moment was by a uniformly distributed load. The results for this are found in figure 5.30 for strong buckling direction and figure 5.31 for weak buckling direction. In the figures, only HEB cross-sections are considered. The results for the other cross-section types are found in appendix E.3 and E.4. Just as for the previous results, both a plastic and an elastic analysis were conducted.



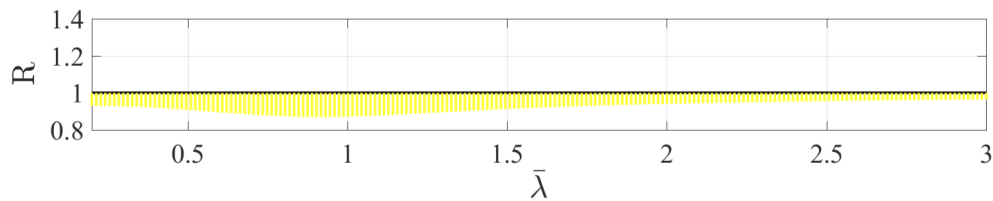
(a) Method 1, plastic analysis



(b) Method 2, plastic analysis

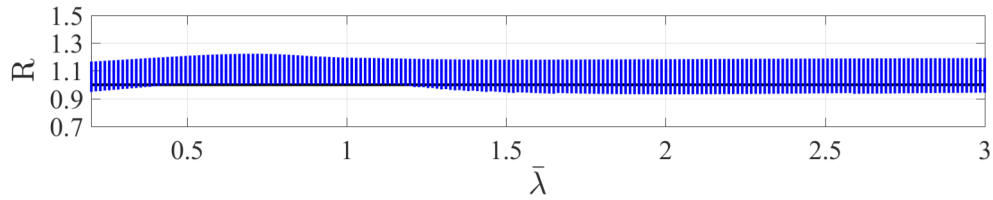


(c) Method 1, elastic analysis

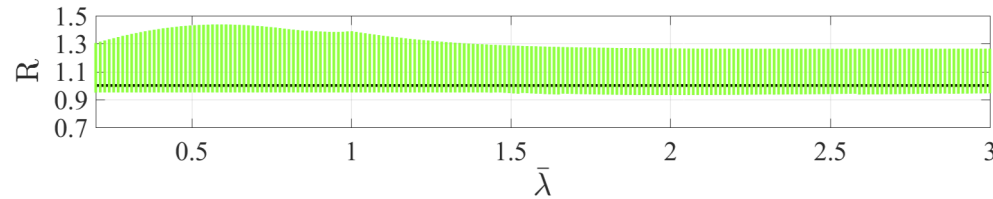


(d) Method 2, elastic analysis

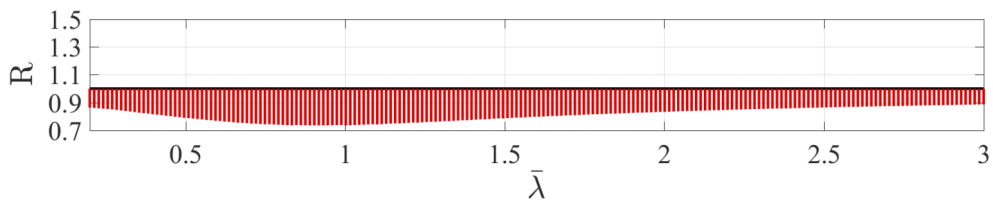
Figure 5.30: Results for beam-columns with HEB cross-sections, steel quality S355 and moment due to uniformly distributed load. Bending about strong axis.



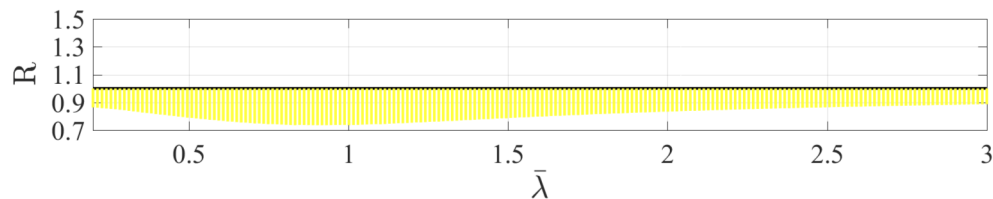
(a) Method 1, plastic analysis



(b) Method 2, plastic analysis



(c) Method 1, elastic analysis

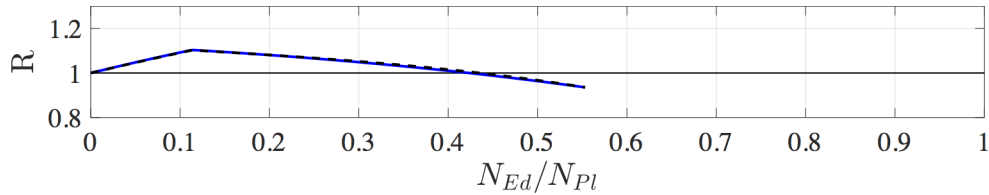


(d) Method 2, elastic analysis

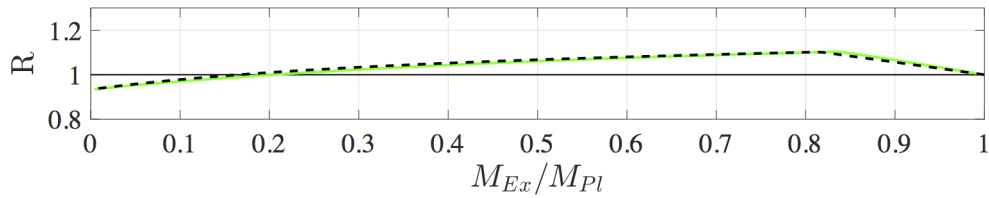
Figure 5.31: Results for beam-columns with HEB cross-sections, steel quality S355 and moment due to uniformly distributed load. Bending about weak axis.

By comparing the results for the different load cases, it was concluded that the results were similar for members subjected to uniform moment as for equal end moment. It was observed that the shape of the curves was mostly the same. However, the elastic analysis only gave results on the safe side while the plastic analysis showed more varying results depending on the combination of axial load and external moment for both strong and weak buckling direction. Just as for a member subjected to an equal end-moment, this load case was also evaluated specifically for a HEB 220 member with intermediate relative slenderness ($\bar{\lambda} = 1$). To enable a more detailed comparison between the load cases, the results are presented together with the results from the load case with equal end-moment in figure 5.32 and 5.33.

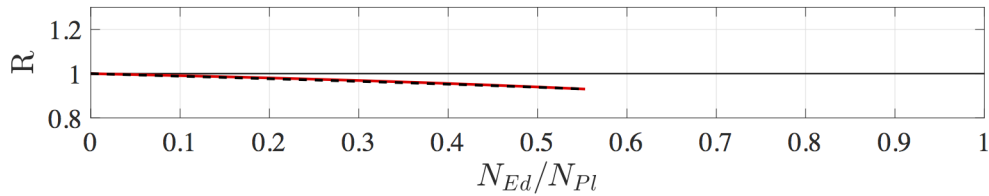
The black line represents the result from the analysis with equal end-moment while the coloured lines represents the results for the moment caused by a uniformly distributed load. As observed, the result was almost equivalent. This was explained with that the different magnitude of external moment due to the change in load conditions was similarly compensated in both the method with initial imperfections as well as Method 1 and 2.



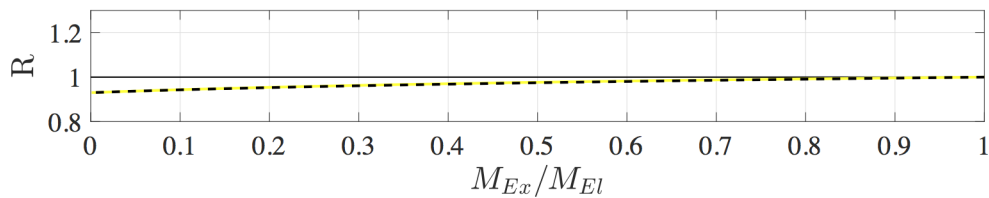
(a) Axial load, plastic analysis



(b) External moment, plastic analysis

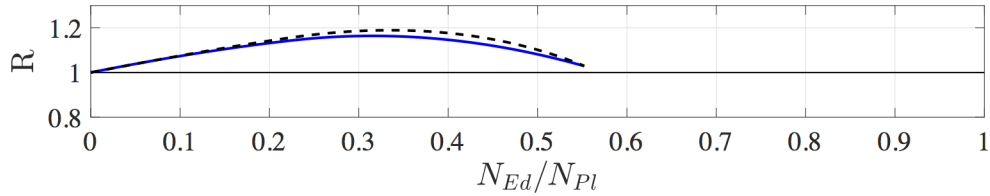


(c) Axial load, elastic analysis

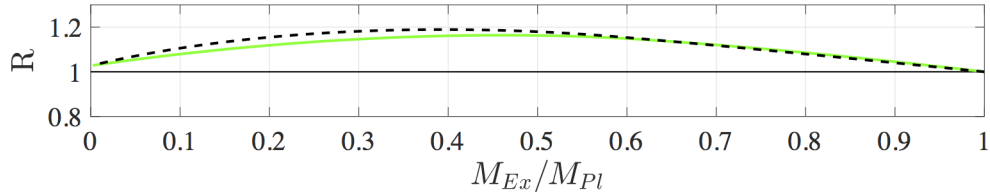


(d) External moment, elastic analysis

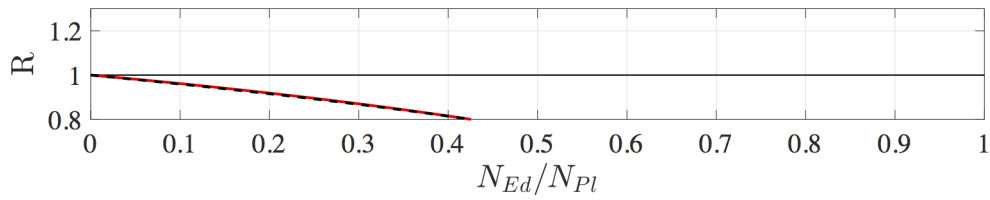
Figure 5.32: Plastic and elastic analysis of a beam-column with a HEB 220 cross-section subjected to different combinations of axial load and external moment caused by an uniformly distributed load. Steel strength class S355, intermediate relative slenderness and strong buckling direction.



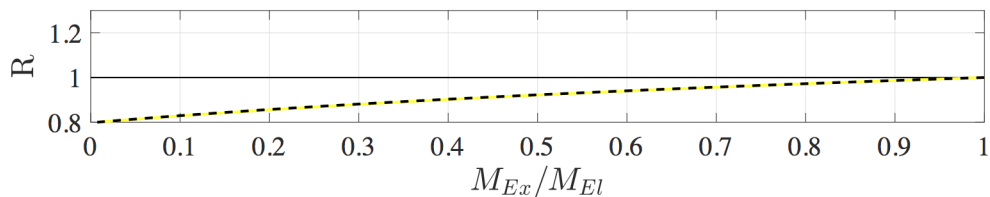
(a) Axial load, plastic analysis



(b) External moment, plastic analysis



(c) Axial load, elastic analysis



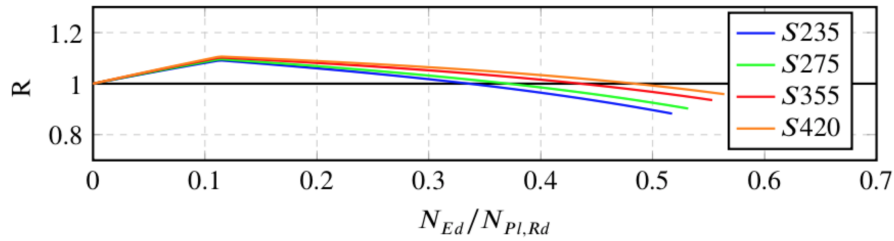
(d) External moment, elastic analysis

Figure 5.33: Plastic and elastic analysis of a beam-column with a HEB 220 cross-section subjected to different combinations of axial load and external moment caused by an uniformly distributed load. Steel strength class S355, intermediate relative slenderness and weak buckling direction.

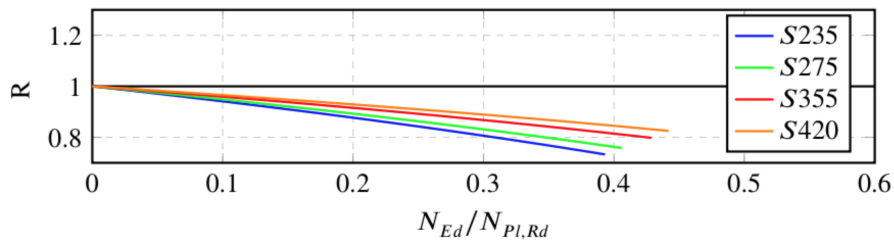
Comparison of different steel strength classes

Also for beam-columns, the effect of different steel strength classes was investigated. Due to the infinite number of axial load and bending moment combinations, the results were also here presented by plotting the ratio, R against the ratio between the axial load N_{Ed} and the maximum axial load $N_{Pl,Rd}$. The beam-column taken as example was one with a HEB 220 cross-section with a ratio based on Method 1. The results are shown in figure 5.34 where the black line represents the ratio (R) equal to 1 while the

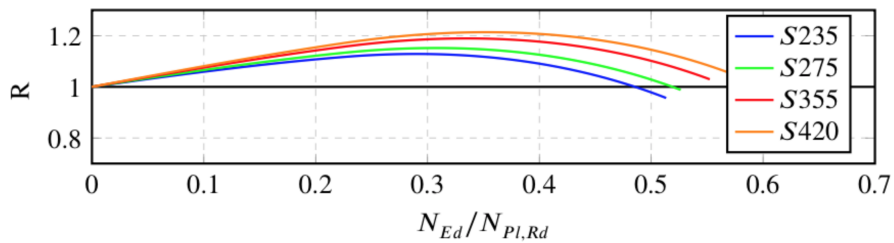
blue, green, red and orange lines represents steel strength classes $S235$ to $S420$, respectively. It was clear that both the magnitude of the ratio and the maximum capacity varied for different steel strength classes for both the plastic and elastic analysis. It was also observed that the biggest difference between steel strength classes occurred for cases with high axial load and low external moment.



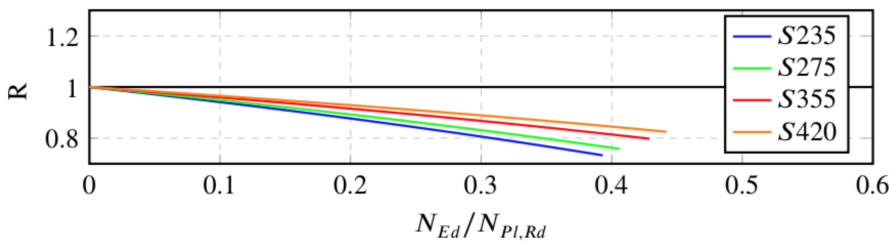
(a) Plastic analysis, strong buckling direction



(b) Elastic analysis, strong buckling direction



(c) Plastic analysis, weak buckling direction

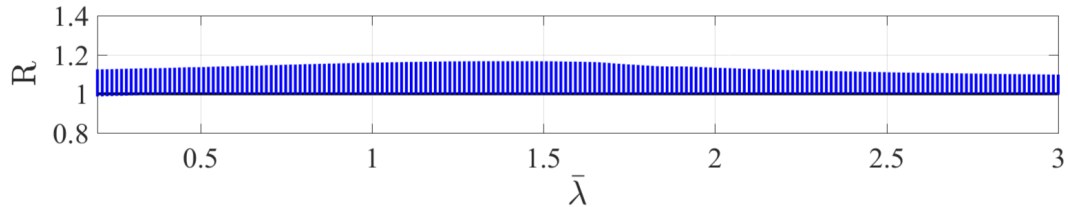


(d) Elastic analysis, weak buckling direction

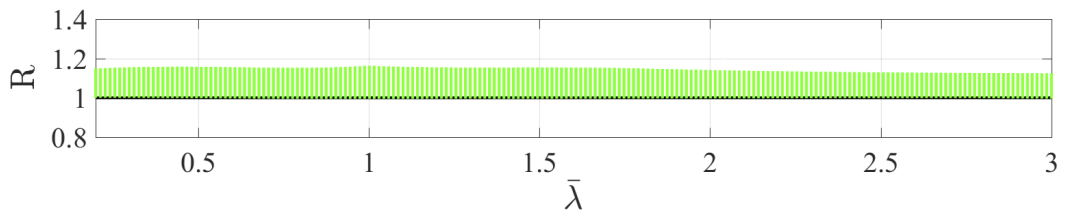
Figure 5.34: Comparison of steel strength classes for a beam-column with a HEB 220 cross-section subjected an axial load and equal external end-moment.

5.3.3 Optimisation of initial bow imperfection

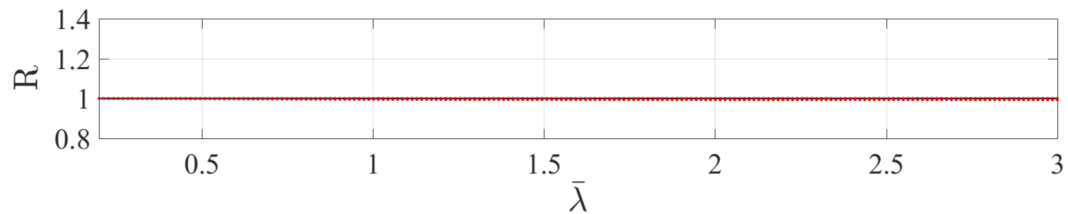
The optimised initial bow imperfection was also applied in the study of beam-columns. Initially, the formulas developed for columns (equation 5.1 and 5.2) were adopted. The results for this regarding HEB cross-sections are found in figure 5.35 for strong buckling direction and figure 5.36 for weak buckling direction.



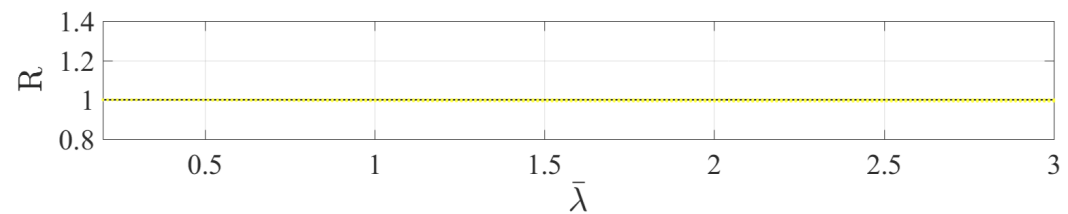
(a) Method 1, plastic analysis



(b) Method 2, plastic analysis

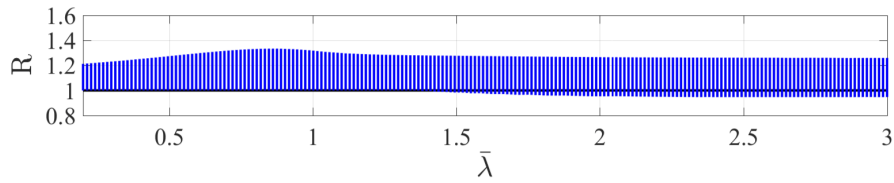


(c) Method 1, elastic analysis

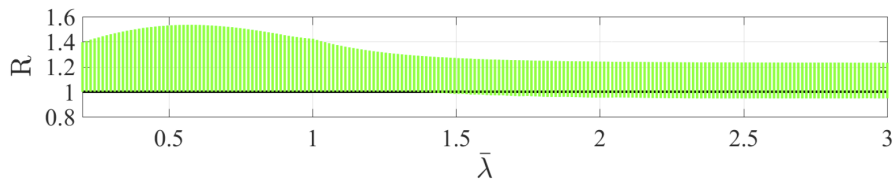


(d) Method 2, elastic analysis

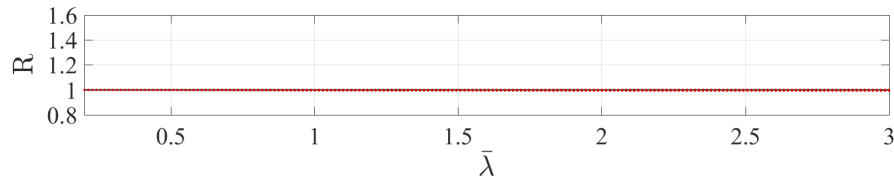
Figure 5.35: Plastic and elastic analysis with new formulas for the initial bow imperfection for a beam-column with a HEB 220 cross-section subjected to different combinations of axial load and external moment caused by an uniformly distributed load. Steel strength class S355, intermediate relative slenderness and strong buckling direction.



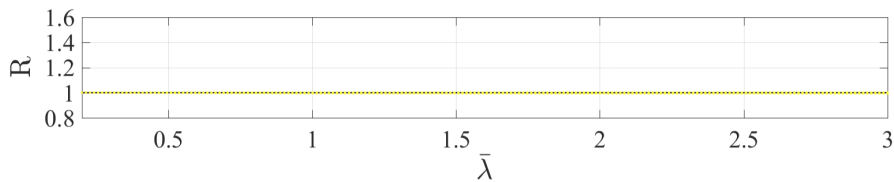
(a) Method 1, plastic analysis



(b) Method 2, plastic analysis



(c) Method 1, elastic analysis

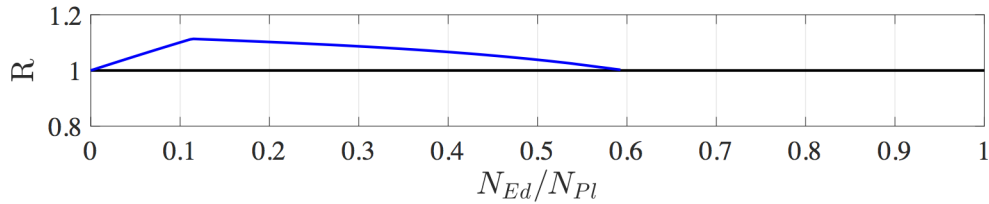


(d) Method 2, elastic analysis

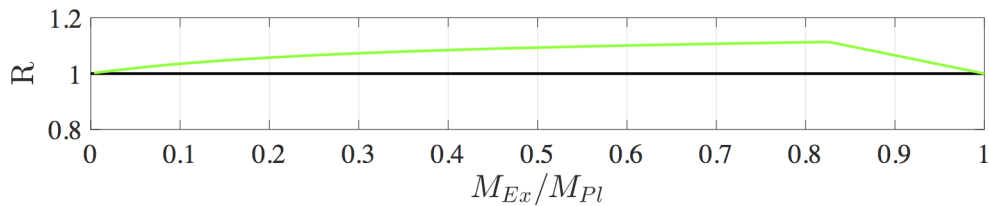
Figure 5.36: Plastic and elastic analysis with new formulas for the initial bow imperfection for a beam-column with a HEB 220 cross-section subjected to different combinations of axial load and external moment caused by an uniformly distributed load. Steel strength class S355, intermediate relative slenderness and weak buckling direction.

The results showed that the new formula for the initial bow imperfection worked well for the elastic analysis. In the plastic analysis it was seen that the new formula worked poorly for both strong and weak buckling direction. Using the new formula enhanced the magnitude of the ratio on the unsafe side and by that generated even more unfavourable results. However, it was also important to notice that the results on the safe side was no longer there and the lower limit of the ratio had a constant value of approximately 1. The results for the HEA, HEM, IPE, VKR and KKR cross-sections were similar and therefore found in appendix E.5 for strong buckling direction and appendix E.6 for weak buckling direction.

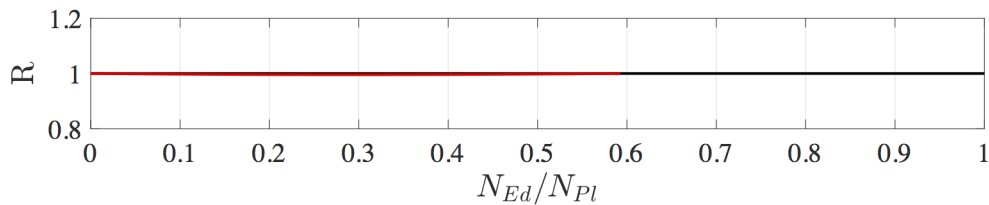
Just as in the previous section, a closer study of the ratio between the external moment and the axial compressive load was made for a HEB 220, which is presented in figure 5.37 and 5.38. For the elastic analysis, all ratios were equal to 1, which was optimal. The results for the plastic analysis showed that the shape of the curve was similar for the new initial imperfection formula as for the old value. The only difference was that the magnitude was higher on the unsafe side which was in accordance with the results presented in figure 5.35 and 5.36.



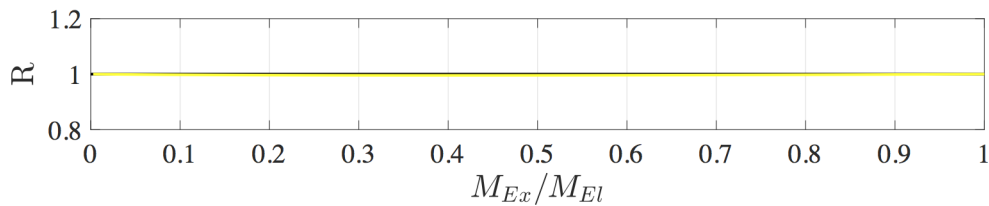
(a) Axial load, plastic analysis



(b) External moment, plastic analysis

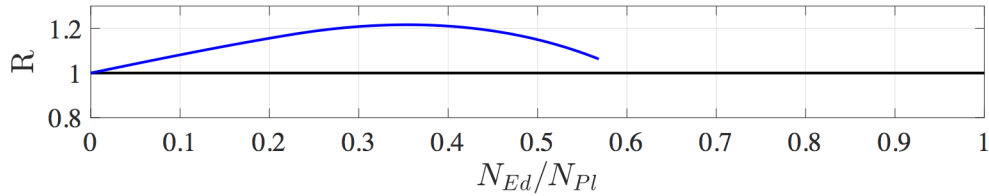


(c) Axial load, elastic analysis

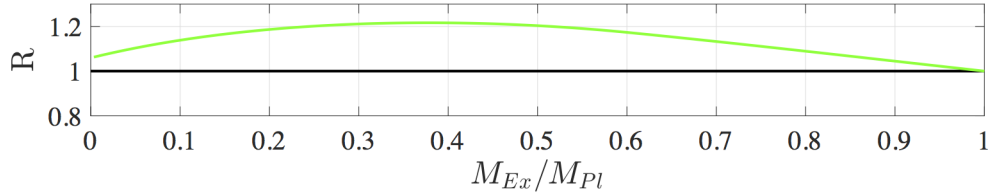


(d) External moment, elastic analysis

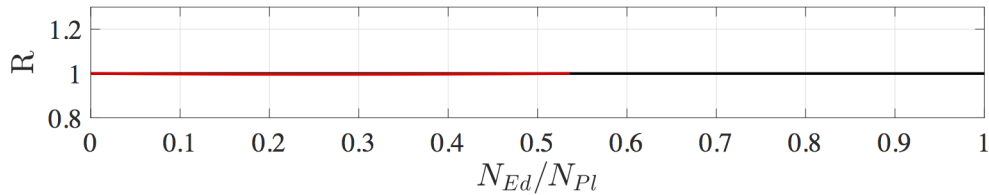
Figure 5.37: Analysis of a HEB 220 member using the improved $e_{0,d}$ formulae. For bending about strong axis, steel strength class S355 and an intermediate relative slenderness.



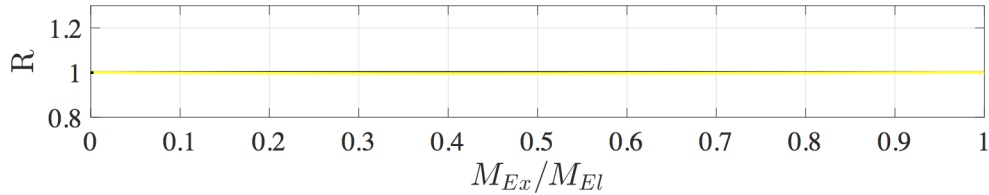
(a) Axial load, plastic analysis



(b) External moment, plastic analysis



(c) Axial load, elastic analysis



(d) External moment, elastic analysis

Figure 5.38: Analyse of a HEB 220 member using the improved $e_{0,d}$ formulae. For bending about weak axis, steel strength class S355 and an intermediate relative slenderness.

The highest deviation of the unsafe results was achieved for a combination of a high external moment and a low axial compression load. It was also seen that for combinations of high axial compression loads and low external moment, which was the case for columns, the ratios were equal to 1. This was in accordance with the results achieved for columns where the new formula fitted well even for the plastic analysis. In the progress of improving the formula for the initial bow imperfection, it became evident that no combination of factors in the formula was reasonable to use to achieve a good approximation.

5.4 Numerical results for beam-columns

Regarding the numerical analysis of beam-columns, only the load case with an external end-moment for IPE 140 and HEB 220 cross-sections in strong buckling direction was investigated. Since Abaqus could not iterate through an infinite combination of axial loads and moments, the ratio between the axial compression load and external moment was constant throughout the analysis. This implied that for each iteration step, the ratio between the axial load and external moment remained the same until the maximum capacity was reached and then the iteration ended. The maximum axial load and external end-moment were collected from the numerical analysis and inserted into the analytical calculation methods, which resulted in either favourable or unfavourable results. The results from the plastic analysis are presented separately for each cross-section in table 5.7a and 5.7b. The second column represents the percent of the maximum capacity from the method with initial imperfections using the axial load and external moment from the numerical analysis. The third and fourth column represents the same, but for Method 1 and 2. The last column shows how many percentage points (*pp.*) the axial load and external moment needed to be increased with to reach full capacity in the method with the initial imperfection.

Table 5.7: Comparison of analytical and numerical results for beam-columns. Strong buckling direction.

(a) HEB 220 cross-section

Relative slenderness $\bar{\lambda}$ [-]	Difference [%] (init. imp.)	Difference [%] (method 1)	Difference [%] (method 2)	Increase [<i>pp.</i>]
0.4	-4.5	2.6	4.5	4.0
1.0	-9.2	0.2	2.7	7.0
1.8	-9.5	1.1	1.6	7.2

(b) IPE 140 cross-section

Relative slenderness $\bar{\lambda}$ [-]	Difference [%] (init. imp.)	Difference [%] (method 1)	Difference [%] (method 2)	Increase [<i>pp.</i>]
0.4	-2.8	3.2	4.4	2.8
1.0	-6.3	0.2	0.9	6.1
1.8	-7.3	0.5	1.6	6.1

Overall, this analysis gave similar results as the numerical analysis of columns did. For the method with an initial bow imperfection, the maximum capacity was lower for the numerical analysis compared to the analytic. One difference between the numerical analysis for columns compared to beam-columns were that for beam-columns, the results from numerical analysis were also directly compared with Method 1 and 2. This gave a much better compatibility where the results were just slightly on the unsafe side. This corroborated the conclusion that the method with an initial bow imperfection overestimated the capacity when used in analytic analysis.

5.5 Summary of results

As stated in section 5.1.4, the comparison between the method with an initial bow imperfection and the buckling curves for columns subjected to only axial compression loads generally showed favourable results. For the strong buckling direction, the results were mostly independent of which cross-section that was analysed since all results were on the safe side considering both the plastic and elastic analysis. However, the elastic analysis showed a slightly lower capacity than the plastic analysis. For the weak buckling direction, the analysis had a larger deviation between different types of cross-sections and analysis type. All results were on the safe side except for the plastic analysis of I and H members. It was also concluded that the results presented in this study was in occurrence with the results presented in the article written by Lindner et al. (2016). The comparison of different steel strength classes showed that the method with an initial bow imperfection reached different capacities for different steel strength classes and that the capacity increased with increasing steel strength class. Calculations with the buckling curve method showed results which were independent of the steel strength class. Thus, it was concluded that the formula for the initial bow imperfection depended on the steel strength class while the method with buckling curves did not.

Since the analysis with an initial bow imperfection mostly showed results on the safe side, the possibility of optimising the method arose. The first optimisation consisted of decreasing the value of the initial bow imperfection and by that reaching higher capacities. The conclusion from this was that the results corresponded better but there were still deviations regarding some values of the relative slenderness and the problem with different capacities for different steel strength classes were still present. The second optimisation of the initial bow imperfection consisted of using the formula presented by Goncalves and Camotim (2005) which was dependent on relative slenderness instead. This gave good results for the elastic analysis but a too high capacity for the plastic analysis. To correct this, the formula was customised to fit the plastic analysis with a factor of the ratio between the plastic and elastic section modulus. The outcome was good for both the plastic and elastic analysis for strong buckling directions for all members. This also solved the problem with the steel strength classes since this new formula was independent of the steel strength class. When regarding weak buckling direction, the use of the new formula for the initial bow imperfection rendered different results. The elastic analysis showed good results for all cross-sections, while the plastic analysis deviated for H and I members. Here, the results were more unfavourable compared to the original values for the initial bow imperfection. To solve this, the formula was further developed by using additional factors for this case specifically, which generated a variation of results. The conclusion was that it was possible to create a formula suitable for the plastic analysis of columns with H and I cross-sections, but it was decided not to further analyse it in this thesis.

Overall, the results from the FE-analysis showed that all examined members experienced a lower capacity than with the analytic calculation. This was the case for both buckling directions but the magnitude of the deviation was greater for H and I cross-sections in weak buckling direction. The optimisation was conducted on the FE-analysis as well, using the same optimised equations for initial bow imperfection that were used in the analytic analysis, see equations 5.1 and 5.2. The results showed that for the elastic analysis, the same equation presented reasonable good results for both buckling directions. For the plastic analysis, the most desirable results were obtained when the equation without the extra factor (equation 5.6) was used. In the analytic analysis, the extra factor was needed to not exceed the capacity

of the buckling curves. Just as for the analytic analysis, the FE-analysis showed slightly less consistent results for weak buckling direction regarding columns with H and I cross-sections.

The analysis of beam-columns showed similar results for both considered load cases. For the plastic analysis of members in strong buckling direction, the results were varying with combinations of axial compression loads and external moments on both safe and unsafe side. The elastic analysis on the other hand presented results exclusively on the safe side regardless of the combination of loads. A closer analyse on a HEB 220 member with the intermediate relative slenderness showed that for the plastic analysis the most unfavourable results were reached with a combination of low axial compression load and high external moment. When the axial load was increased, the maximum capacity decreased and for only axial load the results were on the safe side which was consistent with the results regarding columns. Also, the results from the elastic analysis was consistent with columns for cases with high axial load. The results were generally the same for all types of members, only the magnitude of the ratio varied.

For the weak buckling direction, the results for beam-columns were similar to the results for columns, just as for the strong buckling direction. The general results for weak buckling direction were close to strong buckling direction except for the plastic analysis of H and I members. Another interesting observation for the analysis of weak buckling direction was that the plastic analysis of H and I members also resulted in deviations between Method 1 and 2 where Method 2 showed very high differences. This result was not very reliable thus the conclusion was that either there was something incorrect in the approximation in Method 2 for those members, or the calculations computed in this study was incorrectly interpreted. It should also be noted that Method 1 and 2 are based on an analysis of a lot of different cross-sections and thereby an approximation of all results. The drawn conclusion was therefore that the corroboration between Method 1 and 2 might not be equivalent for all members since some cross-sections might give less accurate results. This might be the case for H and I members when regarding Method 2 and weak axis buckling direction. Just as for columns, the steel strength classes affected the results for beam-columns in the same manner, where higher steel strength class resulted in higher capacities. This was true for all members for both buckling directions.

It was concluded in the optimisation process of beam-columns that the formula derived for columns also gave good results for the elastic analysis for beam-columns in both buckling directions. The conclusion regarding the plastic analysis was that the new formula increased the ratio on the unsafe and decreased the ratio on the safe side which made all results more unfavourable. This was true for both buckling directions. When studying the ratios for the plastic analysis of a HEB 220 member in more detail, it was clear that for combinations of high external moment and low axial load the magnitude of the deviation was the highest. On the other hand, a combination of high axial load and low external moment showed results close to 1, which was the case for a column subjected to only an axial load. The conclusion was that no formula for the initial bow imperfection was reasonable to use to achieve a good approximation for the plastic analysis. This was because the largest deviation of results was reached when the external moment was relatively high. Thus, the part of the total moment that consisted of a second-order moment due to the initial imperfection was low. That meant that no matter how much the value of initial imperfections was lowered and by that obtaining a lower second order moment, the total moment was basically the same. The conclusion drawn from this was that the method with an initial bow imperfection used when calculating the capacity of the beam-column was somehow overestimating the capacity of the member when considering high external moments.

The numerical analysis of beam-columns consisted of a comparison with analytic results only. The analysis considered both buckling directions but did not include the optimisation of the formula for initial bow imperfection. The results did as usual comprehend well with the results achieved when regarding columns, i.e. with lower capacities for numerical analysis compared to analytic analysis. However, the numerical analysis of beam-columns did show good results when being compared to Method 1 and 2, just a bit on the unsafe side. This corroborated the conclusion that the method with initial bow imperfection somehow overestimated the capacity of the member.

5.5.1 Reflections over the deviations in the results

As was presented in chapter 2.4, a difference in capacity between the elastic and plastic analysis was expected. It was clear that results from the elastic analysis only reached a yield moment or load capacity while results from the plastic analysis utilised the plasticity of the member and thus reached higher capacity. Focusing on the comparison between numerical and analytic analysis which was presented in chapter 5.2.2, it was clear that the maximum plastic capacity differed between the two, while the elastic results were mostly similar. This was based on that the curves were aligned until the yield stress was reached. The conclusion of this was that the difference in the final results was because of how the different methods handled the plasticity of the member. This was based in the interpretation of Young's modulus between the analysis types since it defines the relationship between the stress and strain in the material. Thus, a measurement of the stiffness with higher Young's modulus gives a higher stiffness and results in a higher capacity. The relation between stress and strain used in Abaqus for the elastic-plastic behaviour is presented in figure 4.1a. The gradient of the line represents Young's modulus and is assumed constant during the elastic part and when the yield strength is reached, Young's modulus becomes zero during the plastic part of the analysis. This was not the case for analytic calculations where Young's modulus was assumed to be constant during the plastic part as well, see figure 5.39.

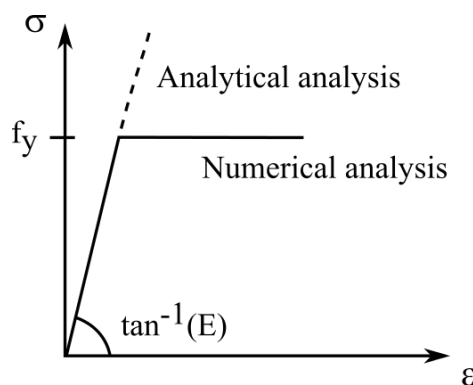


Figure 5.39: Stress-strain relation used in analytic analysis (dotted line) and numerical analysis (solid line).

Since the stress-strain relation used in Abaqus assumed a zero value of the Young's modulus during plasticising of the cross-section, it affected the critical buckling load and the second order moment. As explained in figure 5.40, the cross-section of a member gradually plasticises with increasing load. Thus, for the part of the cross-section that have plasticised the stiffness would be zero, which affected the total stiffness of the cross-section. This meant that for each increasing load step the total stiffness of the cross-section decreased. That resulted in that the maximum capacity was reached quicker in the

numerical analysis compared to the analytic analysis where the stiffness was assumed to be constant all through the plasticising process.

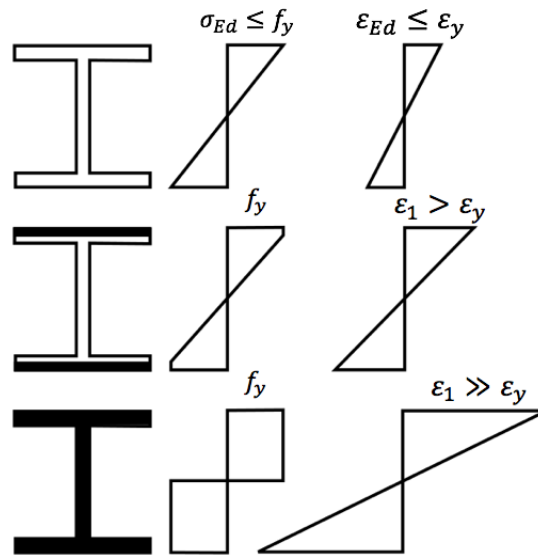


Figure 5.40: Gradually plasticising of cross-section with increased stress.

This could also be expressed as an equivalent moment of inertia I_{eq} where the E and I in equation 2.9 was merged together which generated equation 5.7. Thus, this phenomenon could also be interpreted as a new lower moment of inertia for every step of the cross-section that plasticised where the plasticised part of the cross-section was deemed to be consumed and did not anymore contribute to the plastic capacity.

$$N_{cr} = \frac{\pi^2 I_{eq}}{L^2} \quad (5.7)$$

That meant that in the next load step, the equivalent moment of inertia was a bit smaller than in the previous step, which lead to that the maximum plastic capacity was reached quicker. However, this was only true for the part of the member that was already buckled. Thus, for the load cases used in this thesis it only applied to the middle of the members. So, if the system with an equivalent moment of inertia were to be applied in theory analytically, it would mean that equivalent moment of inertia only should be considered in the buckled part of the member, the rest should be calculated as usual.

This theory explained the differences in the results between numerical and analytic plastic analysis for both columns and beam-columns. It also explained the different behaviour between strong and weak buckling direction as well as for different cross-section types. The bending resistance of the cross-section was mostly in the flanges, which meant that a higher ratio of the flanges compared with the total area resulted in a higher plastic capacity. As long as the plasticity of the cross-section did not yet reach the web, the stiffness was still relatively high. Thus, the capacity was closer to the case of constant stiffness. As soon as the plasticity reached the web, the final capacity was reached almost immediately.

In members where the flanges formed a large part of the total cross-section height, a higher stiffness could be maintained longer before the web started to plasticise. The conclusion was that H members with a relatively large flange height plasticised slower and therefore a final capacity closer to that of analytic analysis was achieved. *I* cross-sections on the other hand had a lower relative flange thickness. Hence, the results in capacities differed more between numerical and analytical analysis. VKR and KKR cross-sections ended up somewhere close to *I* cross-sections but slightly better since the size of flanges were mostly equal but VKR and KKR members have two webs, which contributes twice as much bending resistance as only one web.

In the weak buckling direction, the final plastic capacity was reached much earlier for columns with H and I cross-sections since there are almost no amount of flange area to consider in that direction. Columns with VKR and KKR cross-sections behaved mostly the same for both buckling directions. This was the reason between the more pronounced differences between both buckling directions for H and I members which was presented in section 5.1.4. This might also explain the unfavourable results achieved in the analytic plastic analysis for H and I columns in weak buckling direction. Since the buckling curves was based on physical tests and the real member experienced some of the same stress-strain behaviour as in Abaqus, the maximum capacity was lower compared to the analytic analysis. The solution could be to add an extra factor to the calculation of the initial bow imperfection for the plastic analysis of H and I columns in weak buckling direction. This factor would need to consider the quicker losses in stiffness that the cross-section experiences compared to the strong buckling direction.

This phenomenon also explained why the new formula for the initial bow imperfection needed the extra factor for the plastic analytic analysis compared to plastic numerical analysis, see equation 5.2 and 5.6. The extra factor compensated for the overestimated capacity in the cross-section reached in the analytical analysis when the stiffness was assumed to be constant throughout the whole plasticity process. For the elastic analysis, the same equation could be used since the conditions were the same.

6 Conclusions

For columns, when comparing the method with initial bow imperfection to the method using buckling curves, most results were on the safe side considering both strong and weak buckling direction. Though, there were deviating results for the plastic analysis of both I and H cross-sections in weak buckling direction, where the results were unfavourable. The safe margin for the favourable results together with the unfavourable results opened the possibility to optimise the initial bow imperfection.

In the process of optimising, it was discovered that the new formula for the initial bow imperfection presented in Goncalves and Camotim (2005) generated desirable results for the elastic analysis. However, regarding the plastic analysis the formula needed further improvement to generate good results, which was achieved by adding an extra factor. However, I and H cross-sections, plastic analysis and bending about weak axis still resulted in capacities on the unsafe side. The conclusion regarding this specific case was that an extra factor or another equation was needed to achieve desirable results. One example of such a solution was presented in this study, beyond that this was a problem not further considered in this study.

Additionally, the original expressions for initial bow imperfections, i.e. those in the current version of Eurocode 3, generated different capacities for various steel strength classes. This was a problem because the capacities obtained from the buckling curve method was independent of the steel strength class. However, the result of using the new formulas for the initial bow imperfection was that also this method became independent of steel strength classes which was desirable.

The elastic analysis of beam-columns generated results only on the safe side while the plastic analysis resulted in varying capacities both on safe and unsafe side. Those were the cases for all cross-sections and for both buckling directions. Just as for columns, the only exception was for plastic analysis of I and H cross-sections for weak buckling direction where the results generally were more unfavourable. A closer study of a HEB 220 cross-section showed that the most unfavourable result was obtained when a high external moment was combined with a low axial load. On the other hand, a combination of a low external moment and a high axial load gave similar results as for columns, which was considered reasonable.

Further, the optimised formulae for columns were implemented in the beam-column calculations. For the elastic analysis, these formulae generated excellent results equivalent to a utility ratio off 1. For plastic analysis on the other hand, the results were even more unfavourable compared to the results generated with the use of the original initial bow imperfection from EN-1993-1-1 (2005). Also here, the most unfavourable case was for a combination of a high external moment and low axial load. Therefore, a conclusion was that the method with an initial bow imperfection overestimated the capacity of the members with a relative high external moment compared to axial load. However, an adjustment of the initial bow imperfection was not a solution of the problem since its influence on the total moment was small compared to the external moment.

When the original initial bow imperfection was inserted into the FE-analysis, all results for both columns and beam-columns obtained a lower capacity in the numerical results than in analytical. The deviation

was largest in the plastic analysis for cross-sections in weak buckling direction. When the optimised initial bow imperfection for columns was implemented in Abaqus, the results comprehended well for the elastic analysis. Regarding the plastic analysis, the best correlation to the buckling curves was obtained by slightly adjusting the formula for the initial bow imperfection.

The difference between numerical and analytical results was explained by how the stress-strain relation was treated. Analytically, the modulus of elasticity was assumed to remain constant throughout all calculation steps. Numerically on the other hand, the elastic-perfectly plastic material behaviour was considered by assuming the modulus of elasticity being constant until the yield limit was reached. After that, when the cross-section started to plasticise, it became zero. The meaning of that was that the stiffness of the member decreased with each load step, which in turn affected the moment resistance. Thus, the maximum capacity was reached earlier. This was also the reason for the difference of cross-section type, bending direction and analysis type.

A conclusion for columns was that the new formulae for the initial bow imperfection worked well. For beam-columns the number of numerical analyses was not sufficient to draw any final conclusions, but the analytic analyses gave some optimistic indications. Lastly, it should be perceived that the results and conclusions of this thesis only gave a groundwork of the subject. The next step would be to further corroborate the findings of the numerical analysis with additional members, load cases and boundary conditions. After that, the method should be developed into considering the effect of out-of-plane buckling to finally reach the level of frames and similar structures.

References

- EN-1993-1-1. (2005). *Eurocode 3: Design of steel structures - part 1-1: General rules and rules for buildings*. European Committee for Standardisation.
- EN-1993-1-5. (2006). *Eurocode 3: Design of steel structures - part 1-5: Plated structural elements*. European Committee for Standardisation.
- Bjorhovde, R. (1972). *Deterministic and probabilistic approaches to the strength of steel columns* (Doctoral dissertation, Lehigh University Bethlehem, PA).
- Boissonnade, N., Greiner, R., Jaspart, J.-P., & Lindner, J. (2006). *Rules for member stability in en 1993-1-1: Background documentation and design guidelines*. ECCS-European Convention for Constructional Steelwork.
- Boissonnade, N., Jaspart, J.-P., Muzeau, J.-P., & Villette, M. (2004). New interaction formulae for beam-columns in eurocode 3: The french–belgian approach. *Journal of Constructional Steel Research*, 60(3), 421–431.
- da Silva, L. S., Simões, R., & Gervásio, H. (2010). *Design of steel structures: Eurocode 3, part 1-1, general rules and rules for buildings*. ECCS-European Convention for Constructional Steelwork.
- Al-Emrani, M. (2014). *Finite element analysis (fea) of a girder with corrugated web w.r.t. lateral torsional buckling: Modelling in abaqus*.
- Al-Emrani, M. & Åkesson, B. (2013). *Steel structures course literature - vsm 191*. Department of Civil and Environmental Engineering, Division of Structural Engineering, Chalmers University of Technology.
- Al-Emrani, M., Engström, B., Johansson, M., & Johansson, P. (2013). *Bärande konstruktioner - del 1*. Department of Civil and Environmental Engineering, Division of Structural Engineering, Chalmers University of Technology.
- Galambos, T. V. & Surovek, A. E. (2008). *Structural stability of steel: Concepts and applications for structural engineers*. John Wiley & Sons.
- Gambhir, M. (2004). *Stability analysis and design of structures*. Springer Science & Business Media.
- Goncalves, R. & Camotim, D. (2005). On the incorporation of equivalent member imperfections in the in-plane design of steel frames. *Journal of Constructional Steel Research* 61 (2005) 1226-1240, 61.
- Greiner, R. & Lindner, J. (2006). Interaction formulae for members subjected to bending and axial compression in eurocode 3—the method 2 approach. *Journal of Constructional Steel Research*, 62(8), 757–770.
- Jönsson, J. & Stan, T.-C. (2017). European column buckling curves and finite element modelling including high strength steels. *Journal of Constructional Steel Research*, 128, 136–151.
- Lindner, J., Kuhlmann, U., & Just, A. (2016). Verification of flexural buckling according to eurocode 3 part 1-1 using bow imperfections. *Steel Construction*, 9(4), 349–362.
- SIMULIA. (2014). *Abaqus 6.14 documentation collection: Abaqus analysis user's guide*.
- Szalai, J. & Pappb, F. (2010). On the theoretical background of the generalization of ayrton-perry type resistance formulas. *Journal of Constructional Steel Research* 66 (2010) 670-679, 66.
- Ziemian, R. D. (2010). *Guide to stability design criteria for metal structures*. John Wiley & Sons.

A Considered columns in numerical analysis

The contents of table A.1a and A.1b represents the lengths of the structural members used in the FE-analysis. The lengths were set so that the relative slenderness $\bar{\lambda}$ for each cross-section (with rolled parts neglected) was equal to 0.4, 1.0 and 1.8. Thus, members with low, intermediate and high relative slenderness.

Table A.1: Lengths of members used in the FE-models corresponding to low, intermediate and high relative slenderness.

(a) Strong buckling direction.

Cross-section type	Length, L [mm] (low relative slenderness)	Length, L [mm] (intermediate relative slenderness)	Length, L [mm] (high relative slenderness)
HEB 220	2886	7213	12983
IPE 140	1751	4377	7879
VKR 90 × 50 ($t = 4$)	990	2475	4455

(b) Weak buckling direction.

Cross-section type	Length, L [mm] (low relative slenderness)	Length, L [mm] (intermediate relative slenderness)	Length, L [mm] (high relative slenderness)
HEB 220	1734	4335	7803
IPE 140	512	1279	2302
VKR 90 × 50 ($t = 4$)	618	1544	2780

B Comparison of B21 and B23 beam elements.

Table B.1a and B.1b shows the results obtained when comparing Euler-Bernoulli (B23) och Timoshenko (B22) beam elements. The results are presented as the difference in percent between the non-linear second order FE-analysis and the hand-calculations at critical point. The first table regards axial load and the second total bending moment.

Table B.1: Difference between the results obtained from the non-linear second order buckling analysis and the hand calculations using Euler-Bernoulli or Timoshenko beam elements for a HEB 220 member.

(a) Difference in axial load

Relative slenderness, $\bar{\lambda}$ [–]	Difference [%] (B21 beam elements)	Difference [%] (B23 beam elements)
0.4	–1.35	–1.38
1.0	–4.74	–4.56
1.8	–3.48	–3.38

(b) Difference in bending moment

Relative slenderness, $\bar{\lambda}$ [–]	Difference [%] (B21 beam elements)	Difference [%] (B23 beam elements)
0.4	3.22	2.27
1.0	–8.53	–8.89
1.8	–14.44	–14.61

C Verification of Matlab programme

This appendix presents more data on the verification of Matlab calculations regarding analytic analysis. Both results for columns and beam-columns are presented.

C.1 Columns

The results for a HEB 220 cross-section is presented in table C.1 and for a VKR 90x50x4 cross-section in table C.2. The accuracy is presented in percentage form, thus 100 % equals a perfect match between the results from Matlab and the results from hand calculations.

Table C.1: Verification of Matlab programme compared to hand calculations for HEB 220, steel strength class S355.

Type: HEB 220	Buckling curve	α	$e_{0,d}$	$\bar{\lambda} = 0.4$	$\bar{\lambda} = 1$	$\bar{\lambda} = 1.8$	Status
Strong direction Plastic analysis	b	0.34	$\frac{L}{200}$	99.9%	99.9%	99.9%	OK
Strong direction Elastic analysis	b	0.34	$\frac{L}{250}$	100%	100%	100%	OK
Weak direction Plastic analysis	c	0.49	$\frac{L}{150}$	99.9%	99.8%	99.9%	OK
Weak direction Elastic analysis	c	0.49	$\frac{L}{200}$	99.9%	99.9%	99.9%	OK

Table C.2: Verification of Matlab programme compared to hand calculations for VKR 90 × 50 ($t = 4$), steel strength class S355.

Type: VKR 90x50x4	Buckling curve	α	$e_{0,d}$	$\bar{\lambda} = 0.4$	$\bar{\lambda} = 1$	$\bar{\lambda} = 1.8$	Status
Strong direction Plastic analysis	a	0.21	$\frac{L}{250}$	99.9%	99.8%	99.6%	OK
Strong direction Elastic analysis	a	0.21	$\frac{L}{300}$	99.5%	99.7%	99.8%	OK
Weak direction Plastic analysis	a	0.21	$\frac{L}{250}$	99.8%	99.8%	100%	OK
Weak direction Elastic analysis	a	0.21	$\frac{L}{300}$	100%	99.7%	100%	OK

The comparison between analytic analysis and the results presented by Lindner et al. (2016) for all HEA cross-sections are presented in figure C.1 The results considers plastic analysis for bending about the strong axis and are presented with non-dimensional value j vs. relative slenderness ratio $\bar{\lambda}$. The thick black line represents all results for HEA columns obtained from Matlab. The blue line shows where the initial bow imperfection according to EN-1993-1-1 (2005) is and the green line marks the lowest value

presented in Lindner et al. (2016).

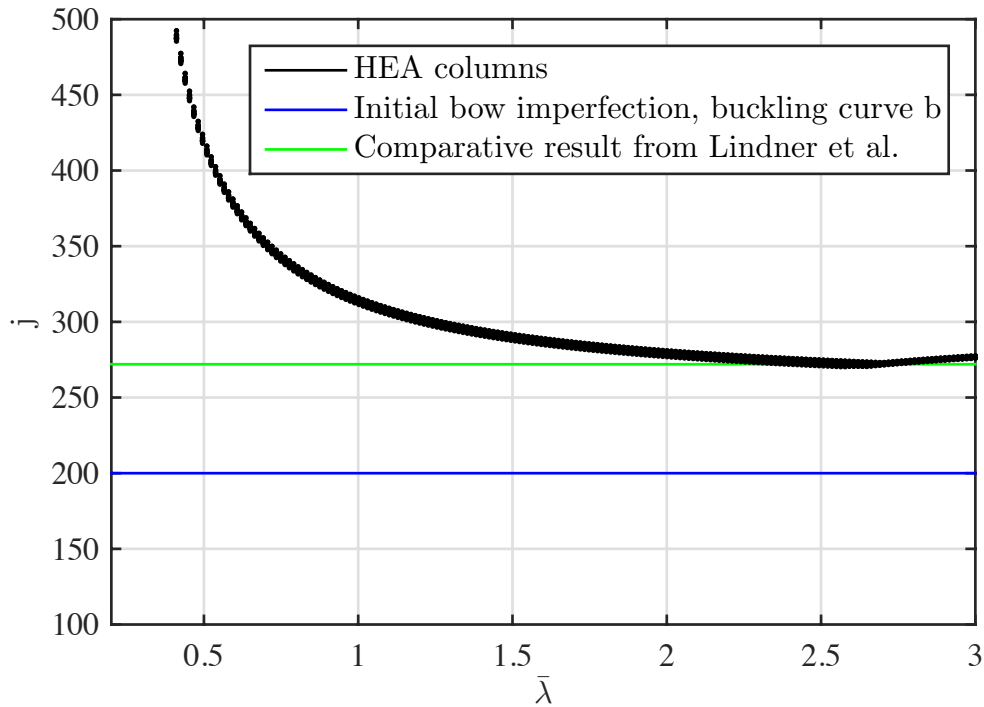


Figure C.1: Verification of results from Matlab calculations with the results presented by Lindner, Kuhlmann, and Just (2016). Results visualised as non-dimensional value j vs. relative slenderness ratio $\bar{\lambda}$.

C.2 Beam-columns

As for part one a HEB 220 cross-section were considered but only the $\bar{\lambda}$ value of 1. The results of the verification of the Matlab programme is presented in percentage form in table C.3 where 100 % equals a perfect match between the results from Matlab and the results from hand calculations

Table C.3: Verification of Matlab programme compared to hand calculations for the methods of Initial imperfections, Method 1 and Method 2 for HEB 220 and a intermediate relative slenderness.

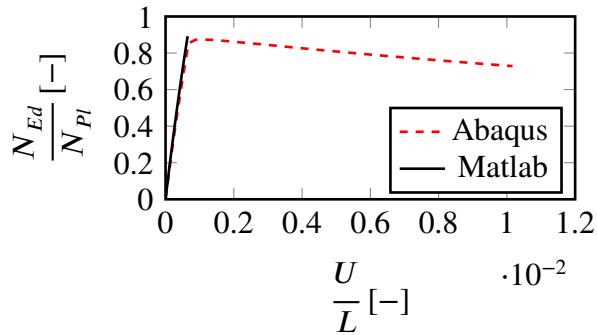
Type: HEB 220	Buckling curve	α	$e_{0,d}$	Initial imperfection	Method 1	Method 2
Strong direction Plastic analysis	b	0.34	$\frac{L}{200}$	99.6%	99.8%	99.8%
Strong direction Elastic analysis	b	0.34	$\frac{L}{250}$	99.9%	99.9%	97%
Weak direction Plastic analysis	c	0.49	$\frac{L}{150}$	99.9%	99.8%	100%
Weak direction Elastic analysis	c	0.49	$\frac{L}{200}$	99.9%	99.9%	100%

D Numerical results for columns

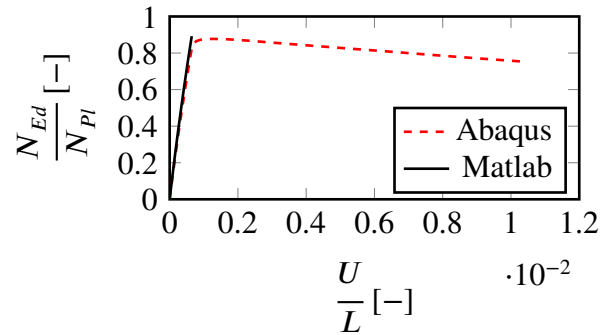
This chapter presents complimentary results regarding numerical analyses of columns.

D.1 Comparison of analytical and numerical results

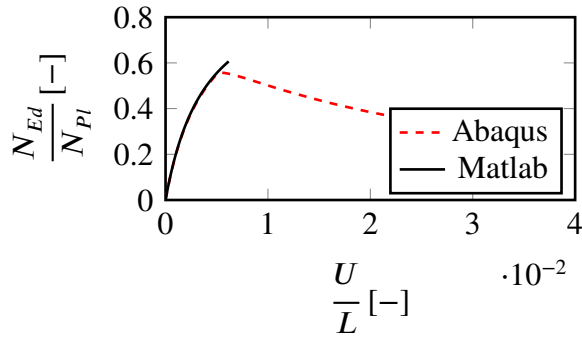
The results from comparing the numerical results obtained in the second order non-linear buckling analysis with analytical results for the IPE and VKR cross-sections and strong buckling direction are found in figure D.1. The black line represents analytic results and the red line numerical results.



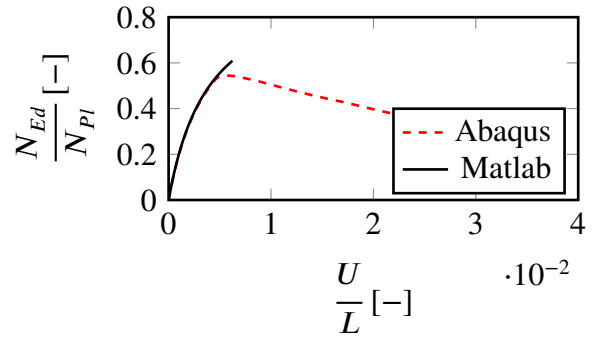
(a) IPE with low relative slenderness



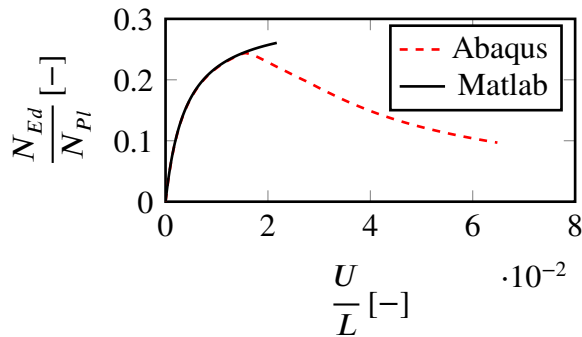
(b) VKR with low relative slenderness



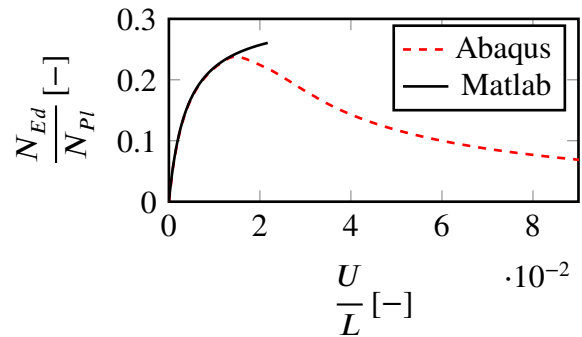
(c) IPE with intermediate relative slenderness



(d) VKR with intermediate relative slenderness



(e) IPE with high relative slenderness



(f) VKR with high slenderness

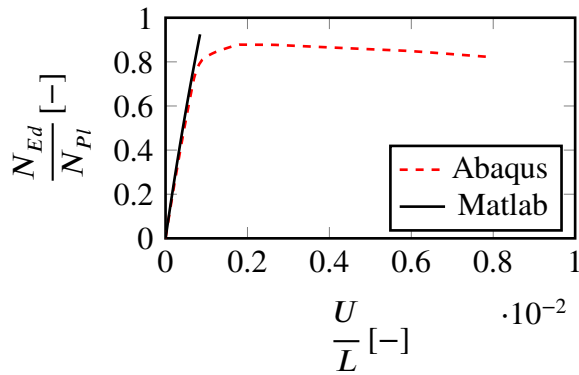
Figure D.1: Ultimate load for IPE 140 and VKR 90 × 50 ($t = 4$) columns. Strong buckling direction.

In table D.1 the values of maximum axial force corresponding to the results in figure D.1 and 5.21 are presented. Negative results indicates that the numerical results from were lower.

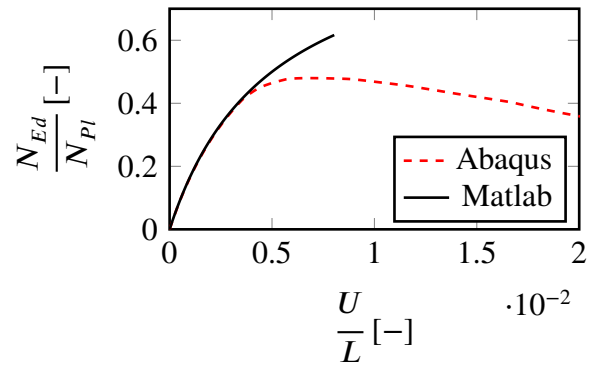
Table D.1: Non-linear second order buckling analysis results for an axially compressed member for HEB 220, IPE 140 and VKR 90 × 50 ($t = 4$) cross-sections. Strong buckling direction. Negative results indicates that the results from FE-analysis was lower than the analytical.

Cross-section type	Difference [%] (low relative slenderness)	Difference [%] (intermediate relative slenderness)	Difference [%] (high relative slenderness)
HEB 220	-1.83	-5.00	-4.76
IPE 140	-2.10	-8.96	-6.85
VKR 90 × 50 ($t = 4$)	-1.71	-11.78	-9.59

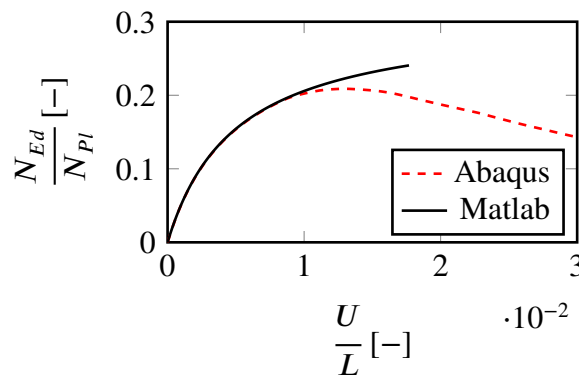
In figure D.2 the results from comparing the numerical results obtained in the second order non-linear buckling analysis with analytical results for the IPE and VKR cross-sections and weak buckling direction are found. The black line represents analytic results and the red line numerical results.



(a) Low relative slenderness



(b) Intermediate relative slenderness



(c) High relative slenderness

Figure D.2: Ultimate load for a IPE 140 column. Weak buckling direction.

In table D.1 the values of maximum axial force corresponding to the results in figure D.2 are presented. Negative results indicates that the numerical results from were lower than the analytical.

Table D.2: Non-linear second order buckling analysis results for an axially compressed member for HEB 220, IPE 140 and VKR 90 × 50 ($t = 4$) cross-sections. Weak buckling direction. Negative results indicates that the results from FE-analysis was lower.

Cross-section type	Difference [%] (low relative slenderness)	Difference [%] (intermediate relative slenderness)	Difference [%] (high relative slenderness)
HEB 220	-6.83	-23.57	-14.56
IPE 140	-5.33	-28.46	-15.21
VKR 90 × 50 ($t = 4$)	-1.78	-7.38	-5.79

D.2 Comparison of optimised plastic analyses

The difference between the analytical and numerical results for the plastic analysis are found in table D.3 for strong buckling direction and D.4 for weak buckling direction. The values are for columns with low and high slenderness.

Table D.3: Difference between the analytical and numerical results, for both Equation 1 and 2, for columns with low and high slenderness. Initial bow imperfection from both new formulas. Plastic analyses for strong buckling direction.

(a) Columns with low relative slenderness.

Cross-section type	Difference, [%] ($e_{0,1}$ from Equation 1)	Difference, [%] ($e_{0,2}$ from Equation 2)
HEB 220	-0.83	0.04
IPE 140	0.14	-0.51
VKR 90 × 50 ($t = 4$)	-0.54	0.44

(b) Columns with high relative slenderness

Cross-section type	Difference, [%] ($e_{0,1}$ from Equation 1)	Difference, [%] ($e_{0,2}$ from Equation 2)
HEB 220	-3.30	-1.15
IPE 140	-3.28	-1.41
VKR 90 × 50 ($t = 4$)	-5.96	-2.61

Table D.4: Difference between the analytical and numerical results, for both Equation 1 and 2, for columns with low and high slenderness. Initial bow imperfection from both new formulas. Plastic analyses for weak buckling direction.

(a) Columns with low relative slenderness.

Cross-section type	Difference, [%] ($e_{0,1}$ from Equation 1)	Difference, [%] ($e_{0,2}$ from Equation 2)
HEB 220	-0.45	2.96
IPE 140	0.44	3.03
VKR 90 × 50 ($t = 4$)	-0.99	-0.36

(b) Columns with high relative slenderness

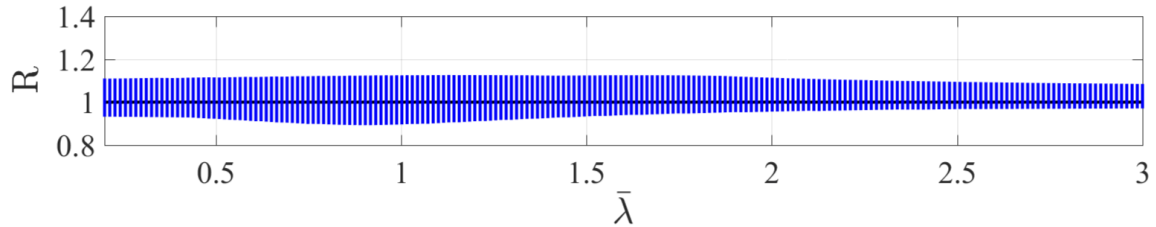
Cross-section type	Difference, [%] ($e_{0,1}$ from Equation 1)	Difference, [%] ($e_{0,2}$ from Equation 2)
HEB 220	-18.26	-6.13
IPE 140	-18.82	-7.03
VKR 90 × 50 ($t = 4$)	-3.58	-1.52

E Analytical results for beam-columns

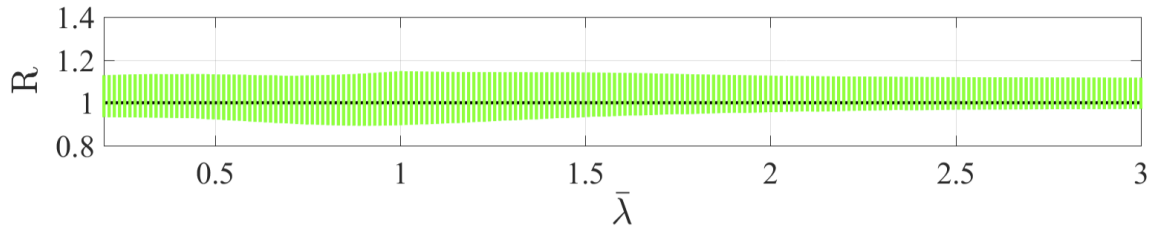
This appendix contains all complimentary results regarding analytical analysis for beam-columns. The appendix is divided into sections depending on load conditions, buckling directions and whether or not the new formula for initial bow imperfection is in use.

E.1 Equal external end-moment (y-y)

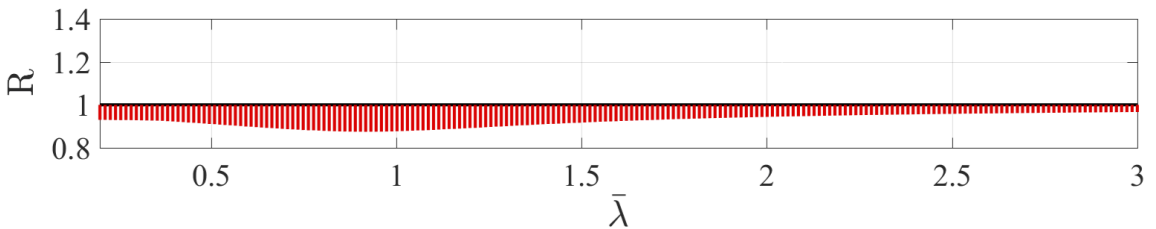
In figure E.1 to E.7 the results for cross-sections HEA, HEM, IPE, VKR and KKR are presented. The analysis was conducted with steel strength class S335 and regarded buckling about the strong axis.



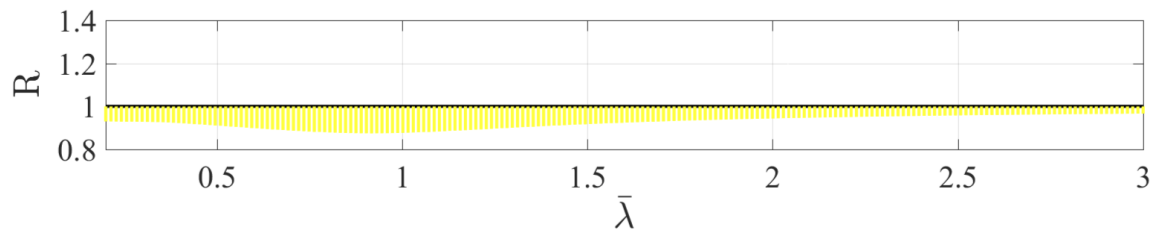
(a) Method 1, plastic analysis



(b) Method 2, plastic analysis

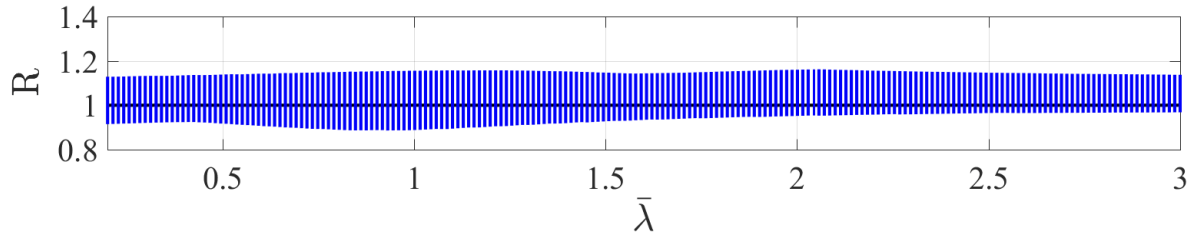


(c) Method 1, elastic analysis

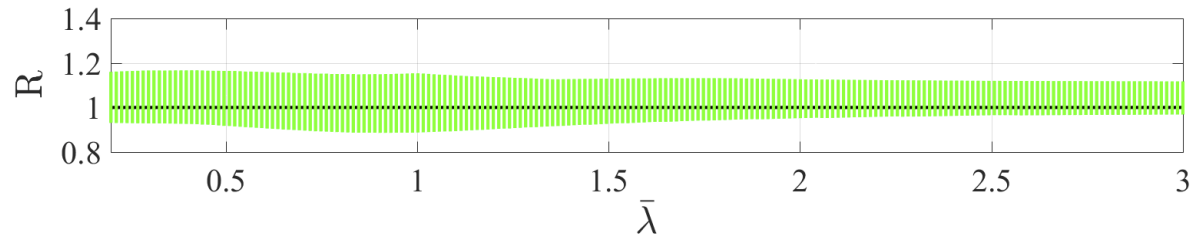


(d) Method 2, elastic analysis

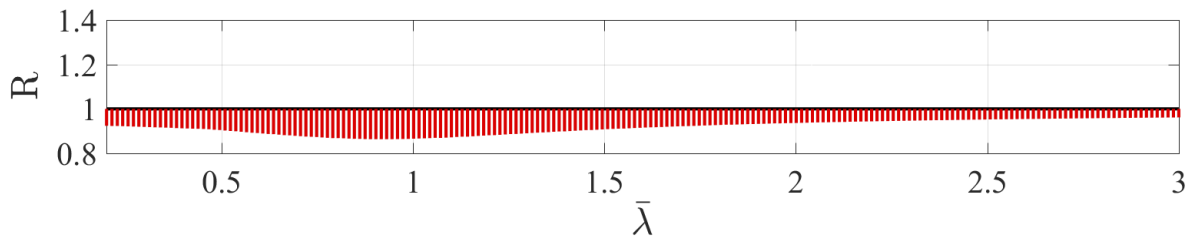
Figure E.1: Results for beam-columns with HEA cross-sections, steel quality S355 and equal end-moments. Bending about strong axis.



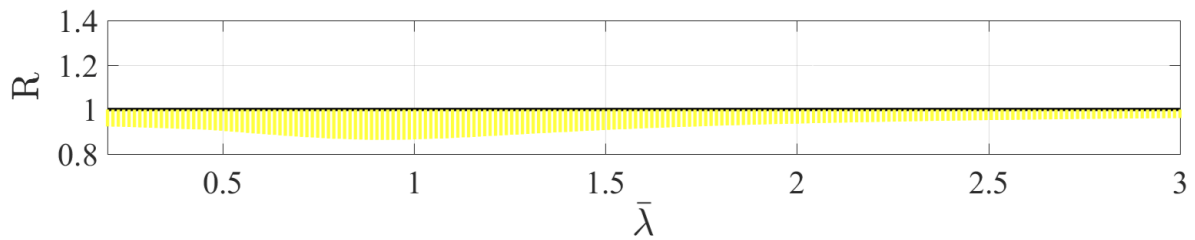
(a) Method 1, plastic analysis



(b) Method 2, plastic analysis

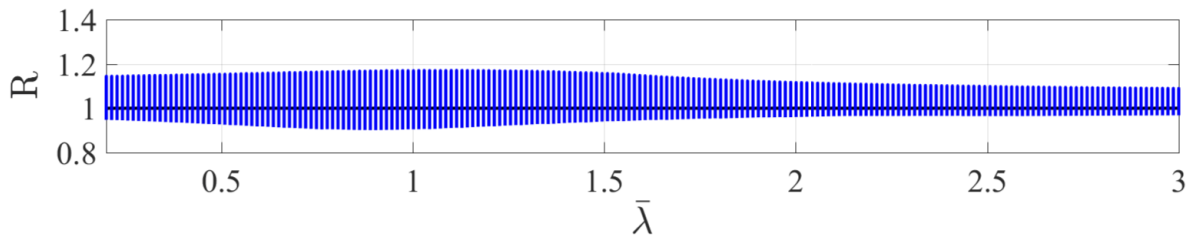


(c) Method 1, elastic analysis

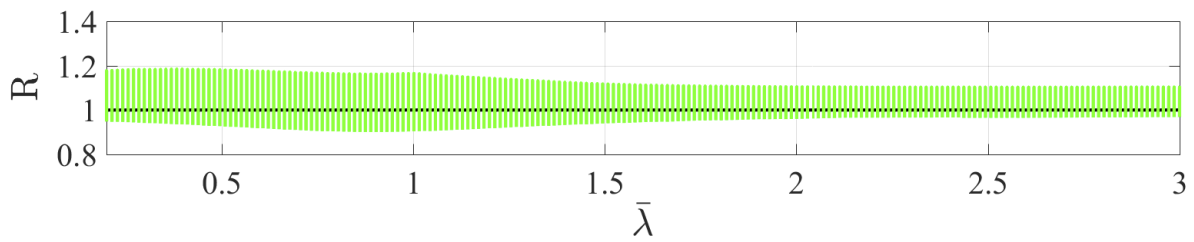


(d) Method 2, elastic analysis

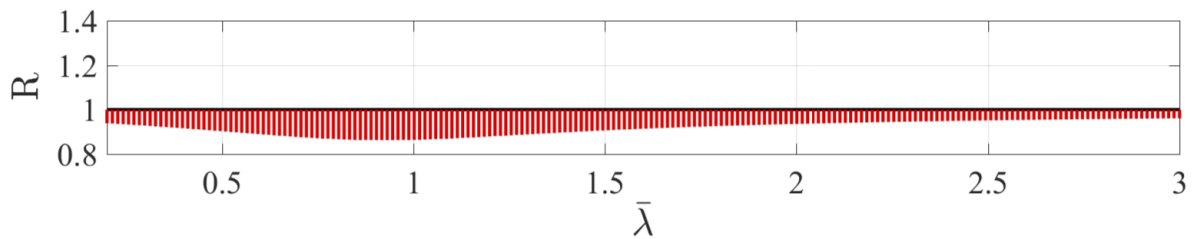
Figure E.2: Results for beam-columns with HEM cross-sections, steel quality S355 and equal end-moments. Strong buckling direction.



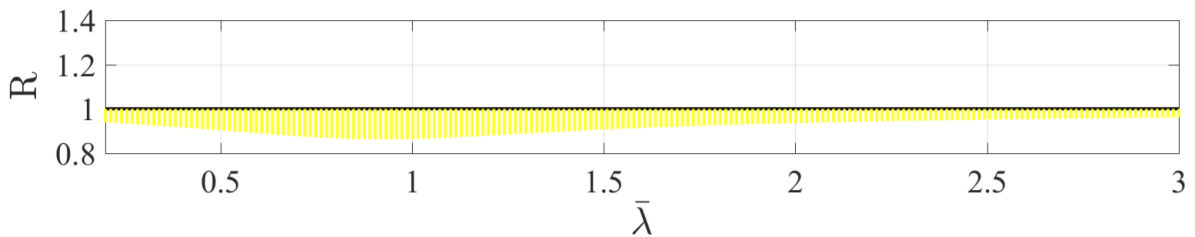
(a) Method 1, plastic analysis



(b) Method 2, plastic analysis

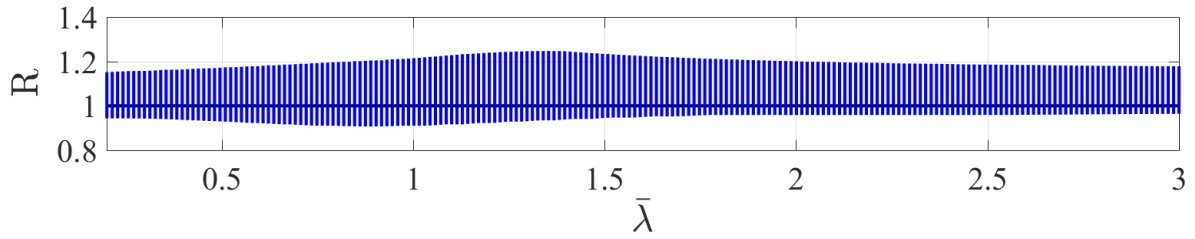


(c) Method 1, elastic analysis

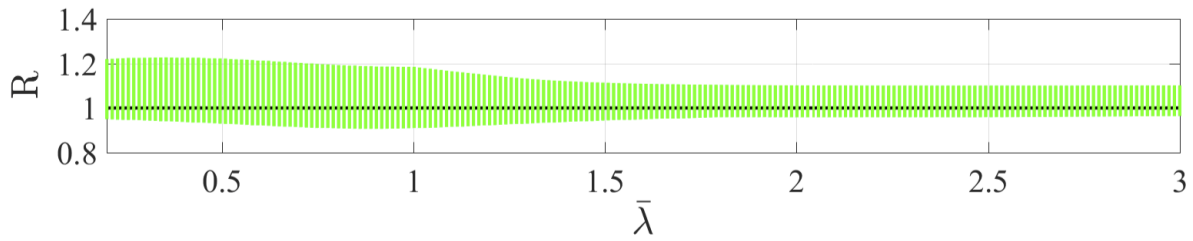


(d) Method 2, elastic analysis

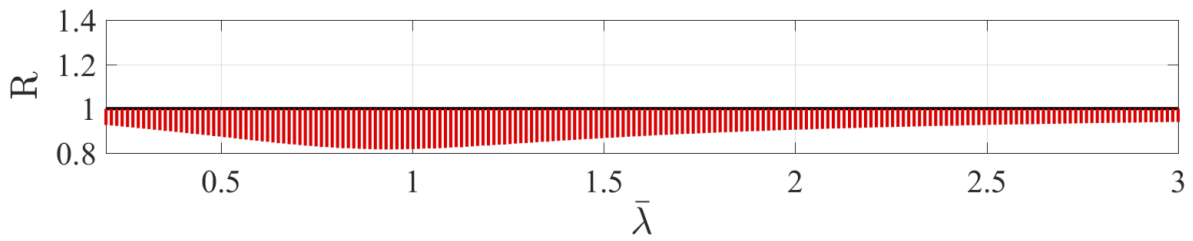
Figure E.3: Results for beam-columns with IPE cross-sections, steel quality S355 and equal end-moments. Bending about strong axis.



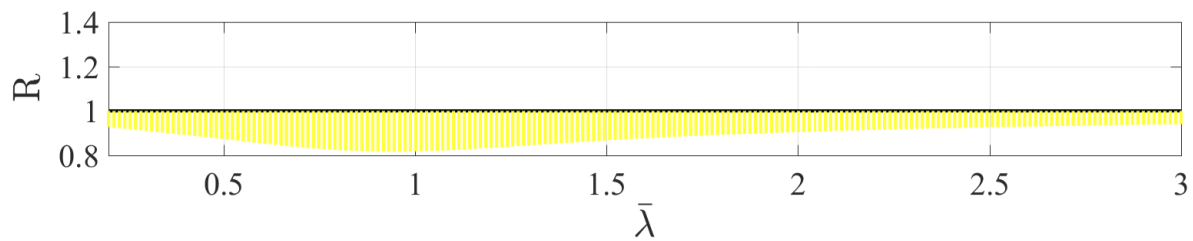
(a) Method 1, plastic analysis



(b) Method 2, plastic analysis

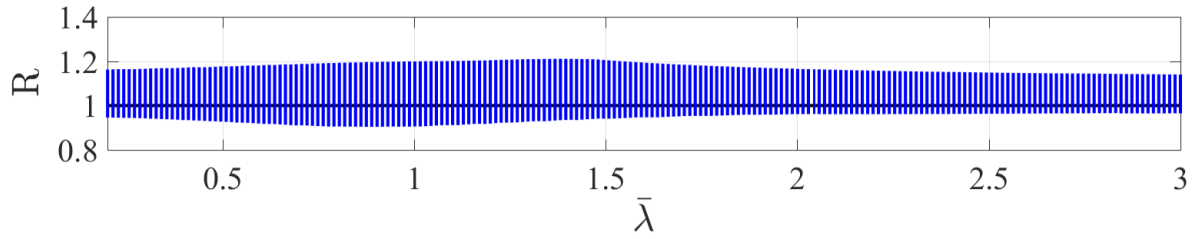


(c) Method 1, elastic analysis

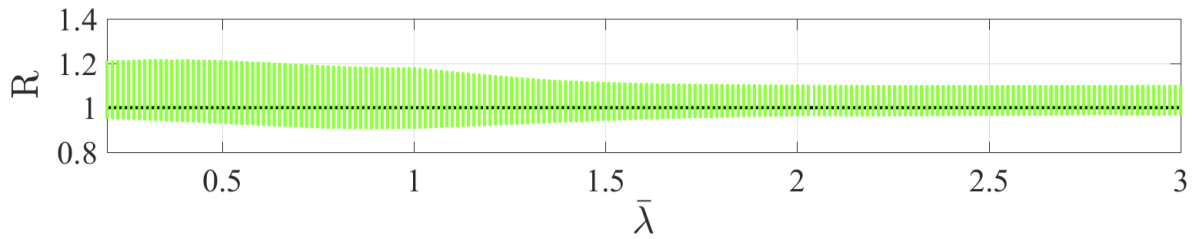


(d) Method 2, elastic analysis

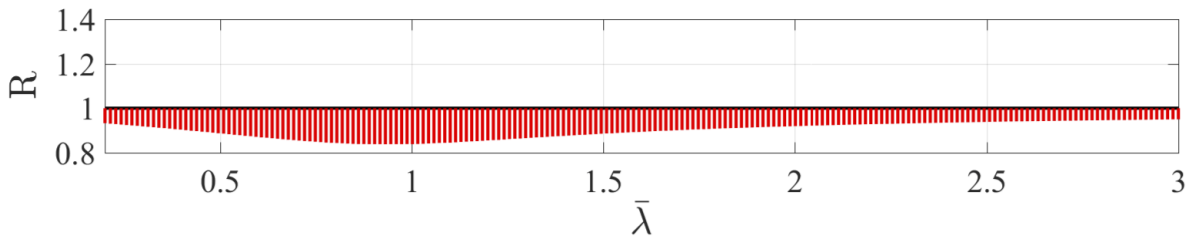
Figure E.4: Results for beam-columns with VKR rectangular cross-sections, steel quality S355 and equal end-moments. Strong buckling direction.



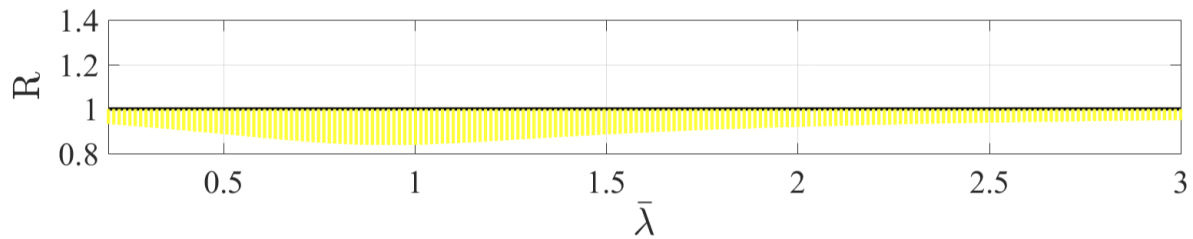
(a) Method 1, plastic analysis



(b) Method 2, plastic analysis

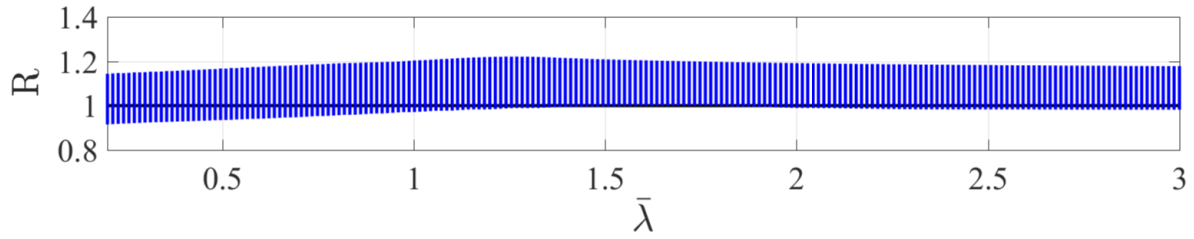


(c) Method 1, elastic analysis

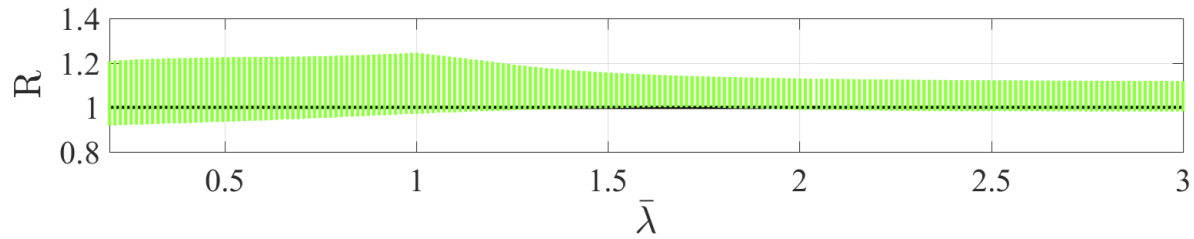


(d) Method 2, elastic analysis

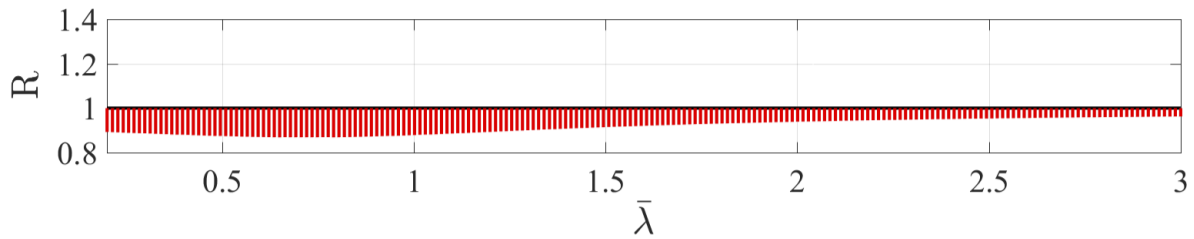
Figure E.5: Results for beam-columns with VKR square cross-sections, steel quality S355 and equal end-moments. Strong buckling direction.



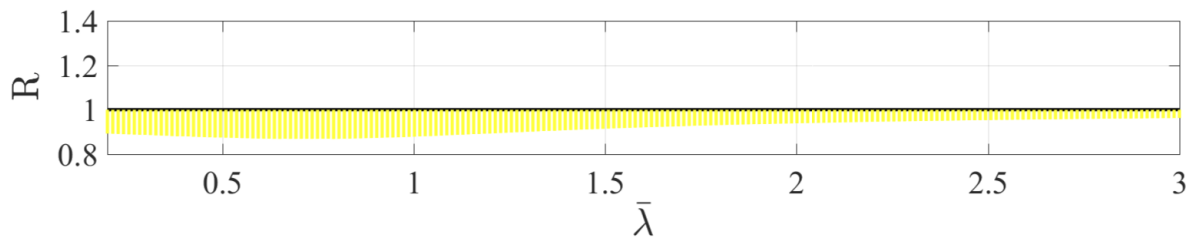
(a) Method 1, plastic analysis



(b) Method 2, plastic analysis

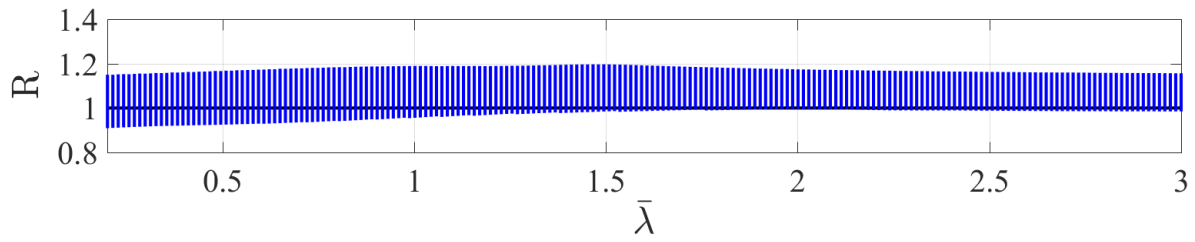


(c) Method 1, elastic analysis

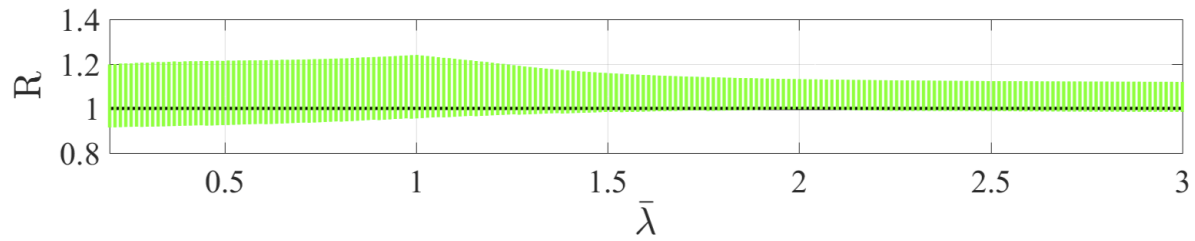


(d) Method 2, elastic analysis

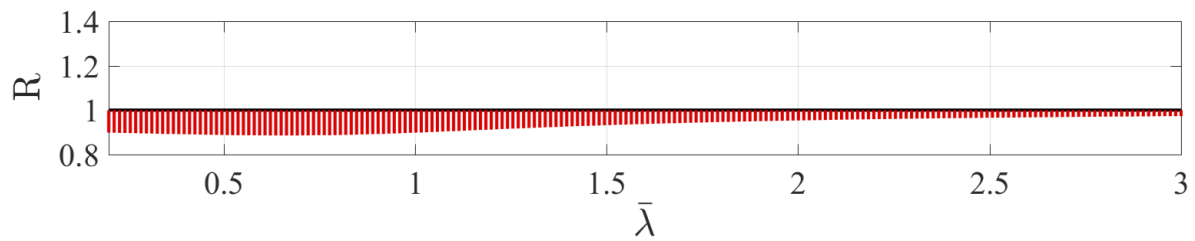
Figure E.6: Results for beam-columns with KKR rectangular cross-sections, steel quality S355 and equal end-moments. Strong buckling direction.



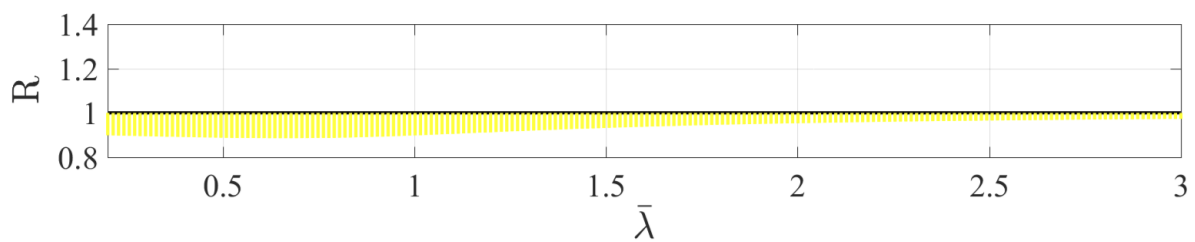
(a) Method 1, plastic analysis



(b) Method 2, plastic analysis



(c) Method 1, elastic analysis

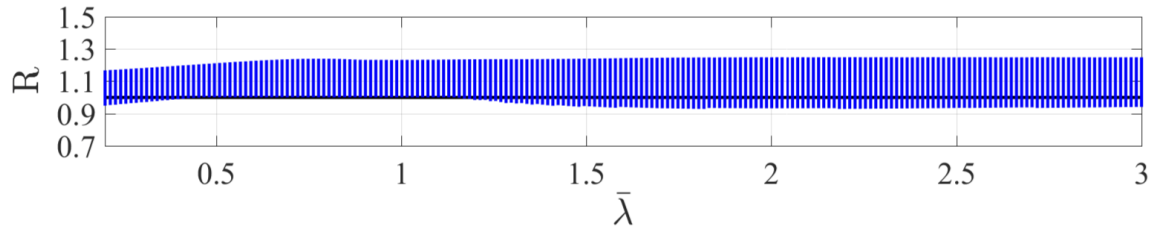


(d) Method 2, elastic analysis

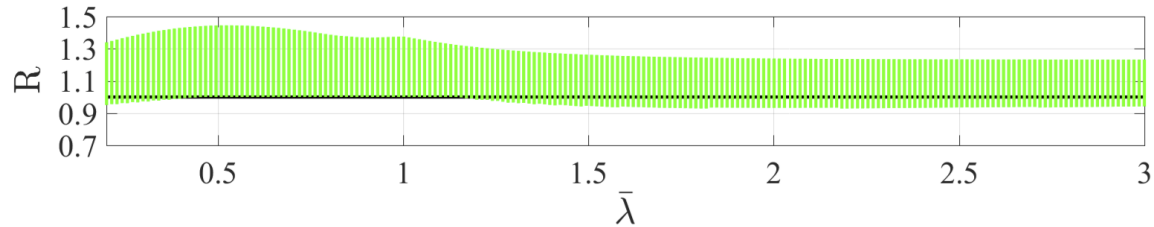
Figure E.7: Results for beam-columns with KKR square cross-sections, steel quality S355 and equal end-moments. Strong buckling direction.

E.2 Equal external end-moment (z-z)

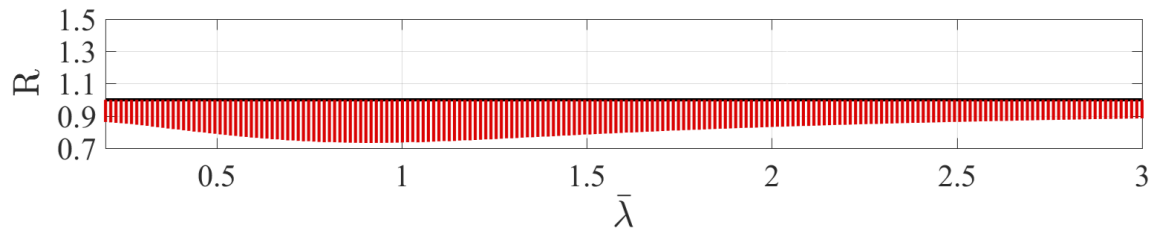
In figure E.8 to E.14 the results for cross-sections HEA, HEM, IPE, VKR and KKR are presented. The analysis was conducted with steel strength class S335 and weak buckling direction.



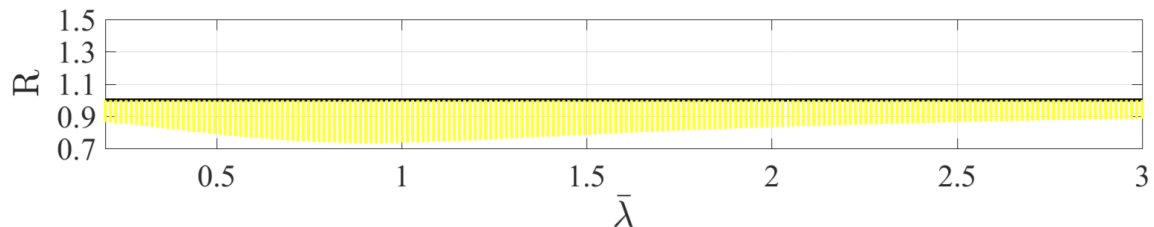
(a) Method 1, plastic analysis



(b) Method 2, plastic analysis

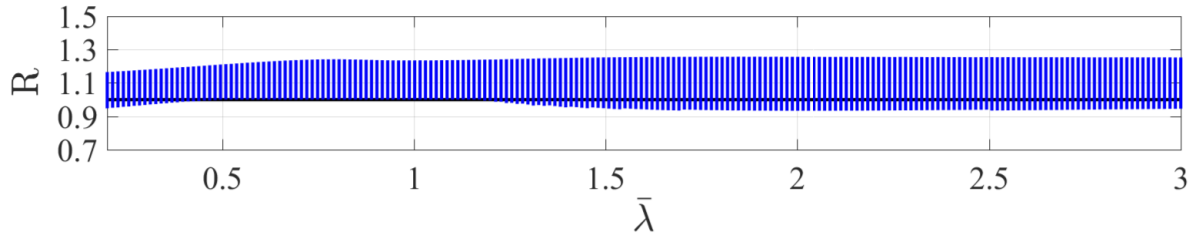


(c) Method 1, elastic analysis

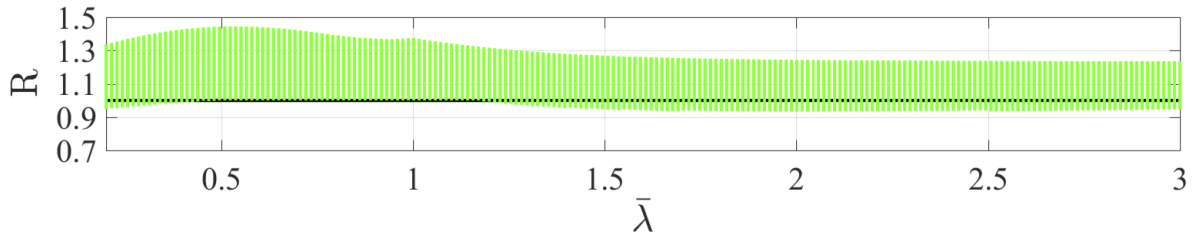


(d) Method 2, elastic analysis

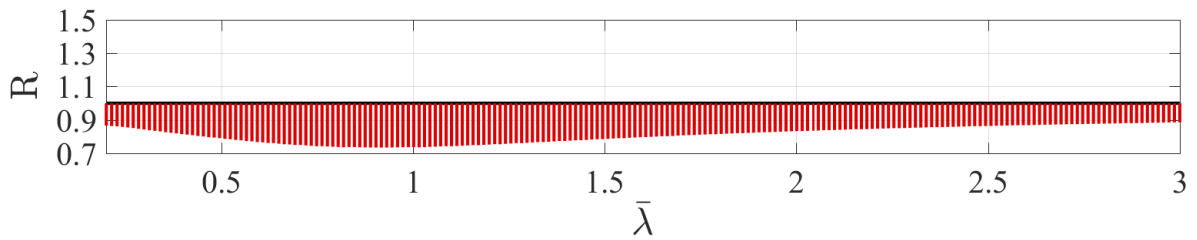
Figure E.8: Results for beam-columns with HEA cross-sections, steel quality S335 and equal end-moments. Weak buckling direction.



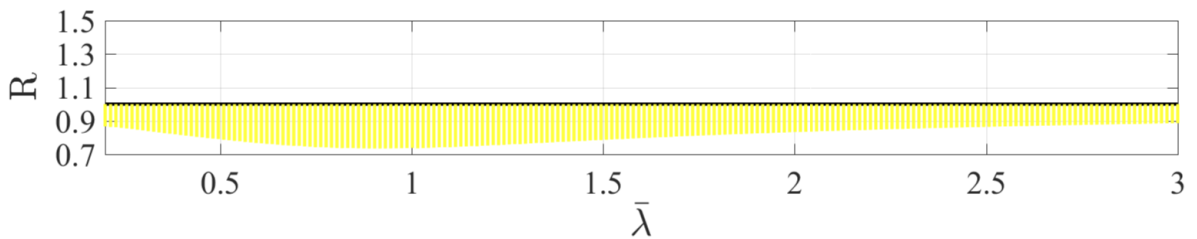
(a) Method 1, plastic analysis



(b) Method 2, plastic analysis

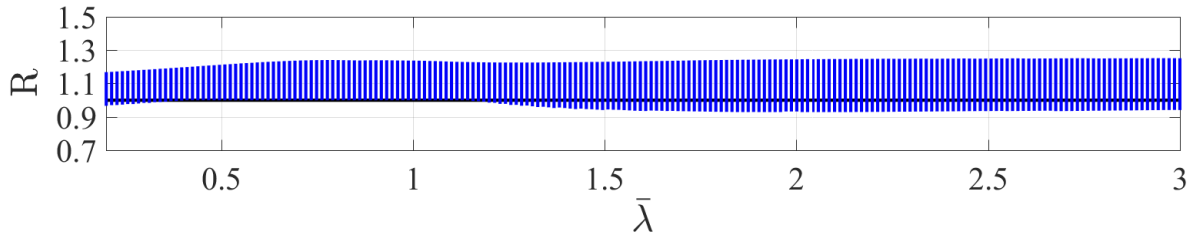


(c) Method 1, elastic analysis

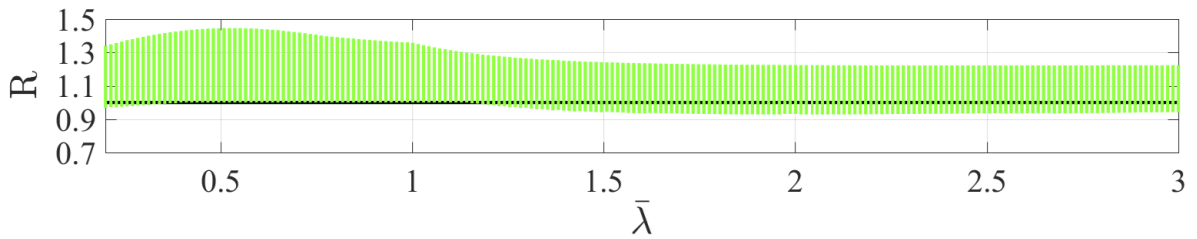


(d) Method 2, elastic analysis

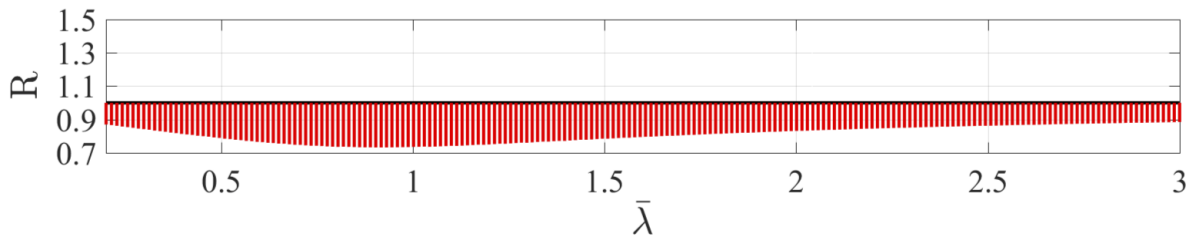
Figure E.9: Results for beam-columns with HEM cross-sections, steel quality S355 and equal end-moments. Weak buckling direction.



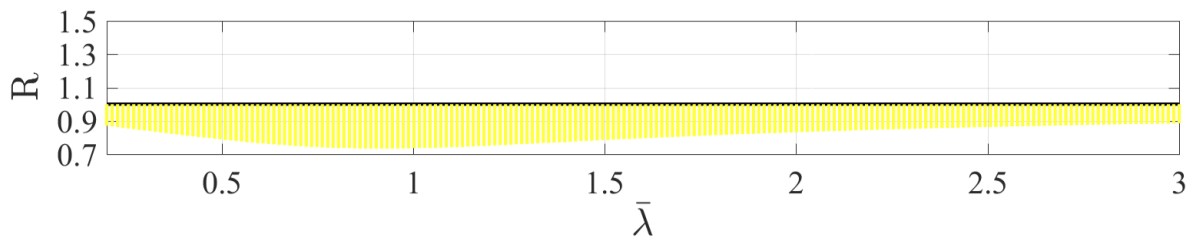
(a) Method 1, plastic analysis



(b) Method 2, plastic analysis

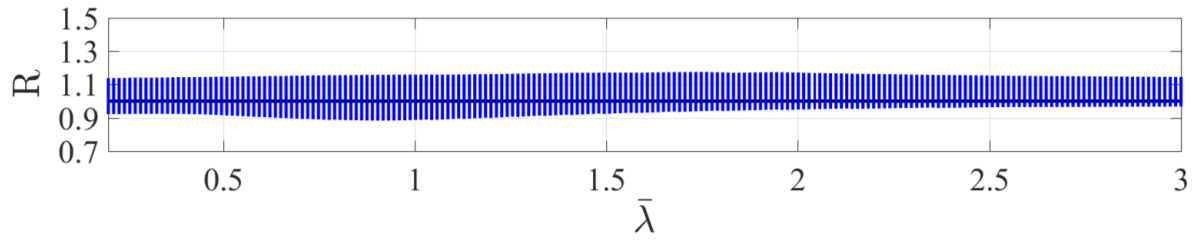


(c) Method 1, elastic analysis

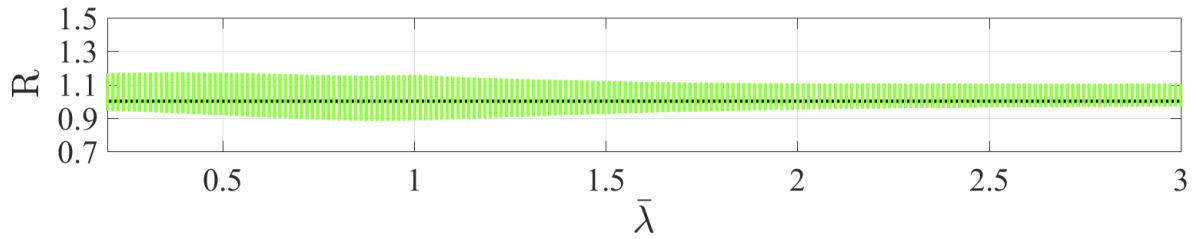


(d) Method 2, elastic analysis

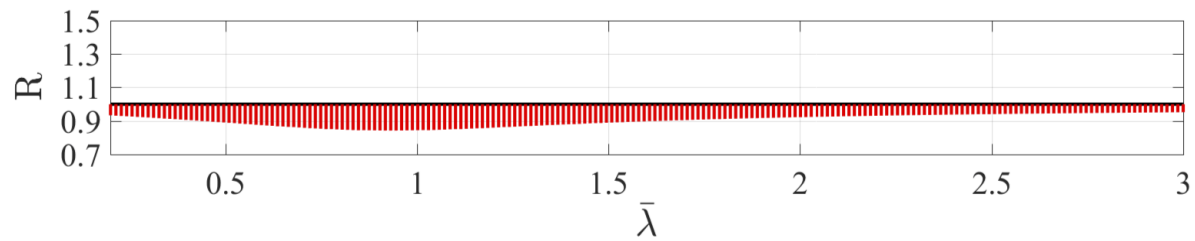
Figure E.10: Results for beam-columns with IPE cross-sections, steel quality S355 and equal end-moments. Weak buckling direction.



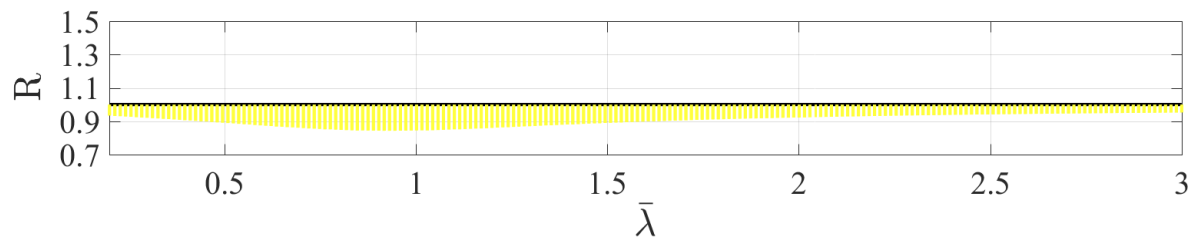
(a) Method 1, plastic analysis



(b) Method 2, plastic analysis

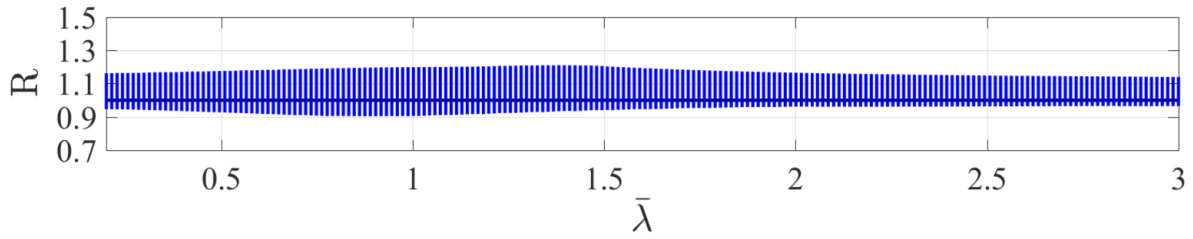


(c) Method 1, elastic analysis

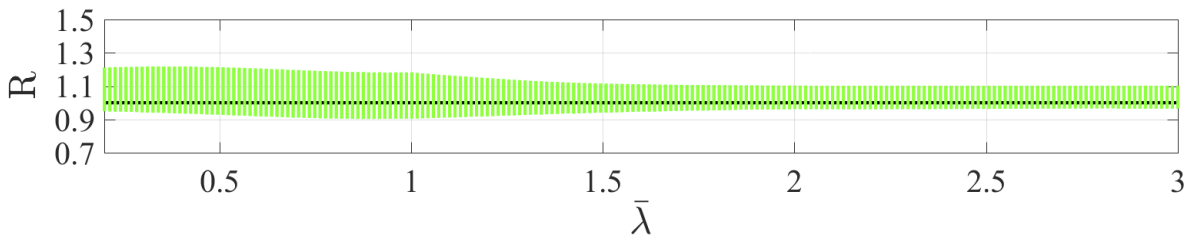


(d) Method 2, elastic analysis

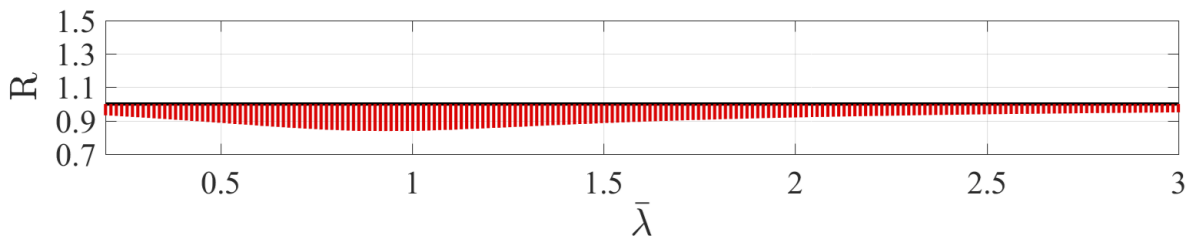
Figure E.11: Results for beam-columns with VKR rectangular cross-sections, steel quality S355 and equal end-moments. Weak buckling direction.



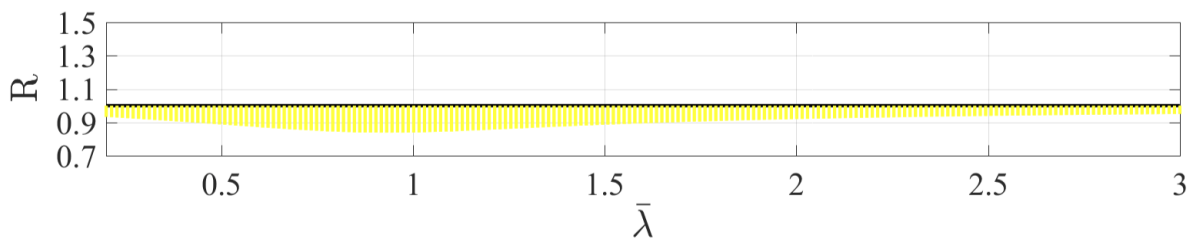
(a) Method 1, plastic analysis



(b) Method 2, plastic analysis

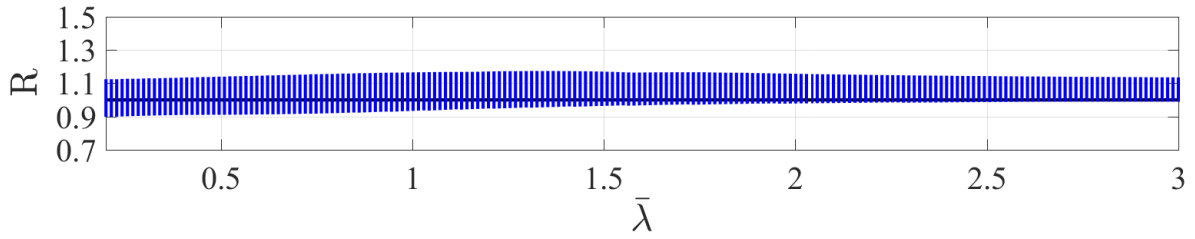


(c) Method 1, elastic analysis

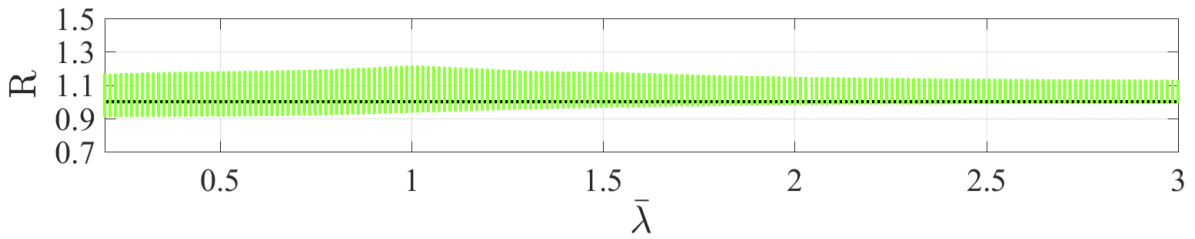


(d) Method 2, elastic analysis

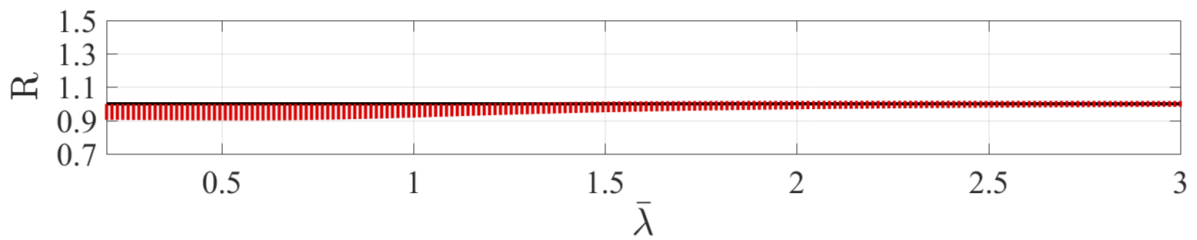
Figure E.12: Results for beam-columns with VKR square cross-sections, steel quality S355 and equal end-moments. Weak buckling direction.



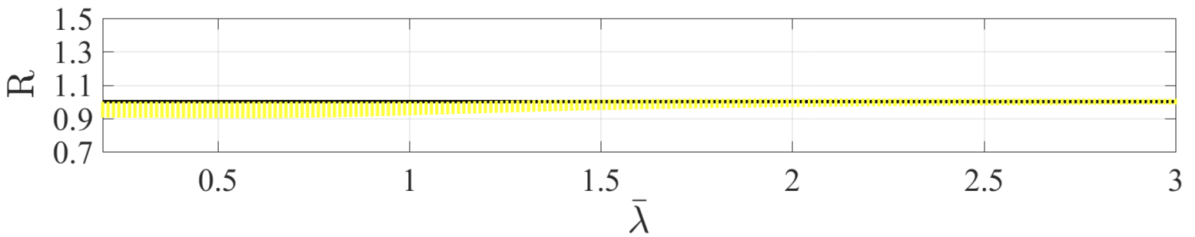
(a) Method 1, plastic analysis



(b) Method 2, plastic analysis

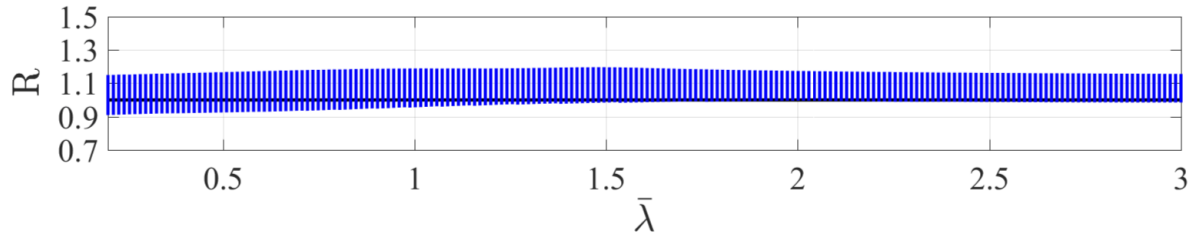


(c) Method 1, elastic analysis

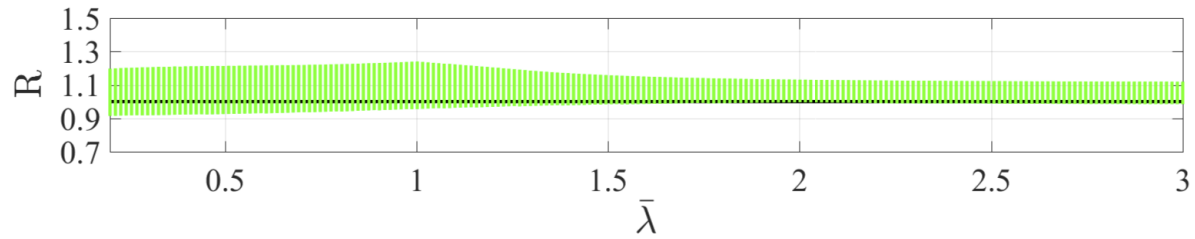


(d) Method 2, elastic analysis

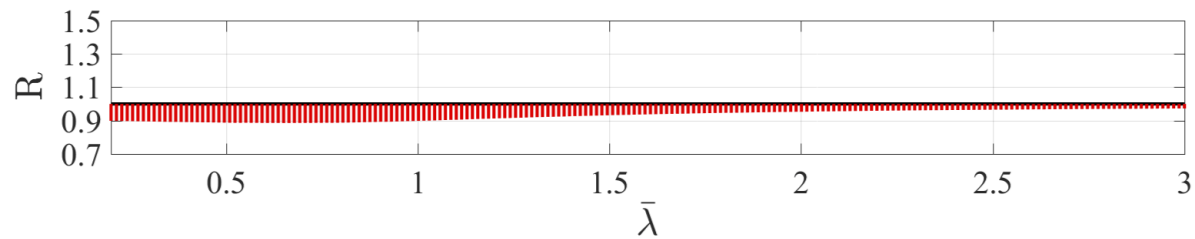
Figure E.13: Results for beam-columns with VKR rectangular cross-sections, steel quality S355 and equal end-moments. Weak buckling direction.



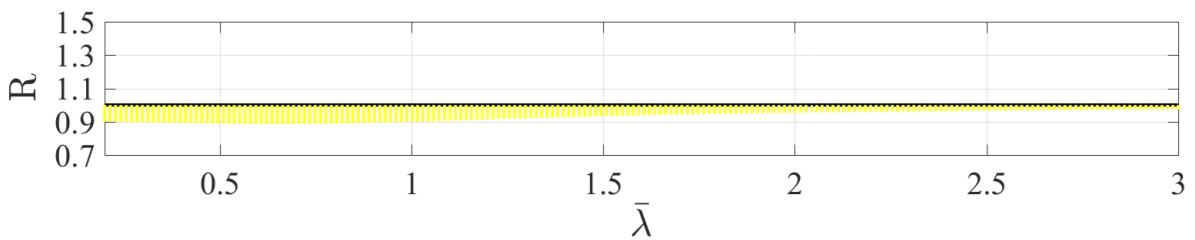
(a) Method 1, plastic analysis



(b) Method 2, plastic analysis



(c) Method 1, elastic analysis

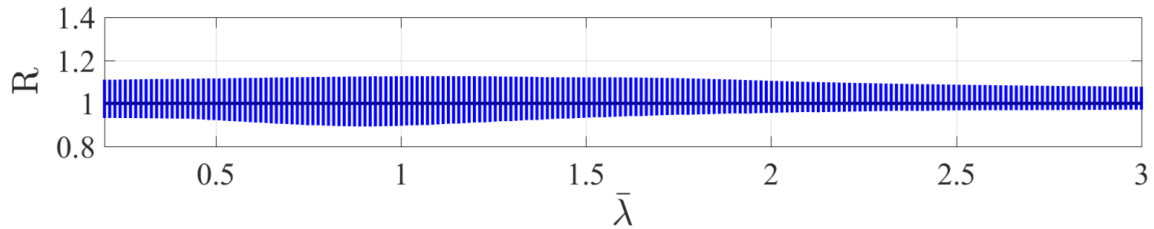


(d) Method 2, elastic analysis

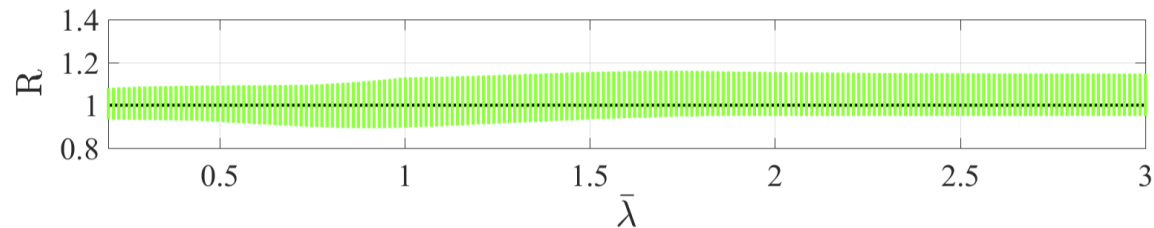
Figure E.14: Results for beam-columns with KKR square cross-sections, steel quality S355 and equal end-moments. Weak buckling direction.

E.3 Uniformly distributed load (y-y)

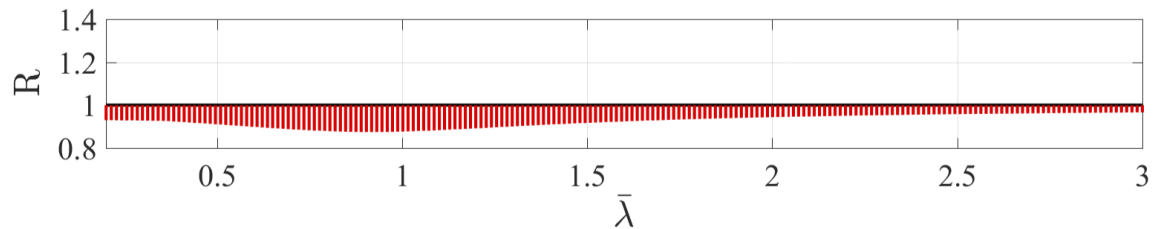
In figure E.15 to E.21 the results for moment due to uniformly distributed load regarding cross-sections HEA, HEM, IPE, VKR and KKR are presented. The analysis was conducted with steel strength class S335 and regarded strong buckling direction.



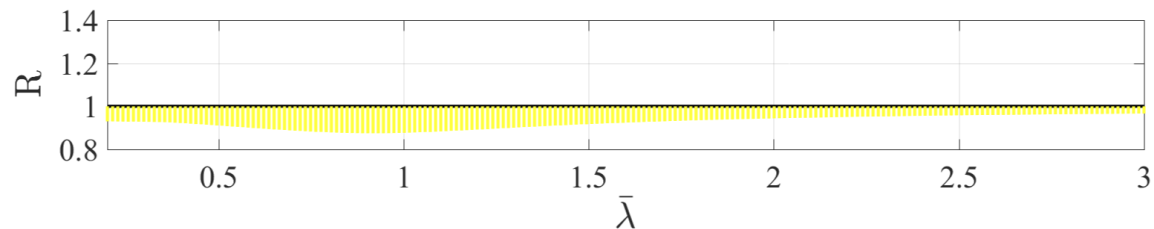
(a) Method 1, plastic analysis



(b) Method 2, plastic analysis

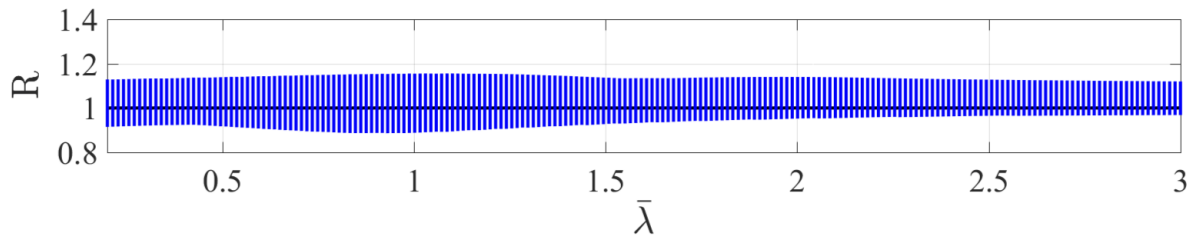


(c) Method 1, elastic analysis

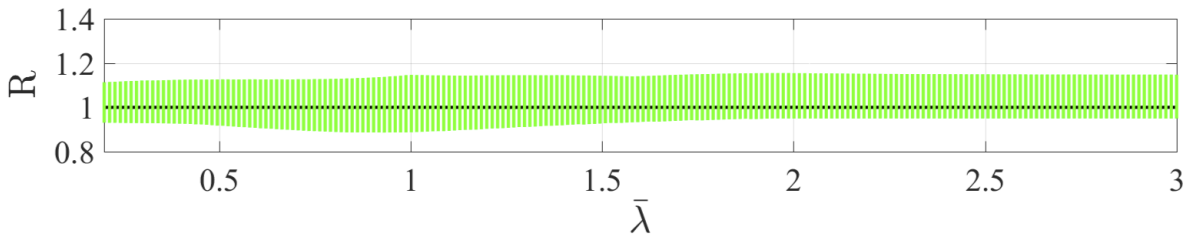


(d) Method 2, elastic analysis

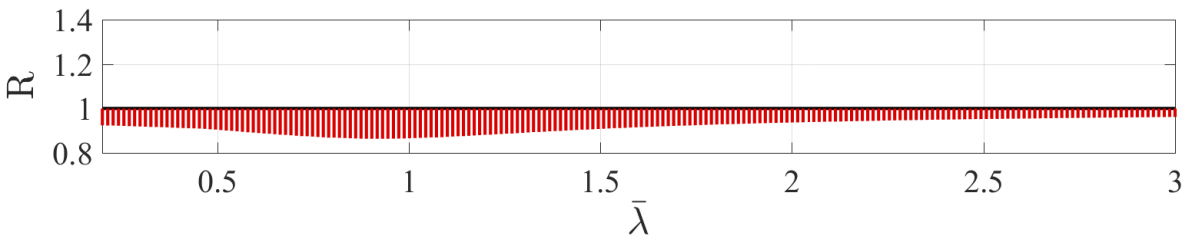
Figure E.15: Results for beam-columns with HEA cross-sections, steel quality S355 and moment due to uniformly distributed load. Strong buckling direction.



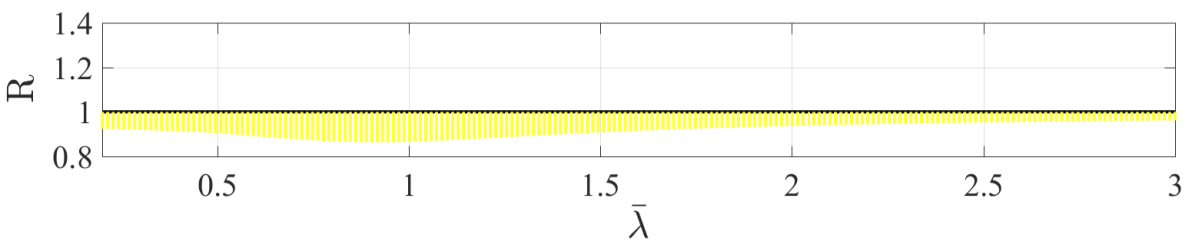
(a) Method 1, plastic analysis



(b) Method 2, plastic analysis

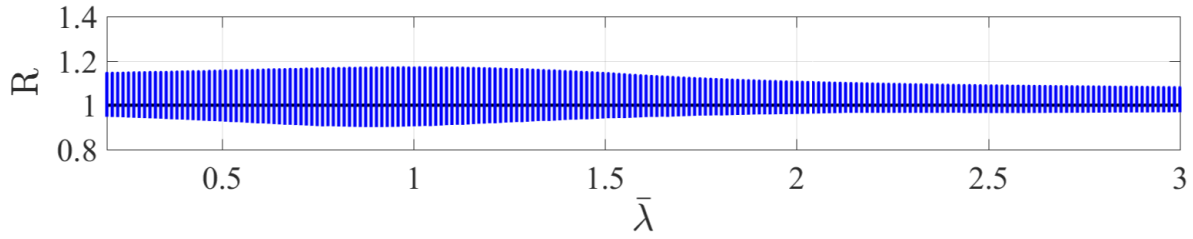


(c) Method 1, elastic analysis

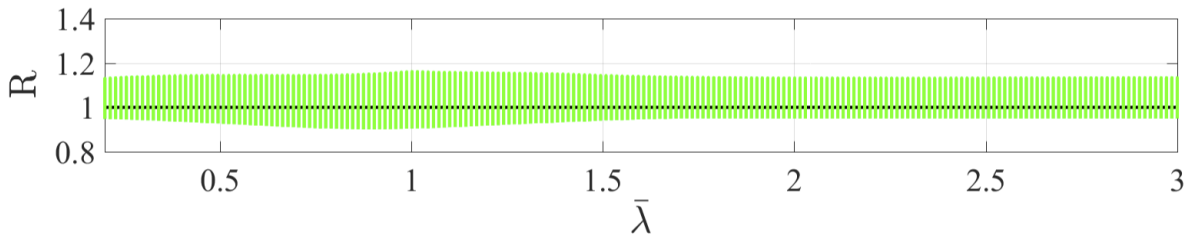


(d) Method 2, elastic analysis

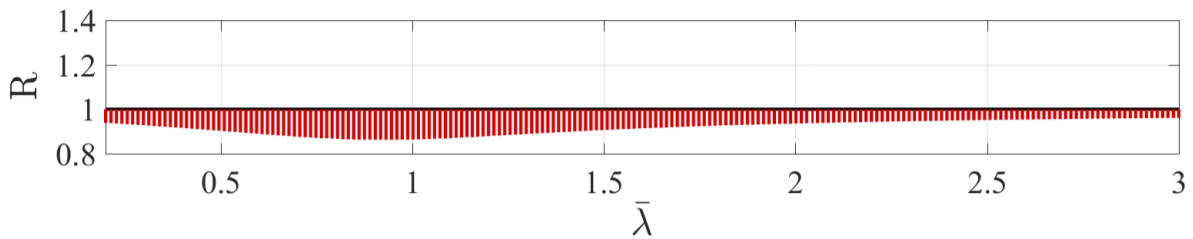
Figure E.16: Results for beam-columns with HEM cross-sections, steel quality S355 and moment due to uniformly distributed load. Strong buckling direction.



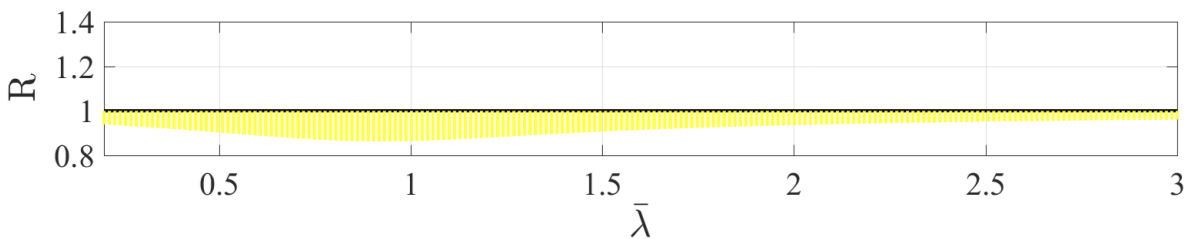
(a) Method 1, plastic analysis



(b) Method 2, plastic analysis

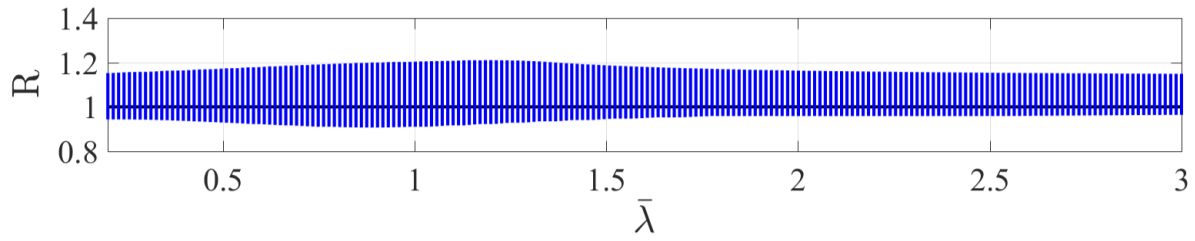


(c) Method 1, elastic analysis

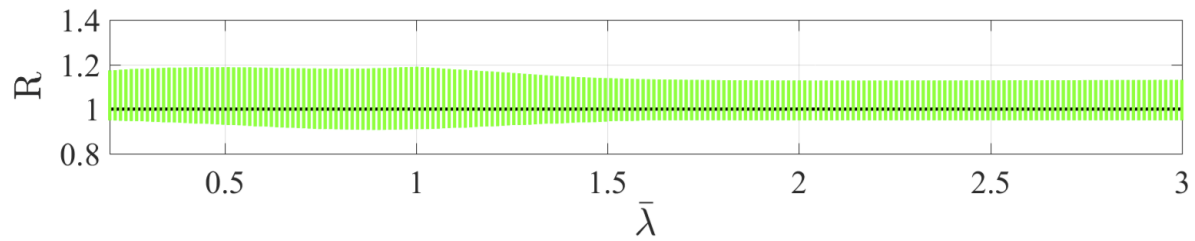


(d) Method 2, elastic analysis

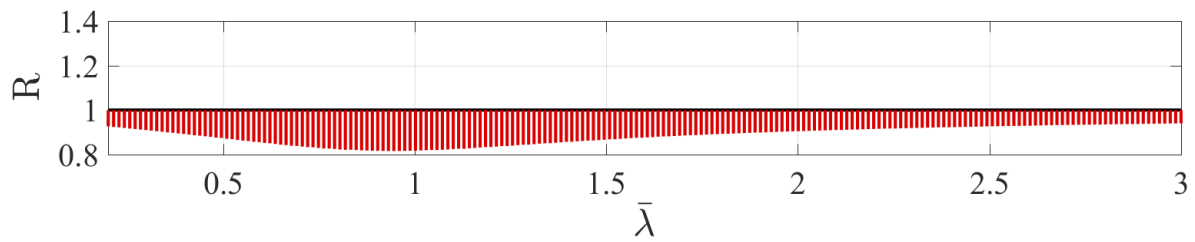
Figure E.17: Results for beam-columns with IPE cross-sections, steel quality S355 and moment due to uniformly distributed load. Strong buckling direction.



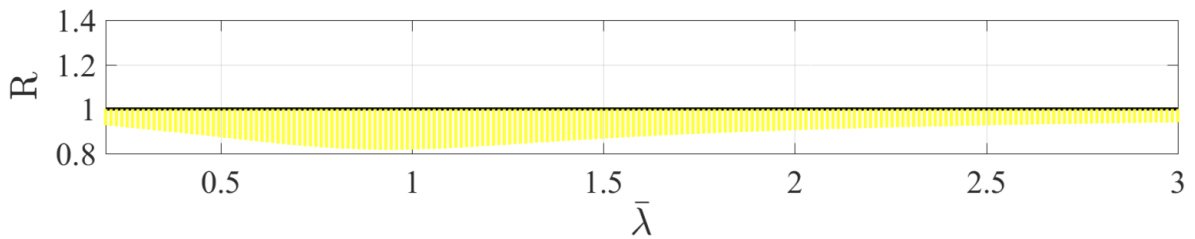
(a) Method 1, plastic analysis



(b) Method 2, plastic analysis

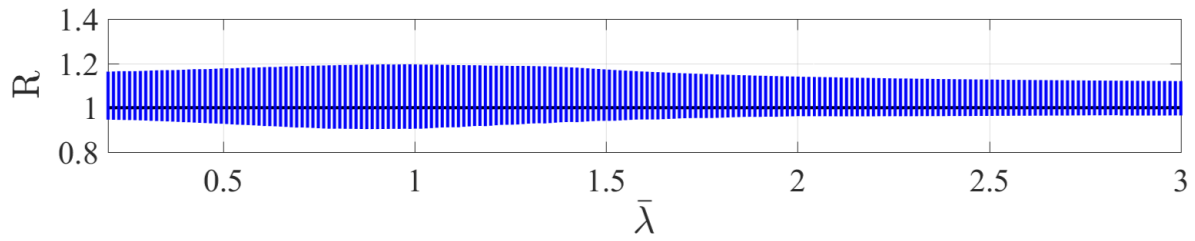


(c) Method 1, elastic analysis

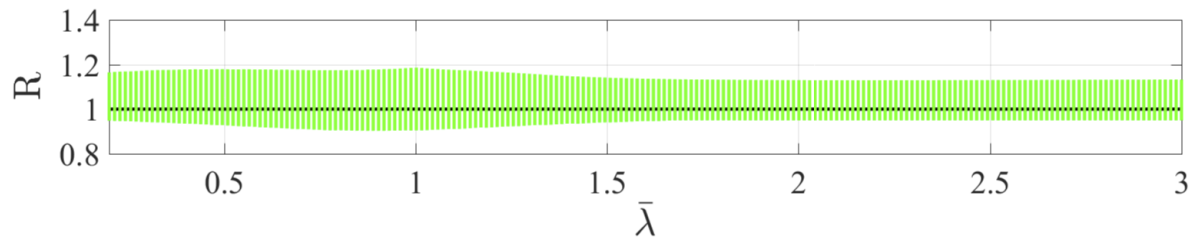


(d) Method 2, elastic analysis

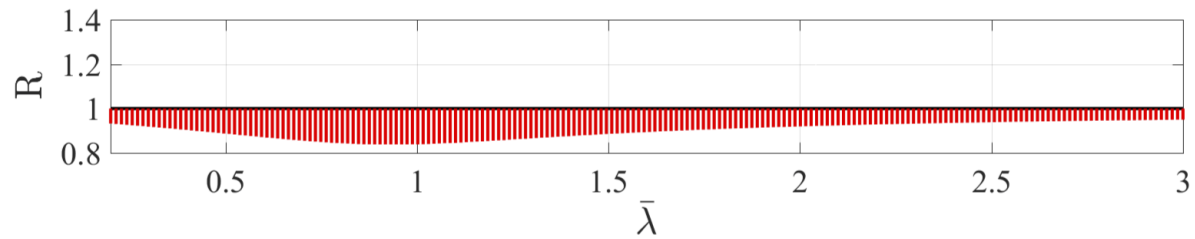
Figure E.18: Results for beam-columns with VKR rectangular cross-sections, steel quality S355 and moment due to uniformly distributed load. Strong buckling direction.



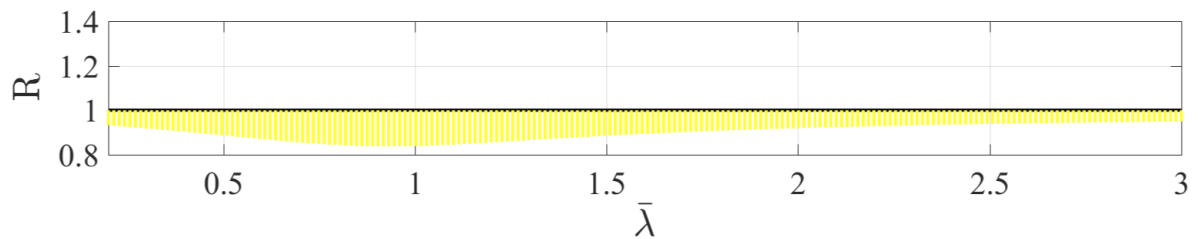
(a) Method 1, plastic analysis



(b) Method 2, plastic analysis

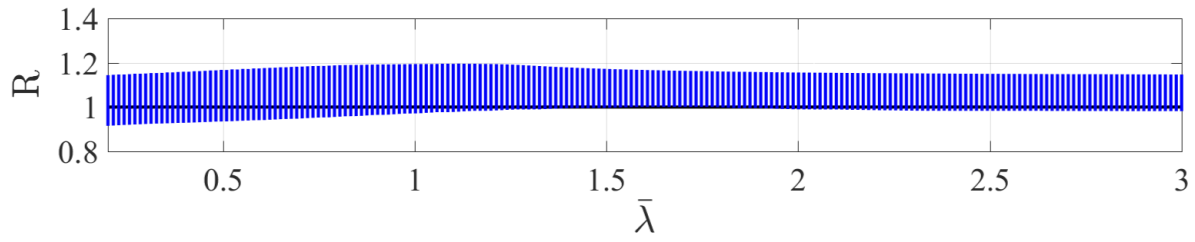


(c) Method 1, elastic analysis

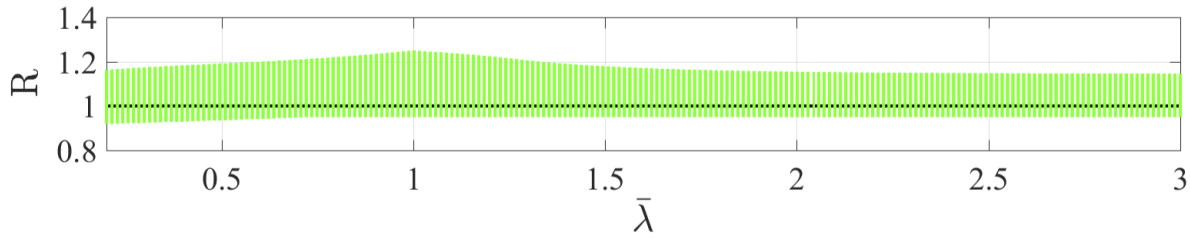


(d) Method 2, elastic analysis

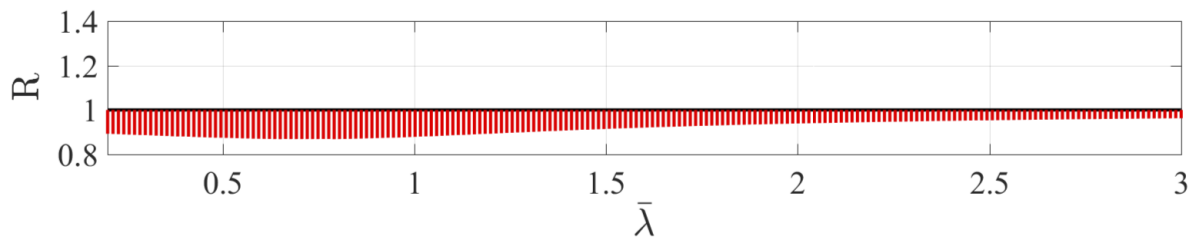
Figure E.19: Results for beam-columns with VKR square cross-sections, steel quality S355 and moment due to uniformly distributed load. Strong buckling direction.



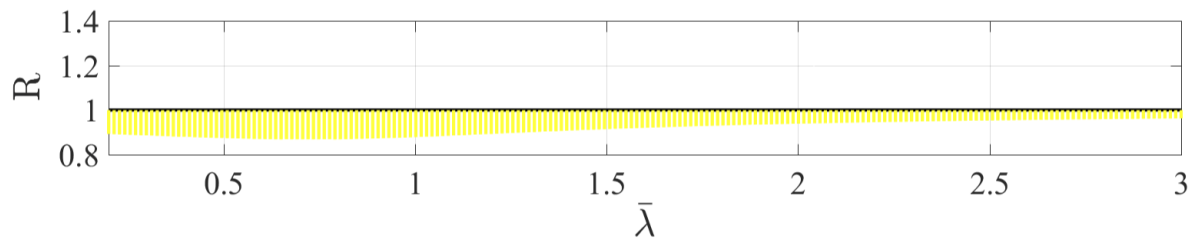
(a) Method 1, plastic analysis



(b) Method 2, plastic analysis

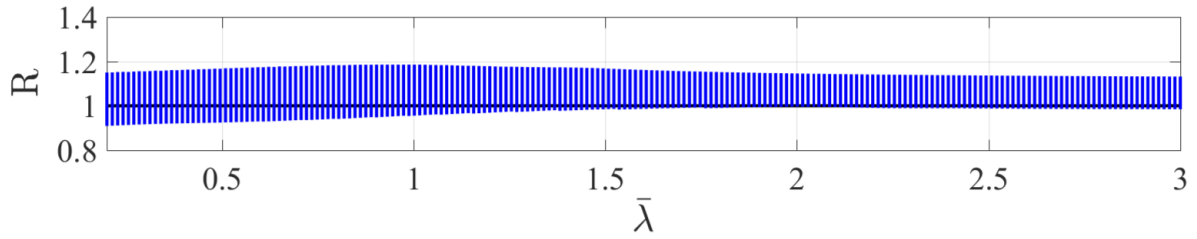


(c) Method 1, elastic analysis

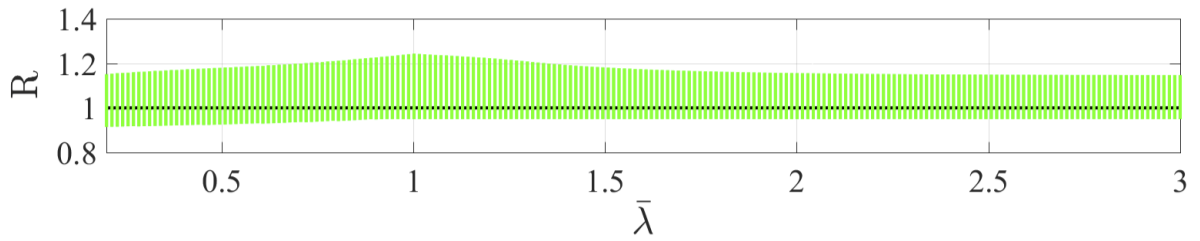


(d) Method 2, elastic analysis

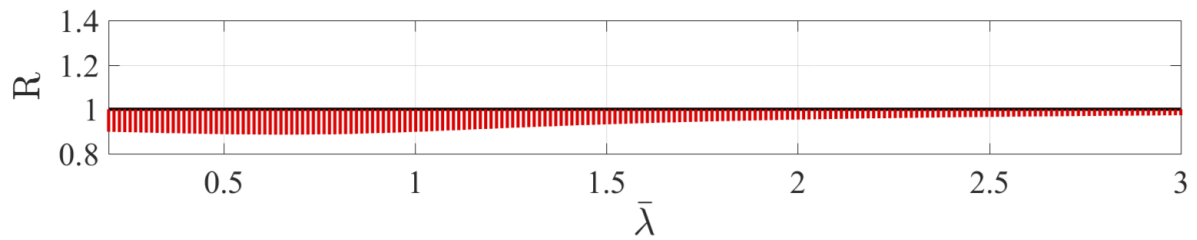
Figure E.20: Results for beam-columns with KKR rectangular cross-sections, steel quality S355 and moment due to uniformly distributed load. Strong buckling direction.



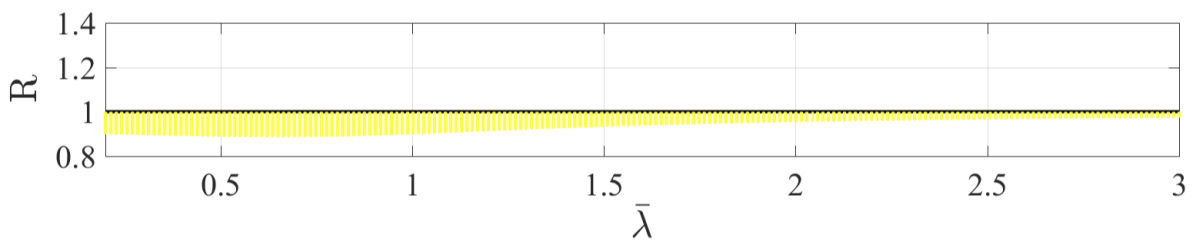
(a) Method 1, plastic analysis



(b) Method 2, plastic analysis



(c) Method 1, elastic analysis

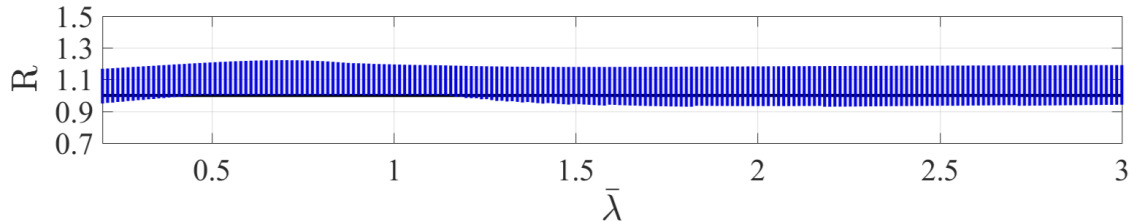


(d) Method 2, elastic analysis

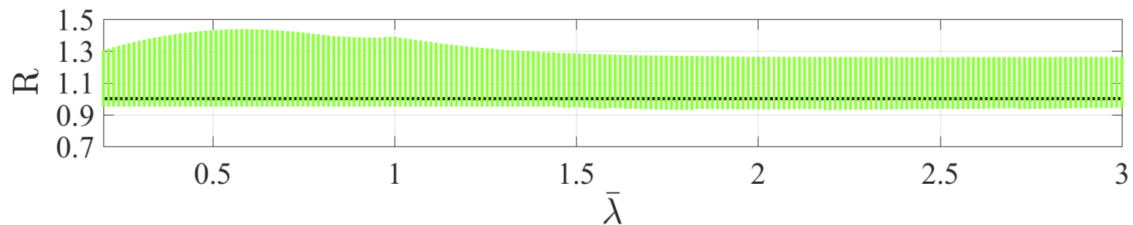
Figure E.21: Results for beam-columns with KKR square cross-sections, steel quality S355 and moment due to uniformly distributed load. Strong buckling direction.

E.4 Uniformly distributed load weak buckling direction (z-z)

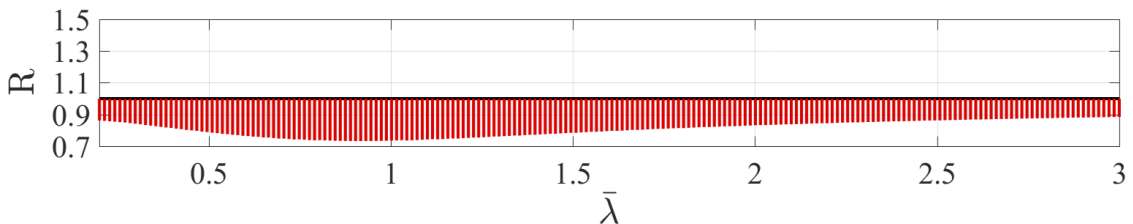
In figure E.22 to E.28 the results for moment due to uniformly distributed load regarding cross-sections HEA, HEM, IPE, VKR and KKR are presented. The analysis was conducted with steel strength class S335 and regarded weak buckling direction.



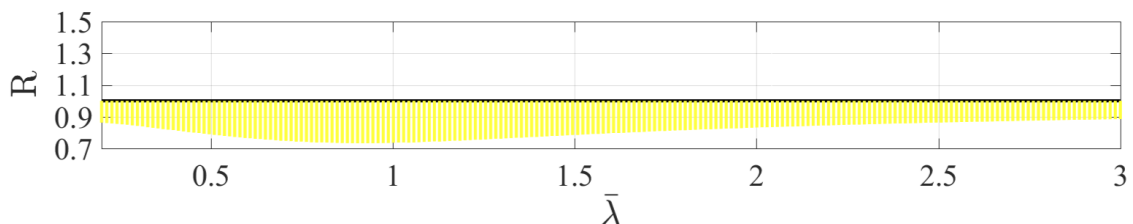
(a) Method 1, plastic analysis



(b) Method 2, plastic analysis

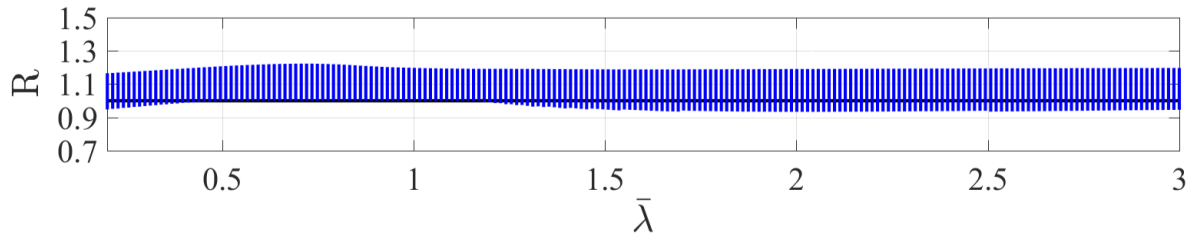


(c) Method 1, elastic analysis

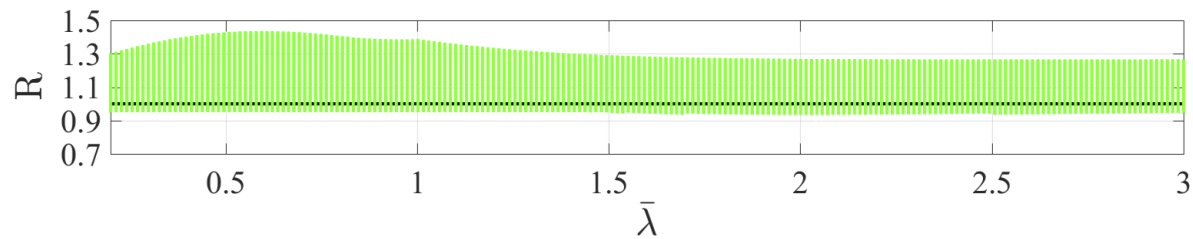


(d) Method 2, elastic analysis

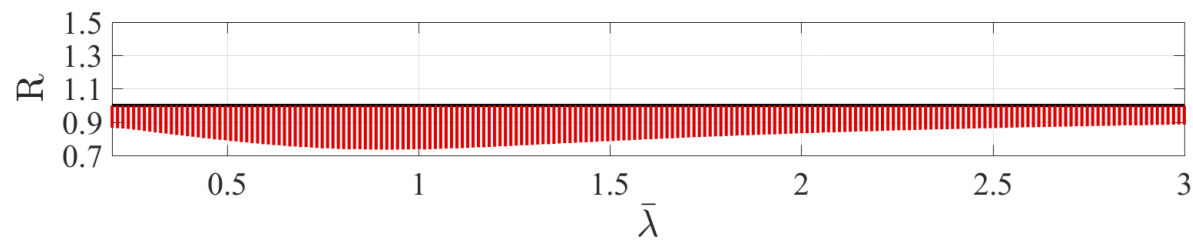
Figure E.22: Results for beam-columns with HEA cross-sections, steel quality S355 and moment due to uniformly distributed load. Weak buckling direction.



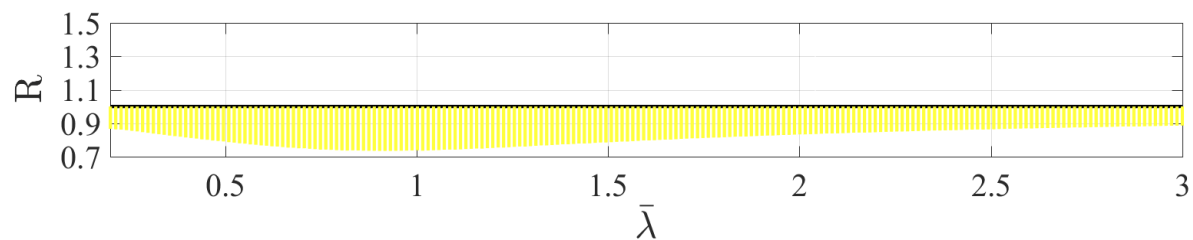
(a) Method 1, plastic analysis



(b) Method 2, plastic analysis

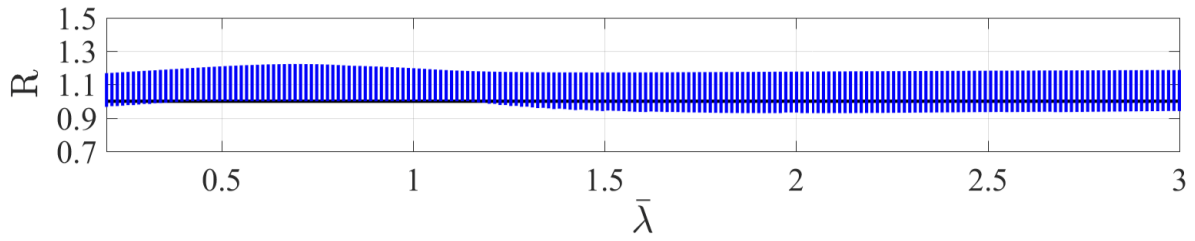


(c) Method 1, elastic analysis

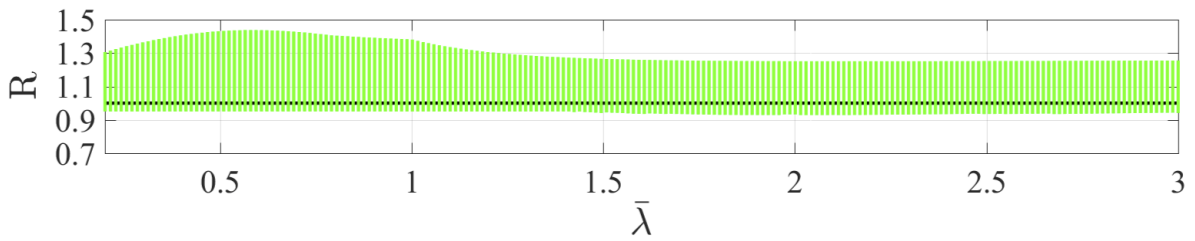


(d) Method 2, elastic analysis

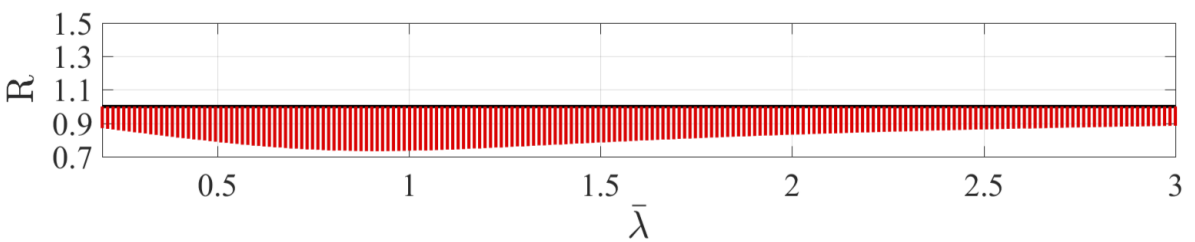
Figure E.23: Results for beam-columns with HEM cross-sections, steel quality S355 and moment due to uniformly distributed load. Weak buckling direction.



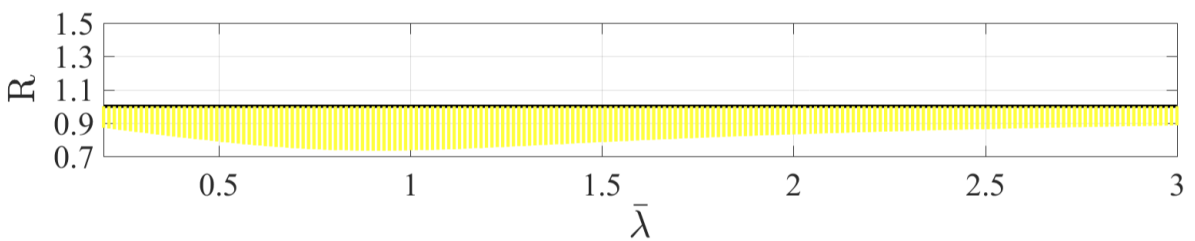
(a) Method 1, plastic analysis



(b) Method 2, plastic analysis

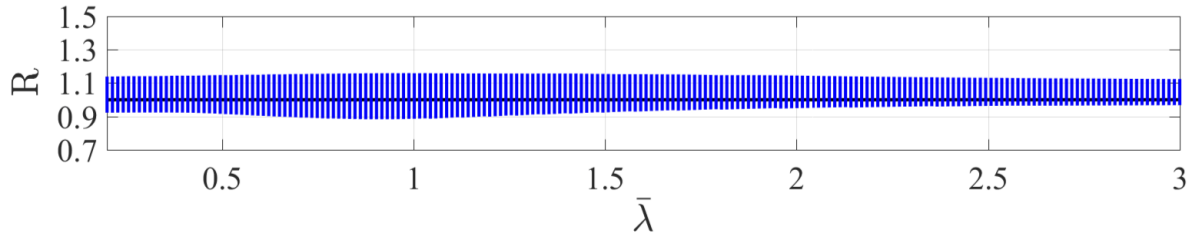


(c) Method 1, elastic analysis

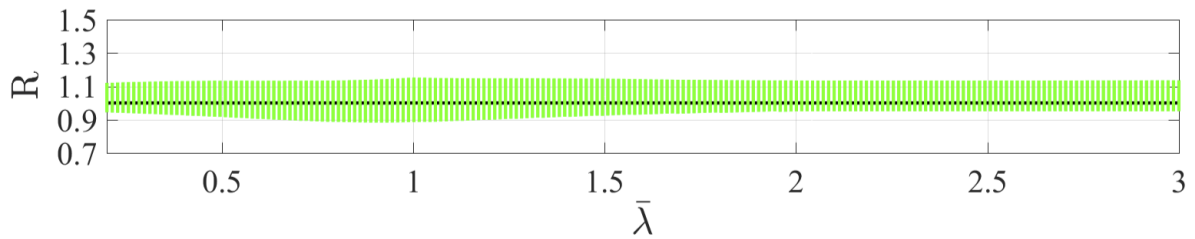


(d) Method 2, elastic analysis

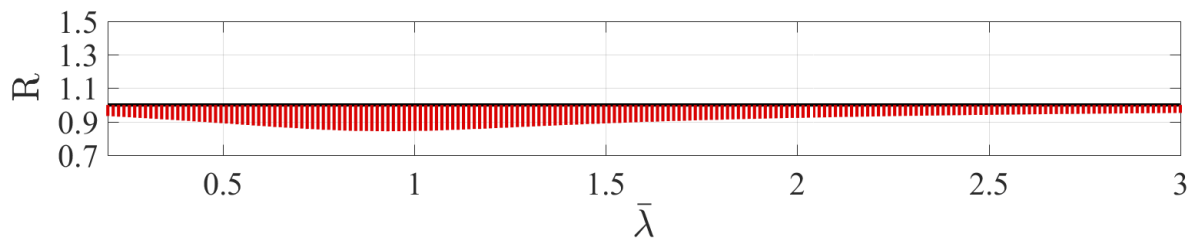
Figure E.24: Results for beam-columns with IPE cross-sections, steel quality S355 and moment due to uniformly distributed load. Weak buckling direction.



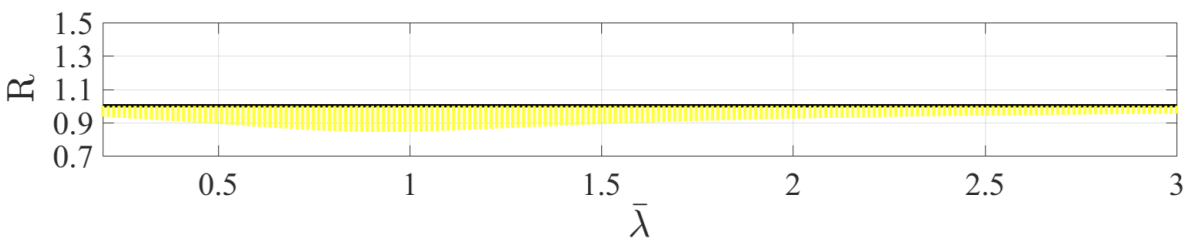
(a) Method 1, plastic analysis



(b) Method 2, plastic analysis

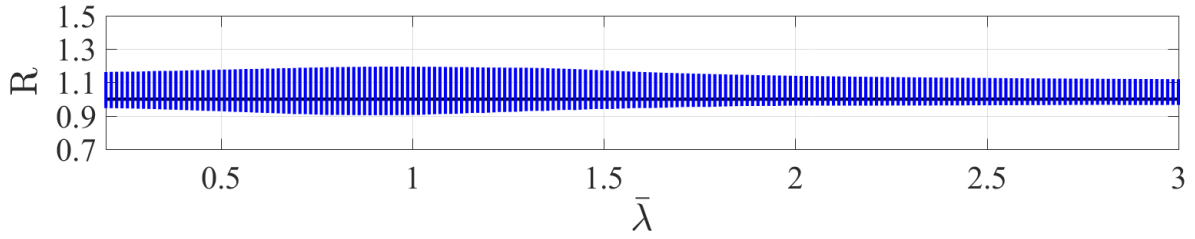


(c) Method 1, elastic analysis

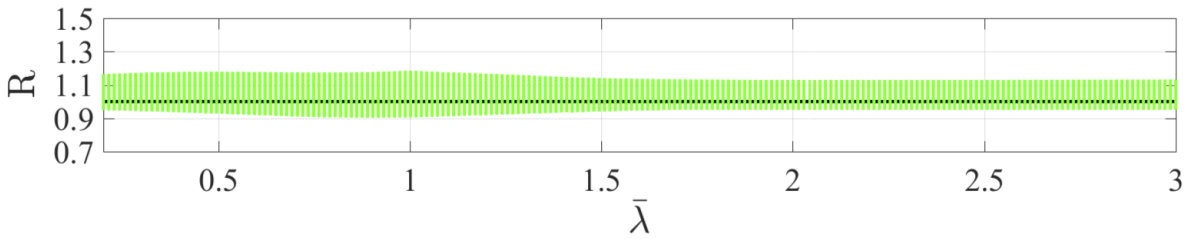


(d) Method 2, elastic analysis

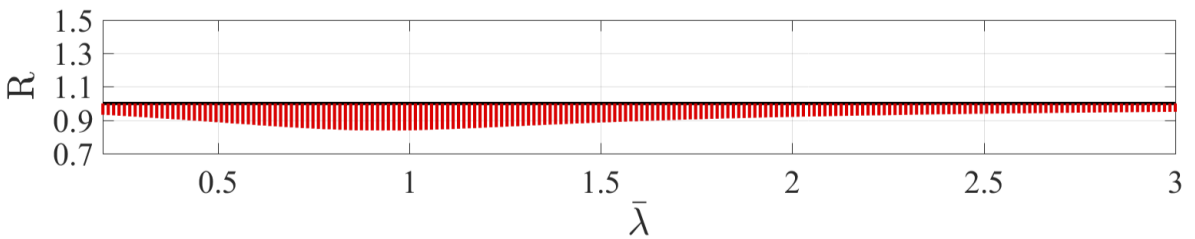
Figure E.25: Results for beam-columns with VKR rectangular cross-sections, steel quality S355 and moment due to uniformly distributed load. Weak buckling direction.



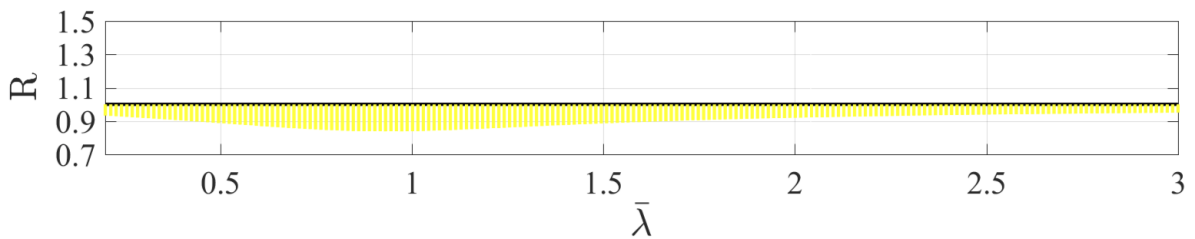
(a) Method 1, plastic analysis



(b) Method 2, plastic analysis

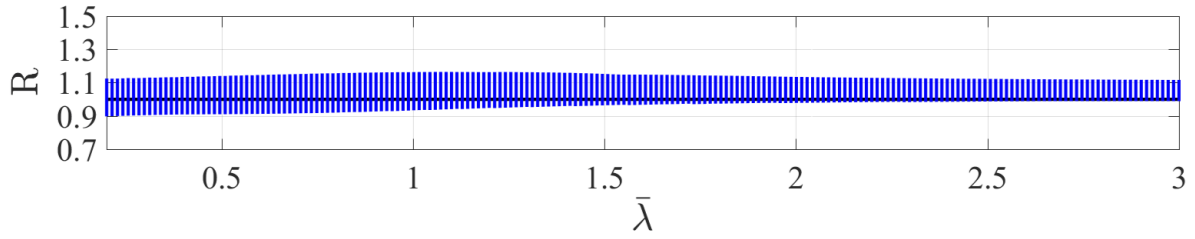


(c) Method 1, elastic analysis

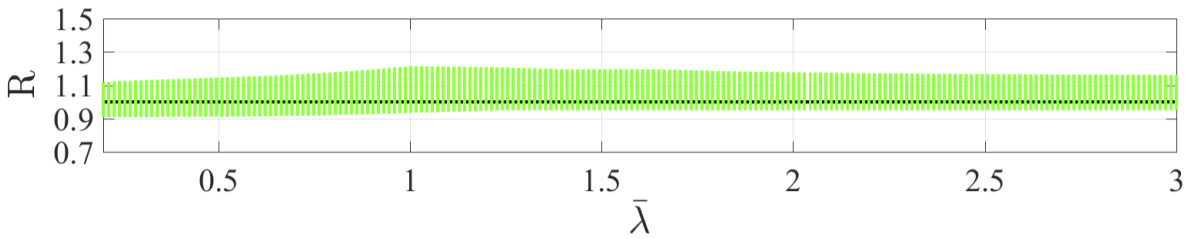


(d) Method 2, elastic analysis

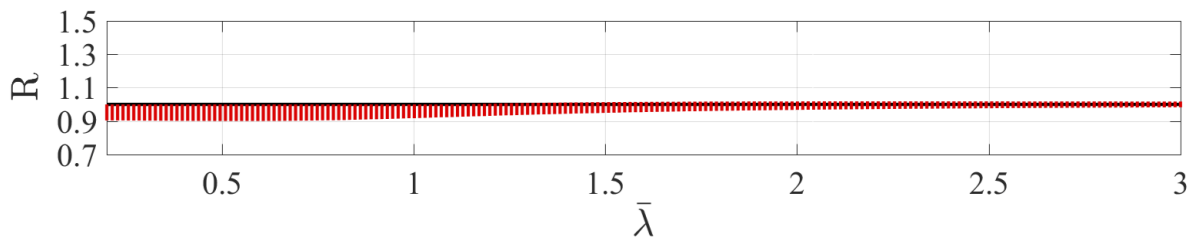
Figure E.26: Results for beam-columns with VKR square cross-sections, steel quality S355 and moment due to uniformly distributed load. Weak buckling direction.



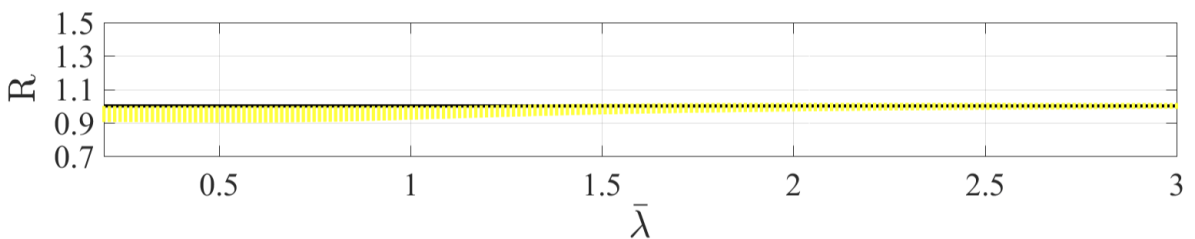
(a) Method 1, plastic analysis



(b) Method 2, plastic analysis

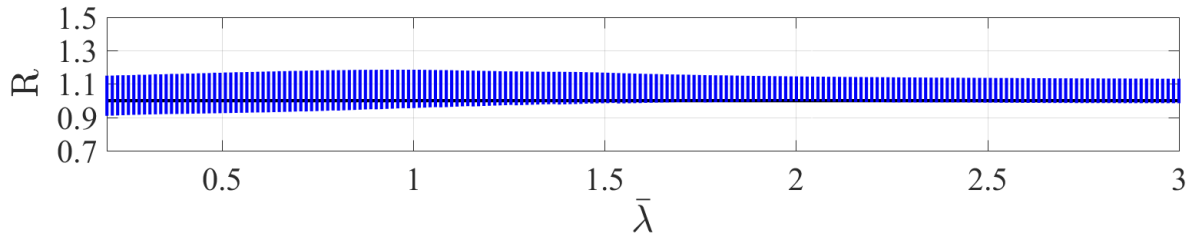


(c) Method 1, elastic analysis

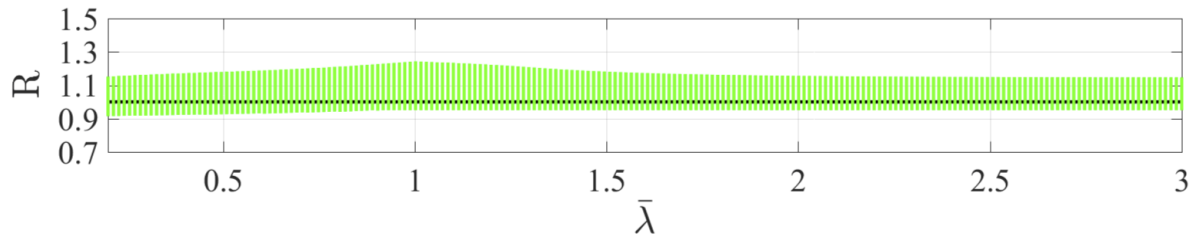


(d) Method 2, elastic analysis

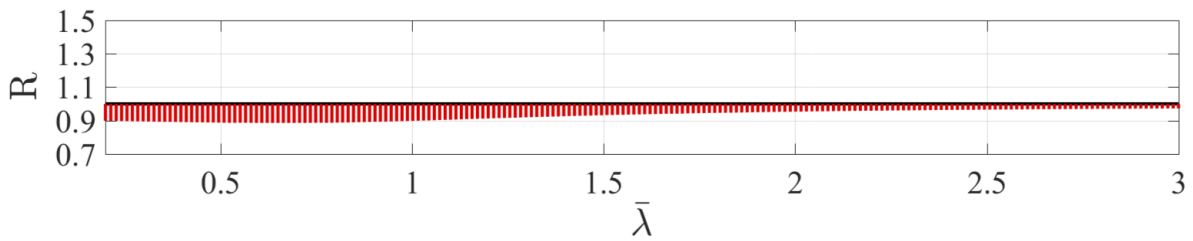
Figure E.27: Results for beam-columns with KKR rectangular cross-sections, steel quality S355 and moment due to uniformly distributed load. Weak buckling direction.



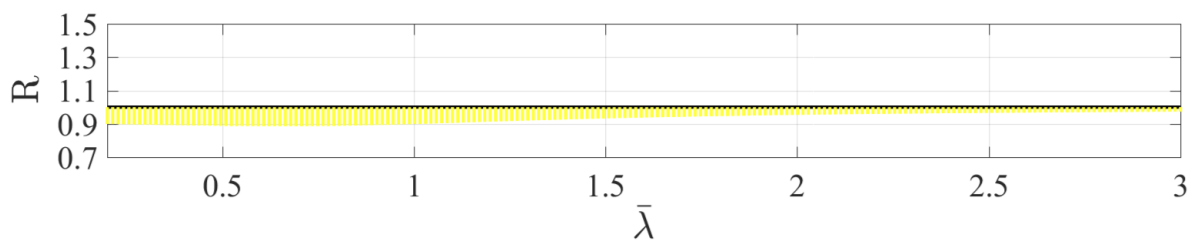
(a) Method 1, plastic analysis



(b) Method 2, plastic analysis



(c) Method 1, elastic analysis

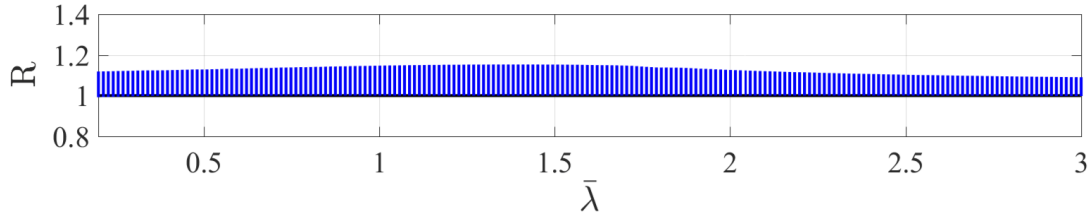


(d) Method 2, elastic analysis

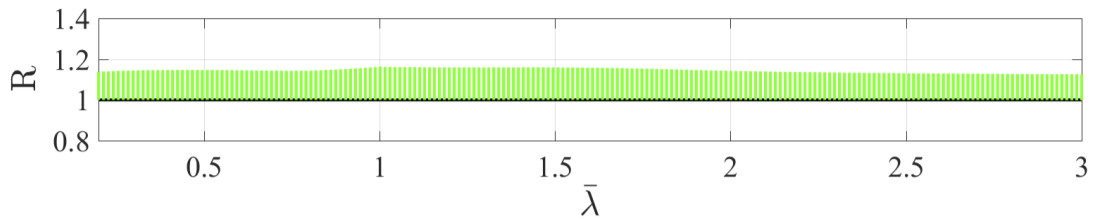
Figure E.28: Results for beam-columns with KKR square cross-sections, steel quality S355 and moment due to uniformly distributed load. Bending about weak axis.

E.5 Optimisation of initial bow imperfection (y-y)

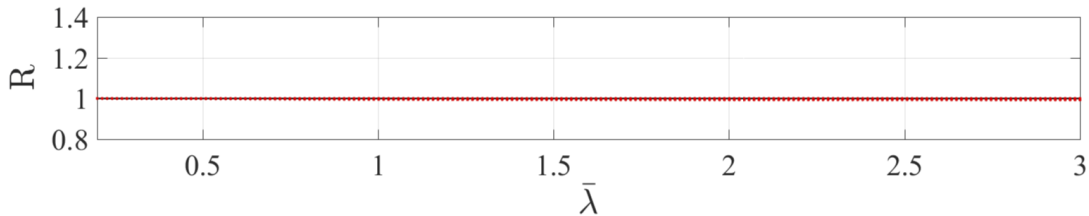
In figure E.29 to E.35 the results from using the new optimised formula for the initial bow imperfection regarding cross-sections HEA, HEM, IPE, VKR and KKR are presented. The analysis was conducted with steel strength class S335 and regarded strong buckling direction.



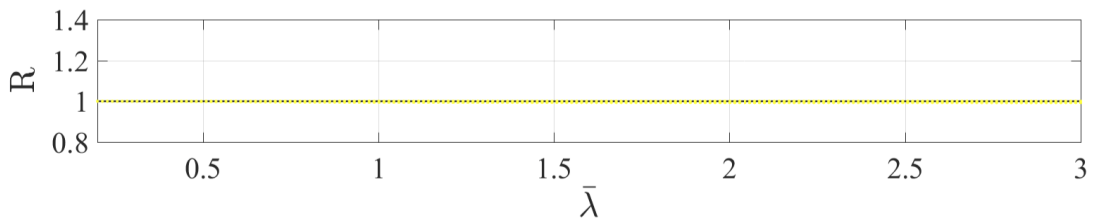
(a) Method 1, plastic analysis



(b) Method 2, plastic analysis

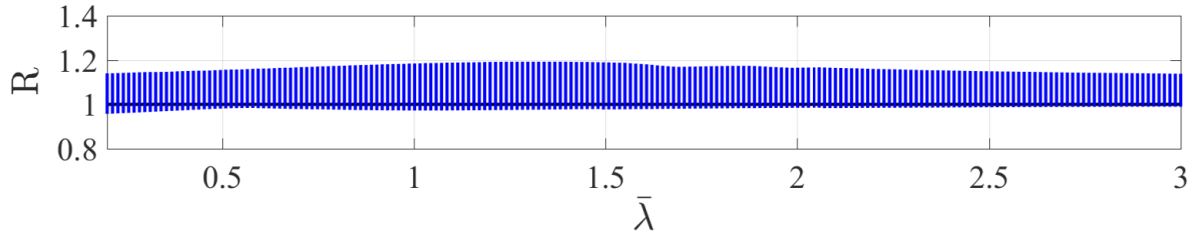


(c) Method 1, elastic analysis

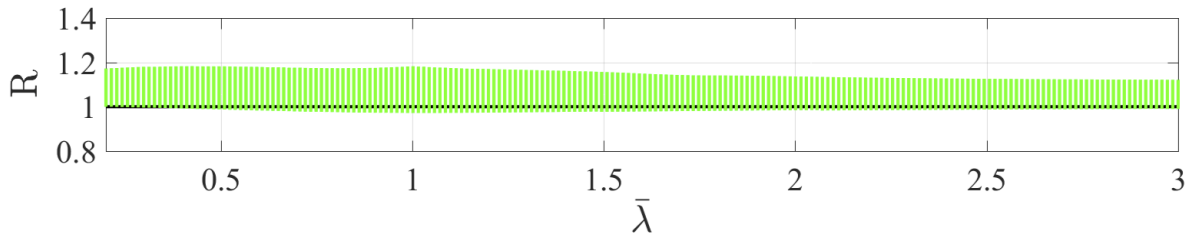


(d) Method 2, elastic analysis

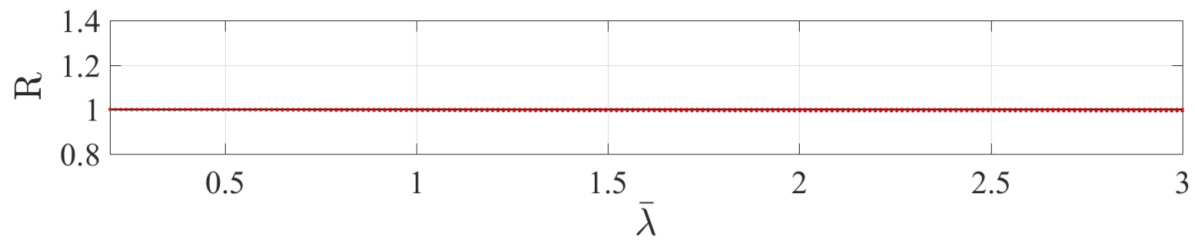
Figure E.29: Results from analysing all HEA beam-columns using the new formulas for initial bow imperfections. The members are subjected to a combination of axial force and external end-moment with steel strength class S335 and strong buckling direction.



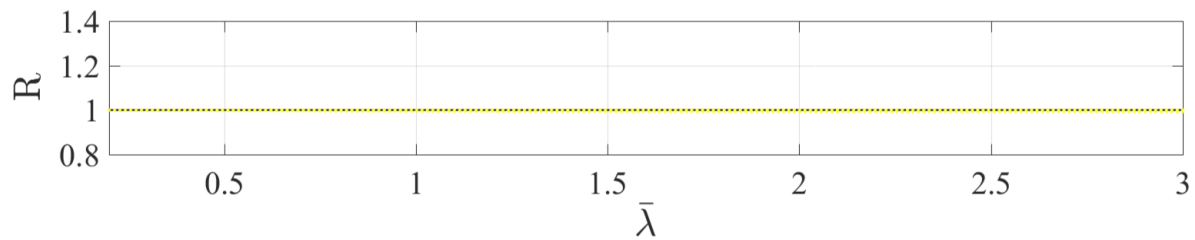
(a) Method 1, plastic analysis



(b) Method 2, plastic analysis

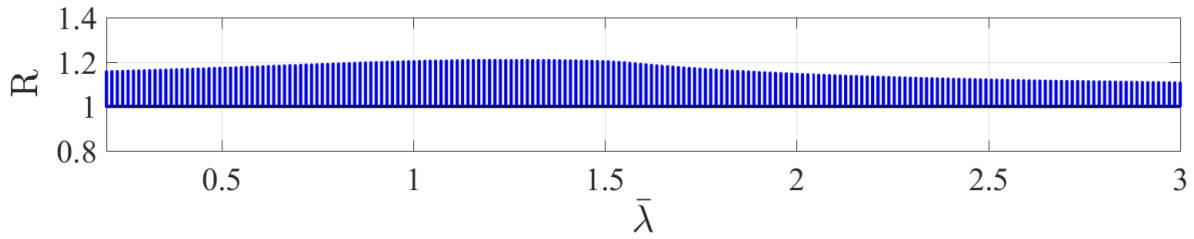


(c) Method 1, elastic analysis

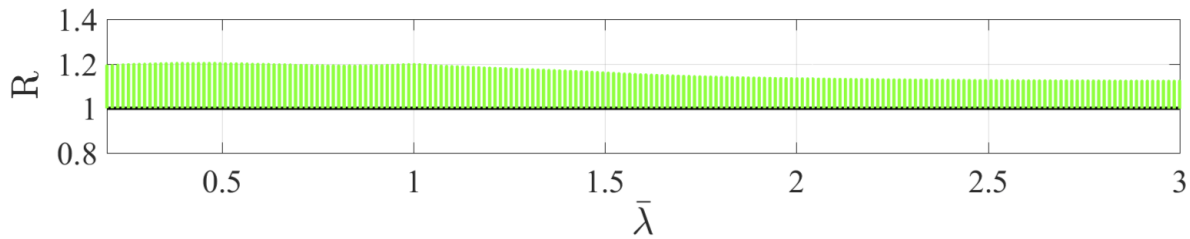


(d) Method 2, elastic analysis

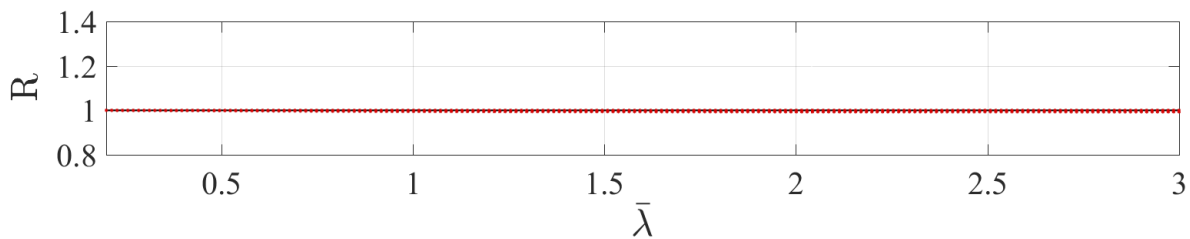
Figure E.30: Results from analysing all HEM beam-columns using the new formulas for initial bow imperfections. The members are subjected to a combination of axial force and external end-moment with steel strength class S355 and strong buckling direction.



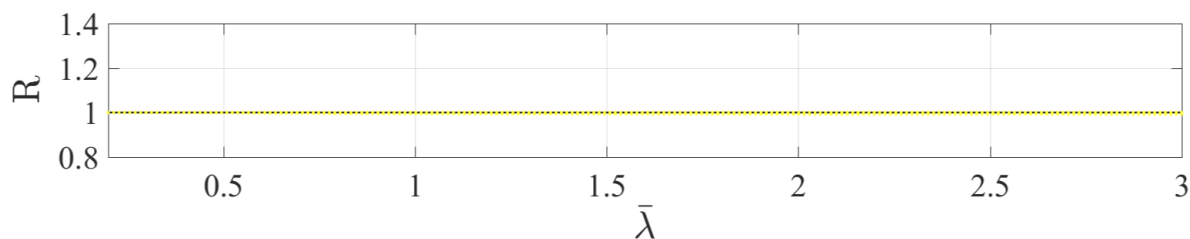
(a) Method 1, plastic analysis



(b) Method 2, plastic analysis

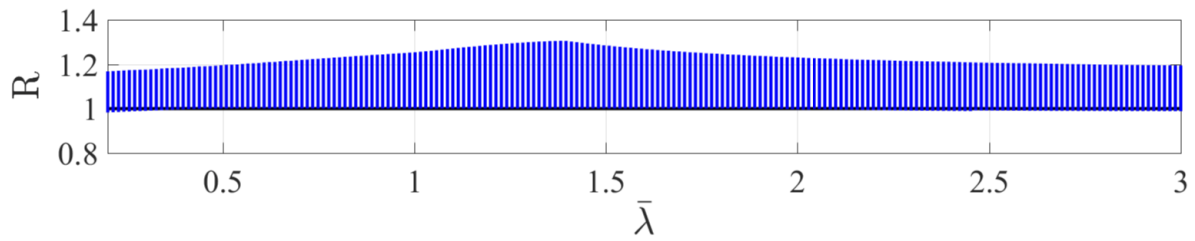


(c) Method 1, elastic analysis

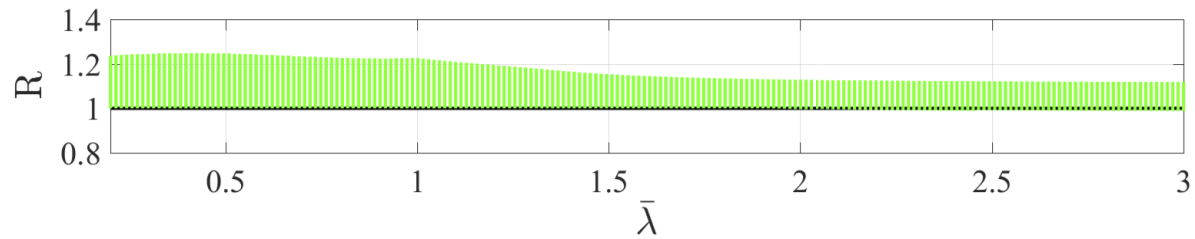


(d) Method 2, elastic analysis

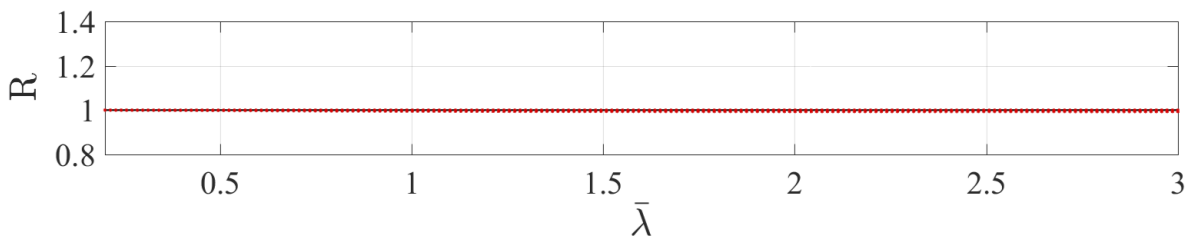
Figure E.31: Results from analysing all IPE beam-columns using the new formulas for initial bow imperfections. The members are subjected to a combination of axial force and external end-moment with steel strength class S355 and strong buckling direction.



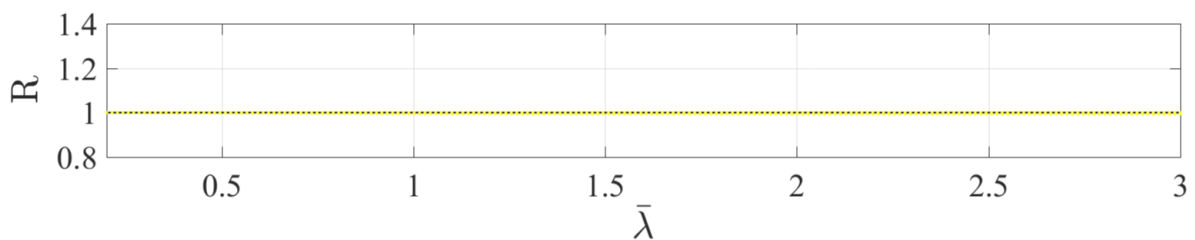
(a) Method 1, plastic analysis



(b) Method 2, plastic analysis

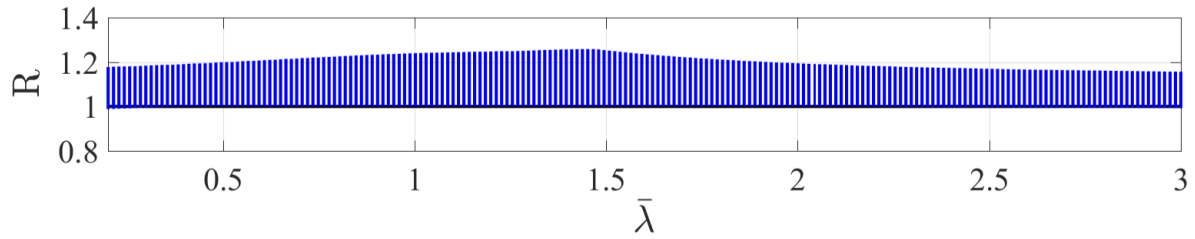


(c) Method 1, elastic analysis

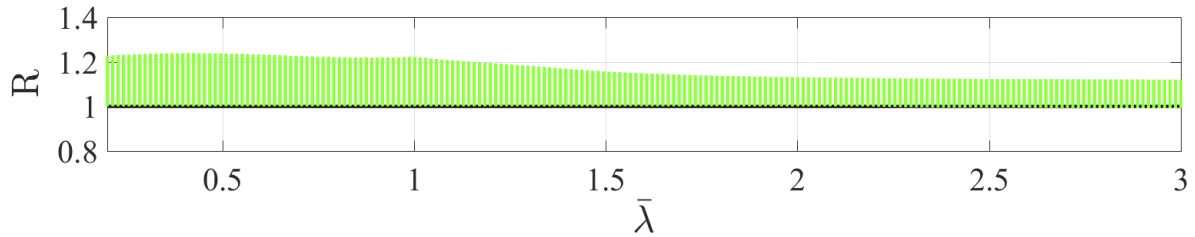


(d) Method 2, elastic analysis

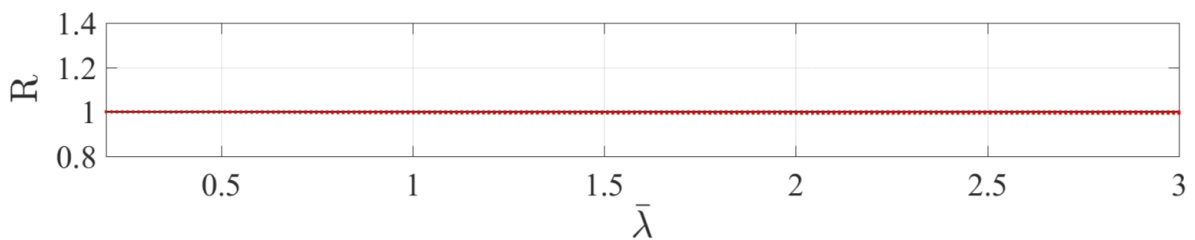
Figure E.32: Results from analysing all VKR rectangular beam-columns using the new formulas for initial bow imperfections. The members are subjected to a combination of axial force and external end-moment with steel strength class S355 and strong buckling direction.



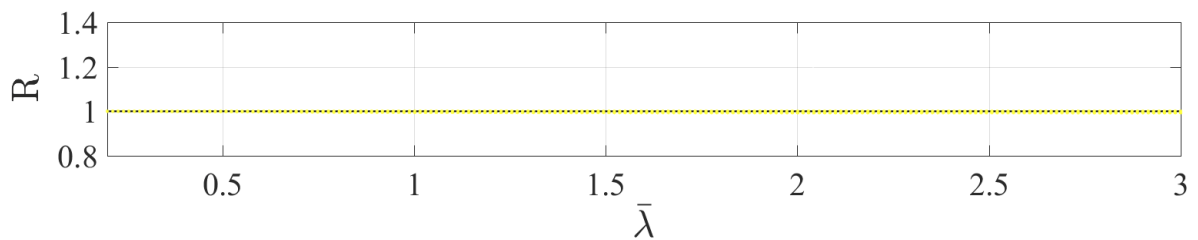
(a) Method 1, plastic analysis



(b) Method 2, plastic analysis

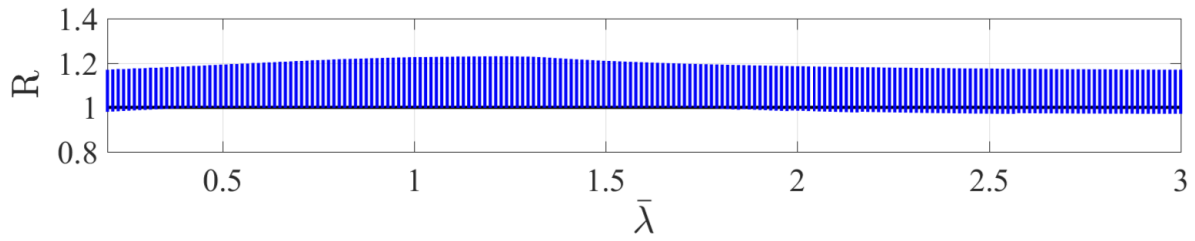


(c) Method 1, elastic analysis

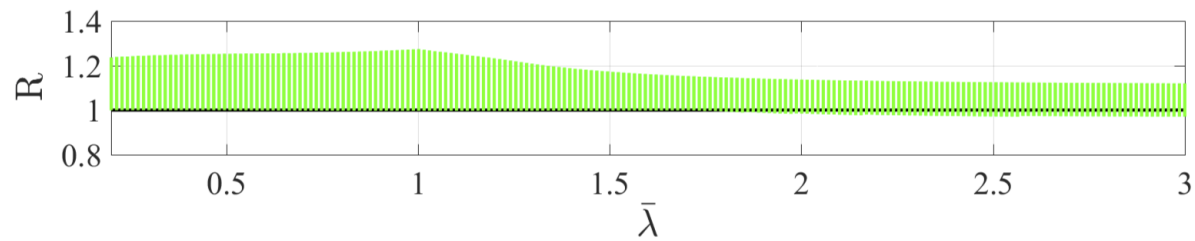


(d) Method 2, elastic analysis

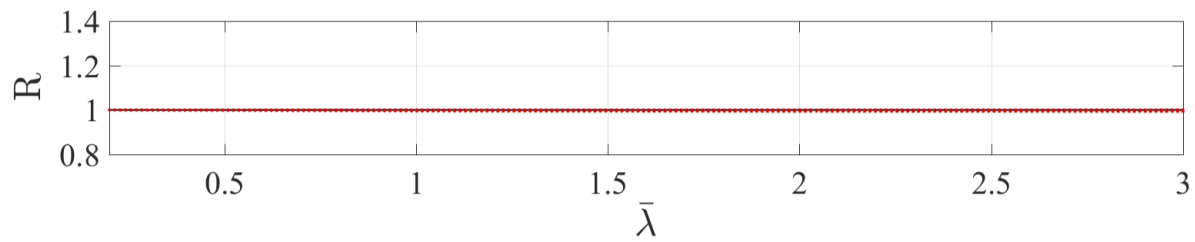
Figure E.33: Results from analysing all VKR square beam-columns using the new formulas for initial bow imperfections. The members are subjected to a combination of axial force and external end-moment with steel strength class S355 and strong buckling direction.



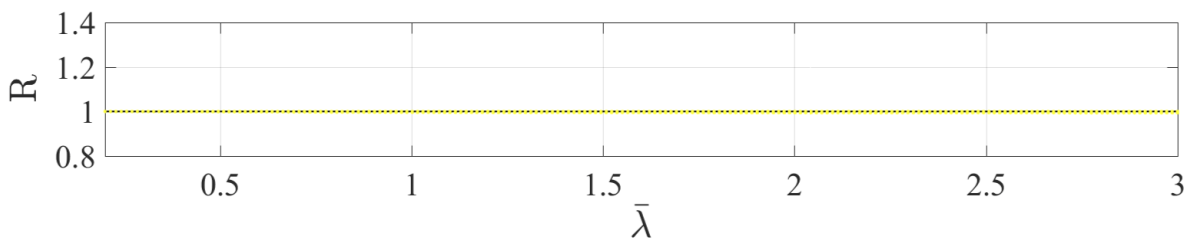
(a) Method 1, plastic analysis



(b) Method 2, plastic analysis

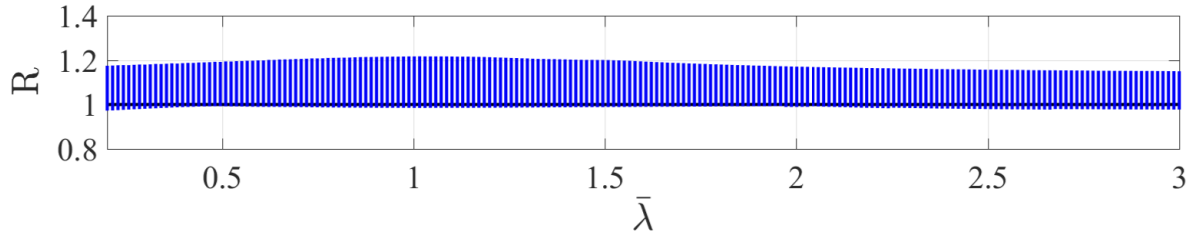


(c) Method 1, elastic analysis

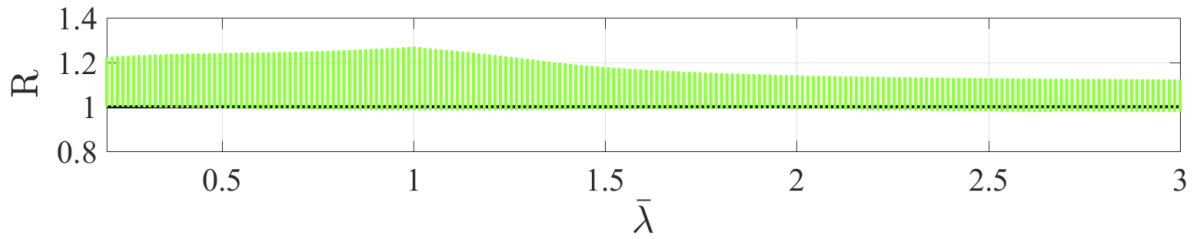


(d) Method 2, elastic analysis

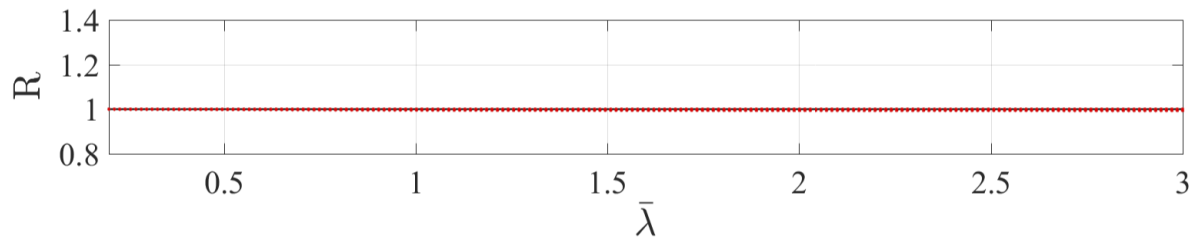
Figure E.34: Results from analysing all KKR rectangular beam-columns using the new formulas for initial bow imperfections. The members are subjected to a combination of axial force and external end-moment with steel strength class S355 and strong buckling direction.



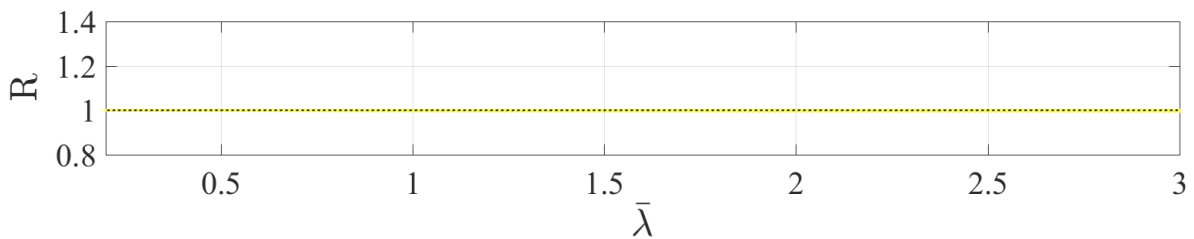
(a) Method 1, plastic analysis



(b) Method 2, plastic analysis



(c) Method 1, elastic analysis

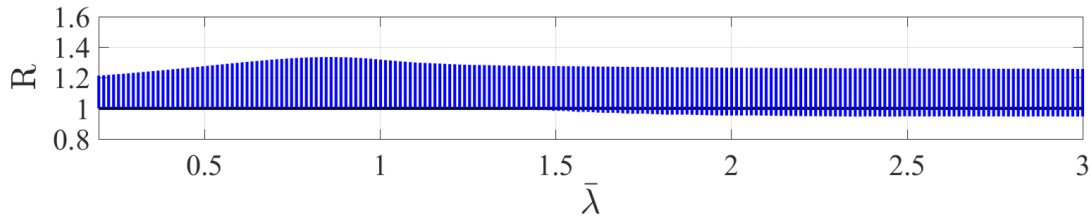


(d) Method 2, elastic analysis

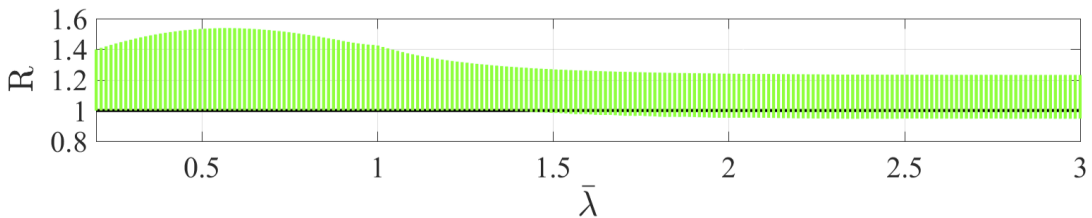
Figure E.35: Results from analysing all KKR square beam-columns using the new formulas for initial bow imperfections. The members are subjected to a combination of axial force and external end-moment with steel strength class S355 and strong buckling direction.

E.6 Optimisation of initial bow imperfection (z-z)

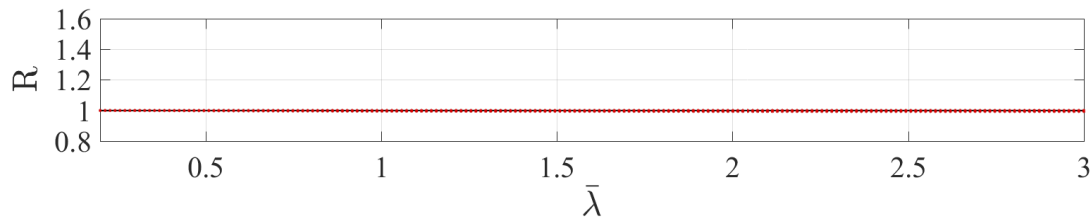
In figure E.36 to E.42 the results from using the new optimised formula for the initial bow imperfection regarding cross-sections HEA, HEM, IPE, VKR and KKR are presented. The analysis was conducted with steel strength class S355 and weak buckling direction.



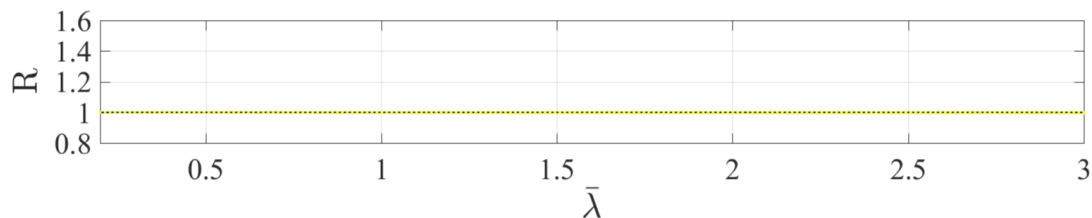
(a) Method 1, plastic analysis



(b) Method 2, plastic analysis

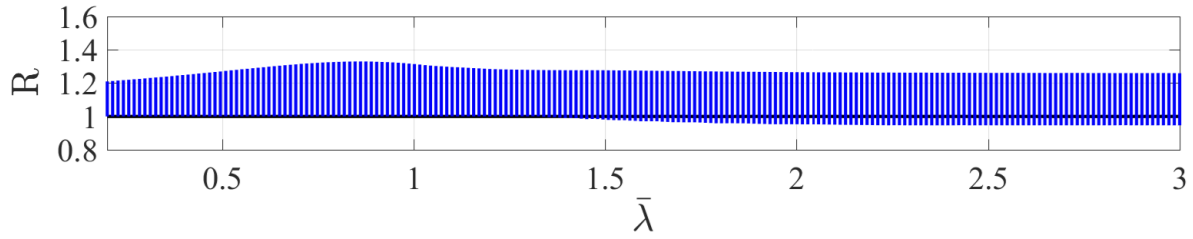


(c) Method 1, elastic analysis

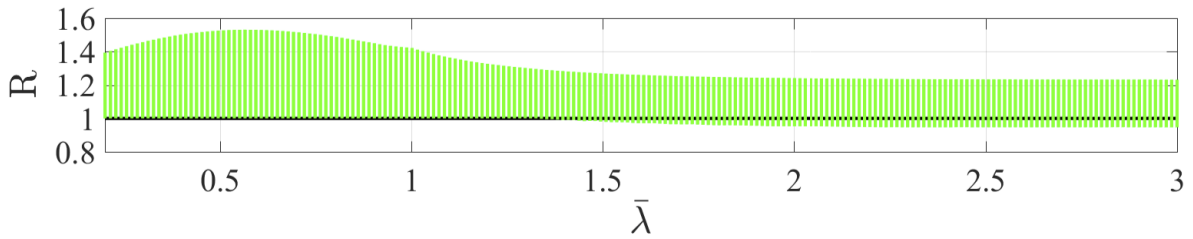


(d) Method 2, elastic analysis

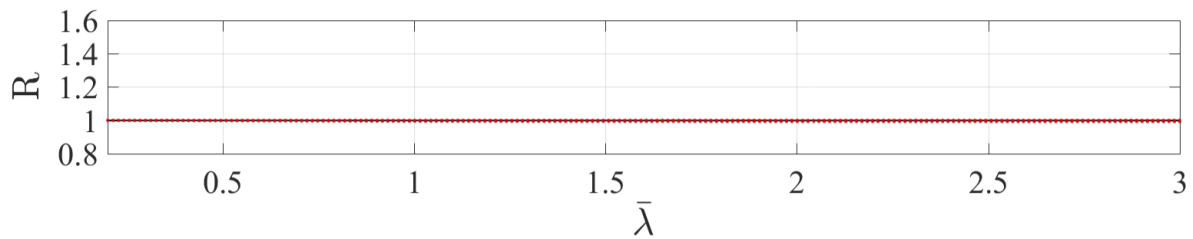
Figure E.36: Results from analysing all HEA beam-columns using the new formulas for initial bow imperfections. The members are subjected to a combination of axial force and external end-moment with steel strength class S355 and weak buckling direction.



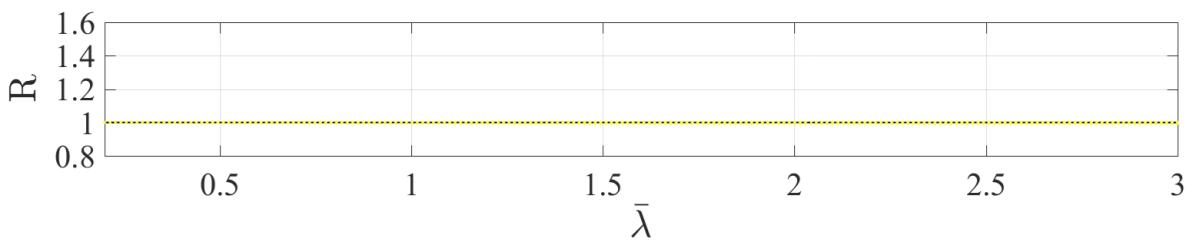
(a) Method 1, plastic analysis



(b) Method 2, plastic analysis

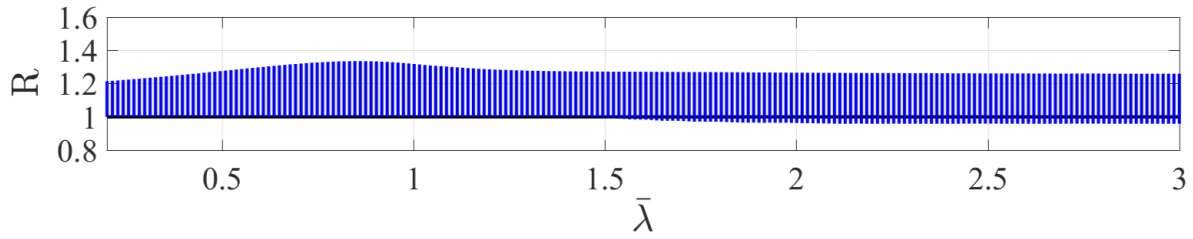


(c) Method 1, elastic analysis

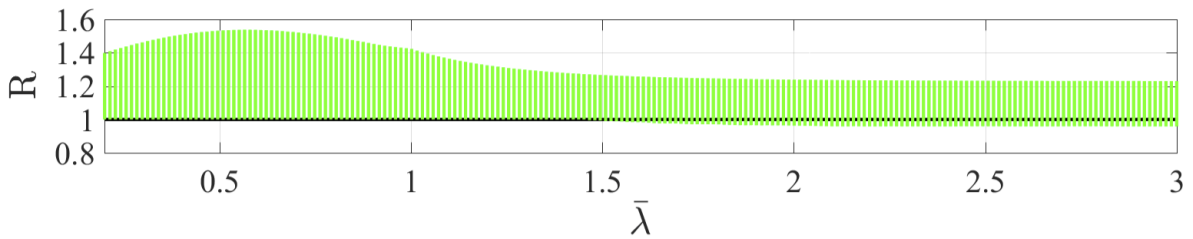


(d) Method 2, elastic analysis

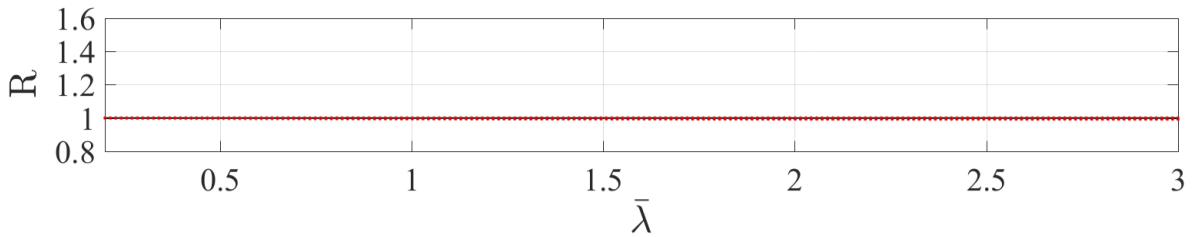
Figure E.37: Results from analysing all HEM beam-columns using the new formulas for initial bow imperfections. The members are subjected to a combination of axial force and external end-moment with steel strength class S355 and weak buckling direction.



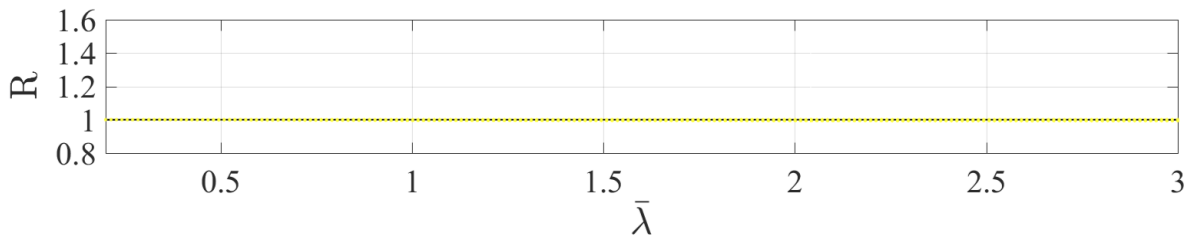
(a) Method 1, plastic analysis



(b) Method 2, plastic analysis

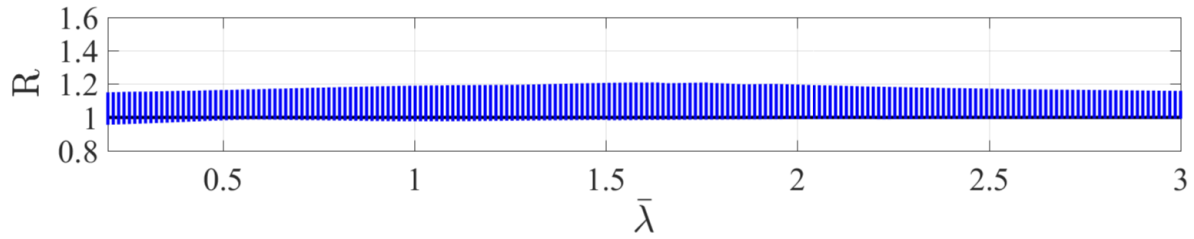


(c) Method 1, elastic analysis

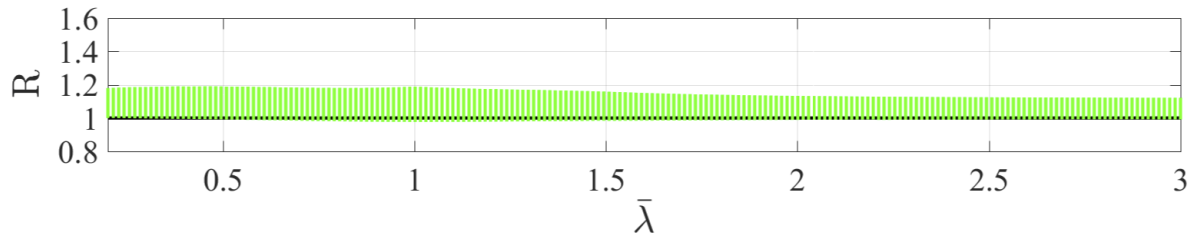


(d) Method 2, elastic analysis

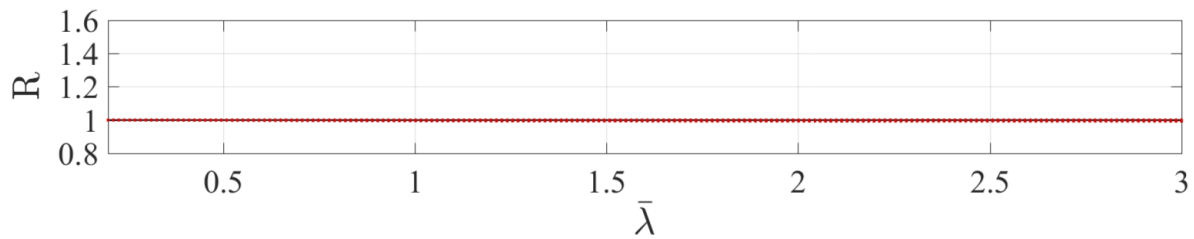
Figure E.38: Results from analysing all IPE beam-columns using the new formulas for initial bow imperfections. The members are subjected to a combination of axial force and external end-moment with steel strength class S355 and weak buckling direction.



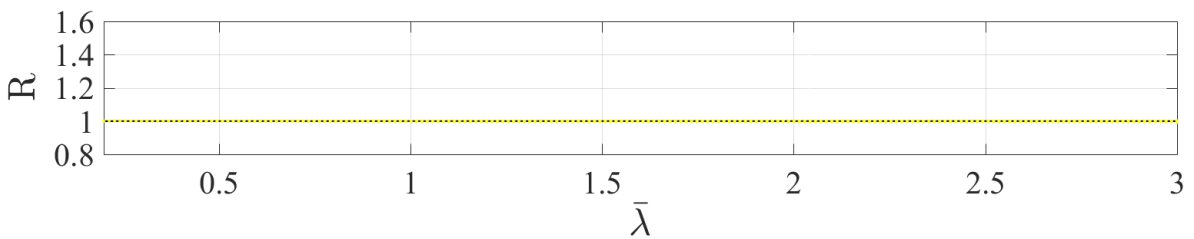
(a) Method 1, plastic analysis



(b) Method 2, plastic analysis

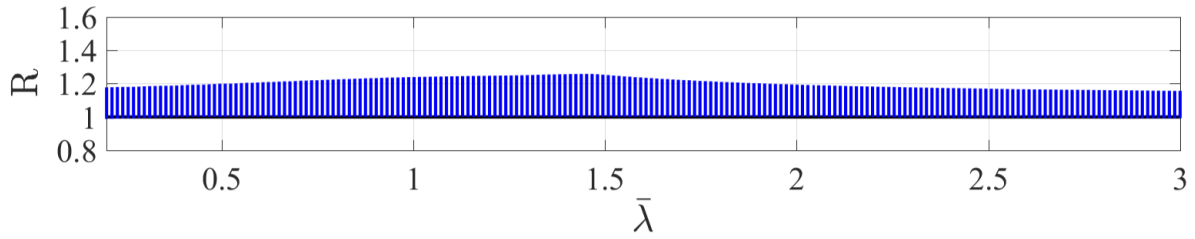


(c) Method 1, elastic analysis

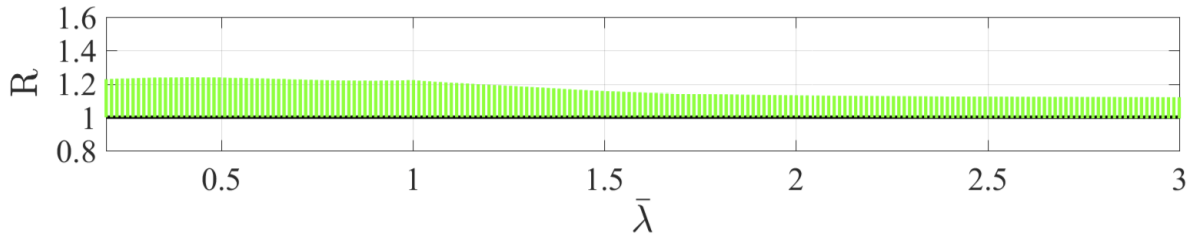


(d) Method 2, elastic analysis

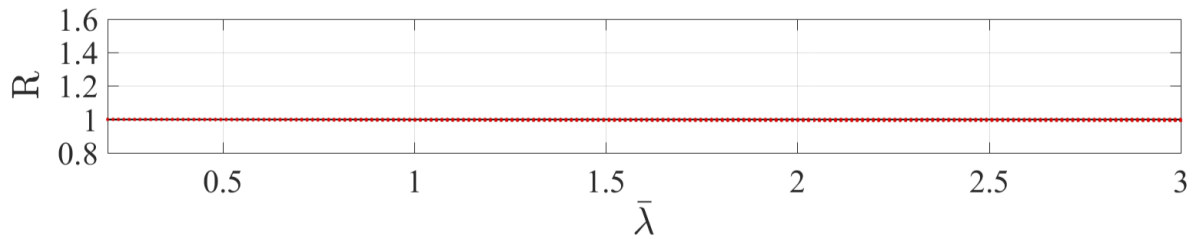
Figure E.39: Results from analysing all VKR rectangular beam-columns using the new formulas for initial bow imperfections. The members are subjected to a combination of axial force and external end-moment with steel strength class S355 and weak buckling direction.



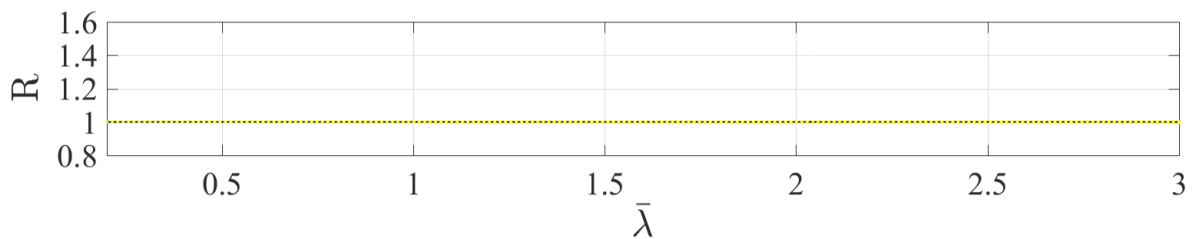
(a) Method 1, plastic analysis



(b) Method 2, plastic analysis

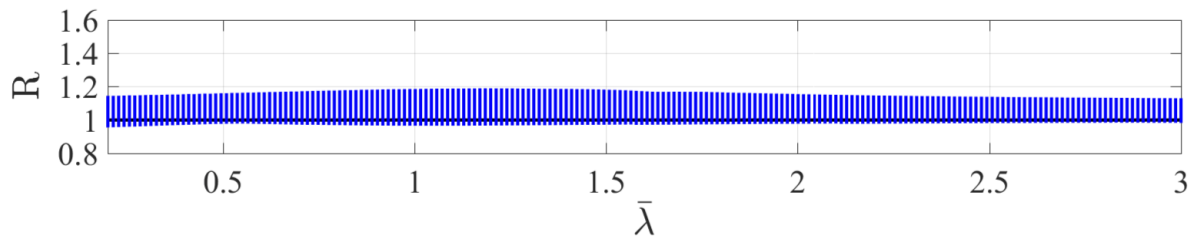


(c) Method 1, elastic analysis

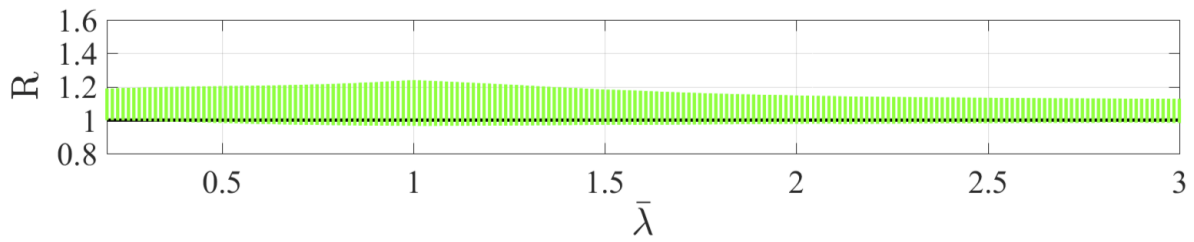


(d) Method 2, elastic analysis

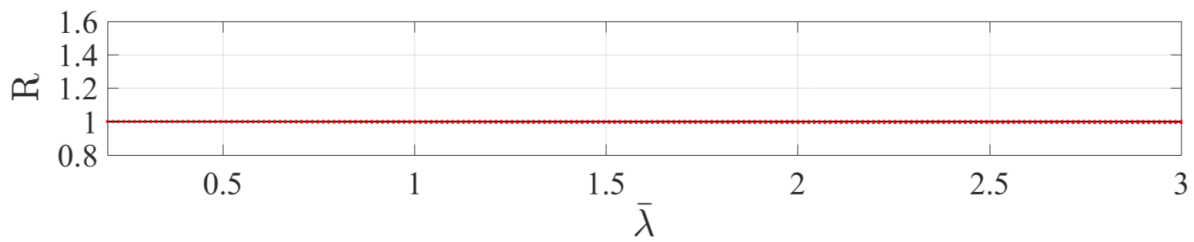
Figure E.40: Results from analysing all VKR square beam-columns using the new formulas for initial bow imperfections. The members are subjected to a combination of axial force and external end-moment with steel strength class S355 and weak buckling direction.



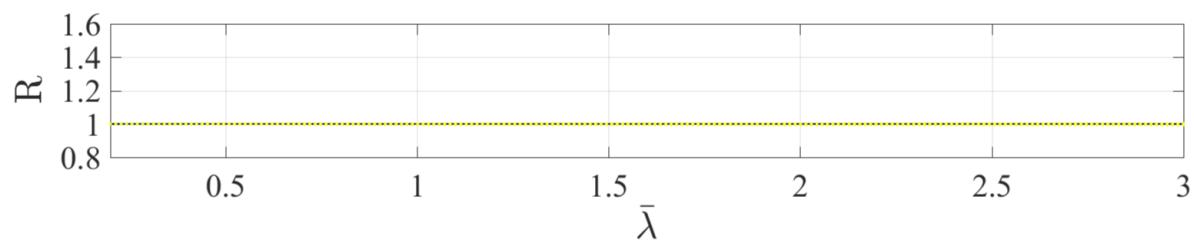
(a) Method 1, plastic analysis



(b) Method 2, plastic analysis

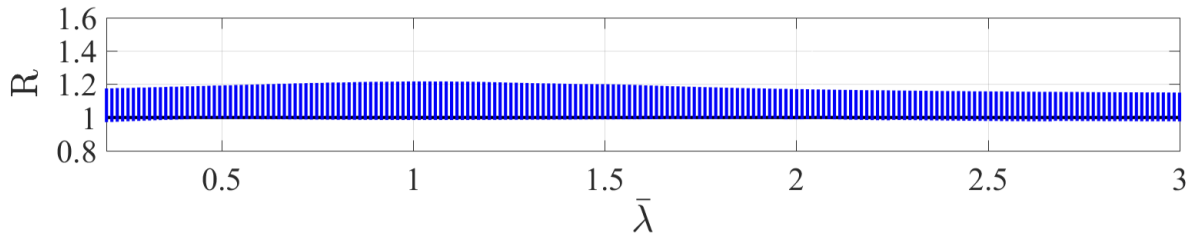


(c) Method 1, elastic analysis

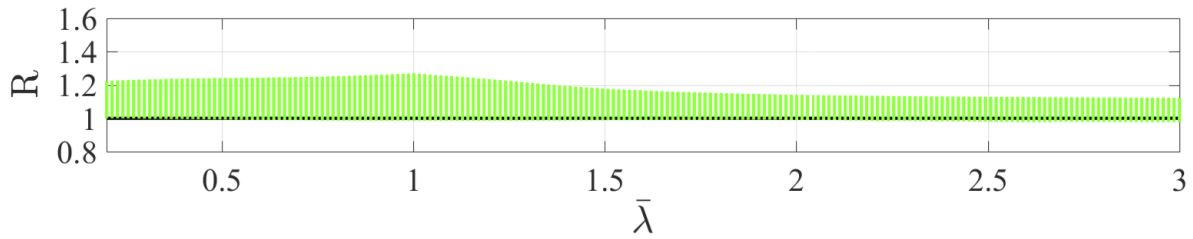


(d) Method 2, elastic analysis

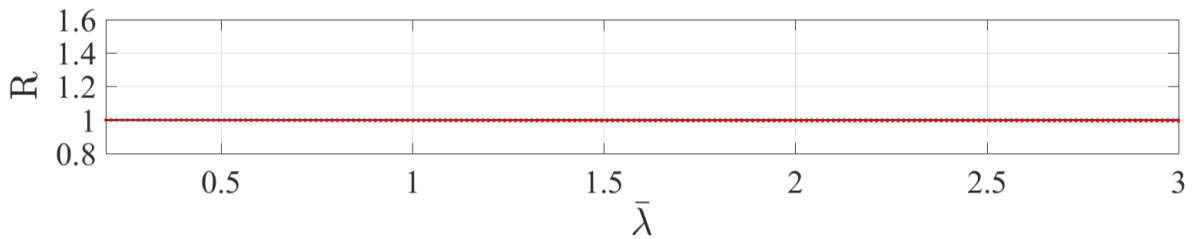
Figure E.41: Results from analysing all KKR rectangular beam-columns using the new formulas for initial bow imperfections. The members are subjected to a combination of axial force and external end-moment with steel strength class S355 and weak buckling direction.



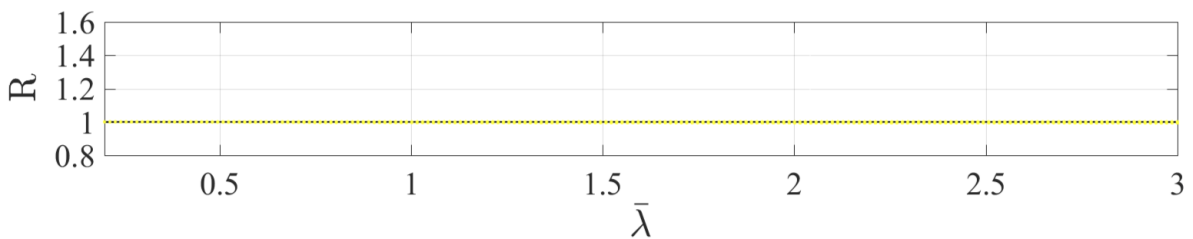
(a) Method 1, plastic analysis



(b) Method 2, plastic analysis



(c) Method 1, elastic analysis



(d) Method 2, elastic analysis

Figure E.42: Results from analysing all KKR square beam-columns using the new formulas for initial bow imperfections. The members are subjected to a combination of axial force and external end-moment with steel strength class S355 and weak buckling direction.